Identification and macrophage-activating activity of glycolipids released from intracellular *Mycobacterium bovis* BCG

. E. Rhoades,[1]* F-. F. Hsu,[2] J. B. Torrelles,[3] J. Turk,[2] D. Chatterjee[3] and D. G. Russell[1]
[1]Department of Microbiology and Immunology, Cornell University, Ithaca, NY 14853, USA.
[2]Department of Internal Medicine, Washington University, St Louis, MO 63110, USA.
[3]Mycobacterial Research Laboratories, Department of Microbiology, Immunology and Pathology, Colorado State University, Ft Collins, CO 80523, USA.

Summary

Intracellular mycobacteria release cell wall glycolipids into the endosomal network of infected macrophages. Here, we characterize the glycolipids of *Mycobacterium bovis* BCG (BCG) that are released into murine bone marrow-derived macrophages (BMMØ). Intracellularly released mycobacterial lipids were harvested from BMMØ that had been infected with ^{14}C-labelled BCG. Released BCG lipids were resolved by thin-layer chromatography, and they migrated similarly to phosphatidylinositol dimannosides (PIM$_2$), mono- and diphosphatidylglycerol, phosphatidylethanolamine, trehalose mono- and dimycolates and the phenolic glycolipid, mycoside B. Culture-derived BCG lipids that co-migrated with the intracellularly released lipids were purified and identified by electrospray ionization mass spectrometry. When delivered on polystyrene microspheres, fluorescently tagged BCG lipids were also released into the BMMØ, in a manner similar to release from viable or heat-killed BCG bacilli. To determine whether the released lipids elicited macrophage responses, BCG lipid-coated microspheres were delivered to interferon gamma-primed macrophages (BMMØ or thioglycollate-elicited peritoneal macrophages), and reactive nitrogen intermediates as well as tumour necrosis factor-alpha and monocyte chemoattractant protein-1 production were induced. When fractionated BCG lipids were delivered on the microspheres, PIM2 species reproduced the macrophage-activating activity of total BCG lipids. These results demonstrate that intra- cellular mycobacteria release a heterogeneous mix of lipids, some of which elicit the production of proin- flammatory cytokines from macrophages that could potentially contribute to the granulomatous response in tuberculous diseases.

Introduction

Recent estimates of the global burden of tuberculosis consider 1.86 billion people to be infected with *Mycobacterium tuberculosis* (Dye *et al.*, 1999), a pathogen respon- sible for more deaths from a single infectious agent than any other per year. The capacity of these bacilli to remain viable in macrophages, cells customarily associated with the elimination of pathogens, appears to be key to the persistence of mycobacterial infections. Upon phagocyto- sis by a host macrophage, bacilli modulate the phago- somes in which they reside into compartments that support bacterial survival and replication (Sturgill- Koszycki *et al.*, 1996; Russell, 2001). Maturation of the phagosomes is interrupted, and fusion with bactericidal lysosomes is avoided. Studies have also indicated that the insidious bacilli exert a subtle influence over the basic function of their host cells, limiting antigen presentation (Gercken *et al.*, 1994; VanHeyningen *et al.*, 1997; Ullrich *et al.*, 2000), suppressing lymphocyte responses (Prasad *et al.*, 1987; Makonkawkeyoon and Kasinrerk, 1989), inducing proinflammatory and immunosuppressive medi- ators (Wallis and Ellner, 1994; Rhoades *et al.*, 1995; Dahl *et al.*, 1996) and suppressing interferon-gamma (IFNγ)- mediated macrophage activation (Sibley *et al.*, 1990; Hussain *et al.*, 1999; Ting *et al.*, 1999). Despite the abun- dant literature on this subject, the identification of the bacterial factors that mediate this complex array of responses is lacking.

Mycobacterial cell wall lipids are ideal candidates for such mediators. The mycobacterial cell wall is covered by a non-covalently associated layer of glycolipids and waxes, some harbouring unusually substituted long- chained acyl moieties unique to *Mycobacterium* spp. (Besra and Chatterjee, 1994; Daffe and Etienne, 1999). There is a body of literature describing the effects of mycobacterial lipids on cells, suggesting that lipids are prime candidates for modulators of the host response. Outer surface lipids are the first mycobacterial compo-

nents to interact with the host, affecting binding to macrophage receptors (Stokes and Speert, 1995; Venisse *et al.*, 1995; Hoppe *et al.*, 1997), and possibly directing early events in the modulation of phagosomal maturation (Goren *et al.*, 1976). Mycobacterial lipids also elicit inflammatory responses. Phosphatidylinositol mannosides and lipoarabinomannans trigger cytokine and chemokine production from mononuclear cells (Roach *et al.*, 1994; Zhang *et al.*, 1995; Dahl *et al.*, 1996; Jones *et al.*, 2001). Trehalose dimycolate (TDM) exerts granulomagenic (Perez *et al.*, 2000; Yamagami *et al.*, 2001) and toxic effects (Silva and Faccioli, 1988) in mice, and complex glycolipids and waxes, including mycolic acids and phthiocerol dimycocerosate, resist degradation and accumulate in chronically infected tissues (Higuchi *et al.*, 1981; Young, 1981), thereby exerting long-term effects at the site of infection (Prasad *et al.*, 1987; Neill and Klebanoff, 1988; Vachula *et al.*, 1990). Much of the existing literature is based on the addition of isolated lipid fractions in suspensions to cell culture, not necessarily reflecting the natural route of delivery nor the combination of lipids occurring naturally in a bacterial infection. The effects of lipids released into the macrophage in a manner mimicking natural infection remains to be characterized.

Previously, we investigated the fate of mycobacterial lipids in *Mycobacterium bovis* BCG-infected cells (Beatty *et al.*, 2000), initiating investigation of the effects of released mycobacterial lipids. Intracellular BCG bacilli released heterogeneous cell wall glycolipids into the endocytic network of infected murine macrophages. The material was released within hours of internalization into early endocytic compartments, after which the glycolipids travelled to late endosomal and lysosomal compartments. Although the lipid nature of the released material was demonstrated, the identity of the released lipids was not reported. Here, we identify the released lipids and demonstrate that BCG glycolipids elicit inflammatory cytokines and reactive nitrogen intermediates in macrophages that have phagocytosed lipid-coated microspheres.

Results

Detection of lipids released into host macrophages

Mycobacterium bovis BCG was labelled metabolically with [^{14}C]-acetate before infecting murine BMMØ. The infected macrophages were lysed after 48 h and fractionated over sucrose, yielding a fraction that was both enriched for early endocytic and plasma membrane compartments (determined by the absence of mature cathepsin D; data not shown) and depleted of intact bacilli (determined by cfu counts). Analysis of this fraction ensured that released BCG lipids were studied instead of lipids that had remained bacteria associated. Bacteria-depleted fractions
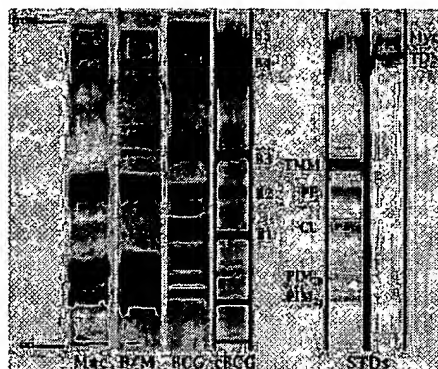

Fig. 1. Comparison of intracellularly released BCG lipids with standards by TLC. ^{14}C-acetate-labelled total lipid extracts were loaded onto a channelled high-performance TLC plate and developed in chloroform–methanol–water (65:25:4) over 10 cm. Radiolabelled lipids were detected by exposing the plate to autoradiography film, and unlabelled lipids and standards were visualized by spraying with sulphuric acid and charring. Lipids were extracted from macrophage cultures or BCG cultures: Mac, radiolabelled, uninfected macrophages; B/M, macrophages infected with radiolabelled BCG; BCG, radiolabelled BCG inoculum; cBCG, unlabelled BCG culture. Standards: PIM$_{2a}$ and PIM$_{2b}$, phosphatidylinositol dimannosides; CL, cardiolipin; PE, phosphatidylethanolamine; TMM, trehalose monomycolate; TDM, trehalose dimycolate; and MycB, mycoside B.

routinely harboured <300 cfu of BCG, a number of bacteria too small to yield detectable radiolabelled lipids. Total lipids in the fraction were extracted in chloroform–methanol (2:1) and resolved on high-performance thin-layer chromatography (TLC) plates in chloroform–methanol–water (65:25:4) (Fig. 1). Comparison with the radiolabelled inoculum (BCG) indicated that a subset of BCG-derived lipids appeared to be present in the infected homogenate of BCG-infected macrophages (B/M), and these lipids were largely absent in radiolabelled lipids of uninfected control macrophages (Mac). The released BCG lipids that aligned with species in an unlabelled BCG culture extract (cBCG) were designated B1–B5. When compared with known lipid standards, B1 and B2 had similar retention factors (R_fs) to diphosphatidylglycerol (labelled as cardiolipin, CL) and phosphatidylethanolamine (PE) respectively. Specific spray reagent tests determined that B1 and B2 contained phosphorus, and B2 contained nitrogen (data not shown). B3 and B4 were glycolipids (indicated by a purple hue after heating) with R_fs similar to trehalose monomycolate (TMM) and trehalose dimycolate (TDM), respectively, and B5 migrated with the solvent front, charring to a similar colour to mycoside B (MycB), a phenolic glycolipid.

The most polar radioactive lipids of the infected homogenate included phosphatidylinositol dimannosides (PIM$_{2a}$ and PIM$_{2b}$, varying in degrees of acylation) that aligned with lipids of both bacterial and macrophage origin. To determine the origin of the homogenate lipids, radioactive

lipids from infected macrophages were resolved in two dimensions on TLC plates (2D TLC). However, the migration of macrophage phospholipids overlapped that of bacterial phospholipids in all two-dimensional solvent systems that we tested. Therefore, we used an alternative radioactive precursor ([^{14}C]-propionate) that is incorporated preferentially by BCG. As shown in Fig. 2, BCG-derived PIMs, B1 and B2 migrated similarly to macrophage-derived lipids (Fig. 2A and B respectively); however, when the spots were recovered from the plate and counted in scintillant, only BCG-derived lipids were radioactive (PIM$_{2a}$ = 5753 d.p.m., PIM$_{2b}$ = 621 d.p.m., B1 = 14 015 d.p.m. and B2 = 8458 d.p.m., in a representative experiment). Similarly, extracts from macrophages that were infected with ^{14}C-propionate-labelled BCG yielded radioactive species that co-migrated with PIM standards (Fig. 2C; PIM$_{2a}$ = 207 d.p.m. and PIM$_{2b}$ = 500 d.p.m.), as well as B1 (359 d.p.m.) and B2 (626 d.p.m.). This method confirmed that B1 and B2 were released intracellularly and indicated that PIM$_2$ was also released from intracellular bacilli. Radioactive lipids were not detected in uninfected macrophages that had been cultured with an equivalent amount (d.p.m.) of [^{14}C]-propionate (Fig. 2D). Visualization of the radioactive lipids by autoradiography revealed that the labelled species present in homogenates of [^{14}C]-BCG-infected macrophages (Fig. 2E) were absent in homogenates of uninfected macrophages that had been cultured with [^{14}C]-propionate (Fig. 2F).

A similar 2D TLC approach was used to demonstrate that extracts of intracellularly released lipids contained species that were present in culture-derived B3, B4 using [^{14}C]-acetate, which was incorporated more efficiently in these lipids than [^{14}C]-propionate. B3 and B4 could be resolved from macrophage lipids and co-migrated with radioactive material from macrophages infected with ^{14}C-acetate-labelled BCG (Fig. 3A, 1057 d.p.m. and 233 d.p.m. respectively). These labelled species were absent in control macrophages (Fig. 3B; 32 d.p.m. and 27 d.p.m. respectively). B5 is labelled more efficiently with [^{14}C]-propionate. When resolved in two dimensions with the B5 standard, we again detected a co-migrating radioactive species (Fig. 3C; 404 d.p.m.) that was not present in the fraction from control macrophages (Fig. 3D; 15 d.p.m.). Macrophage-derived cholesterol (MC) also ran on these plates and, as noted for macrophage phospholipids in Fig. 2, incorporation of the ^{14}C-propionate label was very inefficient.

Mass spectrometric characterization of released mycobacterial lipids

Further characterization of the released lipids required more material than could be harvested from infected mac-
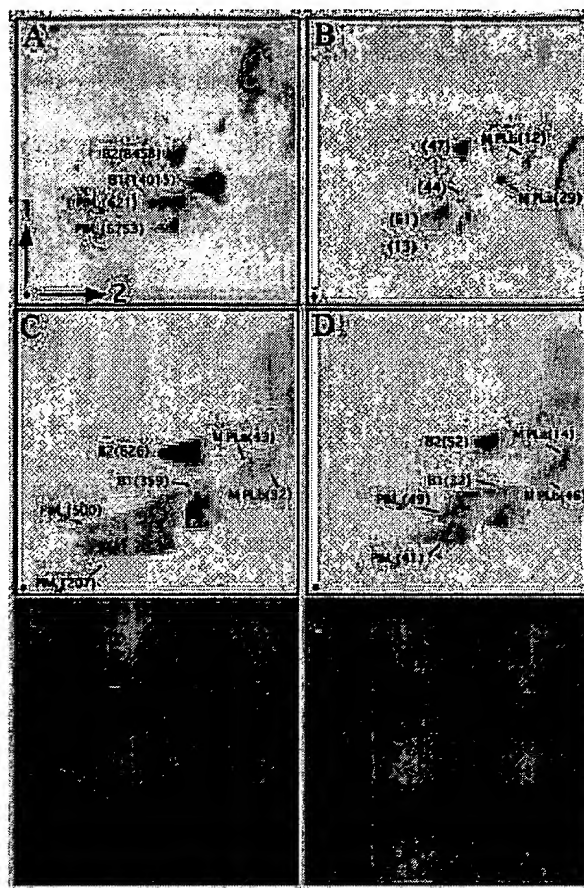
Fig. 2. Intracellularly released lipids co-migrate with BCG culture-derived PIM$_2$, B1 and B2. BCG cultures were metabolically labelled with [^{14}C]-propionate, and macrophages were infected with the radiolabelled bacilli or incubated with an equivalent amount (d.p.m.) of [^{14}C]-propionate. Lipids were extracted from infected or control macrophages and fractionated by preparative TLC to yield polar fractions containing PE and more polar lipids. Equivalent amounts (μg) of homogenate extract fractions were loaded onto TLC plates with lipid standards and resolved in two directions [spot indicates the origin; first direction in chloroform–methanol–water (60:30:6); second direction in propyl acetate–isopropanol–ethanol–6% ammonia (3:9:3:9)]. Lipids were visualized by charring, and co-migrating radioactive lipids were detected by scraping the spots into scintillant. Numbers in parentheses represent the d.p.m. of each charred spot, and background d.p.m. values were routinely <30 d.p.m. (A–D). Alternatively, radiolabelled lipids were visualized by exposing plates to autoradiographic film (E and F).
A. Radiolabelled BCG inoculum.
B. Uninfected macrophages incubated with [^{14}C]-propionate.
C and E. Macrophages infected with ^{14}C-labelled BCG plus PIM$_{2a}$, PIM$_{2b}$, B1 and B2.
D and F. [^{14}C]-propionate-treated control macrophages plus PIM$_{2a}$, PIM$_{2b}$, B1 and B2.

rophages. Therefore, having established that the BCG culture-derived lipids (PIM$_{2a}$, PIM$_{2b}$ and B1–B5) corresponded to the radioactive BCG lipids released inside the macrophage, PIMs and B1–B5 were purified from unlabelled BCG cultures for mass spectrometry. Culture-
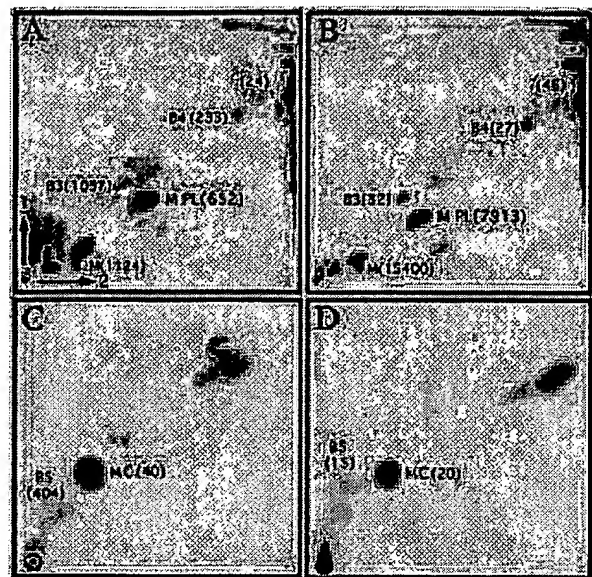
Fig. 3. Intracellularly released lipids co-migrate with BCG culture-derived B3, B4 and B5. For TLC with B3 and B4, BCG cultures were metabolically labelled with [^{14}C]-acetate and, for B5, cultures were metabolically labelled with [^{14}C]-propionate, which labels MycB more readily. Macrophages were infected and harvested as described in the legend to Fig. 2. Equivalent amounts (μg) of whole extracts were co-loaded with standards and resolved in two directions [spot indicates the origin; first direction chloroform–methanol–water (30:8:1); second direction chloroform–acetic acid–methanol–water (60:16:5:2); A and B] or co-loaded with B5 and resolved in the first direction in chloroform–methanol (93:7) and in the second direction in toluene–acetone (90:10); C and D. Lipids were detected as described in the legend to Fig. 2. Background d.p.m. values were between 15 and 50 d.p.m.
A. Macrophages infected with ^{14}C-acetate-labelled BCG plus B3 and B4.
B. [^{14}C]-acetate-treated uninfected macrophages plus B3 and B4.
C. Macrophages infected with ^{14}C-propionate-labelled BCG plus B5.
D. [^{14}C]-propionate-treated uninfected macrophages plus B5.

derived material was characterized using electrospray ionization (ESI) mass spectrometry and collisionally activated dissociation (CAD) tandem mass spectrometry. The major species at m/z 1413 in PIM$_{2a}$ (Fig. 4A) was a [M-H]$^-$ ion of 1-tuberculostearoyl-2-palmitoyl-*sn*-glycero-3-phosphatidylinositol dimannoside ($C_{19:0}/C_{16:0}$-PIM$_2$), containing an additional palmitoyl group ($C_{16:0}$), probably attached to the inositol skeleton. PIM$_{2b}$ (Fig. 4B) had two additional acyl groups. Major ions were observed at m/z 1693, 1679 and 1651, representing the [M-H]$^-$ ions of $C_{19:0}/C_{16:0}$-PIM$_2$ containing additional ($C_{19:0},C_{16:0}$) ($C_{18:0},C_{16:0}$) or ($C_{16:0},C_{16:0}$) acyl groups respectively. The structural assignments were established by their CAD tandem mass spectra (see *Supplementary material*, Figs S1 and S2).

B1 contained DPG [also known as cardiolipin (CL)] and PG (Fig. 4C and D respectively). For DPG, ions in the spectrum represented molecular species bearing different

fatty acyl groups, and the product-ion spectrum of the most abundant, singly charged ion (m/z 1403) yielded ions at m/z 255 ($C_{16:0}$, palmitic acid) and 281 ($C_{18:1}$, oleic acid), identifying the major species as ($C_{18:1}/C_{16:0}$)-DPG (Hsu and Turk, 2001). The CAD tandem mass spectra of minor DPG species revealed the other common fatty acyl substituents as $C_{18:1}/C_{16:1}$ (palmitoleic acid) and $C_{18:1}/C_{18:1}$. The major ion of the spectrum of PG from B1 had a m/z of 747 (Fig. 4D), and the CAD tandem mass spectrum contained carboxylate anions at m/z 255 and 281, corresponding to $C_{18:1}/C_{1:0}$-PG. The fatty acyl constituents for the minor species of PG were identified as $C_{19:0}$(tuberculostearic)/$C_{16:0}$, $C_{18:1}/C_{18:0}$ and $C_{16:0}/C_{16:0}$.

Culture-derived B2 contained PE species as indicated in the negative ion ESI mass spectrum in Fig. 4E. Two major [M-H]$^-$ ions were observed at m/z 716 and 732. CAD tandem mass spectrometry of the major species at m/z 716 yielded carboxylate anion pairs at m/z 281 and 255, identifying the fatty acyl substituent as $C_{18:1}/C_{16:0}$-PE (Hsu and Turk, 2000). The CAD tandem mass spectrum of the other major ion at m/z 732 yielded prominent anion pairs at m/z 297 and 255, arising from the $C_{19:0}/C_{16:0}$-PE. The spectrum also contained the ion pairs at m/z 283 and 269, which revealed the minor $C_{18:0}/C_{17:0}$(heptadecanoic acid)-PE isomer. CAD tandem mass spectrometry also revealed that more than one isomer was present in all the minor species of PE observed for B2, and they contained the same common fatty acyl substituents as those observed for CL and PG (see *Supplementary material*, Fig. S1).

The ESI mass spectrum profile of the culture-derived B3 (Fig. 4F) was similar to that of a TMM standard (inset) from *M. tuberculosis*. The most abundant [M+Li]$^+$ adducts were observed at m/z 1540, 1568 and 1596, and this is consistent with the presence of the ions at m/z 1556, 1584 and 1612 in the ESI mass spectrum of the same mixture observed as the [M+Na]$^+$ adduct ions (data not shown). The mycolic acid compositions of these molecules, as established by tandem mass spectrometry, corresponded to $C_{82}H_{160}O_4$, $C_{84}H_{164}O_4$ and $C_{86}H_{168}O_4$ respectively (see *Supplementary material*, Fig. S2).

To characterize the composition of the culture-derived B5, the ESI mass spectrum observed as the [M+Li]$^+$ ion (Fig. 4G) was compared with that arising from a BCG-derived MycB standard (inset). The most abundant ions were observed at m/z 1472, 1486, 1500 and 1514, representing the various mycoside B species with R$_1$-COOH/R$_2$-COOH long-chain fatty acid substituents, corresponding to $C_{26:0}/C_{26:0}$, $C_{27:0}/C_{26:0}$, $C_{28:0}/C_{26:0}$ and $C_{29:0}/C_{26:0}$ respectively. The fatty acid compositions of the molecules were established by their CAD product-ion spectra (data not shown). The product-ion spectrum of the m/z 1514 contained ions at m/z 1076 and 1118, arising from loss of $C_{28}H_{57}$COOH and $C_{25}H_{51}$COOH respectively. The losses
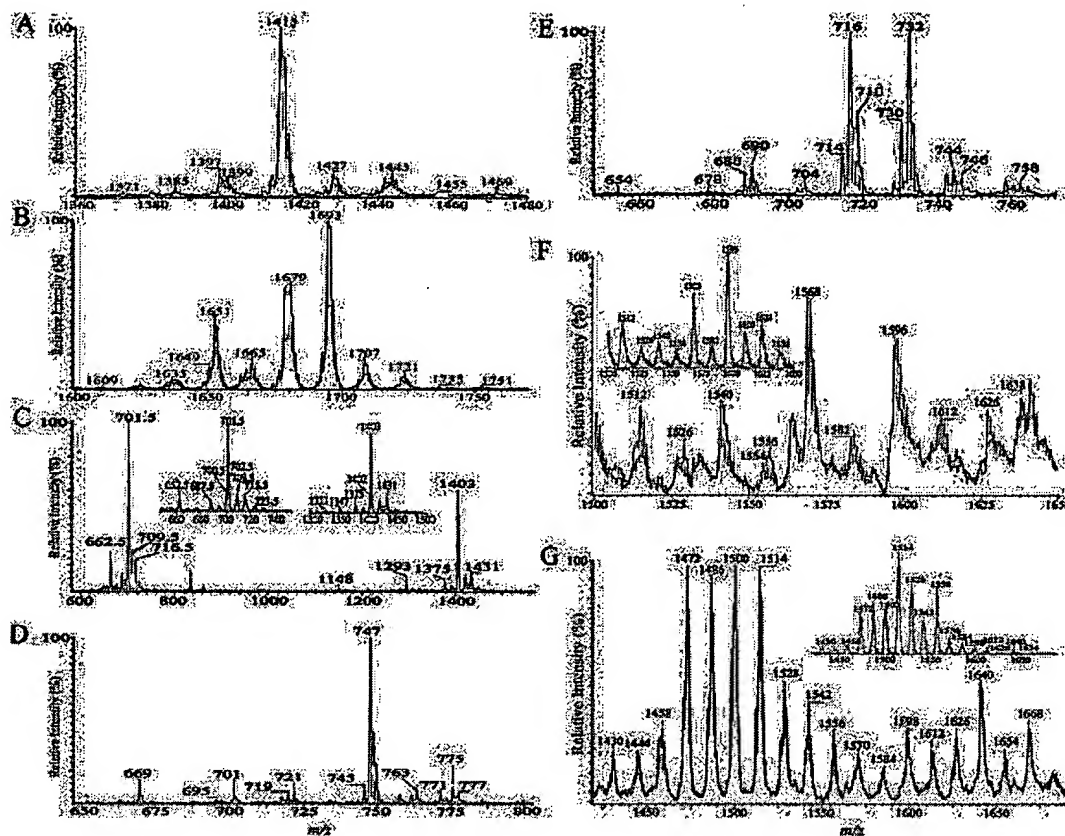
Fig. 4. Mass spectrometry of culture-derived BCG lipids that co-migrate with intracellularly released lipids.
A and B. ESI mass spectra of the [M-H]⁻ ions of 1,2-diacyl-*sn*-glycero-3-phosphatidylinositol dimannoside (PIM₂) species differing in the degree of additional acylation. The major species of PIM₂ₐ (A) at *m/z* 1413 ($C_{16:0}$-$C_{19:0}$/$C_{16:0}$-PIM₂) contains an additional $C1_{6:0}$, whereas the major species of PIM₂ᵦ (B) at *m/z* 1693¹ ($C_{16:0}$, $C_{19:0}$-$C_{19:0}$/$C_{16:0}$-PIM₂) contains additional $C_{16:0}$ and $C_{19:0}$.
C–E. ESI mass spectra of the [M-H]⁻ ions from culture-derived B1 and B2 lipids that contained diphosphatidylglycerol (DPG) and phosphatidylglycerol (PG) from B1 and phosphatidylethanolamine (PE) from B2. The major DPG species was a mixture of ($C_{18:1}$/$C_{16:0}$)($C_{18:1}$/$C_{16:0}$)-DPG that yielded an [M-H]⁻ ion at *m/z* 1403 (C) and an [M-2H]²⁻ ion at *m/z* 701.5. The [M-H]⁻ ion at *m/z* 747 for PG (D) indicated that $C_{18:1}$/$C_{16:0}$-PG was the major species of PG in the mixture. The major ions at *m/z* 716 and 732 (E) arose from the $C_{18:1}$/$C_{16:0}$-PE and ($C_{19:0}$/$C_{16:0}$ + $C_{18:0}$/C17:02)-PE respectively.
F. ESI mass spectrum of the [M + Li]⁺ ions of trehalose monomycolate (TMM) from BCG culture-derived B3 that gave a similar profile to that of an *M. tuberculosis*-derived TMM standard (inset).
G. ESI mass spectrum of the [M + Li]⁺ ions of mycoside B (MycB) from BCG culture-derived B5 that had a similar profile to a BCG-derived MycB standard (inset). The structures of all the molecules were also confirmed by tandem quadrupole mass spectrometry (data not shown).
¹All the *m/z*-values that are shown in the spectra discount mass defect.
²Indicates a minor component.

of the long-chain fatty acid were confirmed by the observation of the ions at *m/z* 916 and 958, arising from the primary loss of the glycoside from the *m/z* 1514 ion to give *m/z* 1354, which undergoes further loss of $C_{28}H_{57}COOH$ or $C_{25}H_{51}COOH$ (see *Supplementary Material*, Fig. S2).

Mass spectrometric identification of B4 could not be performed as all purified B4 samples and TDM standards yielded illegible spectra. It is likely that contaminating detergent used in the culture could not be removed from either the sample or the standard. Therefore, the identity of B4 as TDM was determined by comparing the migration of B4 and *M. tuberculosis* H37Rv-derived TDM standards by 2D TLC (Fig. 5). Lipids from each source migrated and

charred similarly, yielding a characteristic inverted, double rocket-shaped spot that charred with a red–purple hue. A single spot on the co-loaded plate (Fig. 5C) indicated that B4 from BCG and TDM from *M. tuberculosis* belonged to the same class of lipid. The slight difference between the migration of the individual lipids on the singly loaded plates (Fig. 5A and B) is probably caused by heterogeneity in the fatty acyl moieties.

Intracellular release of lipids from bacilli and lipid-coated microspheres

Previously, we demonstrated that fluorophore-labelled
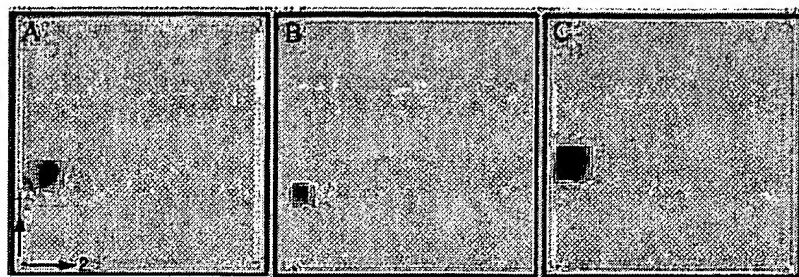
Fig. 5. Culture-derived B4 migrates similarly to trehalose dimycolate by 2D TLC. BCG culture-derived B4 (A), *Mycobacterium tuberculosis*-derived TDM (B) or both lipids (C) were loaded at the origins (indicated by dots) onto TLC plates and developed; first direction chloroform–methanol–water (90:10:1), second direction chloroform–acetic acid–methanol–water (50:60:2.5:3). The lipids were visualized by spraying with sulphuric acid and charring.

surface material was released into the endocytic network of BMMØ from viable intracellular bacilli (Beatty *et al.*, 2000). To determine whether this release depends on the viability of the bacteria, we pulsed BMMØ with Alexa 488-labelled BCG that were alive or heat-killed and observed the cells subsequently by fluorescence microscopy. After 6 h, brightly fluorescent bacilli were located perinuclearly (indicated by the overexposed part of the cells in Fig. 6A and B), and faintly fluorescent material was evident in a vesicular pattern throughout cells that had been pulsed
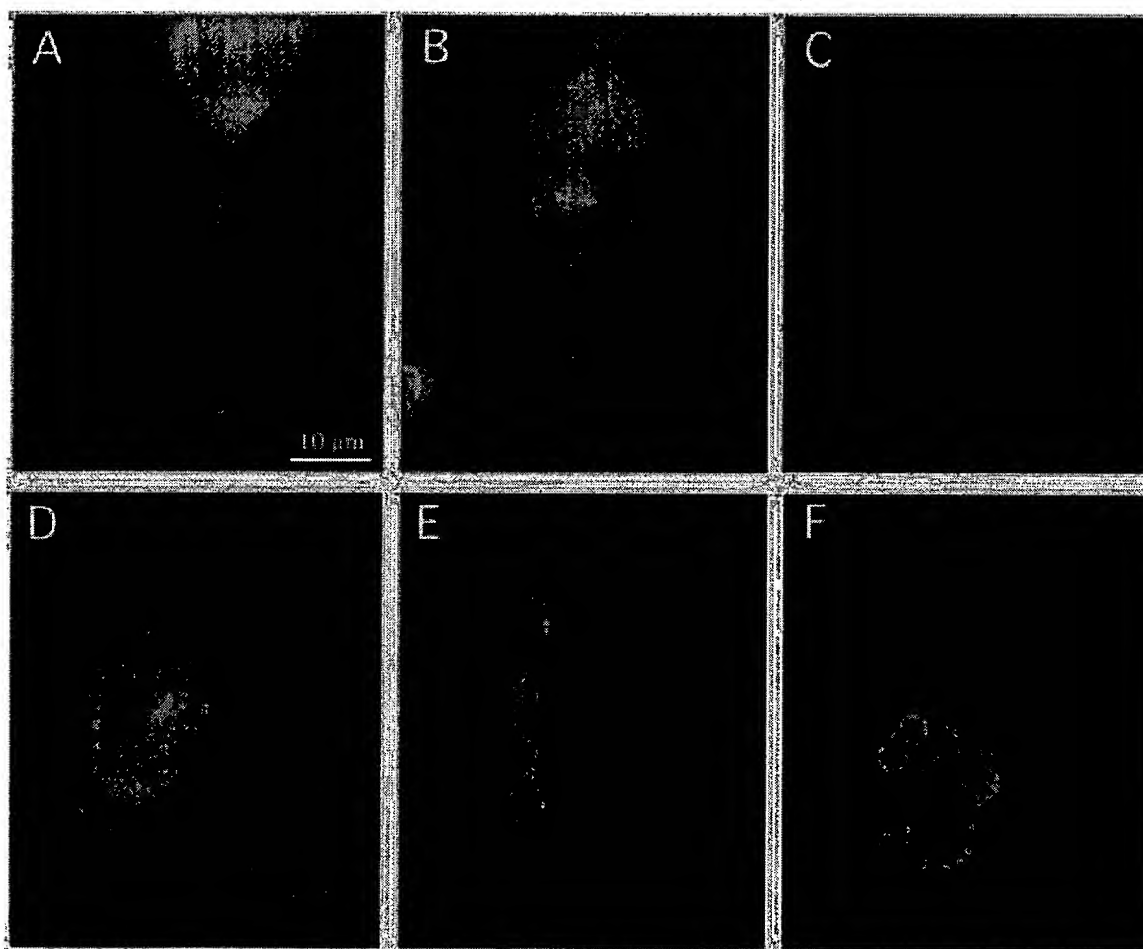
Fig. 6. Intracellular bacilli and lipid-coated microspheres release fluorophore-conjugated glycoconjugates into BMMØ. Macrophages were plated onto glass coverslips and pulsed with Alexa 488-hydrazide-labelled live or heat-killed BCG (A and B). After 6 h, adherent cells were mounted in antifade. Fluorescence microscopy revealed the release of fluorophore-labelled material from both viable (A) and dead (B) intracellular bacilli. Macrophages were also pulsed with polystyrene microspheres (3 µm diameter) that were coated with fluorescein-hydrazide-labelled BCG lipids: no lipid (C), B1 (D), B3 (E) or B4 (F). After 3 h, adherent cells were mounted in antifade. Fluorescent microscopy revealed the release of fluorophore-labelled material from intracellular microspheres (D–F) similar to that seen from the release of glycoconjugates from intracellular bacilli (A and B). Macrophages pulsed with unlabelled microspheres (C) did not contain appreciable amounts of fluorescent vesicles.
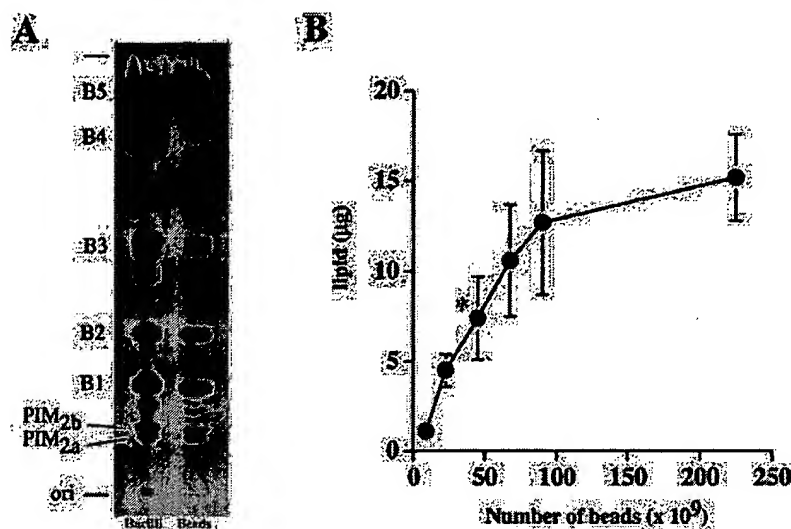
Fig. 7. Microspheres can be coated with total BCG lipids for delivery to macrophages. Polystyrene microspheres (1 μm diameter) were coated with radiolabelled BCG lipids, washed and then extracted in methanol to retrieve all lipids. PIMs and B1–B5 from total BCG lipid extract adhere to the beads (A). The methanol extract of coated beads (Beads) and input lipids (Bacilli) were compared by TLC in chloroform–methanol–water (65:25:4) over 20 cm, and the plate was exposed to autoradiographic film. Beads were coated in an excess of lipid (B). Increasing numbers of beads were coated in a fixed amount of radiolabelled BCG lipid, after which the beads were washed extensively and added directly to scintillant. The amount (in μg) of lipid coated onto the beads was determined by comparison with a standard curve of d.p.m. in known amounts of radiolabelled input lipid. Saturating conditions of bead coating (indicated by the asterisk) were used for lipid bioactivity experiments shown in Fig. 8 to ensure that equal weights of lipids were added to the various macrophage monolayers.

with viable (Fig. 6A) or dead (Fig. 6B) bacilli. Release of Alexa 488-labelled glycoconjugates from viable and heat-killed bacilli was observed as early at 3 h after uptake and was sustained for the duration of all experiments, for as long as 72 h (data not shown).

In order to mimic the natural infection, fractionated BCG-derived lipids were delivered on particles sized similarly (1–3 μm diameter) to mycobacteria. Fluorescent labelling of the lipids allowed visualization of lipid release. Fluorescein hydrazide-labelled BCG lipids were associated with hydrophobic polystyrene microspheres and delivered to adherent BMMØ. The release of these lipids 3 h after delivery is illustrated in Fig. 6, in which we coated the microspheres with the individual fluorescein isothiocyanate (FITC)-labelled lipid species, B1 (Fig. 6D), B3 (Fig. 6E) and B4 (Fig. 6F). Fluorescent vesicular compartments could be distinguished from internalized beads by 3 h. Brightly fluorescent vesicles were observed after delivery of B1- and B2-coated microspheres as early as 90 min. Release of fluorescent material was observed 9 h after delivery (data not shown). Macrophages that were pulsed with unlabelled beads did not contain fluorescent vesicles (Fig. 6C).

Effects of intracellularly released BCG-derived lipids

Having established that BCG-derived lipids could be delivered and released into adherent macrophages, unlabelled lipid fractions were coated onto 1-μm-diameter polystyrene microspheres. Microspheres were coated to saturation in the presence of an excess of lipid, as demonstrated in the graph in Fig. 7. This ensured that a comparable 'dose' was delivered to the cells in all experiments. TLC analysis of lipids recovered from the microspheres after

coating demonstrated that, despite being incubated in a complex mixture of lipids, all pertinent lipids associated with the bead surface and the ratio of lipid species present in the input mixture was reflected in the bound material (Fig. 7A).

Both thioglycollate-elicited peritoneal macrophages (inflammatory-type) and BMMØ (culture-derived) were used to represent macrophages of different maturation status. Monolayers were pulsed with the lipid-coated microspheres, and cytokine levels were assayed in the supernatants after 48 h. Peritoneal macrophages secreted the chemokine MCP-1 in response to lipid-coated beads with or without IFNg priming; however, IFNg priming was required for lipid-mediated induction of tumour necrosis factor (TNF)a and reactive nitrogen intermediates (RNI). BMMØ required IFNg priming for the production of all three mediators. Representative results from macrophages are shown in Fig. 8. Despite being less stimulatory than endotoxin (LPS), total BCG lipids (Total) consistently induced significant levels of TNFa (Fig. 8A) and MCP-1 (Fig. 8B), as well as RNIs (Fig. 8C). BCG lipids did not elicit detectable levels of interleukin (IL)-12p70 or IL-10 (secreted or surface expressed) from primed or unprimed BMMØ (data not shown).

The levels of cytokine production that were induced by purified PIM fractions were comparable with the levels attained with total BCG-derived lipids. And, in all but one case, BCG lipids depleted of PIMs induced significantly lower macrophage responses than total lipids ($^*P < 0.05$, $^{**}P < 0.005$). In IFNγ-primed BMMØ, stimulation with PIM-reconstituted lipids {(P_{2a}+[T]) or (P_{2b}+[T])} restored most of the stimulatory activity of the lipid-coated microspheres and, in IFNγ-primed peritoneal macrophages, reconstitution of PIM-depleted lipids partially restored the TNFα and
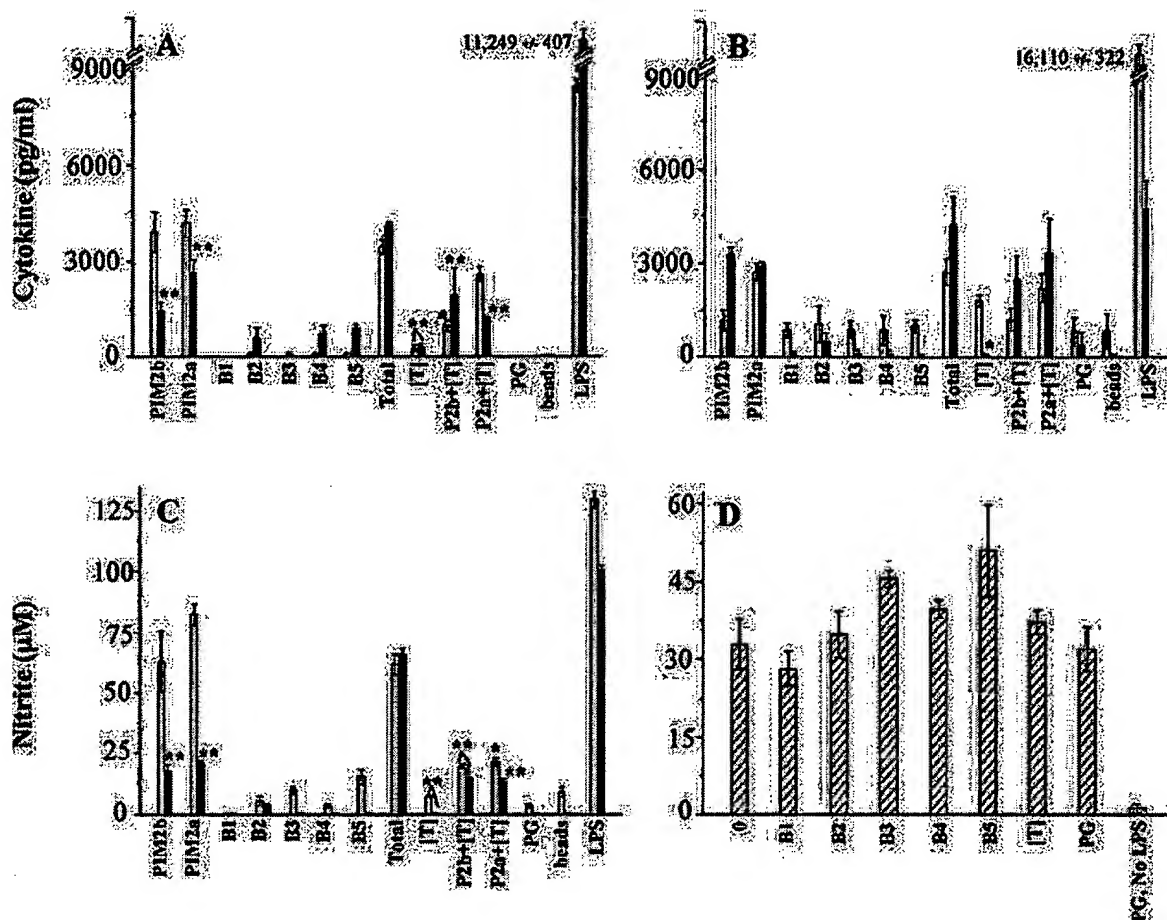
Fig. 8. BCG lipids invoke proinflammatory responses in macrophages. Saturating amounts of BCG-derived lipids (described in the legend to Fig. 7) or LPS (coated in 100 ng ml⁻¹ LPS) were coated onto 1-μm-diameter microspheres and delivered to IFNγ-primed (100 U ml⁻¹) macrophage monolayers except in the case of MCP-1 production by peritoneal macrophages, where unprimed cells were shown. Grey bars, peritoneal macrophages; black bars, BMMØ. After 48 h, culture supernatants were assayed for the release of proinflammatory cytokines TNFα (A), MCP-1 (B) and reactive nitrogen production (C). In the case of MCP-1 production by peritoneal macrophages, unprimed monolayers produced as much MCP-1 as IFNγ-primed monolayers (data not shown). BCG-derived lipid-coated microspheres were delivered to IFNγ-primed peritoneal macrophages and, 2 h later, LPS (5 ng ml⁻¹) was added to detect the suppressive effects of BCG lipids (D). Culture supernatants were assayed for nitrite accumulation as an indicator of macrophage activation. All experiments were performed in triplicate and repeated at least three times, and representative experiments are shown. Data are presented as mean protein or nitrite concentrations with standard deviations. [T], PIM-depleted BCG lipids; $P_{2a}+[T]$, PIM_{2a}-repleted lipids; $P_{2b}+[T]$, PIM_{2b}-repleted lipids; beads, non-coated beads.

RNI production; however, no significant increase in MCP-1 production was detected in unprimed cells. The other purified BCG lipids (B1–B5) were not as stimulatory as the PIM fractions or total lipid. In primed peritoneal macrophages, singly delivered B1–B5 elicited TNFα and MCP-1 levels that rarely exceeded those induced by PIM-depleted lipids or non-coated beads. IFNγ-primed BMMØ consistently responded to B2-, B4- and B5-coated microspheres with low levels of TNFα; however, MCP-1 and RNI levels were similar to negative controls.

It has been reported that mycobacterial lipids inhibit mononuclear cell proliferation and activation (Fournie *et al.*, 1989; Sibley *et al.*, 1990). To investigate whether those BCG lipids that failed to stimulate significant cytok-

ine and RNI production were suppressive rather than stimulatory, peritoneal macrophages were pulsed with lipids before delivery of an activating signal. IFNγ-primed peritoneal macrophages were pulsed with lipid-coated microspheres 2 h before the addition of a low dose of LPS (5 ng ml⁻¹) (Fig. 8D), and RNI production was used as an indicator of macrophage activation. None of the purified BCG lipids interfered with LPS-mediated activation, as evinced by RNI levels comparable with those of LPS-treated macrophages that had been pulsed with non-coated microspheres (0). Indeed, B3- and B5-pretreated macrophages produced slightly more RNI, an effect consistent with the stimulation of RNI observed in Fig. 8C. Treatment of peritoneal macrophages with PG-coated

microspheres in the absence of subsequent LPS activation (PG, no LPS) demonstrated that the peritoneal macrophages were not preactivated.

Discussion

We have demonstrated previously that intracellular *M. bovis* BCG released surface glycoconjugates into the endocytic network of the host macrophage (Beatty *et al.*, 2000). The released material contained unidentified bacterial cell wall lipids that we have now characterized and shown to consist of phospholipids (PG, CL and PE) with short-chain acyl groups and the bacteria-specific lipidoglycans, PIMs, TMM and TDM, and MycB, an *M. bovis*-specific phenolic glycolipid (Brennan, 1988). Comparable experiments conducted with *M. tuberculosis* demonstrated the release of similar classes of glycolipids (data not shown).

We were unable to harvest enough lipids from infected macrophages to identify the released species directly. However, 2D TLC and autoradiography were used to demonstrate that PIMs and B1–B5 lipids from BCG cultures corresponded to the same lipid species that were released intracellularly. The release of PIMs into infected macrophages was reported previously using antibodies that track mycobacterial phospholipid (Xu *et al.*, 1994; Rhoades and Ullrich, 2000). However, in this study, the intracellular release of these bacterial phospholipids was demonstrated via 2D TLC analysis and preferential incorporation of [^{14}C]-propionate into these lipids before infection. It is possible that there are additional mycobacterial lipids released, or that the released lipids are modified structurally by the host. Neither of these possibilities was addressed in this study. It was reported recently that cardiolipin released by intracellular BCG could be modified to its lysoalkyl form by the host macrophage (Fischer *et al.*, 2001). The biological relevance of such a modification was not pursued; however, the authors speculated that lysocardiolipin could exert effects similar to other lysophospholipids, which hinder lymphokine secretion and membrane fusion (Schaible *et al.*, 2000; Fischer *et al.*, 2001).

Once we had established that the bacterial lipid species released into the macrophage corresponded to the peripheral cell wall lipids that could be isolated from BCG in culture, we felt that performing the more demanding physical characterization of this material was justified. Although we acknowledge that there may be small structural differences in either host or pathogen origin between the lipids isolated from infected macrophages and those from bacteria in culture, the released lipids undoubtedly belong to the subclasses identified, namely the phospholipids PG, CL and PE and the lipidoglycans PIM$_2$, TMM,

TDM and MycB. This diversity suggests that the release of lipids is largely independent of lipid structure. Furthermore, intracellular release was not dependent upon the metabolic activity of the bacilli because heat-killed BCG shed fluorescently labelled surface glycoconjugates in a manner indistinguishable from that of viable bacilli. This suggests the absence of a single, specific release mechanism beyond the surfactant-like milieu of the endosomal system, and that the continued synthesis of bacterial cell wall components by viable, intracellular bacteria will be accompanied by a continued release of these lipids.

In previous studies, we have demonstrated that bacterial glycolipids released by intracellular bacterial coalesce in multivesicular lysosomes within their host cell. The multilamellar, membranous bodies that lie within the lumen of these lysosomes act as 'sinks' for the released bacterial components (Beatty *et al.*, 2000; Beatty and Russell, 2001). These vesicular bodies are exocytosed spontaneously by infected macrophages, although their release can be enhanced by treatment of the cells with calcium ionophores (Beatty *et al.*, 2001). The vesicular bodies are relatively uniform in size (100–200 nm), contain host components such as LAMP1 and major histocompatibility complex (MHC) class II molecules and the full array of bacterial lipids (Beatty *et al.*, 2000). Moreover, in tissue culture at least, these vesicles are internalized by neighbouring macrophages and could therefore extend the sphere of influence of the bacterium beyond the confines of its host cell.

Although the granulomagenic properties of isolated mycobacterial lipids have been documented for decades, our appreciation of the role fulfilled by these lipids during the course of the infection is only now starting to emerge. The cellular and molecular events involved in lipid-associated pathology are just recently being elucidated. Surface glycolipids shape the profile of cytokines induced on infection of macrophages by *M. tuberculosis*. Indeed, delipidated mycobacteria elicit markedly less TNFα, IL-1β and MIP-1β, and reconstitution of the bacilli with TDM restores cytokine induction (Indrigo *et al.*, 2002). Trehalose mycolates are known to elicit hypersensitivity responses, and foreign body-type granulomas (Yamagami *et al.*, 2001) prime and induce the production of cytokines (TNFα, IL-1β, IL-6, IL-10, IL-12 and chemokines) (Behling *et al.*, 1993; Perez *et al.*, 2000), induce non-specific resistance to tumours, virus and bacteria and exert direct toxicity (Bekierkunst, 1968; Lepoivre *et al.*, 1982; Numata *et al.*, 1985). PIMs are also known to elicit granulomatous responses (Apostolou *et al.*, 1999; Gilleron *et al.*, 2001). As the host cell for these bacteria, the macrophage is the most likely source of many of the proinflammatory cytokines underlying this response (Roach *et al.*, 1994; Zhang *et al.*, 1995; Perez *et al.*, 2000; Lima *et al.*, 2001). Further-

more, it is possible that the glycolipids, such as PIM and LAM, bind pattern recognition receptors, such as Toll-like receptor-2, triggering cytokine production (Means *et al.*, 1999; Jones *et al.*, 2001).

In order to document the biological activities of the lipids released by the bacteria in the current study, we used 1-μm-diameter polystyrene microspheres to deliver the lipids either individually or in combination to target macrophages. Although we acknowledge that this delivery mechanism does not necessarily reflect the exact presentation of the lipids on viable bacterial surfaces, we feel that presentation of the lipids on particles facilitates intracellular delivery and release that is more physiological than either coating of substrates (Lima *et al.*, 2001) or complexing with albumin (Koster *et al.*, 1987). Moreover, studies with fluorescent lipids delivered on particles generated micrographs that were indistinguishable from those taken from cells infected with bacteria labelled with fluorochrome. Notwithstanding this potential problem, IFNγ-primed macrophages responded to the lipid-coated microspheres with the production of a proinflammatory cytokine and chemokine (TNFα and MCP-1) and a defensive mediator (RNI). In our experiments, exploiting microspheres as a mode of delivery of bacterial lipids, we found that PIM_{2a} or PIM_{2b} was as stimulatory as the total lipid extract. Other glycolipids analysed, including TDM, were not as stimulatory as reported previously (Oswald *et al.*, 1997; 1999; Lima *et al.*, 2001). This disparity may result from the fact that the current study was comparative rather than focusing on a single lipid, or it could reflect the use of microspheres as a delivery vehicle. Our attempts to increase the cellular response by increasing the dose of TDM-coated beads only elicited slightly higher levels of cytokine production (data not shown). It is possible that TDM was not coated onto the microspheres in our study in an orientation that was stimulatory. It has been hypothesized that proper orientation is necessary for the stimulatory effects of this lipidoglycan (Behling *et al.*, 1993). In some other studies, TDM was dried onto wells before the adherence of macrophages (Sakaguchi *et al.*, 2000; Lima *et al.*, 2001), which might elicit a different response from the macrophage. Another group used particles to deliver TDM in a manner similar to ours and reported induction of TNFα and other cytokines (Perez *et al.*, 2000); however, their TDM came from *Mycobacterium smegmatis*, and their macrophage culture medium contained granulocyte–macrophage colony-stimulating factor (GM-CSF), a known modulator of macrophage maturation. Despite the disparity, we feel that our data have validity because our experiments are comparative and document the biological activities of the major species of cell wall lipids that we have shown to be released during intramacrophage infection. Moreover, the delivery of the lipids on beads is likely to be more physiological with respect to dosage and intra-cellular release, even if we are unable to mimic the lipid packing on the bacterial surface.

In a persistent infection, the continued presence of bacteria would provide an enduring source of inflammatory lipids, thereby maintaining the chronic response to this infection. This constant release of peripheral cell wall lipids by intracellular bacteria has to be a costly behaviour, especially for an organism that is thought to be under nutritional stress for at least some stages during infection (Hoener zu Bentrup and Russell, 2001). PIM_2 induces the production of TNFα and MCP-1, which are both known to be strong promoters of a granulomatous response. This behaviour appears to be counterproductive; why would a pathogen that relies on persistence indulge in activities that would sustain an inflammatory response in its host? We feel that the answer to this conundrum lies in the unique structure of the tuberculous granuloma, which retains the reactive lymphocytes at the margin of the granuloma, away from the infected phagocytes at its centre (Gonzalez-Juarrero *et al.*, 2001; Russell, 2001; Russell *et al.*, 2002). Therefore, the granuloma limits the spread of infection and protects the host, but at the cost of inefficient activation of infected macrophages, thus ensuring bacterial persistence. Future studies will focus on the correlation of specific bacterial lipids with the induction of cytokine and chemokine pathways required for the formation and maintenance of the granuloma.

Experimental procedures

Lipid standards

Mycobacterial lipids were kindly provided by several groups: phosphatidylinositol mannoside standards (PIMs) from *M. tuberculosis* H37Rv were supplied by Dr J. Belisle (Colorado State University, CSU, NIH/NIAID tuberculosis research materials contract NOI-AI-75320); trehalose mycolates of *M. tuberculosis* H37Rv were kindly provided by Dr G. Besra (Newcastle upon Tyne, UK). Mycoside B of *M. bovis* BCG was purified as described previously (Chatterjee *et al.*, 1989). Monounsaturated oleoyl-palmitoyl phospholipid standards of bovine origin and TDM from *M. tuberculosis* H37Rv were purchased from Sigma.

Macrophage culture

Female, 6- to 8-week-old BALB/c mice were purchased from Charles River Laboratories and housed under specific pathogen-free conditions. Mice were anaesthetized and sacrificed by cervical dislocation, and the femurs and tibias were harvested. Bone marrow was flushed from the bones with cold cell culture medium {DMEM, 20% L-929 cell-conditioned medium, heat-inactivated sera [10% fetal calf (Summit Biotechnologies), 5% horse (Gibco)], 2 mM L-glutamine, 1 mM sodium pyruvate, 100 U ml⁻¹ penicillin and 100 μg ml⁻¹ streptomycin}. Media components were purchased from Gibco Life Technologies. Bone marrow cells were cultured in bac-

terial grade, 90 mm² Petri dishes (Valmark) at 37°C, 5% CO_2 for 6 days, after which adherent BMMØ were harvested in endotoxin-free PBS or passaged.

Peritoneal macrophages were harvested from mice that had been injected with sterile 3% thioglycollate (Difco Laboratories) intraperitoneally 4 days before. Peritoneal exudate cells were cultured in medium lacking L-929 supernatant. In 96-well tissue culture-treated plates, 2×10^5 cells were primed with 100 U ml⁻¹ recombinant murine IFNγ (R and D Systems) 4–12 h before the delivery of lipid-coated, polystyrene microspheres (1 μm diameter; Polysciences). In some experiments, peritoneal macrophages were subsequently activated with LPS (5 ng ml⁻¹) 3 h after the delivery of lipid-coated microspheres.

For delivery of lipids to cells in culture, BCG-derived lipids or controls (bovine PG or LPS from *Escherichia coli* O26:B6; Sigma) were passively adsorbed onto microspheres in cell culture media. Briefly, lipid (100 μg) was dried aseptically onto the sides of Eppendorf tubes to which 5×10^{10} sterile beads were subsequently added, and coating was facilitated by alternating cycles of vortexing/sonication at 55°C. The microspheres were washed to remove non-associated lipids and suspended in cell culture medium with antibiotics. Approximately 25×10^6 beads were delivered to macrophage monolayers, an amount resulting in the uptake of an average of 15–30 beads by the cells.

For experimental infections, confluent monolayers in 160 mm² tissue culture-treated flasks (Greiner Labortechnik) were infected at a multiplicity of infection (MOI) of 20:1 (bacilli–BMMØ) in the absence of antibiotics. Extracellular bacilli were washed away after a 4 h infection period, and the cells were incubated for as long as another 40 h. To account for the incorporation of radiolabel by macrophages, uninfected BMMØ monolayers were incubated with equivalent c.p.m. of [1,2-¹⁴C]-acetic acid or [1-¹⁴C]-propionic acid and processed identically to infected monolayers.

Mycobacterial culture

Cultures of *M. bovis* BCG (Pasteur) and *M. tuberculosis* H37Rv were maintained in Middlebrook 7H9 medium (Difco Laboratories) with OADC supplement (oleic acid, albumin–Fraction V, dextrose and NaCl) containing 0.05% Tween 80. For radioactive protocols, mid-log phase cultures were resuspended in medium lacking oleic acid and incubated in the presence of [1,2-¹⁴C]-acetic acid (specific activity 100–120 mCi mM⁻¹) or 2 μCi ml⁻¹ [1-¹⁴C]-propionic acid (specific activity 56 mCi mM⁻¹; American Radiolabeled Chemicals) for 16–48 h at 37°C. Radiolabelled bacilli were washed extensively in 0.05% Tween/PBS before extraction of lipids or experimental infections.

Extraction and chromatography of mycobacterial lipids

Mycobacterial cultures were washed in a final wash in PBS, and the pellet was extracted in chloroform–methanol (2:1 v/v) twice at 50°C followed by a Folch wash to remove hydrophilic contaminants. The organic phase was dried and stored at –20°C. Total lipid extracts were fractionated over silica gel-60 (EM Science) in increasing amounts of methanol in chlo-

roform. Waxes and glycosylated mycoserosates eluted in 5% chloroform, glycosylated mycolates between 6% and 20% chloroform, and phospholipids between 7% and 50% chloroform. The fractions were resolved on preparative TLC plates (aluminum-backed, 250-μm-thick silica; EM Science), and individual bands were scraped from the plate and extracted from the silica in chloroform–methanol (2:1). Extracts were purified further by reverse-phase chromatography through C18 Sep-Pak columns (Waters) in increasing amounts of chloroform in methanol. Lipid extracts and radiolabelled extracts were applied to aluminium-backed silica gel-60 TLC plates (EM Science) or channelled high-performance TLC plates (Whatman) and resolved in solvent systems as indicated in the figure legends.

Total lipids were detected by spraying the plates with 50% ethanolic sulphuric acid and charring. Nitrogen-containing and phosphorous-containing lipids were detected with ninhydrin and molybdenum blue spray reagents (Sigma) respectively. Radiolabelled lipids were visualized on autoradiographic film (Amersham) after spraying with En³hance (NEN Life Sciences). Alternatively, sections of charred 2D TLC plates were scraped into scintillation fluid (ICN) and counted on a Wallac 1410 liquid scintillation counter (Pharmacia) for 450 s per sample. Decays per minute (d.p.m.) values were determined using the formula: d.p.m. = [(total c.p.m.–background c.p.m.)/counting efficiency] where counting efficiency = 0.85.

Extraction of intracellularly released mycobacterial lipids

Uninfected BMMØ monolayers or monolayers that had been infected with radiolabelled BCG were washed in ice-cold homogenization buffer (0.5 mM EDTA/EGTA, 20 mM Hepes, 0.05% gelatin, 250 mM sucrose). The macrophages were lysed by repeated passage through 23-gauge needles, and nuclei/debris were removed by several post-nuclear spins at 100 g. The post-nuclear supernatant was layered onto a 12–30% continuous sucrose gradient and centrifuged at 2000 g for 1 h at 4°C. The upper portion of the gradient was layered onto a sucrose step gradient (50%/25%) and centrifuged at 2000 g for 30 min at 4°C. The bacilli-depleted fraction at the top of the 25% step was collected and pelleted at 110 000 g. The pellet was extracted in chloroform–methanol (1:1 v/v) at 4°C for 16 h, followed by (2:1 v/v) at 50°C for 1 h twice with brief sonication and subsequently washed using the Folch method. For 2D TLC analyses, some extracts were fractionated over a silica column.

Western blot analyses of the endocytic compartments in the sucrose gradient fractions were performed as described elsewhere (Ullrich *et al.*, 1999). The bacilli-depleted fraction did not contain hydrolytic, late endocytic or lysosomal compartments, denoted by the absence of the mature form of cathepsin D. Immature forms of cathepsin D were present, indicating that compartments of biosynthetic and/or non-hydrolytic origin were present in the bacilli-depleted fraction.

Mass spectrometry

Electrospray ionization mass spectrometry (ESI/MS) analyses were performed on a Finnigan TSQ-7000 triple-stage

quadrupole mass spectrometer equipped with an electro-spray ion source and controlled by Finnigan ICIS software operated on a DEC alpha station. To analyse lithiated adduct ions ([M+Li]$^+$) in positive ion mode, Na$^+$ was first removed from samples if a high content of Na$^+$ was observed by ESI. To remove Na$^+$, samples were dissolved in chloroform, and an aliquot (100 μl) of LiCl solution (0.6% aqueous) was added. After vortexing, the solution was centrifuged for 5 min (3000 g), and the organic layer was blown to dryness under a stream of nitrogen and redissolved in chloroform–methanol (1:4). The solution yields intense Li$^+$ adduct ion upon MS analysis. Otherwise, to analyse deprotonated anions ([M–H]$^-$) in negative ion mode, samples were prepared in chloroform–methanol (1:4). Samples were infused (1 μl min^{-1}) into the ESI source using nitrogen as the nebulizing gas. The skimmer was at ground potential, and the electrospray needle was set at 4.5 kV. The temperature of the heated capillary was 250°C. The [M+Li]$^+$ ions or the [M–H]$^-$ ions were selected in the first quadrupole (Q1), collided with Ar (2.3 mtorr) in the rf-only second quadrupole (Q2) using a collision energy of 30–70 eV and analysed in the third quadrupole (Q3). Both Q1 and Q3 were tuned to unit mass resolution. Typically, a 1 min period of signal averaging was used for a scan spectrum, and 3–10 min was used for a tandem mass spectrum.

Fluorescent labelling of mycobacterial glycolipids

Surface-exposed terminal oxidizable carbohydrates were labelled with hydrazide or carbazide after periodate oxidation. Briefly, viable or heat-killed (80°C for 30 min) bacilli were washed twice with PBS–0.05% Tween 80 and resuspended in sodium acetate (0.1 M), pH 5.5, containing sodium periodate (1 mM; Sigma). After a 20 min incubation at 4°C with gentle rotation, glycerol (100 nM) was added to quench the reaction. Cultures were washed with PBS–Tween and resuspended in PBS–Tween containing hydrazide- or carbazide-tagged markers (1 mM) (Texas Red, fluorescein, Alexa 4888, biotin; Molecular Probes). After 2 h at room temperature, the cultures were washed with PBS–Tween. Bacterial viability after labelling was consistently 85–90% as determined by counting cfus on Middlebrook 7H10 agar plates (Difco Laboratories). Inoculations were syringe dispersed, and infections were established in BMMØ on 12-mm-diameter glass coverslips at 15:1 MOI. After 3–72 h, the macrophages were washed and fixed in Prolong antifade (Molecular Probes) for fluorescence microscopy.

Alternatively, lipids were extracted from FITC carbazide-labelled BCG. Non-fluorescent polystyrene microspheres (3 μm diameter; Bangs Laboratories) were coated passively in an excess of fluorescent lipid as described above, then washed and delivered to macrophages on glass coverslips. At various time intervals (45 min–9 h), coverslips were rinsed in PBS and mounted directly in Prolong antifade to visualize the intracellular release of fluorescent material.

Cytokine ELISAs and Greiss assay

Macrophage supernatants were harvested 18–55 h after the addition of lipid-coated microspheres. Cytokine enzyme-linked immunosorbent assays (ELISAs) and the Greiss assay were performed on the same supernatants; ELISAs per the manufacturer's recommendations (OptEIA TNFα and MCP-1; BD Pharmingen). To measure nitrite accumulation, equal parts of supernatant and Greiss reagent (1% sulphanilamide, 0.1% naphthylene diamine, 2.5% phosphoric acid) were mixed, and the absorbance was measured at 550 nm. Concentrations of nitrite were determined by comparison with a standard of sodium nitrite. All samples were assayed in triplicate. Data are shown as means ± standard deviation from a representative experiment of two to four independent experiments. Statistical analysis was performed using the two-tailed, paired Student's t-test to determine the significance of changes between treatments.

Supplementary material

The following material is available from http://www.blackwellpublishing.com/products/journals/suppmat/mole/mole3473/mmi3473sm.htm

Fig. S1. Fractionated, culture-derived BCG lipids contained a mixture of species varying in fatty acyl chain length and degree of saturation. The CAD product-ion spectra of the major species of phospholipids of BCG culture-derived lipids are demonstrated. (A) (18:1/16:0)(18:1/16:0)-DPG (Cardiolipin) at m/z 701.6 ([M-2H]$^{2-}$ion), (B) 18:1/16:0-PG at m/z 747, (C) 18:1/16:0-PE at m/z 716, (D) (19:0/16:0+18:0/17:0)-PE at m/z 732, (E) 16:0-19/16:0-PIM$_2$ at m/z 1413, and (F) 16:0,18:1-19:0/16:0-PIM$_2$ at m/z 1677. The fragmentation pathways for identification of the molecular species PIM$_2$ are shown in panel G. The pathways for PG, PE, and DPG have been proposed previously (Hsu & Turk, 2001; Hsu & Turk, 2000).

Fig. S2. CAD product-ion spectra of the major [M+Li]$^+$ ions of (A) trehalose monomycolate (TMM) at m/z 1568, and (B) 29:0/26:0-mycoside B at m/z 1514. The proposed fragmentation pathways for the lithiated species under low-energy CAD are shown in (C) and (D) respectively.

References

Apostolou, I., Takahama, Y., Belmant, C., Kawano, T., Huerre, M., Marchal, G., *et al.* (1999) Murine natural killer T (NKT) cells [correction of natural killer cells] contribute to the granulomatous reaction caused by mycobacterial cell walls. *Proc Natl Acad Sci USA* **96:** 5141–5146.

Beatty, W.L., and Russell, D.G. (2001) Identification of mycobacterial surface proteins released into subcellular com-

partments of infected macrophages. *Infect Immun* **68**: 6997–7002.

Beatty, W.L., Rhoades, E.R., Ullrich, H.J., Chatterjee, D., Heuser, J.E., and Russell, D.G. (2000) Trafficking and release of mycobacterial lipids from infected macrophages. *Traffic* **1**: 235–247.

Beatty, W.L., Ullrich, H.J., and Russell, D.G. (2001) Mycobacterial surface moieties are released from infected macrophages by a constitutive exocytic event. *Eur J Cell Biol* **80**: 31–40.

Behling, C.A., Perez, R.L., Kidd, M.R., Staton, G.W., Jr, and Hunter, R.L. (1993) Induction of pulmonary granulomas, macrophage procoagulant activity, and tumor necrosis factor-alpha by trehalose glycolipids. *Ann Clin Lab Sci* **23**: 256–266.

Bekierkunst, A. (1968) Acute granulomatous response produced in mice by trehalose-6,6-dimycolate. *J Bacteriol* **96**: 958–961.

Besra, G.S., and Chatterjee, D. (eds) (1994) *Lipids and Carbohydrates of Mycobacterium tuberculosis*. Washington, DC: American Society for Microbiology Press.

Brennan, P.J. (1988) *Mycobacterium* and other actinomycetes. In *Microbial Lipids*, Vol. 1. Ratledge, C., and Wilkinson, S.G. (eds). London: Academic Press, pp. 203–298.

Chatterjee, D., Bozic, C.M., Knisley, C., Cho, S.N., and Brennan, P.J. (1989) Phenolic glycolipids of *Mycobacterium bovis:* new structures and synthesis of a corresponding seroreactive neoglycoprotein. *Infect Immun* **57**: 322–330.

Daffe, M., and Etienne, G. (1999) The capsule of *Mycobacterium tuberculosis* and its implications for pathogenicity. *Tuber Lung Dis* **79**: 153–169.

Dahl, K.E., Shiratsuchi, H., Hamilton, B.D., Ellner, J.J., and Toossi, Z. (1996) Selective induction of transforming growth factor beta in human monocytes by lipoarabinomannan of *Mycobacterium tuberculosis*. *Infect Immun* **64**: 399–405.

Dye, C., Scheele, S., Dolin, P., Pathania, V., and Raviglione, M.C. (1999) Consensus statement. Global burden of tuberculosis: estimated incidence, prevalence, and mortality by country. WHO Global Surveillance and Monitoring Project. *J Am Med Assoc* **282**: 677–686.

Fischer, K., Chatterjee, D., Torrelles, J., Brennan, P.J., Kaufmann, S.H., and Schaible, U.E. (2001) Mycobacterial lysocardiolipin is exported from phagosomes upon cleavage of cardiolipin by a macrophage-derived lysosomal phospholipase A2. *J Immunol* **167**: 2187–2192.

Fournie, J.J., Adams, E., Mullins, R.J., and Basten, A. (1989) Inhibition of human lymphoproliferative responses by mycobacterial phenolic glycolipids. *Infect Immun* **57**: 3653–3659.

Gercken, J., Pryjma, J., Ernst, M., and Flad, H.D. (1994) Defective antigen presentation by *Mycobacterium tuberculosis*-infected monocytes. *Infect Immun* **62**: 3472–3478.

Gilleron, M., Ronet, C., Mempel, M., Monsarrat, B., Gachelin, G., and Puzo, G. (2001) Acylation state of the phosphatidylinositol mannosides from *Mycobacterium bovis* bacillus Calmette Guerin and ability to induce granuloma and recruit natural killer T. *J Biol Chem* **276**: 34896–34904.

Gonzalez-Juarrero, M., Turner, O.C., Turner, J., Marietta, P., Brooks, J.V., and Orme, I.M. (2001) Temporal and spatial arrangement of lymphocytes within lung granulomas induced by aerosol infection with *Mycobacterium tuberculosis*. *Infect Immun* **69**: 1722–1728.

Goren, M.B., D'Arcy Hart, P., Young, M.R., and Armstrong, J.A. (1976) Prevention of phagosome-lysosome fusion in cultured macrophages by sulfatides of *Mycobacterium tuberculosis*. *Proc Natl Acad Sci USA* **73**: 2510–2514.

Higuchi, S., Suga, M., Dannenberg, A.M., Jr, Affronti, L.F., Azuma, I., Daniel, T.M., and Petrali, J.P. (1981) Persistence of protein, carbohydrate and was components of tubercle bacilli in dermal BCG lesions. *Am Rev Respir Dis* **123**: 397–401.

Hoener Zu Bentrup, K., and Russell D.G. (2001) Mycobacterial persistence: adaptation to a changing environment. *Trends Microbiol* **9**: 597–605.

Hoppe, H.C., de Wet, B.J., Cywes, C., Daffe, M., and Ehlers, M.R. (1997) Identification of phosphatidylinositol mannoside as a mycobacterial adhesin mediating both direct and opsonic binding to nonphagocytic mammalian cells. *Infect Immun* **65**: 3896–3905.

Hsu, F.-F., and Turk, J. (2000) Charge-remote and charge-driven fragmentation processes in diacyl glycerophosphoethanolamine upon low-energy collisional activation: a mechanistic proposal. *J Am Soc Mass Spectrom* **11**: 892–899.

Hsu, F.-F., and Turk, J. (2001) Studies on phosphatidylglycerol with triple quadrupole tandem mass spectrometry with electrospray ionization: fragmentation process and structural characterization. *J Am Soc Mass Spectrom* **12**: 1036–1043.

Hussain, S., Zwilling, B.S., and Lafuse, W.P. (1999) *Mycobacterium avium* infection of mouse macrophages inhibits IFN-gamma Janus kinase-STAT signaling and gene induction by down-regulation of the IFN-gamma receptor. *J Immunol* **163**: 2041–2048.

Indrigo, J., Hunter, R.L., Jr, and Actor, J.K. (2002) Influence of trehalose 6,6′-dimycolate (TDM) during mycobacterial infection of bone marrow macrophages. *Microbiology* **148**: 1991–1998.

Jones, B.W., Means, T.K., Heldwein, K.A., Keen, M.A., Hill, P.J., Belisle, J.T., and Fenton, M.J. (2001) Different Toll-like receptor agonists induce distinct macrophage responses. *J Leukoc Biol* **69**: 1036–1044.

Koster, F.T., Scollard, D.M., Umland, E.T., Fishbein, D.B., Hanly, W.C., Brennan, P.J., and Nelson, K.E. (1987) Cellular and humoral immune response to a phenolic glycolipid antigen (PhenGL-I) in patients with leprosy. *J Clin Microbiol* **25**: 551–556.

Lepoivre, M., Tenu, J.P., Lemaire, G., and Petit, J.F. (1982) Antitumor activity and hydrogen peroxide release by macrophages elicited by trehalose diesters. *J Immunol* **129**: 860–866.

Lima, V.M., Bonato, V.L., Lima, K.M., Dos Santos, S.A., Dos Santos, R.R., Goncalves, E.D., *et al.* (2001) Role of trehalose dimycolate in recruitment of cells and modulation of production of cytokines and NO in tuberculosis. *Infect Immun* **69**: 5305–5312.

Makonkawkeyoon, S., and Kasinrerk, W. (1989) *In vitro* sup-

pression of interleukin 2 production by *Mycobacterium leprae* antigen. *Clin Exp Immunol* **76**: 398–403.

Means, T.K., Wang, S., Lien, E., Yoshimura, A., Golenbock, D.T., and Fenton, M.J. (1999) Human toll-like receptors mediate cellular activation by *Mycobacterium tuberculosis*. *J Immunol* **163**: 3920–3927.

Neill, M.A., and Klebanoff, S.J. (1988) The effect of phenolic glycolipid-1 from *Mycobacterium leprae* on the antimicrobial activity of human macrophages. *J Exp Med* **167**: 30–42.

Numata, F., Nishimura, K., Ishida, H., Ukei, S., Tone, Y., Ishihara, C., *et al.* (1985) Lethal and adjuvant activities of cord factor (trehalose-6,6′-dimycolate) and synthetic analogs in mice. *Chem Pharm Bull (Tokyo)* **33**: 4544–4555.

Oswald, I.P., Dozois, C.M., Petit, J.F., and Lemaire, G. (1997) Interleukin-12 synthesis is a required step in trehalose dimycolate-induced activation of mouse peritoneal macrophages. *Infect Immun* **65**: 1364–1369.

Oswald, I.P., Dozois, C.M., Fournout, S., Petit, J.F., and Lemaire, G. (1999) Tumor necrosis factor is required for the priming of peritoneal macrophages by trehalose dimycolate. *Eur Cytokine Netw* **10**: 533–540.

Perez, R.L., Roman, J., Roser, S., Little, C., Olsen, M., Indrigo, J., *et al.* (2000) Cytokine message and protein expression during lung granuloma formation and resolution induced by the mycobacterial cord factor trehalose-6,6′-dimycolate. *J Interferon Cytokine Res* **20**: 795–804.

Prasad, H.K., Mishra, R.S., and Nath, I. (1987) Phenolic glycolipid-I of *Mycobacterium leprae* induces general suppression of *in vitro* concanavalin A responses unrelated to leprosy type. *J Exp Med* **165**: 239–244.

Rhoades, E.R., and Ullrich, H.J. (2000) How to establish a lasting relationship with your host: lessons learned from *Mycobacterium* spp. *Immunol Cell Biol* **78**: 301–310.

Rhoades, E.R., Cooper, A.M., and Orme, I.M. (1995) Chemokine response in mice infected with *Mycobacterium tuberculosis*. *Infect Immun* **63**: 3871–3877.

Roach, T.I., Chatterjee, D., and Blackwell, J.M. (1994) Induction of early-response genes KC and JE by mycobacterial lipoarabinomannans: regulation of KC expression in murine macrophages by Lsh/Ity/Bcg (candidate Nramp). *Infect Immun* **62**: 1176–1184.

Russell, D.G. (2001) *Mycobacterium tuberculosis*: here today, here tomorrow. *Nature Rev Mol Cell Biol* **2**: 569–577.

Russell, D.G., Mwandumba, H.C., and Rhoades, E.R. (2002) *Mycobacterium* and the coat of many lipids. *J Cell Biol* **158**: 421–426.

Sakaguchi, I., Ikeda, N., Nakayama, M., Kato, Y., Yano, I., and Kaneda, K. (2000) Trehalose 6,6′-dimycolate (Cord factor) enhances neovascularization through vascular endothelial growth factor production by neutrophils and macrophages. *Infect Immun* **68**: 2043–2052.

Schaible, U.E., Hagens, K., Fischer, K., Collins, H.L., and Kaufmann, S.H. (2000) Intersection of group I CD1 molecules and mycobacteria in different intracellular compartments of dendritic cells. *J Immunol* **164**: 4843–4852.

Sibley, L.D., Adams, L.B., and Krahenbuhl, J.L. (1990) Inhibition of interferon-gamma-mediated activation in mouse macrophages treated with lipoarabinomannan. *Clin Exp Immunol* **80**: 141–148.

Silva, C.L., and Faccioli, L.H. (1988) Tumor necrosis factor (cachectin) mediates induction of cachexia by cord factor from mycobacteria. *Infect Immun* **56**: 3067–3071.

Stokes, R.W., and Speert, D.P. (1995) Lipoarabinomannan inhibits nonopsonic binding of *Mycobacterium tuberculosis* to murine macrophages. *J Immunol* **155**: 1361–1369.

Sturgill-Koszycki, S., Schaible, U.E., and Russell, D.G. (1996) *Mycobacterium*-containing phagosomes are accessible to early endosomes and reflect a transitional state in normal phagosome biogenesis. *EMBO J* **15**: 6960–6968.

Ting, L.M., Kim, A.C., Cattamanchi, A., and Ernst, J.D. (1999) *Mycobacterium tuberculosis* inhibits IFN-gamma transcriptional responses without inhibiting activation of STAT1. *J Immunol* **163**: 3898–3906.

Ullrich, H.J., Beatty, W.L., and Russell, D.G. (1999) Direct delivery of procathepsin D to phagosomes: implications for phagosome biogenesis and parasitism by *Mycobacterium*. *Eur J Cell Biol* **78**: 739–748.

Ullrich, H.J., Beatty, W.L., and Russell, D.G. (2000) Interaction of *Mycobacterium avium*-containing phagosomes with the antigen presentation pathway. *J Immunol* **165**: 6073–6080.

Vachula, M., Holzer, T.J., Kizlaitis, L., and Andersen, B.R. (1990) Effect of *Mycobacterium leprae*'s phenolic glycolipid-I on interferon-gamma augmentation of monocyte oxidative responses. *Int J Lepr Other Mycobact Dis* **58**: 342–346.

VanHeyningen, T.K., Collins, H.L., and Russell, D.G. (1997) IL-6 produced by macrophages infected with *Mycobacterium* species suppresses T cell responses. *J Immunol* **158**: 330–337.

Venisse, A., Fournie, J.J., and Puzo, G. (1995) Mannosylated lipoarabinomannan interacts with phagocytes. *Eur J Biochem* **231**: 440–447.

Wallis, R.S., and Ellner, J.J. (1994) Cytokines and tuberculosis. *J Leukoc Biol* **55**: 676–681.

Xu, S., Cooper, A., Sturgill-Koszycki, S., van Heyningen, T., Chatterjee, D., Orme, I., *et al.* (1994) Intracellular trafficking in *Mycobacterium tuberculosis* and *Mycobacterium avium*-infected macrophages. *J Immunol* **153**: 2568–2578.

Yamagami, H., Matsumoto, T., Fujiwara, N., Arakawa, T., Kaneda, K., Yano, I., and Kobayashi, K. (2001) Trehalose 6,6′-dimycolate (cord factor) of *Mycobacterium tuberculosis* induces foreign-body- and hypersensitivity-type granulomas in mice. *Infect Immun* **69**: 810–815.

Young, D.B. (1981) Detection of mycobacterial lipids in skin biopsies from leprosy patients. *Int J Lepr Other Mycobact Dis* **49**: 198–204.

Zhang, Y., Broser, M., Cohen, H., Bodkin, M., Law, K., Reibman, J., and Rom, W.N. (1995) Enhanced interleukin-8 release and gene expression in macrophages after exposure to *Mycobacterium tuberculosis and* its components. *J Clin Invest* **95**: 586–592.

Improving Protective Immunity Induced by DNA-Based Immunization: Priming with Antigen and GM-CSF-Encoding Plasmid DNA and Boosting with Antigen-Expressing Recombinant Poxvirus[1,2]

Martha Sedegah,[*†] Walter Weiss,[*] John B. Sacci, Jr.,[*†] Yupin Charoenvit,[*] Richard Hedstrom,[*] Kalpana Gowda,[*] Victoria F. Majam,[*] John Tine,[‡] Sanjai Kumar,[*§] Peter Hobart,[¶] and Stephen L. Hoffman[3*]

Intramuscular immunization with a naked DNA plasmid expressing the *Plasmodium yoelii* circumsporozoite protein (p*Py*CSP) protects mice against challenge with *P. yoelii* sporozoites. This protection can be improved either by coadministration of a plasmid expressing murine GM-CSF (pGMCSF) or by boosting with recombinant poxvirus expressing the *Py*CSP. We now report that combining these two strategies, by first mixing the priming dose of p*Py*CSP with pGMCSF and then boosting with recombinant virus, can substantially increase vaccine effectiveness. Not only were immune responses and protection improved but the p*Py*CSP dose could be lowered from 100 μg to 1 μg with little loss of immunogenicity after boost with recombinant poxvirus. Comparing mice primed by the 1-μg doses of p*Py*CSP plus 1 μg pGMCSF with mice primed by 1-μg doses of p*Py*CSP alone, the former were better protected (60% vs 0) and had higher concentrations of Abs (titers of 163, 840 vs 5, 120 by indirect fluorescent Ab test against sporozoites), more ex vivo CTL activity (25% vs 7% specific lysis), and more IFN-γ-secreting cells by enzyme-linked immunospot assay (1460 vs 280 IFN-γ spot-forming cells/10^6 cells). Priming with plasmid vaccine plus pGMCSF and boosting with recombinant poxviruses strongly improves the immunogenicity and protective efficacy of DNA vaccination and allows for significant reduction of dose. *The Journal of Immunology*, 2000, 164: 5905–5912.

I ntramuscular injection of BALB/c mice with plasmid DNA encoding the *Plasmodium yoelii* circumsporozoite protein (*Py*CSP)[4] protects against challenge with *P. yoelii* sporozoites (1), and this protection is dependent on CD8^{+} T cells, IFN-γ, and nitric oxide and is directed against the parasite-infected hepatocyte (2). Protection ranges from 25 to 75% depending on the dosage regimen of vaccine, infectivity, and dose of sporozoites used for challenge (1–3). However, this level of protection is significantly less than the >95% protection in BALB/c mice after immunization with radiation-attenuated sporozoites (4, 5), and we have continued to search for ways to improve the *Py*CSP plasmid

vaccine. We have recently reported that coadministration of *Py*CSP DNA with a DNA plasmid that expresses murine GM-CSF (pGMCSF) (3) improves vaccine efficacy. In a separate paper, we described that boosting of p*Py*CSP DNA-primed animals with recombinant poxvirus expressing the *Py*CSP (rv*Py*CSP) (6) increases protective efficacy. Both these strategies, boosting with recombinant poxvirus (7–13) and the addition of pGMCSF (14–17), have been shown to enhance immunogenicity and protection of several other DNA plasmid vaccines.

In an effort to further improve the protective efficacy of p*Py*CSP DNA vaccine and to reduce the dose of DNA required for immunization, we have combined these two approaches, first priming with p*Py*CSP mixed with pGMCSF and then boosting with rv*Py*CSP. The results demonstrate that this approach leads to greater Ag-specific Ab, IFN-γ, and cytotoxic T cell activity and a significant increase in protective efficacy. Furthermore, priming with a low DNA dose of 1 μg p*Py*CSP and 1 μg pGMCSF gives excellent protection, only slightly less than that achieved after priming with high doses of 100 μg p*Py*CSP and 30 μg pGMCSF.

*Malaria Program, Naval Medical Research Center, Silver Spring, MD 20910; [†]Department of Microbiology, University of Maryland School of Medicine, Baltimore, MD 21201; [‡]Virogenetics Corp., Troy, NY 12180; [§]Department of Molecular Microbiology and Immunology Johns Hopkins University, Baltimore, MD; and [¶]Vical Inc., San Diego, CA 92121

[4] Abbreviations used in this paper: p*Py*CSP, circumsporozoite protein plasmid DNA; *Py*CSP(rv*Py*CSP), recombinant vaccinia virus expressing; pGMCSF, murine GM-CSF plasmid DNA; ELISPOT, enzyme-linked immunospot; IFAT, indirect fluorescent Ab test; ILSDA, inhibition of liver stage development assay.

Materials and Methods

Mice

Female BALB/cByJ (H-2[d]), A/J(H-2[a]), and C57BL/6 (H-2[b])mice, 6–8 wk old, purchased from The Jackson Laboratory, Bar Harbor, ME, were used in all experiments.

Parasites

P. yoelii (17XNL) clone 1.1 parasites were used. Sporozoites for challenges were obtained from infected mosquito glands in M199 medium containing 5% normal mouse serum. All challenges were accomplished by injecting 50–100 sporozoites into the tail vein.

Plasmid immunization

The *P. yoelii* plasmid DNA construct, 1020*Py*CSP, designated here as p*Py*CSP and the murine GM-CSF plasmid, designated here as pGMCSF, used for all the immunizations have been described (3, 6). All DNA for injection was purified using cesium chloride-ethidium bromide density gradient centrifugation as previously described (6). Plasmids stored at −20°C were diluted in PBS (pH 7.2) to the appropriate concentration for injections. Priming with plasmids was done either with p*Py*CSP alone or mixed with pGMCSF. Plasmid DNA lacking the *Py*CSP gene was used as control plasmid and was added to other groups to equalize the total amount of injected plasmid. A 0.3-ml insulin syringe with a 29-gauge 0.5-inch-long needle was used for the i.m. injections in the tibialis anterior muscle of the two hind limbs.

Recombinant vaccinia virus immunization

The construction of *P. yoelii* recombinant vaccinia virus, designated (rv*Py*CSP) used for boosting has already been described (6). Mice were boosted i.p. with rv*Py*CSP at 3, 6, 9, or 12 wk after priming with DNA. The dose of virus was delivered in a total volume of 0.2 ml in PBS, pH 7.2.

Ab response

Indirect fluorescent Ab test (IFAT). The IFAT technique (1) was used to detect anti-*P. yoelii* sporozoite Abs in pooled sera from blood taken just before challenge.

ELISA. Serum Ab levels against recombinant protein or synthetic peptide were determined by standard ELISA protocols as previously described (18), using a full length recombinant *Py*CSP protein produced in yeast (r*Py*CSP) or linear synthetic peptide containing four copies of the major repeat of *Py*CSP protein, $(QGPGAP)_4$, as solid phase Ags. Briefly, 50 μl of 0.1 μg/ml r*Py*CSP or 0.1 μg/ml $(QGPGAP)_4$ in PBS were added into wells of Immunolon II ELISA plates (Dynatech Laboratory, Chantilly, VA) and incubated for 6 h at room temperature. The wells were washed three times with PBS containing 0.05% Tween 20 (washing buffer) and incubated overnight at 4°C with 100 μl 5% nonfat dry milk in PBS (blocking buffer). After three washes with washing buffer, the wells were incubated for 2 h with 50 μl of different dilutions of sera diluted in PBS containing 3% nonfat dry milk (diluting buffer). The wells were washed three times, incubated for 1 h with peroxidase-labeled goat anti-mouse IgG (Kirkegaard and Perry, Gaithersburg, MD) diluted 1:2000 in diluting buffer, then washed again three times. The wells were incubated for 20 min with 100 μl of a solution containing ABTS substrate (2,2′-azinodi(3-ethylbenzthiazoline sulfonate) (Kirkegaard and Perry)) and H_2O_2. Color reaction was measured in a microELISA automated reader (Dynatech, MR5000) at $OD_{410\ nm}$. All reaction steps except blocking were performed at room temperature. Means ± SD of the OD readings of quadruplicate assays were recorded. The results were reported as OD 0.5 units (the reciprocal of the serum dilution at which the mean OD reading was 0.5).

CTL assays

Restimulation CTL assay. ^{51}Cr release assays using bulk cultures was performed as previously described (1). In this method, spleen cells (5 × 10^6) were stimulated in vitro for 7 days with a 16-amino acid peptide, *Py*CSP 280–295 (SYVPSAEQILEFVKQI), which contains the H-2K^d-restricted epitope, *Py*CSP 280–288 (SYVPSAEQI) in 24-well plates at peptide concentration of 2.5 μM. Culture medium used was RPMI supplemented with 10% heat-inactivated FCS, L-glutamine, 50 U/ml each of penicillin and streptomycin, and 2-ME at 5 × 10^{-5} M. P815 (H-2^d) cells (American Type Culture Collection, Manassas, VA) labeled with 0.1 mCi ^{51}Cr (DuPont-New England Nuclear, Boston, MA) and pulsed with the CTL peptide (*Py*CSP 280–288 (SYVPSAEQI)) at 0.025 μM were used as positive target cells. Control targets consisted of unpulsed ^{51}Cr-labeled P815 cells. Varying numbers of effector cells were added to both positive and negative targets at 5000 target cells per well of 96-well U-bottom plates, and 5-h standard chromium release methods were followed. Percent lysis was calculated for both positive and negative targets by the formula: [(experimental cpm − spontaneous cpm)/(maximum cpm − spontaneous cpm)] × 100%. Spontaneous release was defined as background lysis of target cells in presence of medium alone (generally <10% of maximum lysis), and maximum lysis was defined as lysis in the presence of 5% Triton X-100. Net percent specific lysis was calculated as: % lysis of positive targets − % lysis of negative control targets.

Ex vivo CTL assay. Freshly isolated immune spleen cells were used without the 7-day in vitro restimulation period. In this method, varying numbers of freshly isolated spleen cells were added to 5000 peptide-pulsed, ^{51}Cr-labeled P815 target cells with medium containing 2% rat T-cell stim

(Collaborative Biomedical Products, Bedford, MA) in 96-well U-bottom plates. Both positive targets, ^{51}Cr-labeled P815 cells pulsed with the CTL peptide (*Py*CSP 280–288 (SYVPSAEQI)) at 0.025 μM, and control targets, consisting of unpulsed ^{51}Cr-labeled P815, cells were tested. A 12-h chromium release method was followed. Net percent specific lysis was calculated as: % lysis of positive target cells − % lysis of negative control target cells.

ELISPOT assay for detection of Ag-specific IFN-γ-secreting CD8$^+$ T cells

The numbers of *Py*CTL epitope-specific IFN-γ-producing CD8$^+$ T cells were determined using freshly isolated spleen cells from mice that had received their second immunization 14 days earlier. These measurements were made after 24–28 h incubation of spleen cells with irradiated P815 target cells pulsed with a 1 μM concentration of the H-2^d-restricted *Py*CSP peptide SYVPSAEQI as previously described (6, 19). Nitrocellulose plates (96-well, Millipore, Bedford, MA) were coated with 75 μl PBS containing 1 μg/ml purified rat anti-mouse IFN-γ mAb (PharMingen, San Diego, CA). After overnight incubation at room temperature, the wells were washed 6 times with culture medium and incubated for 1 h with 100 μl culture medium containing 10% FCS. Irradiated P815 target cells (100 μl of 2 × 10^5 cells/ml) were placed in the Ab-coated wells. The starting concentration for the freshly isolated unrestimulated effector cells was 1–4 × 10^6/ ml, and 2-fold dilutions in duplicate were assayed. One set of duplicate cells was cocultured with irradiated P815 cells, which had been incubated with 1 μM SYVPSAEQI. The other set of cells was cocultured with irradiated P815 cells that had not been incubated with peptide. After incubation at 37°C and 5% CO_2 for 24–28 h, the plates were washed six times with PBS containing 0.05% Tween 20 (PBS/T). The wells were then incubated with 100 μl of a solution of 1 μg/ml biotinylated anti-mouse IFN-γ-mAb (PharMingen) in PBS/T. After overnight incubation at 4°C, wells were washed with PBS/T and 100 μl peroxidase-labeled streptavidin (Kirkegaard and Perry) at a dilution of 1/1000 in PBS/T, was added to each well. After 1 h incubation at room temperature, wells were washed twice with PBS/T and twice with PBS. The spots were developed by following the instructions provided with the DAB Reagent set (Kirkegaard and Perry Laboratories). After 10–15 min, the number of spots corresponding to IFN-γ-producing cells in wells containing the different spleen cell dilutions was determined using a stereomicroscope. The results were expressed as the number of IFN-γ-secreting cells per 10^6 spleen cells. Net spots per 10^6 spleen cells were calculated as: number of spots with peptide pulsed targets − number of spots with unpulsed targets.

Inhibition of liver stage development assay (ILSDA)

Cell culture. Mouse hepatocytes were obtained by in situ collagenase perfusion of mouse liver as previously described (20). Briefly, livers were perfused in situ sequentially with HBSS and a collagenase solution. The cell suspension generated was then centrifuged over a Percoll gradient to remove dead cells. The hepatocytes were then seeded onto 8-well Lab-Tek chamber slides in complete medium (EMEM with Earle's balanced salts supplemented with 0.2% BSA (fraction 5), 10% FCS, 2% penicillin-streptomycin solution, insulin, 1% L-glutamine solution (100×), and 1% nonessential amino acids solution (100×)) at a concentration of 1 × 10^5 cells/ well. The slides were incubated overnight at 37°C in a 5% CO_2, 95% air environment. The medium was changed the following day and fresh media containing dexamethasone (7 × 10^{-4}) was added to the cultures.

ILSDA: restimulated spleen cells. Hepatocyte cultures, which had been seeded onto 8-well chamber slides 24 h previously, were incubated with 7.5 × 10^4 *P. yoelii* sporozoites for 3 h. The cultures were then washed with medium and incubated for 24 h. Immune spleen cells, which had been restimulated with peptide *Py*CSP 280–295, were tested for their ability to inhibit the development of liver stage parasites. Spleen cells from naive mice were stimulated and tested in the same manner as the immunized mouse spleens and used as a control. Stimulated spleen cells (5 × 10^5) were added to the liver cultures and allowed to remain in culture with the infected hepatocytes for an additional 24 h. Assays were run in triplicate. The chamber slides were then fixed for 10 min in ice-cold absolute methanol and stained with NYLS3 mAb (21) and a FITC-labeled goat anti-mouse IgG. The stained parasites on the slides were then viewed and counted using an epifluorescence microscope. The slide reader was blinded and did not know which group received which vaccine combination. Percent inhibition was then calculated and expressed as a percentage according to the formula: % inhibition = [1 − (mean number of parasites in experimental wells/mean number of parasites in control wells)] × 100.

ILSDA: serum. The biological activity of the Abs produced by the various regimens was assessed in an ILSDA. Hepatocyte cultures, seeded onto

Table I. *Increasing the booster dose of recombinant vaccinia expressing PyCSP increases protection[a]*

Prime (DNA)	Boost (Recombinant Vaccinia Expressing PyCSP) (PFU)	Protected/ Total	% Protection
100 µg PvCSP	1×10^8	10/10	100
100 µg PyCSP	2×10^7	8/10	80
100 µg PyCSP	1×10^7	4/10	40
100 µg empty plasmid	1×10^8	0/10	0
Naive		0/10	0

[a] BALB/c mice received 100 µg PyCSP plasmid DNA i.m. and $\times 10^7$, 2×10^7, or 10^8 PFU recombinant vaccinia expressing PyCSP i.p. 9 wk later. Control mice received 100 µg empty plasmid DNA and were boosted with $\times 10^8$ PFU recombinant vaccinia. Two weeks after the boost, all mice were challenged with 50 *P. yoelii* sporozoites (χ^2 for linear trend, 6.180; p = 0.013).

Table II. *Addition of GM-CSF expressing plasmid increases protection by boost[a]*

Expt.	Prime-Boost	Protected/Total	% Protection
1	DG-V	8/10	80
	D-V	4/10	40
	DG-DG	1/10	10
	D-D	0/10	0
	CG-V	0/10	0
	Naive	0/10	0
2	DG-V	7/8	87.5
	dg-V	7/8	87.5
	D-D	2/8	25
	CG-V	1/8	12.5
	Naive	0/8	0
3	DG-V	8/10	80
	D-V	5/10	50
	DG-DG	2/10	20
	D-D	1/10	10
	CG-V	1/10	10
	dg-V	6/10	60
	dg-dg	3/10	30
	d-V	0/10	0
	d-d	0/10	0
	cg-V	0/10	0
	dg (0.1 µg)-V	3/10	30
	dg (0.01 µg)-V	0/10	0
	dg (0.001 µg)-V	1/10	10

[a] In three experiments, BALB/c mice were immunized with DNA i.m., boosted 3 wk later with DNA i.m. or recombinant vaccinia virus i.p., and challenged with 50 *P. yoelii* sporozoites 2 wk after the booster dose of recombinant vaccinia. D, 100 µg pPyCSP; G, 30 µg pGMCSF; d, 1 µg pPyCSP; g, 1 µg pGMCSF; c, 1 µg control plasmid; V, 2×10^7 PFU rvPyCSP. In the last three groups of Experiment 3, the amounts of plasmid DNA were progressively reduced 10-fold.

8-well chamber slides and allowed to attach overnight, were used. After 24 h of incubation at 37°C in an atmosphere of 5% CO_2 in air, medium was removed, and 7.5×10^4 salivary gland dissected sporozoites suspended in 25 µl of medium, and 25 µl of varying dilutions of sera from immunized mice or medium were added. After 3 h incubation, the cultures were washed to remove sporozoites that did not invade hepatocytes, and fresh medium was added. Assays were run in triplicate. After a further 24 h, the medium was changed, and at 48 h the cultures were fixed and incubated with a mAb directed against liver stage parasites of *P. yoelii* (NYLS3) and a FITC-labeled goat anti-mouse IgG. The slide reader was blinded and did not know which group received which vaccine combination. The stained parasites on the slides were then viewed and counted as already described: % inhibition = [1 − (mean number of parasites in cultures with immune serum/mean number of parasites in cultures with medium control)] × 100.

Protection against challenge

Immunized mice were challenged i.v. with 50 to 100 infective *P. yoelii* sporozoites 2 wk after the second immunization, and protection was defined as absence of patent parasitemia in Giemsa-stained blood smears during the 14-day follow-up period.

Statistical analysis

Simple linear regression was performed using SPSS for Windows version 8.0 (SPSS, Chicago, IL). Comparisons between groups were also performed using the same SPSS for Windows version 8.0. χ^2 was used except when any cell contained fewer than five observations; then Fisher's exact test (two-tailed) was substituted.

Results

Effect of dose of rvPyCSP used for boosting after pPyCSP priming

In our previous publication using DNA priming followed by recombinant vaccinia boosting in the *Py* malaria model, we used 1×10^7 rvPyCSP PFU as the viral dose and were able to achieve 69% protection. We wished to know whether increasing the viral dose would increase the immune response. The results in Table I show that larger doses of virus provided better protection. Nine weeks after DNA priming, boosting with 1×10^8 PFU rvPyCSP resulted in a 100% protection, whereas a boost with 1 or 2×10^7 rvPyCSP PFU resulted in 40 and 80% protection. As in our previous studies (6), boosting with recombinant virus did not protect unless there had been a previous immunization with pPyCSP.

Priming with pPyCSP and pGMCSF and boosting with rvPyCSP induces increased protection against malaria

Because pGMCSF can enhance DNA immune responses to pPyCSP (3), we wished to know whether a mixture of pPyCSP and pGMCSF would improve priming for rvPyCSP. Our strategy was to use a suboptimal immunization schedule giving lower levels of protection to easily detect immune enhancement. We primed with a single dose of DNA followed 3 wk later by a boost with 2×10^7 PFU of rvPyCSP, a less than optimal amount of virus. Table II

shows the results of three separate protection experiments admixing pGMCSF in the prime-boost regimen. In Experiment 1, using high doses of plasmid (100 µg pPyCSP and 30 µg pGMCSF), priming with admixtures of pGMCSF protected better than did priming with pPyCSP alone. In Experiment 2, we compared smaller and larger doses of DNA for priming. When a mix of the two plasmids was used, protection was maintained although plasmid doses were reduced 30- to 100-fold (1 µg pPyCSP plus 1 µg pGMCSF). In Experiment 3, we systematically compared low and high plasmid doses and extended the plasmid titration down to 0.001 µg of each DNA. Experiment 3 confirmed the results of Experiments 1 and 2 and showed that some protection was achieved with as little as 0.1 µg priming doses of pPyCSP and pGMCSF. It thus appears that pGMCSF is a powerful enhancer of pPyCSP at the priming step. Summing the results of the three experiments, we found that priming with high dose PyCSP plus GM-CSF DNA (DG-V) protected 23 of 28 mice (82%), whereas priming with low dose PyCSP plus GM-CSF (dg-V) protected 13 of 18 mice (72%) (comparison of DG-V vs dg-V (p = 0.430, χ^2 test)). This degree of protection with dg-V, 13 of 18 mice (72%) was higher than that recorded for recombinant virus boosting with high dose PyCSP plasmid priming D-V, 9 of 20 mice (45%) (comparison of dg-V vs D-V, p = 0.089, χ^2 test). Furthermore, the degree of protection by dg-V, 13 of 18 mice (72%), was significantly better than that recorded for recombinant virus boosting with low dose PyCSP plasmid priming alone, d-V, 0 of 10 mice (0%) (comparison of dg-V vs d-V, p = 0.00023, Fisher's exact test, two-tailed), or two doses of high dose PyCSP plus GMCSF plasmid DG-DG, 3 of 20 mice (15%) (comparison of dg-V vs DG-DG, p = 0.0004, χ^2). This is an important improvement in

A

% Lysis

B

Net no. of IFN-γ SFCs per 10^6 cells
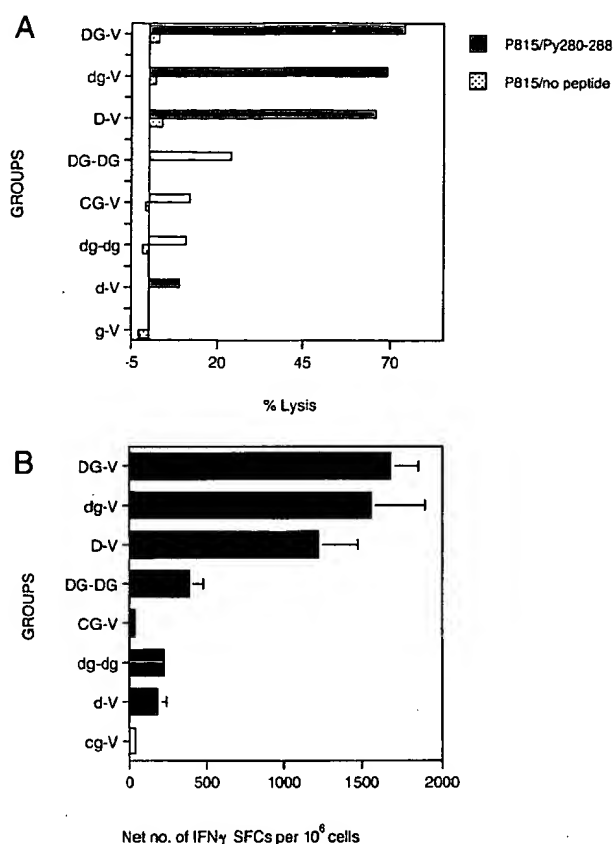
FIGURE 1. *A*, CTL activity. BALB/c mice were immunized and pooled splenocytes harvested from two unchallenged mice 2 wk after last immunizing dose. Spleen cells were restimulated for 7 days in vitro with PyCSP 280–295 (SYVPSAEQILEFVKQI) peptide. Immunization codes are as in Table II. Restimulated cells were used in a CTL assay with target cells pulsed with the K^d-restricted peptide, PyCSP 280–288, or with unpulsed target cells at an E:T ratio of 7:1. *B*, IFN-γ ELISPOT. Spleen cells from the same mice as in *A* were incubated for 24–28 h with irradiated target cells pulsed with the K^d-restricted peptide, PyCSP 280–288, and IFN-γ production was assessed by ELISPOT. SFC, spot-forming cells.

antimalarial immunity. Not only does the addition of pGMCSF to the priming dose increase protection but it also allows a large decrease in the amount of DNA required for immunization.

Table III. *CTL, ILSDA, and protection in mice immunized with the prime-boost regimen[a]*

Prime-Boost Immunization	% Protection	CTL Response (% net specific lysis)[b] (E:T, 10:1)	Inhibition of Liver Stage Development (ILSDA) (%)
DG-V	87.5	87	73
dg-V	87.5	77	50
D-D	25	40	45
CG-V	12.5	37	20
Naive	0	0	

[a] Splenocytes from two unchallenged BALB/c mice in Table II, Experiment 2, were restimulated in vitro with peptide PyCSP 280–295, and cultures were used both for CTL assays and to eliminate *P. yoelii*-infected hepatocytes in vitro. In the ILSDA, the mean number of parasites ± SD in control wells was 53 ± 5. Immunization codes are as in Table II.

[b] Percent lysis was calculated for both positive and negative targets by the formula: [(experimental cpm − spontaneous cpm)/(maximum cpm − spontaneous cpm)] × 100%. Net percent specific lysis was calculated as: % lysis of positive target cells − % lysis of negative control target cells.

In vitro immune responses to PyCSP are increased after immunization with pPyCSP and pGMCSF and boosting with rvPyCSP

Having determined that pGMCSF improved priming, we wished to know whether any in vitro measures of immunity correlated with increased protection. We measured T cell and Ab responses in mice immunized with or without pGMCSF at the priming dose.

T cell responses to the PyCSP 280–288 K^d-restricted epitope.

The results of an experiment comparing T cell responses to the K^d-restricted epitope PyCSP 280–288 (SYVPSAEQI) among mice receiving the various immunizations are shown in Fig. 1. Fig. 1*A* shows CTL activity against targets cultured with peptide PyCSP 280–288 after 7 days of in vitro restimulation of splenocytes with PyCSP 280–295 (SYVPSAEQILEFVKQI) peptide. Fig. 1*B* shows the number of cells producing IFN-γ in the same spleens. In the ELISPOT assay, spleen cells were incubated for 24–28 h with P815 cells pulsed with the PyCSP 280–288 peptide, and IFN-γ spot-forming cells were counted. Spleens from two mice per group were pooled for these assays. CTL activity and IFN-γ-producing cells was highest in the DG-V group with dg-V and D-V next highest in that order.

Table IV. *Inhibition of sporozoite invasion of hepatocytes by sera from mice immunized with different regimens[a]*

Group	Serum Dilution	Mean ± SD Schizonts/Well	% Inhibition	ELISA Against Recombinant PyCSP	ELISA Against QGPGAP Peptide
DG-V	1:25	7 ± 2	82	306,000	14,900
	1:50	16 ± 3	57		
dg-V	1:25	6 ± 4	83	170,700	10,200
	1:50	20 ± 2	45		
D-V	1:25	15 ± 3	59	143,400	6,400
	1:50	30 ± 2	19		
DG-DG	1:25	25 ± 5	32	38,400	3,500
	1:50	32 ± 3	14		
D-D	1:25	23 ± 3	37	9,600	800
	1:50	27 ± 2	27		
Media		37 ± 1			

[a] The ability of Abs to inhibit the development of liver stage parasites was tested using pooled sera from 10 BALB/c mice per group obtained just before challenge. In this experiment, mice were boosted at 6 wk after the first immunizing DNA dose and challenged 14 days later. Immunization codes are as in Table II.

Table V. *Association between immune responses and protection*[a]

Group	% Protected	IFA Against Parasites	ELISA Against Recombinant Protein	ELISA Against QGPGAP Peptide	IFN-γ Secreting CD8 T Cells/Million Splenocytes	Direct CTL (E:T 320:1) (% net specific lysis)	Restimulated CTL (E:T 2.5:1) (% net specific lysis)
DG-V	80	655,360	112,640	7,680	3,440	55	84
dg-V	60	163,840	34,133	700	1,460	25	61
D-V	50	163,840	34,133	1,280	900	24	77
DG-DG	30	163,840	25,600	1,000	580	20	75
dg-dg	30	20,240	6,080	320	400	19	41
0.1 dg-V	30	5,120	ND	ND	840	5	78
D-D	10	20,480	3,529	175	360	11	68
CG-V	10	640	500	0	40	11	27
0.001 dg-V	10	640	ND	ND	20	4	53
d-V	0	5,120	1,867	0	280	7	48
cg-V	0	2,560	933	0	40	5	25
0.01 dg-V	0	1,280	ND	ND	20	1	29
d-d	0	160	150	0	0	7	2
r^2		0.84	0.88	0.77	0.90	0.90	0.71

[a] Pooled sera from 10 BALB/c mice in each group taken before challenge (50 *P. yoelii* sporozoites) and pooled splenocytes from 2 unchallenged mice taken 14 days after last booster dose in each group in Table II, Experiment 3, were used for in vitro assays of humoral and cellular immunity (see text for details). Immunization codes are as in Table II. r^2 values represent the proportion of the variance in "% Protected" explained by the individual outcome variables as calculated by simple linear regression.

ILSDA.

ILSDA is an in vitro assay system that quantifies the reduction of malaria infected hepatocytes after the addition of cells or serum. In mice from Experiment 2 in Table II, splenocytes from two mice per group were pooled and restimulated for 7 days with the *Py*CSP 280–295 peptide. These cultures were then divided; one-half were used for a CTL assay, and one-half were used for ILSDA. Table III compares results for CTL, ILSDA, and protection in these groups. All three measures of immunity showed a consistent ranking of response with the highest levels of in vitro activity seen in the mice primed with high doses of p*Py*CSP plus pGMCSF plasmids.

The ability of Abs produced by the different immunization regimen to inhibit the entry and development of sporozoites in hepatocytes was also investigated. Pooled sera from the best protected groups regimens DG-V and dg-V gave the highest inhibitory effect, up to 82% (Table IV). Our experience with passive transfer of protective mAbs (22) and immunization with synthetic peptides (23) has indicated that only levels of inhibition >90–95% have a high predictive value for protection.

Correlation of Ab and T cell responses with protection

Table V is a summary of our analysis of mice from Table II, Experiment 3. Abs to *Py*CSP were measured three ways: by IFAT against *P. yoelii* sporozoites (column 3), and by ELISA using as capture Ag either a full length recombinant *Py*CSP protein produced in yeast (column 4), or a synthetic 18-mer peptide representing three copies of the 6-aa *Py*CSP repeat motif (column 5). T cell responses to the *Py*CSP 280–288 epitope were measured using three methods: ELISPOT measuring IFN-γ producing cells (column 6), and two CTL assays measuring lysis from splenocytes, either directly from spleens without restimulation (column 7), or after 7 days of culture with *Py*CSP 288–295 peptide (column 8). High dose DNA priming with p*Py*CSP + pGMCSF plasmids followed by boosting with recombinant virus gave the highest protection, as well as the highest levels of T cell and Ab responses by every measure. Other immunization regimens, using less DNA with or without virus boosting, gave less protection and lower Ab and T cell responses to the K^d-restricted epitope, *Py*CSP 280–288 (SYVPSAEQI) in vitro. There is a strong association between protection, and all measured immune responses as measured by simple linear regression. From this analysis, we conclude that overall immunity is increased by p*Py*CSP + pGMCSF DNA priming, but we cannot determine which immune responses are responsible for protection.

Mechanisms of protection after immunizing with plasmids and boosting with rvPyCSP

To understand the immune mechanisms responsible for protection in the DNA prime-viral boost immunizations, we tried to abrogate protection by injecting immunized mice with mAbs to IFN-γ and CD4 or CD8. We first tested mice immunized without the addition of pGMCSF (Table VI). Mice were primed with 100 µg p*Py*CSP and boosted with 2 × 10^7 PFU rv*Py*CSP 9 wk later. Administration of an anti-CD8 mAb, which removed >99% of all $CD8^+$ T cells, eliminated protection ($p = 0.0001$, Fisher's exact test, two-tailed). (Table VI, Experiment A). A single i.v. injection of 1 mg anti-IFN-γ mAb at the time of challenge reduced protection from 80% to 30% (Table VI, Experiment B) ($p = 0.069$, Fisher's exact test, two-tailed). These data indicated that the mechanism of protection with this prime-boost regimen was similar to that induced by p*Py*CSP immunization alone and probably involved $CD8^+$ T cells that recognize infected hepatocytes and produced IFN-γ. Our previous data (2, 24, 25) indicate that the IFN-γ either induces the infected hepatocyte to produce nitric oxide, which eliminates the infected hepatocyte, or induces mononuclear cells to produce IL-12, which leads to production of IFN-γ by other T cells or NK cells (26).

We then attempted to repeat these in vivo depletion experiments in mice immunized with with p*Py*CSP + pGMCSF and rv*Py*CSP (Table VI, Experiment C). Results revealed that after treatment with the anti-CD4 mAb, $CD4^+$ T cells were depleted at least 98.3, 97.9, and 98.8% in the D-V, DG-V, and dg-V groups, respectively. $CD8^+$ T cells were depleted at least 99.3, 99.5, and 99.4% in the D-V, DG-V, and dg-V groups, respectively, after treatment with the anti-CD8 mAb. In the low dose plasmid group (dg-V), treatment with anti-CD8 mAb completely eliminated protection ($p = 0.0009$, Fisher's exact test, two-tailed). However, in the high dose plasmid group (DG-V), this same Ab reduced immunity, but 45% of the mice remained protected ($p = 0.414$, Fisher's exact test, two-tailed), even though >99% of $CD8^+$ T cells were removed by the Ab treatment. Treatment with anti-IFN-γ mAb only reduced protection to 83% in the DG-V group ($p = 0.640$, Fisher's exact test, two-tailed), and to 58% in the dg-V group ($p = 0.155$ Fisher's

Table VI. *Effect of in vivo administration of Abs to $CD8^+$ T cells, $CD4^+$ T cells, and IFN-γ on protection[a]*

Expt.	Prime-Boost	Ab	Protected/Total	% Protection
A	D-V	Control	9/10	90
	D-V	Anti-CD8	0/10	0
	Naive	None	0/10	0
B	D-V	Control	8/10	80
	D-V	Anti-IFNγ	3/10	30
	Naive	None	0/10	0
C	DG-V	Anti-CD4	12/12	100
	DG-V	Anti-CD8	5/12	45
	DG-V	Anti-IFNγ	10/12	83
	DG-V	Control	8/10	80
	dg-V	Anti-CD4	10/12	83
	dg-V	Anti-CD8	0/11	0
	dg-V	Anti-IFNγ	7/12	58
	dg-V	Control	11/12	92
	Naive	None	0/10	0

[a] In three experiments, BALB/c mice were first immunized and then treated with mAbs before challenge with 50 *P. yoelii* sporozoites in an attempt to abrogate protection. Immunization codes are as in Table II. The reduction in protection by treatment with anti-CD8 mAb in the D-V group ($p = 0.0001$) in Experiment A and the dg-V group ($p = 0.0009$) in Experiment C was complete. The reduction in protection in the D-V group ($p = 0.069$, Fisher's exact test, two-tailed) by treatment with the anti-IFN-γ mAb was incomplete, but approached the level of statistical significance.

exact test, two-tailed), as compared with 30% in the previous D-V experiment. These data do not allow an unequivocal assignment of immune effector function in protection with the dg-V and DG-V prime-boost regimens. It appears that immune effector function with low doses of pGMCSF DNA priming is dependent on $CD8^+$ T cells. However, with large plasmid doses of pGMCSF DNA, the fact that we cannot completely abrogate protection means either that the mAb treatment cannot neutralize higher levels of $CD8^+$ T cells and IFN-γ, or that additional immune effector functions have come into play.

Genetic control of protection from prime/boost immunization

A/J and C57BL/6 mice were immunized with DNA i.m., boosted 12 wk later with DNA i.m. or recombinant vaccinia virus i.p. Mice were bled for serum at week 14 and then challenged with *P. yoelii* sporozoites (100 sporozoites for A/J mice and 50 sporozoites for C57BL/6 mice) to measure protection. Table VII shows protection data comparing the prime-boost immunization to other regimens of immunization. In the past, A/J mice have been difficult to protect with vaccination using p*Py*CSP alone (2). It appears the DG-V regimen is slightly more effective than other immunization regimens in A/J mice (Table VII). Only the DG-V regimen was significantly better than its control, CG-V ($p = 0.0171$, Fisher's exact

test, two-tailed) The DG-V regimen elicited the highest levels of Abs against sporozoites (Table VII), and sera from mice immunized with this regimen had the highest inhibitory activity against sporozoite invasion and development within hepatocytes in vitro (Table VIII). This supported the interpretation that Abs might play a major role in the protection seen. However, in efforts to determine a protective role for $CD8^+$ T cells in A/J mice, the nine mice that had been protected by the DG-V regimen in Table VII were treated with a control Ab or an anti-CD8 mAb. In these mice, Ab injections for depletions were started at 68 days after boost with recombinant virus and these depleted mice were rechallenged at 74 days after boost, and 57 days subsequent to first challenge. Three of the five mice (60%) treated with the control Ab were still protected, but none of the four mice treated with the anti-CD8 mAb were protected. The numbers of animals are too few to draw firm conclusions. However, the data support the interpretation that $CD8^+$ T cells were required for the protection in the four previously protected A/J mice despite the high levels of inhibitory Abs. C57BL/6 mice were not significantly protected by any prime-boost regimen and may require immunization with additional Ags to achieve T cell-mediated protection or further optimization of the regimen.

Table VII. *Protection of A/J and C57BL/6 mice by* Py*CSP immunization[a]*

Prime-Boost	A/J Protected/Challenged	IFAT Titer	C57BL/6 Protected/ Challenged	IFA Titer
DG-V	9/20 (45)	163,840	3/16 (19)	81,920
D-V	6/20 (30)	40,960	3/16 (19)	20,480
DG-DG	6/20 (30)	20,480	1/16 (6)	5,120
D-D	1/20 (5)	5,120	3/16 (19)	2,560
CG-V	2/20 (10)	640	0/16 (0)	80
Naive	0/20 (0)	<10	1/15 (7)	<10

[a] A/J and C57BL/6 mice were immunized with DNA i.m. and boosted 12 wk later with DNA i.m. or recombinant vaccinia virus i.p. D, 100 μg p*Py*CSP, G, 30 μg pGMCSF, C, 100 μg control plasmid, V, 2 × 10^7 PFU rv*Py*CSP. Mice were bled for serum at wk 14 and then challenged with *P. yoelii* sporozoites (100 sporozoites for A/J mice and 50 sporozoites for C57BL/6 mice) to measure protection. Ab levels against sporozoites were measured by the IFAT described in *Materials and Methods*. Only the protection by the DG-V (9 of 20) regimen was statistically significant ($p = 0.0171$, Fisher's exact test, two-tailed) compared with its control CG-V (2 of 20).

Table VIII. *Inhibition of sporozoite invasion by sera from A/J mice immunized with different regimens*

Prime-Boost	Mean ± SD Schizonts/Well	% Inhibition	ELISA Against Recombinant Protein	ELISA Against QGPGAP Peptide
DG-V	2 ± 1	93	184,300	10,700
D-V	5 ± 2	86	102,400	10,700
DG-DG	13 ± 5	63	21,300	1,600
D-D	25 ± 5	32	6,400	500
CG-V	33 ± 2	10	1,000	<100
Media	37 ± 1			

a A/J mice were immunized at 0 and 12 wk and bled for serum at wk 14, and all sera were tested at a final dilution of 1:25. Immunization regimens were as in Table VII.

Discussion

Since our first descriptions of a protective DNA malaria vaccine in mice (1) and the safety and immunogenicity of a DNA malaria vaccine in humans (27), our goals have been to improve DNA vaccines by: 1) increasing protective efficacy, 2) increasing Ab response, and 3) decreasing on a dose. Although the protective efficacy of our plasmid DNA malaria vaccines has been consistent, they do not completely protect mice challenged with highly infective *P. yoelii* sporozoites. In most of our experiments, immunization with two or three doses of 100 μg *Py*CSP plasmid DNA alone has protected only 25–50% of BALB/c mice against challenge with 50 or 100 *P. yoelii* sporozoites (3, 6). CD8$^+$ T cells are the most important effector cells in this model system, but protection is also dependent on IFN-γ induction of nitric oxide that apparently mediates killing of developing liver stage parasites (2, 26). One method for increasing the protection from a DNA vaccine is to include more than one malarial Ag. With mixtures of plasmids, immune responses are made independently to each plasmid Ag, and protection is apparently additive (2). However, even with multiple Ags, we have not consistently protected all animals and all mouse strains against malaria. Therefore, a major goal has been to improve protection from our *P. yoelii* DNA vaccines.

Our second goal has been to increase the humoral response to DNA vaccines. Results of the first human trial of a DNA malaria vaccine showed no Ab responses in any volunteer despite the induction of CTL responses in the majority of vaccinees (27). In mice, Ab responses after i.m. plasmid immunization vary widely, from moderately strong to undetectable, depending on the encoded Ag (2). Abs to malaria Ags are an important source of protection, particularly against the blood stages of malaria, and we have tried to devise ways to boost the Ab response to DNA vaccines.

Our third goal has been to decrease the amount of plasmid needed for immunization. In our first clinical trial (27), volunteers received three doses of 20, 100, 500, or 2500 μg of *Plasmodium falciparum* CSP plasmid DNA. CTL assays were positive more often in the 2500- and 500-μg groups than in the 20- and 100-μg groups. Obviously, reducing the dose would reduce the cost of production of a vaccine that is intended in large part for population groups with few financial resources. Epidermal administration of DNA on gold beads by a gene gun has been shown to require less DNA per dose, often <4 μg (28) but requires a complex technology that may be impractical for a vaccine which will be used in the developing world. Furthermore, in a recent study of a simian HIV DNA vaccine, rhesus monkeys primed with DNA administered by the intradermal route and boosted with recombinant fowlpox were protected. However, monkeys primed with the same DNA delivered on gold particles by gene gun were not protected (29).

Recent publications from our laboratory have identified two methods for increasing both CD8 T$^+$ cell responses and Abs to p*Py*CSP. When plasmid encoding murine GMCSF is mixed with

*Py*CSP plasmid, protection is doubled and Abs to *Py*CSP increase 8-fold, and CD4$^+$ and CD8$^+$ T cell responses increase 4-fold (3). It appears that the GMCSF causes an influx of APC into the injected muscle, leading to stronger Ag-specific immune responses.[5] The second novel approach we have described is combining plasmid vaccination as a first dose followed by a vaccination with a recombinant poxvirus expressing the same Ag as the second dose (6). This "DNA prime-viral boost" technique increases protective efficacy, Abs, and T cell responses. We do not understand why the combination of DNA followed by poxvirus is superior to two doses of DNA or two doses of virus, but recombinant poxviruses also boost immune responses primed by recombinant adenoviruses (30). Similar data with the DNA prime-viral boost have been generated by other laboratories studying malaria in mice (7, 8) and simian HIV in rhesus monkeys (29).

In this paper, we describe the combination of these two approaches: priming with p*Py*CSP + pGMCSF plasmids followed by boosting with recombinant poxvirus. The results are remarkable. Using this combined method, we have been able simultaneously to achieve all three of our goals for plasmid DNA vaccination: protective efficacy and T cell responses were increased; Abs were enhanced; and we were able to reduce the dose of DNA required for priming by 1–2 logs. If this same approach can be made to work in humans, it will be an important advance toward an effective malaria vaccine.

Despite these impressive results, there are important shortcomings of the prime-boost vaccine, in terms of both our understanding and application. As mentioned above, we are still unsure how GMCSF enhances priming and why poxvirus boosting is so effective. Also, we have not completely defined the immune effector mechanisms that are responsible for immunity in the prime-boost model of *Py*CSP in BALB/c mice. In all our previous experience, in vivo treatments of immunized mice with mAbs to CD8$^+$ T cells, or to IFN-γ always abrogated immunity. This has allowed us to conclude unambiguously that these two aspects of the immune response were most significant in killing malaria parasites. However, these in vivo depletions have not completely neutralized immunity in the prime-boost experiments. This may indicate that additional arms of the protective immune response such as specific Abs or CD4$^+$ T cells are playing an important role in protecting these mice. Alternatively, our inability to abrogate the protective immune responses with anti-CD8 and anti-IFN-γ mAbs may simply reflect the very high levels of immune responses, which cannot be completely neutralized by the in vivo Ab treatments we used. Preliminary analysis of our data by multiple regression techniques also seems to indicate that the high levels of specific Ab in our mice may be contributing to the high levels of protection.

Although BALB/c mice have superior protection from the prime-boost PyCSP vaccine, protection in other strains of mice is much less complete. A/J mice have a modest level of protection (45%) from this same vaccine, whereas C57BL/6 mice show little if any protection. Although both the A/J and C57BL/6 of these strains show important increases in specific serum Abs from the prime-boost vaccine, the levels in the C57BL/6 mice are not as high. In the small number of animals tested, depletion of CD8$^+$ T cells eliminated protection in the AJ mice previously protected, whereas 60% of mice receiving control Abs were still protected (>10 wk since the last immunization). Seeing protection in a previously unprotected strain (A/J) just by improving the immunization regimen suggests that further optimization of immunization regimens may increase this protection further. We are optimistic that the inclusion of several parasite Ags in the prime-boost format will allow an expanded vaccine to protect a wider range of mouse strains. An analogous multigene vaccine would hopefully be similarly effective in a wide range of human HLA types.

Acknowledgments

References

1. Sedegah, M., R. Hedstrom, P. Hobart, and S. L. Hoffman. 1994. Protection against malaria by immunization with plasmid DNA encoding circumsporozoite protein. Proc. Natl. Acad. Sci. USA 91:9866.

2. Doolan, D. L., M. Sedegah, R. C. Hedstrom, P. Hobart, Y. Charoenvit, and S. L. Hoffman. 1996. Circumventing genetic restriction of protection against malaria with multigene DNA immunization: CD8+ T cell-, interferon-, and nitric oxide-dependent immunity. J. Exp. Med. 183:1739.

3. Weiss, W. R., K. J. Ishii, R. C. Hedstrom, M. Sedegah, K. Barnhart, D. Klinman and S. L. Hoffman. 1998. A plasmid encoding murine granulocyte-macrophage colony-stimulating factor increases protection conferred by a malaria DNA vaccine. J. Immunol. 161: 2325.

4. Hoffman, S. L., E. D. Franke, M. R. Hollingdale, and P. Druilhe. 1996. In Malaria Vaccine Development: A Multi-Immune Response Approach. S. L. Hoffman, ed. Chap 3. American Society for Microbiology, Washington, DC.

5. Miller, L., and S. L. Hoffman. 1998. Research toward vaccines against malaria. Nat. Med. (Suppl.) 4:520.

6. Sedegah, M., T. R. Jones, M. Kaur, R. Hedstrom, P. Hobart, J. A. Tine, and S. L. Hoffman. 1998. Boosting with recombinant vaccinia increases immunogenicity and protective efficacy of malaria DNA vaccine. Proc. Natl. Acad. Sci. USA 95:7648.

7. Li, S., M. Rodrigues, D. Rodriguez, J. R. Rodriguez, M. Esteban, P. Palese, R. S. Nussenzweig, and F. Zavala. 1993. Priming with recombinant influenza virus followed by administration of recombinant vaccinia virus induces CD8$^+$ T-cell-mediated protective immunity against malaria. Proc. Natl. Acad. Sci. USA 90:5214.

8. Schneider, J., S. C. Gilbert, T. J. Blanchard, T. Hanke, K. J. Robson, C. M. Hannan, M. Becker, R. Sinden, G. L. Smith, and A. V. S. Hill. 1998. Enhanced immunogenicity for CD8+ T cell induction and complete protective efficacy of malaria DNA vaccination by boosting with modified vaccinia virus Ankara. Nat. Med. 4:397.

9. Plebanski, M., S. C. Gilbert, J. Schneider, C. M. Hannan, G. Layton, T. J. Blanchard, M. Becker, G. L. Smith, G. Butcher, R. Sinden, et al. 1998. Protection from Plasmodium berghei infection by priming and boosting T cells to a single class 1-restricted epitope with recombinant carriers suitable for human use. Eur. J. Immunol. 28:4345.

10. Leong, K. H., A. J. Ramsey, I. A. Ramshaw, M. J. Morin, H. L. Robinson, and D. B. Boyle. 1995. Generation of enhanced immune responses by consecutive immunization with DNA and recombinant fowl pox vectors. In Vaccines 95. R. M. Chanock, F. Brown, H. S. Ginsberg, and E. Norrby, eds. Cold Spring Harbor Laboratory, pp. 327–331.

11. Rothel, J. S., D. B. Boyle, G. W. Both, A. D. Pye, J. G. Waterkeyn, P. R. Wood, and M. W. Lightowlers. 1997. Sequential nucleic acid and recombinant adeno-

12. Richmond, J. F., F. Mustafa, S. Lu, J. C. Santoro, J. Weng, M. O'Connell, E. M. Fenyo, J. L. Hurwitz, D. C. Montefiori, and H. L. Robinson. 1997. Screening of HIV-1 Env glycoproteins for the ability to raise neutralizing antibody using DNA immunization and recombinant vaccinia virus boosting. Virology 230:265.

13. Irvine, K. R., R. S. Chamberlain, E. P. Shulman, D. R. Surman, S. A. Rosenberg, and N. P. Restifo. 1997. Enhancing efficacy of recombinant anticancer vaccines with prime/boost regimens that use two different vectors. J. Natl. Cancer Inst. 89:1595.

14. Lieschke, G. J., and A. W. Burgess. 1992. Granulocyte colony-stimulating factor and granulocyte-macrophage colony-stimulating factor (2). N. Engl. J. Med. 327:99.

15. Kuzrock, R., M. Talpaz, and J. U. Gutterman. 1992. Very low doses of GM-CSF administered alone or with erythropoietin in aplastic anemia. Am. J. Med. 933:41.

16. Estey, E. H., R. Kurzrock, M. Talpaz, K. B. McCredie, S. O'Brien, H. M. Kanrarjian, M. J. J. Keating, A. B. Deisseroth, and J. U. Gutterman. 1991. Effects of low doses of recombinant human granulocyte-macrophage colony-stimulating factor (GM-CSF) in patients with myelodysplastic syndromes. Br. J. Haematol. 77:291.

17. Simons, J. W., E. M. Jaffee, C. E. Weber, H. I. Levitsky, W. G. Nelson, M. A. Carducci, A. J. Lazenby, L. K. Cohen, C. C. Finn, S. M. Clift, et al. Bioactivity of autologous irradiated renal cell carcinoma vaccines generated by ex vivo granulocyte-macrophage colony-stimulating factor gene transfer. Cancer Res. 57:15337.

18. Charoenvit, Y., S. Mellouk, C. Cole, R. Bechara, M. Leef, M. Sedegah L. F. Yuan, F. A. Robey, R. L. Beaudoin, and S. L. Hoffman. 1991. Monoclonal but not polyclonal antibodies protect against Plasmodium yoelii sporozoites. J. Immunol. 146:1020.

19. Rodriguez, M., S. Li, K. Murata, D. Rodriguez, J. R. Rodrigues, I. Bacik, J. R. Bennink, J. W. Yewdell, A. Garcia-Sastre, R. Nussenzweig, M. Esteban, P. Palese, and F. Zavala. 1994. Quantification of antigen specific CD8$^+$ T cells using an ELISPOT assay. J. Immunol. 153:4636.

20. Hoffman, S. L., D. Isenbarger, G. Long, M. Sedegah, A. Szarfman, L. Waters, M. R. Hollingdale, P. H. Van der Meide, D. S. Finbloom, and W. R. Ballou. 1989. Sporozoite vaccine induces genetically restricted T-cell elimination of malaria from hepatocytes. Science 244:1078.

21. Charoenvit, Y., S. Mellouk, M. Sedegah, T. Toyoshima, M. F. Leef, P. de la Vega, R. L. Beaudoin, M. Aikawa, V. Fallarme, and S. L. Hoffman. 1995. 17 kDa Plasmodium yoelii hepatic and erythrocytic stage proteins the target of protective antibodies. Exp. Parasitol. 80:419.

22. Charoenvit, Y., S. Mellouk, C. Cole, R. Bechara, M. F. Leef, M. Sedegah, L. F. Yuan, F. A. Robey, R. L. Beaudoin, and S. L. Hoffman. 1991. Monoclonal, but not polyclonal, antibodies, protect against Plasmodium yoelii sporozoites. J. Immunol. 146:1020.

23. Wang, R., Y. Charoenvit, G. Corradin, R. Porrozzi, R. L. Hunter, G. Glenn, C. R. Alving, P. Church, and S. L. Hoffman. 1995. Induction of protective polyclonal antibodies by immunization with a Plasmodium yoelii circumsporozoite protein multiple antigen peptide vaccine. J. Immunol. 154:2784.

24. Mellouk, S., S. J. Green, C. A. Nacy, and S. L. Hoffman. 1991. IFN-γ inhibits development of Plasmodium berghei exoerythrocytic stages in hepatocytes by an L-arginine-dependent effector mechanism. J. Immunol. 146:3971.

25. Mellouk, S. 0., S. L. Hoffman, Z. Z. Liu, P. de la Vega, T. R. Billiar, and A. K. Nussler. 1994. Nitric oxide-mediated antiplasmodial activity in human and murine hepatocytes induced by γ interferon and the parasite itself: enhancement by exogenous tetrahydrobiopterin. Infect. Immun. 62:4043.

26. Doolan, D. L., and S. L. Hoffman. 1999. IL-12 and NK cells are required for antigen-specific adaptive immunity against malaria initiated by CD8$^+$ T cells in the Plasmodium yoelii model. J. Immunol. 163:884.

27. Wang, R., D. L. Doolan, P. L. Thong, R. C. Hedstrom, K. M. Coonan, Y. Charoenvit, T. R. Jones, P. Hobart, M. Margalith, J. Ng, et al. 1998. Induction of antigen-specific cytotoxic T lymphocytes in humans by a malaria DNA vaccine. Science 282:476.

28. Tang, D., M. DeVit, and S. A. Johnston. 1992. Genetic immunization is a simple method for eliciting an immune response. Nature 356:152.

29. Robinson, H. L., D. C. Montefiori, R. P. Johnson, K. H. Manson, M. L. Kalish, J. D. Lifson, T. A. Rizvi, S. Lu, S. L. Hu, G. P. Mazzara, et al. 1999. Neutralizing antibody-independent containment of immunodeficiency virus challenges by DNA priming and recombinant pox virus booster immunizations. Nat. Med. 5:526.

30. Rodrigues, E. G., F. Zavala, D. Eichinger, J. M. Wilson, and M. Tsiji. 1997. Single immunizing dose of recombinant adenovirus efficiently induces CD8$^+$ T cells mediated protective immunity against malaria. J. Immunol. 158:1268.

31. Guide for the Care and Use of Laboratory Animals. 1996. Institute of Laboratory Animal Resources Commission on Life Sciences, National Research Council, National Academy Press, Washington, DC. .

Molecular recognition of pathogen attack occurs inside of plant cells in plant disease resistance specified by the *Arabidopsis* genes *RPS2* and *RPM1*

R. Todd Leister*, Frederick M. Ausubel[†], and Fumiaki Katagiri*[†‡]

*Department of Biological Sciences, University of Maryland, Baltimore County, 1000 Hilltop Circle, Baltimore, MD 21250; and [†]Department of Molecular Biology, Massachusetts General Hospital and Department of Genetics, Harvard Medical School, Boston, MA 02114

ABSTRACT   The *Arabidopsis thaliana* disease resistance genes *RPS2* and *RPM1* belong to a class of plant disease resistance genes that encode proteins that contain an N-terminal tripartite nucleotide binding site (NBS) and a C-terminal tandem array of leucine-rich repeats. *RPS2* and *RPM1* confer resistance to strains of the bacterial phytopathogen *Pseudomonas syringae* carrying the avirulence genes *avrRpt2* and *avrB*, respectively. In these gene-for-gene relationships, it has been proposed that pathogen avirulence genes generate specific ligands that are recognized by cognate receptors encoded by the corresponding plant resistance genes. To test this hypothesis, it is crucial to know the site of the potential molecular recognition. Mutational analysis of RPS2 protein and *in vitro* translation/translocation studies indicated that RPS2 protein is localized in the plant cytoplasm. To determine whether avirulence gene products themselves are the ligands for resistance proteins, we expressed the *avrRpt2* and *avrB* genes directly in plant cells using a novel quantitative transient expression assay, and found that expression of *avrRpt2* and *avrB* elicited a resistance response in plants carrying the corresponding resistance genes. This observation indicates that no bacterial factors other than the avirulence gene products are required for the specific resistance response as long as the avirulence gene products are correctly localized. We propose that molecular recognition of *P. syringae* in *RPS2*- and *RPM1*-specified resistance occurs inside of plant cells.

In plants, robust defense responses to invading phytopathogens often conform to a gene-for-gene relationship: resistance to a pathogen is only observed when the pathogen carries a specific avirulence (*avr*) gene and the plant carries a corresponding resistance (*R*) gene (1–3). Because *avr-R* gene-for-gene relationships are observed in many plant-pathogen systems and are accompanied by a characteristic set of defense responses, a common molecular mechanism underlying *avr-R* gene mediated resistance has been postulated (4). One simple model which explains gene-for-gene relationships is that pathogen *avr* genes directly or indirectly generate a specific molecular signal (ligand) that is recognized by cognate receptors encoded by plant *R* genes. Recent cloning of plant resistance genes and corresponding pathogen avirulence genes provided the tools for a direct test of this ligand-receptor model (5).

In the phytopathogenic interaction between the small flowering plant *Arabidopsis thaliana* and the bacterial phytopathogen *Pseudomonas syringae*, two *R* genes, *RPS2* (6, 7) and *RPM1* (8), and three corresponding *avr* genes, *avrRpt2* (9), *avrRpm1* (10), and *avrB* (11), have been isolated. *RPS2* confers resistance to *P. syringae* strains expressing *avrRpt2* (12, 13) and *RPM1* confers resistance to *P. syringae* expressing *avrRpm1*

(14) or *avrB* (15). *RPS2* and *RPM1* belong to a major class of plant resistance genes which encode proteins containing nucleotide binding sites (NBS) and leucine-rich repeats (LRR) and which confer resistance to bacterial, fungal, or viral pathogens (5). The structural conservation among *R* genes is consistent with the presence of a common molecular mechanism underlying gene-for-gene mediated disease resistance.

The hypersensitive response (HR) is the most characteristic defense response associated with gene-for-gene interactions (1). The HR involves rapid plant cell death localized at the site of infection. Using the HR as a marker for disease resistance, a transient expression assay for RPS2 function was previously developed that involves biolistic introduction of an *RPS2* cDNA clone into plant cells (7). In this assay, expression of a β-glucuronidase (GUS)-encoding reporter gene cointroduced with *RPS2* is monitored as an indicator of the HR: when the HR causes plant cell death, low levels of GUS activity are observed.

Here we report that the *RPS2* gene product is probably localized in the plant cell cytoplasm. We also report that when transiently expressed in plants, two *P. syringae avr* genes, *avrRpt2* and *avrB*, can elicit an HR in a gene-for-gene specific manner. For these experiments, the transient expression assay was enhanced to make it quantitative. We propose that molecular recognition of the pathogen in *RPS2*- and *RPM1*-specified resistance occurs inside of plant cells.

MATERIALS AND METHODS

A. thaliana plants representing four different *R* gene genotypes were used; ecotype Columbia (Col-0) wild type (phenotype, RPS2 RPM1; genotype, *RPS2/RPS2 RPM1/RPM1*), rps2-101C (rps2 RPM1; *rps2-101C/rps2-101C RPM1/RPM1*; Col-0 background) (7, 16), ecotype Niederzenz (Nd-0) wild type (RPS2 rpm1; *RPS2/RPS2 Δrpm1/Δrpm1*) (8, 14); and a hybrid line derived from a cross between rps2-101C and Nd-0 with an *rps2-101C/rps2-101C Δrpm1/Δrpm1* genotype (phenotype rps2 rpm1) (7). Plants were grown at 22°C with ≈80% relative humidity with a 12 hr light/12 hr dark cycle in environment-controlled growth chambers.

The *avrRpt2* and *avrB* genes were amplified by PCR using Pfu polymerase (Stratagene) from plasmids pLH12 (13) and pPSG0002 (17), respectively, using the primers, AVRT1 and AVRT2 for *avrRpt2* and AVRB1 and AVRB2 for *avrB*: AVRT1, 5'-CGCGGATCCACCATGATGAAAATTGCTC-CAGTTG-3'; AVRT2, 5'-GGAGCGCGGCCGCTTGTCAT-GATGCCGCCACGTG-3'; AVRB1, 5'-CGCGGATCCACC-ATGGGCTGCGTCTCGTC-3'; AVRB2, 5'-GGAGCGCG-GCCGCTATACATTTAAAAGCAATC-3'. These primers

Abbreviations: *avr* gene, avirulence gene; *R* gene, resistance gene; HR, hypersensitive response; NBS, nucleotide binding site; LRR, leucine-rich repeats; GUS, β-glucuronidase; LUC, luciferase.
[‡]To whom reprint requests should be addressed. e-mail: katagiri@umbc.edu.

were designed to change the sequence preceding the initiation codon into a eukaryote-type translation initiation site (18). Each PCR product was digested with *Bam*HI and *Not*I and cloned into the *Bam*HI–*Not*I site of the plant transient expression vector pKEx4tr (7) to obtain pExavrRpt2 and pExavrB, respectively. These plasmids were used for transient expression of the *avr* genes. A full-length *RPS2* cDNA (clone 11) (7) in pKEx4tr was used for transient expression and *in vitro* translation of *RPS2*. The *RPS2* mutant I353K was created using PCR by changing the ATC codon of isoleucine 353 into the lysine codon AAG. Similarly, the *rps2-101C* nonsense mutation (7) was recreated by changing nucleotide G704 to A. These RPS2 wild-type and mutant genes in pKEx4tr were cut out with *Pme*I and *Sac*I, and cloned into the *Sma*I–*Sac*I site of pBI1Rpro11 (a derivative of the plant transformation vector pBI121 (Clonetech) in which the cauliflower mosaic virus *35S* promoter was replaced with the 1.4-kb *RPS2* promoter region; F.K. and F.M.A., unpublished) to obtain pR11-I353K, pR11-101C, and pR11-X11, respectively. These plasmids were used for generating transgenic plants. *RPM1* cDNA clones were isolated from an *A. thaliana* cDNA library (7) in pKEx4tr by hybridization screening using a DNA probe based on the sequence of *RPM1* (8). Three clones were purified, and one of the two full-length clones (clone 7), whose 5' end starts at nucleotide number −86, was used for transient expression. pKEx4tr-G (7) was used for the *GUS* construct. The luciferase (*LUC*) construct p35S-LUC (19) was a gift from M. Bustos. Generation of transgenic plants and analysis of the plants for a macroscopic HR were performed as described (7).

For transient expression, gold biolistic particles (1 μm in diameter) were coated with DNA as described (7). Note that all genes for transient expression were linked to the cauliflower mosaic virus *35S* promoter. pKEx4tr-G (1.4 μg) and 2.0 μg of one of the *avr* gene constructs were used for coating each mg of gold particles. When an *R* gene was included in the assay, 0.1 μg of *RPS2* clone 11 or 2.0 μg of *RPM1* clone 7, respectively, was used for each mg of gold particles. In all cases, the total amount of DNA/mg of gold particles was adjusted to be the same by addition of pKEx4tr. When the *LUC* gene was used for a reference of transformation efficiency, 1.8 μg of p35S-LUC was used for each mg of gold particles. These *LUC*-coated particles were mixed with the particles coated with *GUS* and the relevant test gene in the ratio of 1:5.6. Bombardment was carried out with a Bio-Rad PDS-1000/He machine and in each bombardment experiment, 0.5 mg of gold particles and six leaves of *A. thaliana* (5–6 weeks old) were used. After a 27-hr incubation at room temperature in the dark, the leaves were either histochemically stained for GUS activity (20) or homogenized for quantitation of the GUS and LUC activities (19). The GUS and LUC activities of leaves that were not bombarded were used as blank values. The relative GUS activities (GUS activity/LUC activity) in a single series of experiments were renormalized by setting the mean value of the *GUS* only samples to be 100. All transient expression experiments were repeated at least twice to confirm reproducibility.

The *RPS2* cDNA clone 11 digested with *Not*I was transcribed *in vitro* using T7 RNA polymerase and the resulting *RPS2* RNA or β-lactamase RNA (Promega) were used for *in vitro* translation. The *in vitro* translation/translocation experiments were performed using rabbit reticulocyte lysate and canine pancreatic microsomes (Promega) with [^{35}S]methionine according to the supplier's instruction. Fractionation of the proteins after the reaction and a posttranslation procedure (see Fig. 3B) were performed essentially according to Sakaguchi *et al.* (21). The proteins were resolved by 7.5% SDS/PAGE, and the autoradiograms of the gels were obtained by a PhosphorImager. Each lane in Fig. 3 corresponds to 9 μl of reaction.

```
374  LSLEVVNYAKGLPLALKVWGSLL  396  N
      |  :|      ||||||   :|:  :
337  LAEIIVSKCGGLPLALITLGGAM  359  RPS2

337  LAEIIVSKCGGLPLALKTLGGAM  359  I353K
```

FIG. 1. The I353K mutation in the putative transmembrane region of RPS2. The putative transmembrane region of RPS2 protein (*Middle*) (7) is compared with the corresponding region of N (*Top*) (23). Identical and similar residues between the two proteins are indicated by vertical lines and colons, respectively, between the two sequences. The putative transmembrane region of RPS2, predicted by ALOM (22), is underlined. The corresponding region of the I353K mutant is shown at *bottom*. The mutated amino acid residue in I353K and the corresponding residues in N and RPS2 are shown in boldface. The numbers indicate the amino acid residue numbers in each protein.

RESULTS

Evidence That RPS2 Is a Cytoplasmic Protein. A direct approach for detection of *R* gene products in plants is technically challenging due to the low abundance of the R proteins. An anti-RPS2 antibody, which apparently has high affinity for *in vitro*-translated RPS2 protein, barely detected the protein in plant extracts by Western blot analysis (F.K. and F.M.A., unpublished work). Therefore, we used indirect approaches to investigate the subcellular localization of RPS2.

The computer program ALOM (22) predicts that one polypeptide region (amino acid residues 340–356) of RPS2 is membrane-integrated (7) whereas the corresponding region of the protein encoded by the tobacco mosaic virus resistance gene *N* (amino acid residues 377–393; Fig. 1) (23), which also belongs to the NBS-LRR class, is not membrane-integrated. The corresponding region of RPM1 (8) is not predicted to be membrane-integrated either (not shown). It seems unlikely that one of the corresponding polypeptide regions of functionally and structurally related proteins is membrane-integrated and the others are not. A mutation (I353K) was created in RPS2 by changing isoleucine 353 to lysine, the corresponding residue in N (Fig. 1). To analyze the activity of the I353K mutant, which ALOM does not predict to be membrane-integrated, transgenic rps2-101C mutant plants carrying the I353K transgene linked to the *RPS2* promoter (F.K. and F.M.A., unpublished work) were constructed. As controls, transgenic rps2-101C mutant plants carrying a wild-type *RPS2* transgene and an *rps2-101C* mutant transgene were also constructed. One-month old primary transformants were challenged with a high dose (0.5 × 10⁷ colony-forming unit/ml) of *P. syringae* pv. *phaseolicola* (*Psp*) 3121 ± *avrRpt2* and observed 20 hr after inoculation (Fig. 2A). When challenged with *Psp* 3121 carrying a vector control, none of the transgenic plants showed detectable change. When challenged with *Psp* 3121 carrying *avrRpt2*, all seven independent transgenic lines transformed with the *RPS2* wild-type gene showed a typical macroscopic HR (Fig. 2A *Right*), indicating complementation of the mutant phenotype, whereas none of 20 independent transgenic lines transformed with the *rps2-101C* gene showed an HR (Fig. 2A *Center*). Among 24 independent lines transformed with I353K, 17 lines showed as strong an HR as the plants transformed with the wild-type gene (Fig. 2A *Left*), and five lines showed a weak HR (not shown). The occurrence of a small number of transgenic lines showing a weak HR may indicate that the activity of the I353K gene may be slightly weaker than the wild-type gene. Nevertheless, these results demonstrate that the I353K mutation, which would disrupt the transmembrane-integrated property of this region of RPS2, does not significantly affect RPS2 function, indicating that the polypeptide region is unlikely to be transmembrane.

As a second indirect approach, we examined the localization of RPS2 in an *in vitro* translation/translocation system that
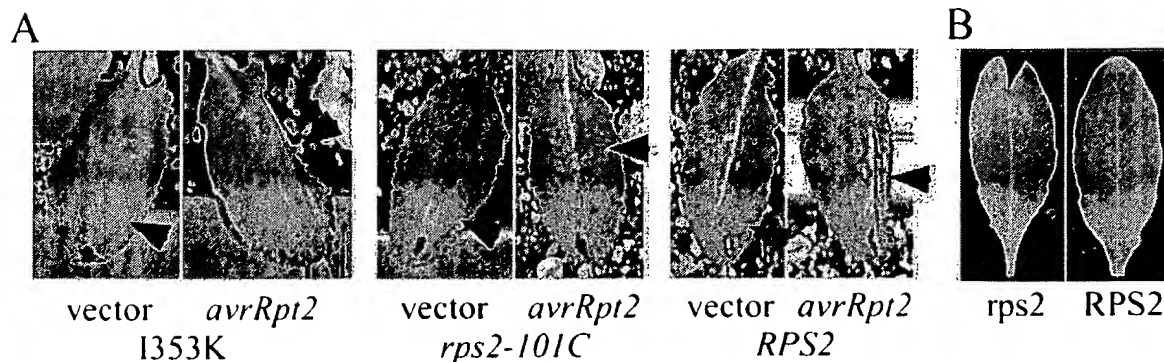
Plant Biology: Leister et al.

Proc. Natl. Acad. Sci. USA 93 (1996)   15499

A   B

vector avrRpt2   vector avrRpt2   vector avrRpt2   rps2   RPS2
    I353K   rps2-101C   RPS2

FIG. 2.   (A) The I353K RPS2 mutant gene can complement an rps2 mutant phenotype in transgenic plants. One-month old rps2-101C plants transformed with I353K (Left), with a rps2-101C mutant gene (Center), and with the RPS2 wild-type gene (Right) were inoculated at 0.5 × 10^7 colony-forming unit/ml with Psp 3121 carrying a vector control (pLAFR3) or carrying avrRpt2. Only one-half of each leaf (arrowhead) was inoculated. The photographs were taken 20 hr after inoculation. (B) Transient expression of avrRpt2 causes a reduction of cointroduced GUS gene expression in RPS2 plants. Leaves of RPS2 wild-type (Right) and rps2-101C mutant (Left) plants were bombarded with biolistics carrying the avrRpt2 and GUS constructs. After a 27-hr incubation, the leaves were histochemically stained for GUS activity. The cells that express GUS enzyme at a high level are visualized as blue dots on the leaves.

utilizes rabbit reticulocyte lysate and dog pancreatic microsomes. In this procedure, if a protein, labeled with ^{35}S by in
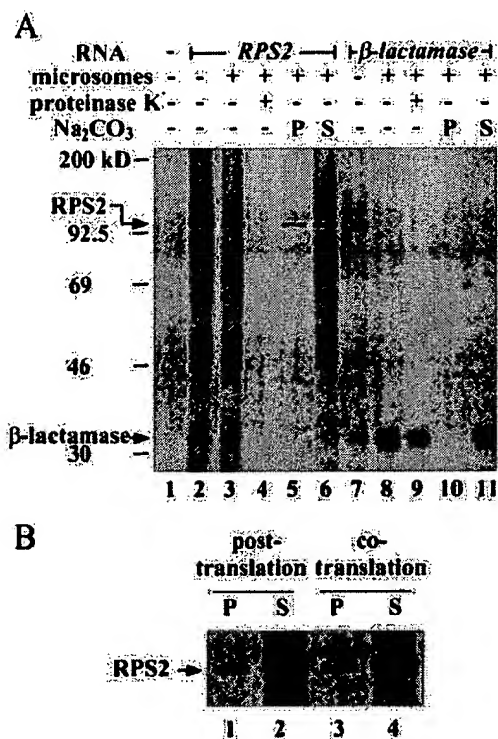

FIG. 3.   Subcellular localization of RPS2 by in vitro translation/translocation. (A) RPS2 appears to be cytoplasmic. RPS2 RNA (lanes 2–6) and β-lactamase RNA (a positive control for translocation; lanes 7–11) were translated either in the presence (lanes 3–6 and 8–11) or absence (lanes 2 and 7) of dog pancreatic microsomes. Lane 1 shows a no RNA control for translation. The reactions were treated with proteinase K (lanes 4 and 9) or fractionated by ultracentrifugation into precipitate (lanes 5 and 10) and supernatant (lanes 6 and 11) fractions after Na$_2$CO$_3$ treatment. The positions of molecular weight markers, RPS2, and β-lactamase are indicated on the left. (B) RPS2 detected in the precipitate fraction is an artifact. The microsomes were either included in the translation reaction as in the standard procedure (cotranslation; lanes 3 and 4) or added after the translation reaction was terminated with cycloheximide (posttranslation; lanes 1 and 2). The reactions were fractionated into precipitate (lanes 1 and 3) and supernatant fractions (lanes 2 and 4) after Na$_2$CO$_3$ treatment.

vitro translation, has a signal peptide for secretion, the protein is cotranslationally transported into microsomes. Proteinase K treatment and ultracentrifugation after Na$_2$CO$_3$ treatment allow protein localization to be classified as cytoplasmic, membrane-integrated, or secreted (21). A cytoplasmic protein remains outside of microsomes, so that it is sensitive to proteinase K and is recovered in the supernatant after centrifugation. A secreted protein is transported into microsomes but remains soluble, so that it is protected from proteinase K and recovered in the supernatant after centrifugation. A membrane-integrated protein can be partially protected from proteinase K and it is precipitated with the membrane after centrifugation. Fig. 3A shows the results of this analysis, including β-lactamase as a positive control for translocation. β-Lactamase, which is a secreted protein, was protected from proteinase K (lane 9) and detected in the soluble fraction after Na$_2$CO$_3$ treatment (lane 11), demonstrating the high efficiency of the translocation system. In vitro-translated RPS2 migrated with an apparent molecular weight consistent with that calculated from its deduced amino acid sequence (105 kDa; lane 2). RPS2 was not protected from proteinase K (lane 4). The major portion of RPS2 was detected in the soluble fraction after Na$_2$CO$_3$ treatment (lane 6), but a significant amount was also detected in the precipitate fraction (lane 5). The amount of this precipitate remained the same in the absence of the translocation system (posttranslation, Fig. 3B), indicating that the precipitate was an artifact. These results indicate a cytoplasmic localization for RPS2. Although the results must be interpreted with caution because of the use of a heterologous in vitro system, taken together with the mutagenesis results described above, they suggest that RPS2 is a cytoplasmic protein.

When Transiently Expressed in Plants, avrRpt2 Can Elicit a Specific Resistance Response. If RPS2 is indeed cytoplasmic and if it is the primary receptor for the avrRpt2-generated ligand, the ligand must also be present in the plant cytoplasm. A possible ligand for RPS2 is the avrRpt2 gene product itself. If AvrRpt2 protein were expressed in plant cells, it would most likely be located in the plant cytoplasm because it is a hydrophilic protein and does not have an obvious signal peptide (9). Based on these considerations, we tested whether expression of avrRpt2 in plants can elicit a specific resistance response.

Transient expression by biolistic bombardment was used for this purpose. Based on the same principle as the transient expression assay for RPS2 (7), reduced expression of a cointroduced GUS gene was used as an HR indicator. In Fig. 2B,

the *avrRpt2* construct was cointroduced with the *GUS* construct into either RPS2 wild-type (*Right*) or rps2-101C mutant (*Left*) plants, and plant cells that expressed GUS were visualized by histochemical staining (blue dots in the figure). The GUS expression in wild-type plants was reduced compared with that in the rps2 mutant plants, indicating the occurrence of the HR in an *RPS2*-dependent manner. Therefore, *avrRpt2* can elicit a resistance response with gene-for-gene specificity when expressed in plants.

A Quantitative Transient Expression Assay for the Resistance Response. A problem associated with biolistic bombardment is that the efficiency of transient transformation varies to a great extent both for each bombardment and for different areas of the target in a single bombardment. To quantitate the assay, a reference for transformation efficiency must be included. This was achieved by introducing a second reporter gene, *LUC* (24), linked to the *35S* promoter, into cells different from the cells into which the *GUS* and *avrRpt2* genes were introduced. Gold particles were coated either with the *LUC* construct or with the *GUS* and *avrRpt2* constructs, the particles were mixed and then bombarded together. Because a relatively small number of plant cells are transformed by the biolistics procedure, the cells transformed with *LUC* and the cells transformed with the *GUS* and *avrRpt2* are statistically different and far apart. Because the HR is a local event (1), *LUC* expression is not expected to be affected very much by an HR occurring in other cells. Therefore, LUC activity represents the relative transformation efficiency in a particular bombardment and can be used as a reference to normalize the GUS activity.

Using this quantitative transient expression assay, *avrRpt2* was examined in RPS2 and rps2 plants which had either an RPM1 or rpm1 phenotype (Fig. 4, second row of each panel). Irrespective of the RPM1 phenotype, expression of *avrRpt2* caused ≈50% reduction of the normalized GUS activity in RPS2 plants (*A* and *C*) compared with the activity in rps2 plants (*B* and *D*). Another *P. syringae* avirulence gene *avrB*, which corresponds to the *RPM1* resistance gene, was also examined (Fig. 4, third row of each panel). Similar to the results obtained with *avrRpt2*, irrespective of the RPS2 phenotype, expression of *avrB* caused more than 85% reduction of the normalized GUS activity in RPM1 plants (*A* and *B*) compared with the activity in rpm1 plants (*C* and *D*). Thus the gene-for-gene relationship for *avrRpt2* and *avrB* is strictly conserved in this assay, confirming that the assay indeed reflects a specific resistance response. Two different *P. syringae* *avr* genes with distinct specificities can elicit a specific resistance response when expressed in plants, and no other bacterial components are required for this response.

The reduction of GUS activity reflects both the percentage of dead cells and how quickly the cells die. The reduction of GUS activity caused by *avrRpt2* was smaller than that caused by *avrB* (Fig. 4). This is consistent with the observation that the HR caused by *avrB* is faster than the one caused by *avrRpt2* when the *avr* genes are carried by a *P. syringae* strain (25).

In the case of *avrB* expression in RPM1 wild-type plants, we often observed a statistically significant reduction of *LUC* reference gene expression (typically 50–70% reduction) compared with the *LUC* expression in controls in which no avirulence genes were expressed (not shown). Therefore, the actual reduction of relative GUS activity in the case of *avrB-RPM1* interactions was even greater than that shown in Fig. 4. A similar reduction in *LUC* expression was not observed in any of the other assay conditions, including the case in which *avrRpt2* was expressed in RPS2 wild-type plants. This difference in *LUC* gene expression between the *avrRpt2-RPS2* and *avrB-RPM1* interactions may be correlated with different gene induction patterns that are observed between these two interactions (25, 26).

The Specific Resistance Response Can Be Elicited by Transiently Expressed *avr* and *R* Genes. The results of the transient
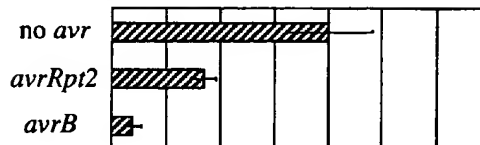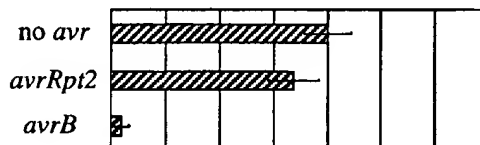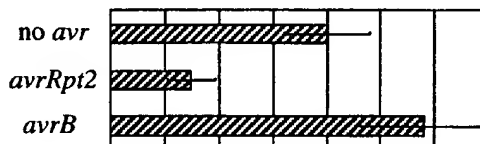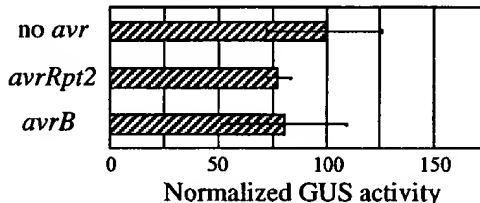

FIG. 4. avrRpt2 and *avrB* can elicit a specific resistance response when expressed in plants. RPS2 RPM1 (*A*), rps2 RPM1 (*B*), RPS2 rpm1 (*C*), and rps2 rpm1 (*D*) plants were bombarded with biolistics carrying the GUS and the indicated *avr* gene constructs. Each bar represents the mean value of four bombardment events. (Bars = SEM.)

expression of the avirulence genes prompted us to test whether the assay works when both *avr* and *R* genes are transiently expressed. In the following experiments, rps2 rpm1 double mutant plants were used for biolistic bombardment. The *avr* gene, *R* gene, and *GUS* gene constructs were used to coat one set of gold particles and the *LUC* gene construct was used to coat another set. As shown in Fig. 5*A*, when *avrRpt2* and *RPS2* were transiently expressed together, reduction of GUS activity was observed, but was not observed when *RPS2* was expressed together with *avrB*. Similarly, reduction of GUS activity was observed when *RPM1* was transiently expressed together with *avrB*, but not when *RPM1* was expressed together with *avrRpt2* (Fig. 5*B*). This strict conservation of the gene-for-gene specificity indicates that the transient expression assay can be used for functional analysis of both *avr* and *R* genes.

As in the experiment described in Fig. 4, the *avrB-RPM1* interaction resulted in greater reduction of the GUS activity than the *avrRpt2-RPS2* interaction, when both the *avr* and *R* genes were transiently expressed (Fig. 5). A significant reduction of *LUC* reference gene expression specific to the *avrB-RPM1* interaction was also observed in this experiment (not shown).

DISCUSSION

To determine where the molecular recognition occurs between *avr*-generated signals and *R*-gene mediated responses in gene-
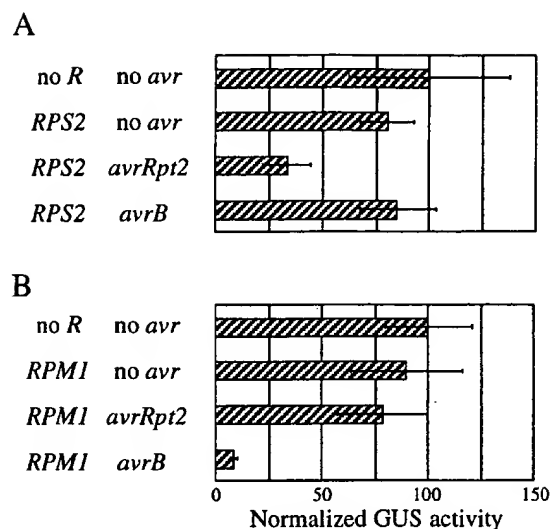
A

| no R   no avr |
| RPS2   no avr |
| RPS2   avrRpt2 |
| RPS2   avrB |

B

| no R   no avr |
| RPM1   no avr |
| RPM1   avrRpt2 |
| RPM1   avrB |

0   50   100   150

Normalized GUS activity

FIG. 5. Both avirulence and resistance genes can be analyzed by transient expression. rps2 rpm1 plants were bombarded with biolistics carrying the *GUS* gene, the indicated *R* gene, and the indicated *avr* genes. Each bar represents the mean value of four bombardment events. (Bars = SEM.)

for-gene relationships, we investigated the subcellular localization of RPS2 and the effects of directly expressing *avr* genes in plants. Mutational analysis of the putative transmembrane region of RPS2 and *in vitro* translation/translocation analysis suggested that RPS2 is a cytoplasmic protein. RPM1 is also likely to be cytoplasmic because *RPS2* and *RPM1* belong to the same class of *R* genes (8). Expression in plants of *avrRpt2* and *avrB*, *avr* genes corresponding to *RPS2* and *RPM1*, respectively, elicited resistance responses in a gene-for-gene specific manner. This indicates that these *avr* gene products are the only bacterial components required for the gene-for-gene interaction as long as they are correctly localized. Judging from their amino acid sequences (9, 11), the *avr* gene products are also likely to be cytoplasmic when expressed in plants. Therefore, we propose that the molecular recognition involved in the *RPS2*- and *RPM1*-specified resistance takes place inside of plant cells.

A corollary of the notion that *R* gene mediated recognition of *avr* gene signals occurs in the cytoplasm is that *avr* gene products themselves directly interact with the corresponding *R* gene products although this notion does not exclude other possibilities. For example, the *avr* gene products could be enzymes that modify a plant product into specific ligands. However, we prefer the direct interaction model for the following reasons. First, it has been speculated that the LRR of an NBS-LRR gene product is a determinant of *avr* gene specificity (27). Because LRR structures are generally involved in protein-protein interactions (28), it is likely that the ligands would be proteins. Second, in most cases, the genetically identifiable factors involved in specificity determination in resistance are a single *R* gene and a single corresponding *avr* gene (1). If *avr* genes generate signals through indirect mechanisms, more genes required for the specificity determination might have been identified. This view of an NBS-LRR resistance gene product as an intracellular receptor is compatible with the fact that tobacco mosaic virus resistance gene *N* is also an NBS-LRR gene (23) because the products of the viral genes, one of which should be the corresponding avirulence gene, accumulate inside of plant cells.

For the molecular recognition to occur inside plant cells, the *avr* gene products must be transported into plant cells from bacteria. For most *P. syringae avr* genes, including the two *avr*

genes used in this study, the bacterial *hrp* (hypersensitive response and pathogenicity) gene cluster is required to elicit the specific resistance response in plants (29, 30). Some of the genes in the *hrp* cluster encode components of a type III protein secretion system (31). Bacterial pathogens of mammals, such as *Salmonella*, *Shigella*, and *Yersinia*, apparently use the type III secretion pathway to transfer proteins important for pathogenicity directly into mammalian cells (32). By analogy, *P. syringae* could also use a type III secretion system to directly transfer *avr* gene products into plant cells. The *hrp* cluster is also required for pathogenicity (33), suggesting that the type III secretion system may also transfer virulence gene products into plant cells.

To demonstrate effects of avirulence gene expression in plants, we used transient expression using biolistic bombardment. The principle of the assay, in which reduction of a cointroduced reporter gene expression is used as an indicator of the HR, was initially developed by us to demonstrate complementation of an rps2 mutant phenotype by an *RPS2* cDNA clone (7). In this study, we showed that the transient expression assay can also be used to monitor the activity of a cloned *avr* gene by delivering the *avr* gene constructs biolistically into plant cells. (Fig. 2B). While this work was in progress, Gopalan *et al.* also reported that *avrB* can elicit a specific resistance response when expressed in plants using a transient expression assay that is essentially the same as the assay used in Fig. 2B (29).

One shortcoming of the biolistic mediated transient expression assay is that the transformation efficiency varies to a large extent, both with respect to independent bombardments and to different areas of the target. To compensate for this variability, our original assay for RPS2 function involved infection of only one half of each leaf with *P. syringae* carrying avrRpt2; the uninfected half of the leaf served as a reference for the transformation efficiency (7). However, the assay for *avr* genes used in Fig. 2B did not include an internal reference for transformation efficiency. We therefore modified the transient expression assay by including a second reporter gene (*LUC*) delivered on a separately coated set of biolistic particles in the same bombardment event (Fig. 4). Using this quantitative assay, we have unequivocally demonstrated that transient expression of *avrRpt2* or *avrB* in plants elicits an HR in a gene-for-gene specific manner (Fig. 4).

We further extended the application of the functional transient expression assay by simultaneously assaying for both *avr* and *R* gene functions (Fig. 5). This rapid assay will be applicable to studies of many other gene-for-gene plant-pathogen systems for three reasons. First, biolistic transient transformation is applicable to many plant species. Second, the HR is a characteristic resistance response in gene-for-gene resistance. Third, simultaneous bombardment of *avr* and *R* genes is not limited by pathogen type. This assay may also be used for a rapid determination of whether a particular *R* gene can function in a heterologous host.

1. Keen, N. T. (1992) *Plant Mol. Biol.* 19, 109–122.
2. Lamb, C. J., Lawton, M. A., Dron, M. & Dixon, R. A. (1989) *Cell* 56, 215–224.

3. Flor, H. H. (1971) *Annu. Rev. Phytopathol.* **9**, 275–296.
4. Gabriel, D. W. & Rolfe, B. G. (1990) *Annu. Rev. Phytopathol.* **28**, 365–391.
5. Staskawicz, B. J., Ausubel, F. M., Baker, B. J., Ellis, J. G. & Jones, J. D. G. (1995) *Science* **268**, 661–667.
6. Bent, A. F., Kunkel, B. N., Dahlbeck, D., Brown, K. L., Schmidt, R., Giraudat, J., Leung, J. & Staskawicz, B. J. (1994) *Science* **265**, 1856–1860.
7. Mindrinos, M., Katagiri, F., Yu, G.-L. & Ausubel, F. M. (1994) *Cell* **78**, 1089–1099.
8. Grant, M. R., Godiard, L., Straube, E., Ashfield, T., Lewald, J., Sattler, A., Innes, R. W. & Dangl, J. L. (1995) *Science* **269**, 843–846.
9. Innes, R. W., Bent, A. F., Kunkel, B. N., Bisgrove, S. R. & Staskawicz, B. J. (1993) *J. Bacteriol.* **175**, 4859–4869.
10. Dangl, J. L., Ritter, C., Gibbon, M. J., Mur, L. A. J., Wood, J. R., Goss, S., Mansfield, J., Taylor, J. D. & Vivian, A. (1992) *Plant Cell* **4**, 1359–1369.
11. Tamaki, S., Dahlbeck, D., Staskawicz, B. & Keen, N. T. (1988) *J. Bacteriol.* **170**, 4846–4854.
12. Dong, X., Mindrinos, M., Davis, K. R. & Ausubel, F. M. (1991) *Plant Cell* **3**, 61–72.
13. Whalen, M. C., Innes, R. W., Bent, A. F. & Staskawicz, B. J. (1991) *Plant Cell* **3**, 49–59.
14. Debener, T., Lehnackers, H., Arnold, M. & Dangl, J. L. (1991) *Plant J.* **1**, 289–302.
15. Bisgrove, S. R., Simonich, M. T., Smith, N. M., Sattler, A. & Innes, R. W. (1994) *Plant Cell* **6**, 927–933.
16. Yu, G.-L., Katagiri, F. & Ausubel, F. M. (1993) *Mol. Plant–Microbe Interact.* **6**, 434–443.
17. Staskawicz, B., Dahlbeck, D., Keen, N. & Napoli, C. (1987) *J. Bacteriol.* **169**, 5789–5794.
18. Kozak, M. (1987) *Nucleic Acids Res.* **15**, 8125–8148.
19. Chern, M.-S., Bobb, A. J. & Bustos, M. M. (1996) *Plant Cell* **8**, 305–321.
20. Jefferson, R. A. (1987) *Plant Mol. Biol. Rep.* **5**, 387–405.
21. Sakaguchi, M., Tomiyoshi, R., Kuroiwa, T., Mihara, K. & Omura, T. (1992) *Proc. Natl. Acad. Sci. USA* **89**, 16–19.
22. Klein, P., Kanehisa, M. & DeLisi, C. (1985) *Biochim. Biophys. Acta* **815**, 468–476.
23. Whitham, S., Dinesh-Kumar, S. P., Choi, D., Hehl, R., Corr, C. & Baker, B. (1994) *Cell* **78**, 1101–1105.
24. de Wet, J. R., Wood, K. V., Helinski, D. R. & DeLuca, M. (1985) *Proc. Natl. Acad. Sci. USA* **82**, 7870–7873.
25. Reuber, T. L. & Ausubel, F. M. (1996) *Plant Cell* **8**, 241–249.
26. Ritter, C. & Dangl, J. L. (1996) *Plant Cell* **8**, 251–257.
27. Lawrence, G. J., Finnegan, E. J., Ayliffe, M. A. & Ellis, J. G. (1995) *Plant Cell* **7**, 1195–1206.
28. Kobe, B. & Deisenhofer, J. (1993) *Nature (London)* **366**, 751–756.
29. Gopalan, S., Bauer, D. W., Alfano, J. R., Loniello, A. O., He, S. Y. & Collmer, A. (1996) *Plant Cell* **8**, 1095–1105.
30. Pirhonen, M. U., Lidell, M. C., Rowley, D. L., Lee, S. W., Jin, S., Liang, Y., Silverstone, S., Keen, N. T. & Hutcheson, S. W. (1996) *Mol. Plant–Microbe Interact.* **9**, 252–260.
31. Huang, H. C., Lin, R. H., Chang, C. J., Collmer, A. & Deng, W. L. (1995) *Mol. Plant–Microbe Interact.* **8**, 733–746.
32. Rosqvist, R., Hakansson, S., Forsberg, A. & Wolf-Watz, H. (1995) *EMBO J.* **14**, 4187–4195.
33. Lindgren, P. B., Peet, R. C. & Panopoulos, N. J. (1986) *J. Bacteriol.* **168**, 512–522.

Tolerance to Self Gangliosides Is the Major Factor Restricting the Antibody Response to Lipopolysaccharide Core Oligosaccharides in *Campylobacter jejuni* Strains Associated with Guillain-Barré Syndrome

Tyrone Bowes,[1,2] Eric R. Wagner,[1] Judith Boffey,[1] Dawn Nicholl,[1] Lynne Cochrane,[1] Mustapha Benboubetra,[1] Joe Conner,[2] Keiko Furukawa,[3] Koichi Furukawa,[3] and Hugh J. Willison[1]*

University Department of Neurology, Institute of Neurological Sciences, Southern General Hospital, Glasgow, Scotland G51 4TF[1], Department of Biological Sciences, Glasgow Caledonian University, Glasgow, Scotland G4 0BA,[2] United Kingdom, and Department of Biochemistry II, Nagoya University School of Medicine, Nagoya, Japan[3]

Guillain-Barré syndrome following *Campylobacter jejuni* infection is frequently associated with anti-ganglioside autoantibodies mediated by molecular mimicry with ganglioside-like oligosaccharides on bacterial lipopolysaccharide (LPS). The regulation of antibody responses to these T-cell-independent antigens is poorly understood, and only a minority of *Campylobacter*-infected individuals develop anti-ganglioside antibodies. This study investigates the response to gangliosides and LPS in strains of mice by using a range of immunization strategies. In normal mice following intraperitoneal immunization, antibody responses to gangliosides and LPS are low level but can be enhanced by the antigen format or coadministration of protein to recruit T-cell help. Class switching from the predominant immunoglobulin M (IgM) response to IgG3 occurs at low levels, suggesting B1-cell involvement. Systemic immunization results in poor responses. In GalNAc transferase knockout mice that lack all complex gangliosides and instead express high levels of GM3 and GD3, generation of anti-ganglioside antibodies upon immunization with either complex gangliosides or ganglioside-mimicking LPS is greatly enhanced and exhibits class switching to T-cell-dependent IgG isotypes and immunological memory, indicating that tolerance to self gangliosides is a major regulatory factor. Responses to GD3 are suppressed in knockout mice compared with wild-type mice, in which responses to GD3 are induced specifically by GD3 and as a result of polyclonal B-cell activation by LPS. The anti-ganglioside response generated in response to LPS is also dependent on the epitope density of the ganglioside mimicked and can be further manipulated by providing secondary signals via lipid A and CD40 ligation.

Guillain-Barré syndrome (GBS) is an acute, postinfectious polyneuropathy that is believed to have an autoimmune basis (21–23, 27, 29, 64, 66). It is associated with a wide range of precipitating bacterial and viral infections, including *Campylobacter jejuni* enteritis in 10 to 50% of cases depending on geographical region (5, 30, 46). In addition to immune responses specific to the preceding infection, 40% of post-*Campylobacter* infection GBS sera contain transient immunoglobulin M (IgM), IgA, and IgG antibodies to a variety of self gangliosides, including GM1, GM2, GD1a, GalNAc-GD1a, GD1b, GD3, GT1a, and GQ1b, which are believed to be among the principal pathogenic factors (7, 8, 28, 37, 65). Gangliosides are a family of sialic-acid-containing glycosphingolipids distributed throughout the body but highly enriched in the nervous system, where they are capable of acting as targets for anti-ganglioside autoantibodies (22, 34, 35, 60).

One of the mechanisms by which anti-ganglioside antibodies arise in GBS is through molecular mimicry with microbial oligosaccharides, including those borne by *Campylobacter* species (43, 56). Chemical and structural analysis of lipopolysaccharide (LPS) and lipooligosaccharide (LOS) outer core oligosaccharide (core OS) structures from *C. jejuni* serotypes isolated from GBS and non-GBS patients have identified sialylated moieties with configurations identical to those of several gangliosides (9, 11, 42, 44, 45, 50). For example, LPSs from *C. jejuni* HS:19, a serotype commonly associated with GBS, have been shown to contain GM1-, GD1a-, GD3-, and GT1a-like motifs, and antibody mimicry is supported by the finding that immunization of experimental animals with these LPSs produces the corresponding anti-ganglioside antibody response (4, 18). Serotyping studies have determined that certain *C. jejuni* serotypes, including HS:19, have greater potential for triggering GBS, and this may be due to quantitative differences in ganglioside-like LPS and LOS epitopes compared with non-GBS-associated strains (9, 44, 50).

Whereas *C. jejuni* is one of the commonest causes of acute diarrhea worldwide, affecting approximately 1% of the U.S. population per annum, GBS has a much lower incidence of 1.5/100,000 population, and thus it is estimated that only 0.01% of *C. jejuni* infections trigger GBS (2, 30). Although the absence of ganglioside mimics on some *C. jejuni* LPSs may be

---

* Corresponding author. Mailing address: University Department of Neurology, Institute of Neurological Sciences, Southern General Hospital, Glasgow G51 4TF, Scotland, United Kingdom. Phone: 44 141 201 2464. Fax: 44 141 201 2993. E-mail: h.j.willison@udcf.gla.ac.uk.

TABLE 1. Ganglioside-like structures present on LPSs from
C. jejuni strains

Ganglioside mimicked	Presence[a] of structure on LPS:				
	HS:3	HS:4	HS:19 (GM1^{+} GD1a^{+})	HS:10[d]	HS:19 (GM1^{+} GT1a^{+})[e]
GM1	−	+[b]	+[c]	−	+
GD1a	−	+	+	−	−
GD3	−	−	−	+	−
GT1a	−	−	−	−	+

[a] +, present; −, absent.
[b] HS:4 LPS bears GD1a and GM1 at a ratio of 9:1 (50).
[c] HS:19 LPS bears GD1a and GM1 at a ratio of 1:1 (50, 51) and is referred to here as HS:19(GM1^{+} GD1a^{+}).
[d] HS:10 was previously referred to as PG836 (48).
[e] HS:19(GM1^{+} GT1a^{+}) was previously referred to as OH4384 (11).

part of the explanation for this, clinical studies have demonstrated that even when humans are exposed to *C. jejuni* strains possessing ganglioside-like epitopes, their presence is not sufficient in itself to trigger the production of anti-ganglioside antibodies.

The host and microbial factors that determine whether any individual will mount an immune response to core OS structures that mimic self gangliosides are likely to be multifactorial. One confounding microbial factor is the presence of high levels of phase variation in *C. jejuni* LOS that may alter the level and nature of the mimic in any one strain (19, 36). Antibody responses to carbohydrate structures, including LPS, are T cell independent (TI) and arise early in ontogeny from B1 B cells, which produce a large pool of IgM class natural antibodies acting as an early defense against invading microorganisms (17, 41, 57). B1 B cells do not switch class to T-cell-dependent (TD) isotypes, form memory cells, or affinity mature (39).

In GBS, anti-ganglioside antibodies do switch class to the TD IgG1 and IgG3 isotypes, suggesting they may have arisen from conventional B2 cells and were able to recruit T-cell help or other accessory signals (55, 62). Whether the help comes from intermolecular cooperativity (uptake of carbohydrate-protein complexes by carbohydrate-specific B-cell receptors [BCR] and subsequent presentation of peptides to conventional T helper cells), presentation via CD1 and LPS signaling via Toll receptors, or other noncognate pathways is unknown.

A limitation of pathophysiological studies of anti-ganglioside antibody-mediated neuropathy has been the inability to generate high-titer IgG antibody responses in mice. Many studies have shown that mice immunized with gangliosides using a variety of immunization strategies generate poor antibody responses. This unresponsiveness has been attributed to poor immunogenicity, T-cell independence, and tolerance (32, 38, 49). The extent to which tolerance for self gangliosides is responsible for limiting the antibody response to core OS structures in *C. jejuni* has not been explored. We have previously shown that mice immunized with O:3 LPS, which does not contain a self ganglioside core OS structure, produce a vigorous antibody response to O:3 LPS compared with the poor response to self ganglioside-mimicking LPSs (18).

The red blood cell glycolipid antigens that define the ABO blood group system are also examples of carbohydrate antigens under strict tolerance control, which when disrupted can lead to severe antibody-mediated disease (61). In humans, natural anti-Gal antibodies, reactive with alpha-Gal epitopes that are absent in humans, comprise 1% of total human immunoglobulins and have a major role in mediating nonprimate xenograft rejection (14). In the alpha-1,3-galactosyltransferase knockout mouse, which lacks the ability to synthesize alpha-Gal epitopes, high levels of antibody to alpha-Gal can be induced by immunization with alpha-Gal antigen, in contrast with the absence of responses in wild-type mice (14). Similar studies of GalNAc transferase knockout (GalNAcT^{−/−}) mice, which contain high levels of GM3 and GD3 but lack all complex gangliosides, have demonstrated vigorous antibody responses in ganglioside-deficient mice immunized with ganglioside-protein conjugates; this also suggests that self gangliosides play an important role in inducing tolerance (38).

In this study, we have examined the roles of T-cell help, noncognate accessory signals, and tolerance in enhancing or restricting the antibody response in the mouse to ganglioside-mimicking LPS core OS structures. We have approached this by using GalNAcT knockout mice, in which one would predict that autoreactive B cells specific for complex gangliosides would not be eliminated but that the mice would be highly tolerant to LPS bearing GD3-like ganglioside mimics. In order to determine whether tolerance could be overcome by immunological manipulations, we also investigated the roles of different adjuvants and accessory stimuli, including anti-CD40
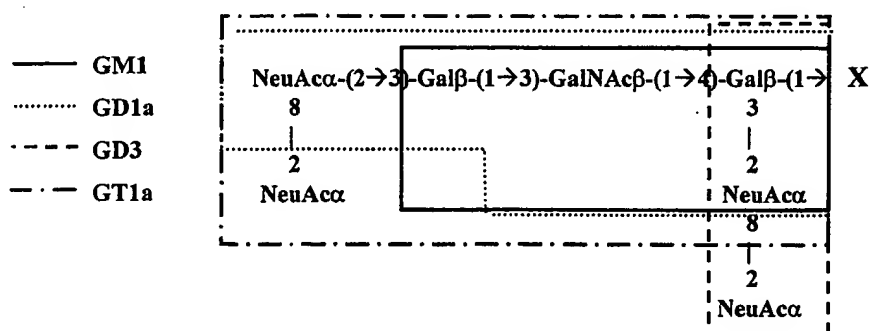

FIG. 1. Oligosaccharide structures. The whole structure of GQ1b is shown, but this has not been found in *C. jejuni*. NeuAc, *N*-acetyl neuraminic acid; X, Glc (1→1) ceramide (gangliosides) or the remaining core OS-lipid A (LPSs).

antibodies, and the role of lipid A signaling mediated through CD14 in C3H/HeN and C3H/HeJ mice.

MATERIALS AND METHODS

Animals. Female BALB/c, C3H/HeN, and LPS-hyporesponsive C3H/HeJ mice were supplied by Harlan, UK Ltd., Bicester, United Kingdom. Mice lacking a functional GalNAcT gene (GalNAc$^{+/+}$) and wild-type homozygous Gal-NAc$^{-/-}$ mice were generated and genotyped as described previously (59). The animals were housed and handled under University of Glasgow institutional guidelines and United Kingdom Home Office licensing. Food and water were supplied ad libitum.

C. jejuni. *C. jejuni* serostrains and isolates with structurally defined core OSs that were used in this study are shown in Table 1, and the oligosaccharide structures are shown in Fig. 1. The HS:19 (formerly O:19) and HS:4 serostrains, the OH4384 isolate of the HS:19 serostrain (11), and the PG836 isolate of the HS:10 serostrain (48, 54) were provided by J. Penner and D. Woodward, Centre for Disease Control, Ottawa, Ontario, Canada (42, 50, 51). The HS:3 serostrain was provided by A. Moran, Galway, Eire (10). For clarity, HS:19 is referred to as HS:19(GM1$^+$ GD1a$^+$), the isolate OH4384 is referred to as HS:19(GM1$^+$ GT1a$^+$), and the isolate PG836 is referred to as HS:10. The bacteria were grown on blood agar plates in a microaerobic atmosphere and harvested in distilled water after 48 h of growth. The bacteria were killed by heating them at 60°C for 1 h. LPS was isolated by hot phenol-water extraction, quantitated, analyzed for purity by silver staining after sodium dodecyl sulfate-polyacrylamide gel electrophoresis and thin-layer chromatography, resuspended in distilled water, and stored at −20°C (18).

Liposomes. Extruded liposomes were made according to protocols provided by Lipex Biomembranes Inc., Vancouver, Canada (40). Cholesterol, sphingomyelin, dicetylphosphate, and ganglioside GQ1b, GD1a, GM1, or GD3, supplied by Sigma Chemicals (Poole, Dorset, United Kingdom), were dissolved in chloroform-methanol (1:1) to yield stock solutions at 10 μg/ml and used to create liposomes with a molar ratio of 5:4:1:1, respectively. In order to generate a final volume of 1 ml of liposomes (sufficient for immunization of 10 mice with 100 μl of resuspended liposomes each), the lipid mixture was dried under nitrogen and resuspended to 5 ml in phosphate-buffered saline (PBS), pH 7.4. To create ovalbumin (ova)-containing liposomes, the PBS contained ova at 5 mg/ml. The mixture was alternately vortexed (Rotamixer; Fisher Scientific, Loughborough, United Kingdom) and sonicated (Nusonics; Quayle Dental, Worthing, United Kingdom) at room temperature for up to 15 min until the dried lipid was released from the walls of a 15-ml tube and the suspension was uniformly milky. The suspension was frozen and thawed five times by plunging it alternately into liquid nitrogen and a 37°C water bath to create multilamellar vesicles. This mixture was clarified by centrifugation at 600 × g (2,000 rpm in a Beckman GS6R benchtop centrifuge) for 15 min, and the pellet was discarded. Unilammelar liposomes were then created by repeated extrusion (10 times) through an N$_2$-driven extruder (Lipex Biomembranes Inc.) using a double 0.4-μm-pore-size polycarbonate fiber filter (no. 110605; Nuclepore). The extruded liposomes were then ultracentrifuged at 110,000 × g (35,000 rpm; Beckman LS50B centrifuge) for 1 h and resuspended in 1 ml of PBS for immunization in a final volume of 100 μl/mouse. The final product is referred to according to its constituents, e.g., ova-GD1a liposomes. In some immunization experiments in which liposomes were compared with simpler lipid preparations, gangliosides were dried on glass vessels and then resuspended by being vortexed and sonicated for 15 to 30 min in PBS containing 5 mg of ova/ml. In the series of experiments with anti-CD40 antibodies, LPS liposomes, without any protein adjuvant, were created by sonication of cholesterol, phosphatidylcholine, and HS:4 or HS:19(GM1$^+$ GT1a$^+$) in a ratio of 5:4:1 in liposomes, which were then admixed by gentle vortexing with 0.5 mg of monoclonal anti-CD40 antibody or the control MAb, GL117 (25)/mouse.

Immunizations. The mice were first immunized at 6 to 8 weeks of age via the footpad (FP), subcutaneous (s.c.), or intraperitoneal (i.p.) route and subsequently on up to three further occasions at 2- to 4-week intervals. Immunizations comprised final volumes of 100 μl per mouse. The animals were studied in groups of three to eight either in single or in duplicated experiments. In experiments using protein adjuvant, the mice were primed with ova (60 μg/mouse) in alum (Alhydrogel 2%; Superfos Biosector, Frederikssund, Denmark) or in complete Freund's adjuvant (CFA; Sigma Chemicals). For ova-liposome immunizations, the mice were initially primed with ova-alum and then immunized 7 to 10 days later via the i.p. route with liposomes containing 100 μg of ganglioside per mouse. Subsequent immunizations were administered at 2-week intervals. Mice immunized with LPS were given 100 μg of LPS per mouse in a 100-μl final volume of CFA (1:1, admixed by vortexing to emulsion for 30 min). For subse-

quent immunizations, LPS was delivered in incomplete Freund's adjuvant (IFA) at 2- to 3-week intervals. Serial blood samples were collected at multiple time points via the tail vein and stored at −20°C for measuring antibody responses. Prebleeds were performed in selected experiments, and significant antibody responses to gangliosides were never seen in these samples. All immunization and venipuncture procedures conformed to United Kingdom Home Office and University of Glasgow institutional guidelines.

Detection of antibodies to gangliosides, LPS, and ova. All gangliosides (GM1, GD1a, GD3, and GQ1b) supplied by Sigma Chemicals have an estimated purity of >95%. GT1a is a rare ganglioside species and is not available in sufficient quantities in purified form for these studies; thus, sera were screened against GQ1b, because it has a structure almost identical to that of GT1a, with which it invariably has immunological cross-reactivity (Fig. 1). Mouse sera were tested for IgG and IgM responses to gangliosides by enzyme-linked immunosorbent assay (ELISA) as previously described (63). Immunolon 2 microtiter plates (Dynatech, Chantilly, Va.) were coated with 200 ng of ganglioside per well in methanol. Each sample was also screened against a methanol-treated, ganglioside-free control well from which background OD readings were obtained. Some serum samples were assayed to determine the isotype (subclass and light-chain type) of the anti-ganglioside antibody response using anti-mouse IgG1, -2a, -2b, and -3 and kappa- and lambda-specific antibodies (diluted 1/3,000). All secondary antibodies were supplied by Sigma Chemicals or by Southern Biotechnology Associates Inc., Birmingham, Ala. The ELISA results for ganglioside-free control wells are shown alongside those for ganglioside-coated wells in all figures in order to demonstrate the nonspecific background signals seen in this glycolipid ELISA, particularly for IgM class antibodies. These nonspecific signals are believed to be increased as a result of polyclonal activation of predominantly IgM-secreting B cells producing natural antibodies that often yield high background levels. Such responses were seen particularly with LPS immunizations. Background OD levels are especially prominent in these assays because of the absence of detergent in the washing and blocking buffers: glycolipids bind polystyrene poorly and are further stripped from ELISA wells by detergents, rendering the assay uselessly insensitive. Antibodies to LPS were detected by coating Immunolon 2 plates with 10 μg of LPS/μl (100 μl per well) in PBS (pH 7.4) overnight at 4°C and then discarding the unbound supernatant. Subsequent steps were performed as for anti-ganglioside antibodies. Antibodies to ova were detected by coating ELISA wells with 100 μl of 10-μg/ml ova per well in bicarbonate coating buffer, pH 9.6, and the same procedure described above was followed except for the addition of 0.05% Tween 20 to the PBS washing buffer.

Statistical analysis. Antibody responses in groups of animals were analyzed for significant intragroup differences using Student's *t* test.

RESULTS

Immunization of BALB/c mice with ganglioside liposomes with and without adjuvants through FP, s.c., and i.p. routes. In order to determine the level of immunological tolerance to gangliosides in mice with a normal complement of self gangliosides, groups of BALB/c mice (*n* = 3) were immunized with the self ganglioside GM1 or GQ1b incorporated into liposomes via the FP, s.c., or i.p. route using a range of immunization strategies. The effect of providing either a TH2- or TH1-type helper environment with ova-alum or ova-CFA priming and subsequent delivery of ova encapsulated in liposomes was examined. Ova-liposomes were also compared with delivery of gangliosides and ova simply admixed by vortexing.

Priming with ova-alum and subsequent immunization with GM1-ova liposomes via the i.p. route yielded significantly elevated anti-GM1 IgM titers compared with undetectable titers following the same regime via FP immunization (mean OD, 0.32 compared with 0.02; *P* = 0.004; three mice in each group; data from bleeds collected 10 days after the second immunization). The anti-GM1 IgM titers obtained via the i.p. route appeared after the first immunization, decayed rapidly, and reappeared at a similar titer on subsequent immunizations (data not shown). These data indicated that the peritoneal compartment, which principally contains B1 cells, could be
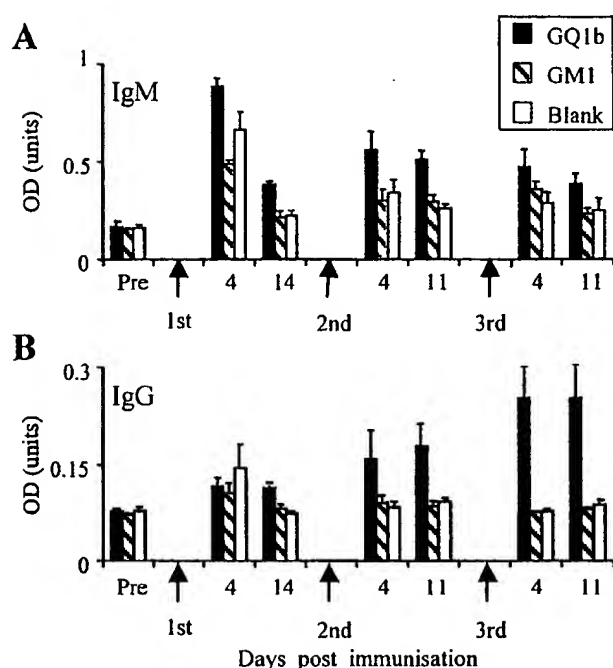
FIG. 2. Anti-ganglioside IgM (A) and IgG (B) responses in BALB/c mice (n = 3) following i.p. immunization with GQ1b-ova liposomes. The error bars indicate SD. The mice were primed with ova-alum and then immunized on day 7 with GQ1b-ova liposomes and bled 4 and 14 days later. The mice were reimmunized 2 and 4 weeks following the initial immunization and rebled 4 and 11 days later. A diminishing IgM response and rising IgG response to GQ1b can be clearly seen upon repeated immunization. The IgG subclass of the anti-GQ1b response was exclusively IgG3 (mean OD at 1:200 serum dilution, 0.61 ± 0.16 SD).

more readily stimulated to produce anti-GM1 IgM antibody-secreting B cells than the systemic B2 compartment, which would be stimulated by FP immunization. Sequential immunizations, via either the FP or i.p. route, with GM1 liposomes in the absence of any ova priming or subsequent ova administration yielded mean OD values for IgG and IgM antibodies to GM1 at or close to zero. These data indicate that exposure of any naturally occurring GM1-specific B cells to GM1 liposomes alone, in either the conventional B2- or i.p. B-cell compartments, is not in itself a sufficient stimulus to induce secretion of anti-GM1 IgM antibodies.

In order to examine the class-switching characteristics of ganglioside-ova liposome administration in the peritoneal compartment, groups of mice were primed with ova-alum and then immunized with GQ1b-ova liposomes via the i.p. route. As described above for GM1-ova liposomes and anti-GM1 antibodies, immunization via the i.p. route with GQ1b-ova liposomes induced anti-GQ1b IgM antibodies. Class switching to IgG clearly occurred, albeit at a low level, after the second and third immunizations in a pattern suggestive of a secondary immune response (Fig. 2). No response to GM1 was seen, indicating the specificity of the response for GQ1b. Subclass analysis of the IgG response demonstrated all the anti-GQ1b IgG activity to be IgG3, the IgG subclass most usually seen when B1 cells switch class. These data indicate that i.p. immunization with ganglioside-ova liposomes stimulates B1 B cells

to secrete anti-ganglioside antibodies that have the capacity to switch to IgG3.

In control experiments, anti-ova IgM and IgG antibodies were highly elevated in all groups of mice primed via either the FP or i.p. route with ova-alum or ova-CFA and subsequently boosted with ganglioside-ova liposomes. The mice showed a primary and then a secondary immune response to ova, with diminution of IgM titers and increase of IgG titers over time, indicating that ova is being efficiently delivered and processed (data not shown).

In order to establish the effectiveness of extruded liposomes compared with simpler lipid preparations, immunizations of groups of mice (n = 3) with extruded GM1-ova liposomes or GM1 vortexed with ova in PBS were compared. The former was efficient at inducing anti-GM1 antibodies, whereas the latter failed to induce any anti-GM1 antibody responses (data not shown). This indicates that the preparation of uniform extruded liposomes with encapsulated ova is a necessary part of the immunization protocol. In experiments comparing the effects of CFA and alum as priming agents in conjunction with ova, no significant differences were observed in total IgM or IgG anti-ganglioside antibody titers when immunizations were performed via either the s.c. or i.p. route (data not shown).

These data indicate that in normal mice, the B-cell pool that can be expanded to secrete antibodies to self gangliosides requires an appropriate antigen configuration (in this case extruded liposomes) in the presence of accessory signals (provided by ova as an adjuvant) and is largely limited to an IgM and IgG3 response in the peritoneal compartment, suggestive of involvement principally of B1 B cells. The conventional B2 B-cell pool, stimulated by s.c. or FP immunization, is highly tolerant of self gangliosides.

Immunization of GalNAcT$^{-/-}$ and GalNAcT$^{+/+}$ mice with ganglioside liposomes. In order to study the effect of tolerance to self gangliosides on antibody responses, mice with or without complex gangliosides were immunized with GD1a, GQ1b, or GD3. GalNAcT$^{-/-}$ mice possess only GM3 and GD3, whereas wild-type GalNAcT$^{+/+}$ mice possess a normal complement of simple and complex gangliosides. Groups of GalNAcT$^{-/-}$ or GalNAcT$^{+/+}$ mice (three to five mice per group) were first primed i.p. with ova-alum and then immunized i.p. with GQ1b-ova or GD1a-ova liposomes. All immunized GalNAcT$^{-/-}$ mice developed highly elevated anti-GQ1b or anti-GD1a antibody responses that switched to IgG after the second and third immunizations, consistent with secondary immune responses (Fig. 3). As observed for BALB/c mice, GQ1b-ova liposomes also induced very modest IgM and IgG antibody responses in wild-type GalNAcT$^{+/+}$ mice; however, they were especially small in the IgG class compared to IgG responses in GalNAcT$^{-/-}$ mice. The IgG subclass response in GQ1b-ova liposome-immunized GalNAcT$^{-/-}$ mice was restricted to IgG3 and IgG1, suggesting possible involvement of peritoneal B1 B cells to account for the IgG3 and a TH2-driven B2 response accounting for the IgG1 that would be expected following priming with the TH2-type adjuvant, ova-alum (data not shown).

Despite the development of a high anti-GQ1b IgG response in the GalNAcT$^{-/-}$ mice, the IgM response to GQ1b in the GalNAcT$^{-/-}$ mice was insignificantly elevated compared with either the anti-GD1a IgM response in GalNAcT$^{-/-}$ mice or
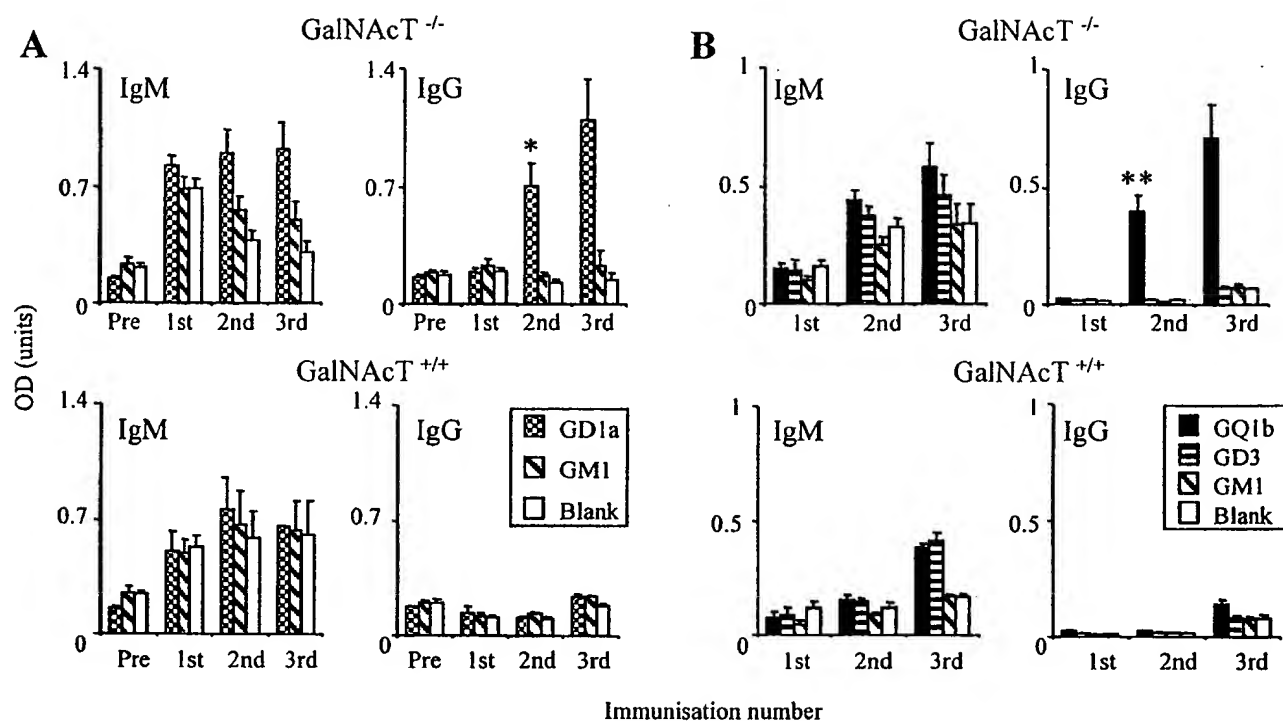
FIG. 3. Anti-ganglioside antibody responses in GalNAcT$^{-/-}$ and GalNAcT$^{+/+}$ mice following i.p. immunization with GD1a-ova liposomes (A) and GQ1b-ova liposomes (B). The error bars indicate SD. Group sizes were as follows: GD1a-ova liposomes, $n = 8$ (GalNAcT$^{-/-}$) and $n = 5$ (GalNAcT$^{+/+}$); GQ1b-ova liposomes, $n = 5$ (GalNAcT$^{-/-}$) and $n = 3$ (GalNAcT$^{+/+}$). The mice were primed with ova-alum and immunized on day 7 with GQ1b-ova or GD1a-ova liposomes. The mice were further immunized at 2-week intervals and bled 4 days after each immunization. Elevated IgG anti-GD1a antibody titers are evident in GalNAcT$^{-/-}$ mice compared with GalNAcT$^{+/+}$ mice, and they increase upon subsequent immunization (*, $P < 0.005$ after the second immunization). Elevated IgG anti-GQ1b antibody titers are evident in GalNAcT$^{-/-}$ mice compared with GalNAcT$^{+/+}$ mice (**, $P < 0.001$ after the second immunization).

the anti-GQ1b IgM response in wild-type mice (Fig. 3). Furthermore, GalNAcT$^{+/+}$ mice immunized with GQ1b also developed a greater anti-GD3 response than GalNAcT$^{-/-}$ mice. GQ1b shares a disialosyl epitope with GD3 (Fig. 1), sited on the terminal galactose of the ganglioside core. IgM antibodies frequently react with this epitope, irrespective of any adjacent oligosaccharide structure, and many human and mouse IgM MAbs cross-react with GQ1b, GD3, and other disialylated structures, including bacterial LPS. These data indicate that the anti-disialosyl IgM response, which most likely arises from the i.p. B1 pool, is suppressed in GalNAcT$^{-/-}$ mice (which contain large amounts of GD3 compared with the wild type) but that the matured IgG anti-GQ1b response, which is specific for a unique GQ1b epitope(s) not shared by GD3, is suppressed in the wild type (which contains GQ1b) but not suppressed in the GQ1b-deficient, GD3-rich GalNAcT$^{-/-}$ mouse.

In order to directly address the antibody response to GD3, we immunized GalNAcT$^{-/-}$ (GD3-high) and GalNAcT$^{+/+}$ (GD3-normal) mice ($n = 5$) with GD3-ova liposomes and found the GalNAcT$^{-/-}$ mice to be completely unresponsive to GD3. In comparison, anti-GD3 responses were seen in four of five wild-type mice in the IgM class, which switched in three of four mice to produce low levels of anti-GD3 IgG (Fig. 4). These data indicate that normal mice possess a pool of GD3-reactive B cells (most likely i.p. B1 cells) that can be expanded by i.p. immunization with GD3 to secrete predominantly IgM

antibodies and can be suppressed by high levels of endogenous GD3.

Immunization of GalNAcT$^{-/-}$ and GalNAcT$^{+/+}$ mice with C. jejuni LPSs bearing ganglioside-like core OS structures. Our previous studies have shown that immunization of mice with C. jejuni LPSs containing ganglioside-mimicking core OS structures, using a variety of immunization protocols and mouse strains, leads to the generation of anti-ganglioside antibodies. However, the responses are generally poor, highly variable between animals, and principally IgM class. In order to determine the degree to which tolerance to self gangliosides might be limiting this response, we immunized GalNAcT$^{-/-}$ and GalNAcT$^{+/+}$ mice (three to five mice per group) with HS:4 and HS:19(GM1$^+$ GT1a$^+$) LPSs emulsified in CFA (a TH1-driving adjuvant) followed by serial immunizations with LPS in IFA (Fig. 5). LPS from HS:4, which predominantly bears a GD1a-like epitope, induced high levels of IgG class antibody to GD1a in GalNAcT$^{-/-}$ mice by the third immunization, in contrast with no response in wild-type GD1a-containing GalNAcT$^{+/+}$ mice and no response to the structurally dissimilar ganglioside GM1 (Fig. 5A). In the IgM class, it is clearly evident that nonspecific background signals are greatly increased upon immunization with LPS in both GalNAcT$^{-/-}$ and GalNAcT$^{+/+}$ mice, as manifested by equivalently high OD readings from non-ganglioside-coated blank wells and from the ganglioside-coated wells; this is interpreted as due to nonspe-
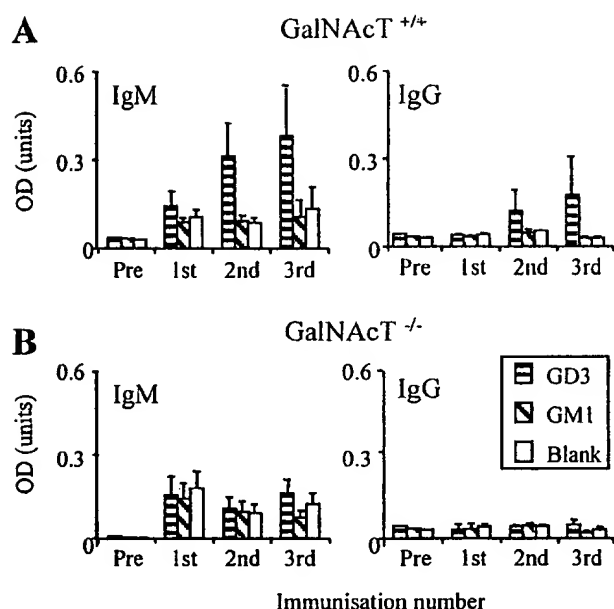
A   GalNAcT $^{+/+}$

B   GalNAcT $^{-/-}$

Immunisation number

FIG. 4. Anti-ganglioside antibody responses in GalNAcT$^{+/+}$ (A) and GalNAcT$^{-/-}$ (B) mice (two groups; $n = 5$) following repeated i.p. immunizations with GD3-ova liposomes. The error bars indicate SD. The mice were primed with ova-alum, immunized on day 7 with GD3-ova liposomes, and bled 4 days later. The mice were reimmunized at 2-week intervals and bled 4 days after each immunization. Anti-GD3 IgM and IgG antibody responses are depressed in the GD3-rich GalNAcT$^{-/-}$ mice compared with GalNAcT$^{+/+}$ mice, but this did not reach statistical significance ($P = 0.08$ post-third immunization for IgM, and $P = 0.3$ for IgG).

cific polyclonal activation of B1 cells and underlines the importance of including these control data. LPS from HS:19(GM1$^+$ GT1a$^+$)-induced high levels of IgG class antibody to both GQ1b and GM1 in GalNAcT$^{-/-}$ mice (which lack GT1a, GQ1b, and GM1) compared with those in wild-type GalNAcT$^{+/+}$ mice (Fig. 5B). Sera were screened against GQ1b because it has a structure almost identical to that of GT1a, with which it invariably has immunological cross-reactivity (Fig. 1; also see Materials and Methods). IgG subclass analysis revealed class switching to IgG3 > IgG2b = IgG2a > IgG1, suggesting B1 switching to IgG3 and B2 switching to the TH1-preferred IgG2a/b and -3 subclasses had occurred (data not shown). In a larger group of 11 GalNAcT$^{-/-}$ mice immunized with HS:19(GM1$^+$ GD1a$^+$) LPS in CFA followed by IFA, a similar subclass pattern was observed.

In order to more formally demonstrate the presence of B-cell memory for gangliosides, GalNAcT$^{-/-}$ and GalNAcT$^{+/+}$ mice ($n = 4$) received a primary immunization with HS:19(GM1$^+$ GD1a$^+$) LPS in CFA, were screened for IgG anti-GD1a on day 7, and then were boosted on day 20 and rescreened on day 24. The anti-GD1a IgG response in GalNAcT$^{-/-}$ mice showed typical characteristics of an antigen-specific memory response, being absent on day 7 (mean OD, 0.009 ± 0.007 standard deviation [SD]) and present on day 25 (mean OD, 0.41 ± 0.23 SD). No anti-GD1a IgG responses were observed in GalNAcT$^{+/+}$ mice (mean OD on day 7, 0.002 ± 0.001 SD; day 25, 0.015 ± 0.015 SD). Subsequent

immunizations further magnified the IgG response (data not shown). These results indicate that tolerance to self gangliosides is the major factor limiting a class-switched memory response to ganglioside-mimicking core OS structures in *C. jejuni* LPS.

Analysis of individual GalNAcT$^{-/-}$ mice immunized with HS:19(GM1$^+$ GT1a$^+$) LPS showed that two of four generated both anti-GQ1b and GM1 responses, whereas two of four developed anti-GQ1b responses alone. The ratio of GT1a to GM1 on HS:19(GM1$^+$ GT1a$^+$) is unknown, but the quantitatively major structure might be predicted to induce antibodies more favorably than the less abundant structure. In order to address this directly, we immunized groups of GalNAcT$^{-/-}$ and GalNAcT$^{+/+}$ mice (four to five mice per group) with HS:4 and HS:19(GM1$^+$ GD1a$^+$) LPSs that are known to contain GD1a/GM1 ratios of 9:1 and 1:1, respectively. In the group of eight GalNAcT$^{-/-}$ mice immunized with HS:4, GD1a was clearly immunodominant over GM1, with only anti-GD1a responses being seen, whereas in the group immunized with HS:19(GM1$^+$ GD1a$^+$) LPS, antibody responses to both GD1a and GM1 were present (Table 2). Among HS:19(GM1$^+$ GD1a$^+$) LPS-immunized GalNAcT$^{-/-}$ mice, four developed an antibody response to GD1a alone and one developed an antibody response to GM1 alone, which persisted on secondary immunization. However, of the three mice that responded to both GD1a and GM1 on primary immunization, two of three failed to mount a secondary response to GM1 but did respond to GD1a. Two of eight GalNAcT$^{+/+}$ mice immunized with HS:19(GM1$^+$ GD1a$^+$) LPS developed low-magnitude but nevertheless significant IgG responses to GD1a (data not shown), and none of eight GalNAcT$^{+/+}$ mice immunized with HS:4 LPS developed IgG responses to either GM1 or GD1a.

In control immunization experiments with *C. jejuni* serostrain HS:3 LPS, which is not associated with GBS and lacks any ganglioside-like epitopes, neither GalNAcT$^{-/-}$ nor GalNAcT$^{+/+}$ mice developed anti-ganglioside antibodies, but they did possess strong antibody responses to HS:3 LPS epitopes when screened in ELISA against HS:3, confirming that the immunization was effectively delivered (data not shown).

Immunization of GalNAcT$^{-/-}$ mice with *C. jejuni* HS:10. Experiments with GD3-ova liposomes showed complete unresponsiveness of GalNAcT$^{-/-}$ mice to immunization with GD3, compared with responding wild-type mice, suggesting a high level of B-cell tolerance induced by overexpression of GD3 in GalNAcT$^{-/-}$ mice. However, among GalNAcT$^{-/-}$ mice immunized with HS:19(GM1$^+$ GT1a$^+$), two of four animals with anti-GQ1b antibodies also developed anti-GD3 responses, and two of four GalNAcT$^{+/+}$ mice developed anti-GD3 antibodies without anti-GQ1b antibodies. This suggests that there is an intrinsic pool of GD3-specific B cells that do not respond to immunization with our schedule of GD3-ova liposomes in GalNAcT$^{-/-}$ mice but are not entirely suppressed following immunization with GD3-like oligosaccharides associated with a highly potent immunomodulator like LPS. To explore this further, GalNAcT$^{-/-}$ mice ($n = 6$) were immunized with LPS from the *C. jejuni* strain HS:10, which contains GD3-like structures in its LPS. No significant anti-GD3 IgM responses were seen. However, three of six mice developed low-level IgG antibodies to GD3 after the third immunization (mean OD, 0.18 ± 0.08 SD; $n = 6$ mice), indicating that tolerance to GD3 can
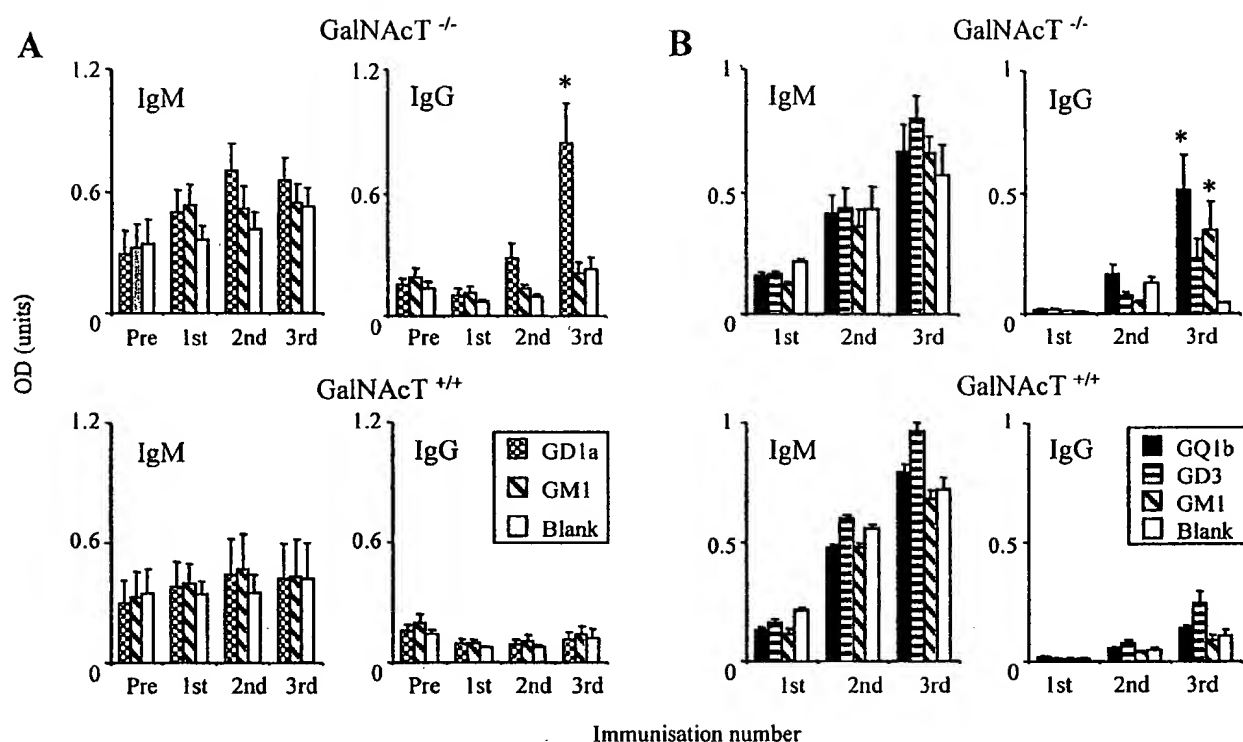
FIG. 5. Anti-ganglioside antibody responses in GalNAcT$^{-/-}$ and GalNAcT$^{+/+}$ mice after i.p. immunization with HS:4 LPS (A) or HS:19(GM1$^+$ GT1a$^+$) LPS (B) in CFA and subsequently at 2-week intervals with LPS in IFA. The error bars indicate SD. The group sizes were as follows: HS:4 group, $n = 9$ (GalNAcT$^{-/-}$ mice) and $n = 7$ (GalNAcT$^{+/+}$ mice); HS:19(GM1$^+$ GT1a$^+$) group, $n = 5$ (GalNAcT$^{-/-}$ mice) and $n = 3$ (GalNAcT$^{+/+}$ mice). All sera were screened 4 days after each immunization. IgG anti-ganglioside antibodies, corresponding to the core OS structure on the immunizing LPS [GD1a for HS:4 LPS; GT1a and GM1 for HS:19(GM1$^+$ GT1a$^+$) LPS], appear after the second and third immunizations in significantly greater amounts in GalNAcT$^{-/-}$ than in GalNAcT$^{+/+}$ mice (*, $P < 0.05$). In the ganglioside ELISA, GQ1b is substituted for GT1a (see Materials and Methods for details).

be overcome when the GD3-like epitope is delivered on LPS, even in GD3-ova liposome-unresponsive mice. GalNAcT$^{-/-}$ mice immunized with other LPS species which do not contain GD3 or GD3-like epitopes did not generate anti-GD3 responses, indicating that the anti-GD3 response is not simply due to a polyclonal activating effect of LPS in this mouse strain.

Anti-ganglioside responses in C3H/HeN and C3H/HeJ mice immunized with ganglioside-bearing LPS. Our experiments comparing anti-ganglioside antibody responses following immunization with ganglioside-mimicking LPS species or native

TABLE 2. Immune responses to GM1 and GD1a in GalNAcT$^{-/-}$ mice immunized with HS:4 and HS:19(GM1$^+$ GD1a$^+$) LPSs

Characteristic	Value	
	HS:4	HS:19(GM1$^+$ GD1a$^+$)
GM1/GD1a ratio	1:9	1:1
No. of animals immunized	8	8
No. of responders		
GM1 alone	0	1
GD1a alone	8	4
GM1 and GD1a	0	3[a]

[a] In the three mice that developed both anti-GD1a and -GM1 IgG responses after two immunizations, no response to GM1 could be detected in two of three mice on subsequent boosts, although a secondary response to GD1a was observed.

gangliosides suggest that in some situations, such as that seen with HS:10 LPS and GD3, the LPS provides a stronger antigenic stimulus than the ganglioside. In order to determine whether the lipid A component of LPS is providing any accessory help to B cells in generating antibody responses to LPS core OS structures, we examined antibody responses in C3H/HeJ mice. Lipid A associates with lipid binding protein, binds to CD14 on B cells, and signals via the transmembrane Toll receptor, Tlr4. C3H/HeJ mice harbor a mutation in the Toll receptor which renders them unresponsive to lipid A signaling via CD14, but BCR and other accessory signaling pathways remain intact. HS:4 LPS, which bears the immunodominant GD1a structure, was used to examine core OS responses in LPS-responsive C3H/HeN and LPS-unresponsive C3H/HeJ mice (Fig. 6). All C3H/HeN mice showed some anti-GD1a antibody response, whereas responses were significantly attenuated in C3H/HeJ mice, with only two of five mice developing very low-level anti-GD1a IgG antibodies. The mean anti-GD1a responses were greater in magnitude and developed earlier in C3H/HeN than in C3H/HeJ mice. The profile of anti-GD1a antibodies over time did not show any clear secondary response, remaining at constant levels upon subsequent immunizations (data not shown). This is consistent with the tolerance to GD1a one would predict in a GD1a-bearing mouse and from the lack of a substantial GD1a-specific B-cell
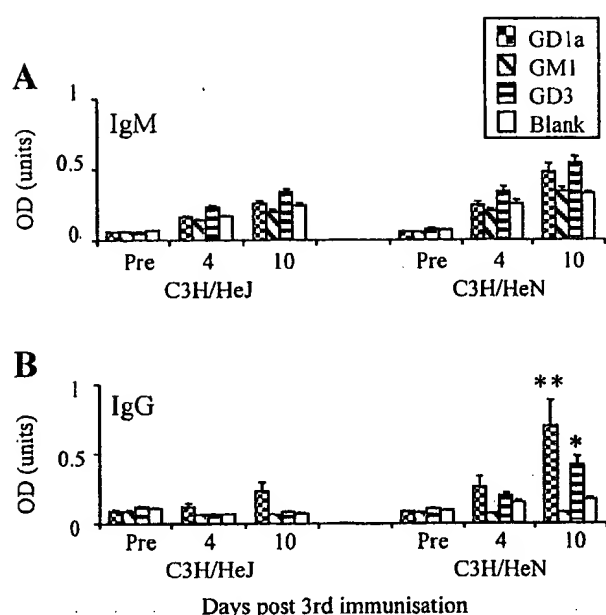
FIG. 6. Anti-ganglioside IgM (A) and IgG (B) antibody responses following HS:4 LPS immunization of C3H/HeN and C3H/HeJ (LPS low responder) mice. The error bars indicate SD. HS:4 LPS bears a GD1a-like epitope. Groups of mice ($n = 5$) received serial immunizations with HS:4 LPS in CFA-IFA at 2-week intervals, and sera were assayed on days 4 and 10 following each immunization. C3H/HeN mice showed significantly greater IgG responses than C3H/HeJ mice to GD3 (*, $P = 0.002$), and elevated IgG responses to GD1a, compared with C3H/HeJ mice (**, $P = 0.066$).

FIG. 7. Anti-ganglioside IgM (A) and IgG (B) antibody responses in BALB/c mice immunized with HS:19(GM1$^+$ GT1a$^+$) LPS coadministered with anti-CD40 antibody or control antibody, GL117. Groups of BALB/c mice ($n = 4$) were immunized i.p. with HS:19(GM1$^+$ GT1a$^+$) LPS and anti-CD40 antibody or GL117 and then reimmunized on day 21 and bled on day 28 (7 days post-second immunization). Mice treated with anti-CD40 antibody showed slightly greater anti-GQ1b and anti-GD3 responses than control antibody-treated mice (*, $P < 0.005$; **, $P < 0.05$), but there was no significant difference in anti-GM1 antibody responses.

memory compartment. Interestingly, C3H/HeN mice also mounted a modest anti-GD3 response, despite the absence of GD3 on HS:4 LPS, suggesting that the anti-GD3 antibodies have arisen through polyclonal B-cell activation by LPS, which included a pool of GD3-specific B1 cells. C3H/HeJ mice did not exhibit this anti-GD3 response, again suggesting it is due to Lipid A-mediated polyclonal activation. Thus, the data indicate that the lipid A component of LPS mediates an important signaling pathway that helps B cells respond to ganglioside-like core OS structures.

Effect of CD40 activation in enhancing anti-LPS core OS responses in BALB/c mice. B cells proliferate and differentiate into antibody-forming cells in response to CD40 ligation, either provided naturally by cognate TH cell interactions or via experimental mechanisms, such as anti-CD40-stimulating antibodies. Since LPS lacks protein and thus has no clearly identified mechanism for recruiting T-cell-dependent help in the mouse, we examined the possibility that coadministration of anti-CD40 antibodies with ganglioside-mimicking LPS might provide the accessory help that would also result in breaking tolerance to self gangliosides. Groups of BALB/c mice ($n = 4$) were immunized with HS:4 or HS:19(GM1$^+$ GT1a$^+$) LPS containing liposomes admixed with anti-CD40 antibody or the control antibody GL117 (0.5 mg/mouse) in the absence of any protein adjuvant. Sera studied by ELISA for anti-ganglioside and anti-LPS antibodies on day 7 following HS:4 immunization with CD40 or GL117 exhibited an increase in the nonspecific background signal, more marked with the CD40 antibody (IgM
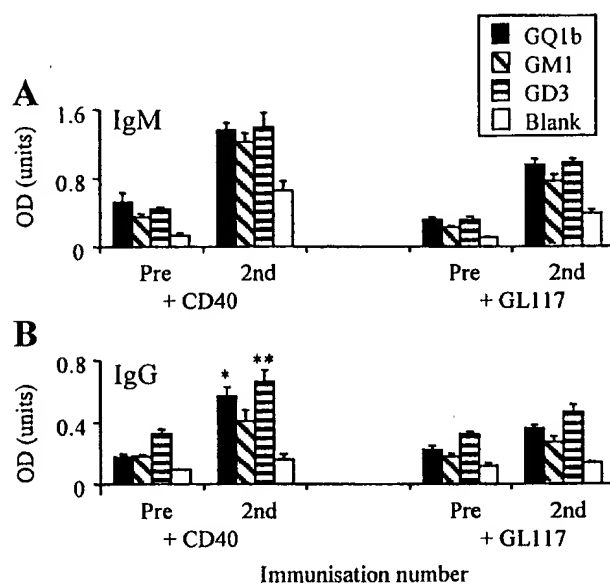
mean OD on day 0, 0.15 ± 0.04 SD; day 7, 0.87 ± 0.08 SD) than control antibody (mean OD on day 0, 0.10 ± 0.005 SD; day 7, 0.19 ± 0.04 SD). This elevation in background, attributed to elevated serum IgM and IgG as a result of nonspecific polyclonal B-cell activation, partially obscured any underlying ganglioside- or LPS-specific responses, making interpretation difficult. Although anti-GD3 IgM and IgG responses were elevated above background level, they did not reach significance compared with the control antibody GL117. However, the absence of GD3 on HS:4 LPS again indicates that anti-GD3 antibodies form part of the natural memory repertoire.

On day 28 following immunization with HS:19(GM1$^+$ GT1a$^+$) LPS, background IgM levels had fallen compared with day 7 (data not shown), and enhancement of the ganglioside-specific signal, expected to comprise GQ1b, GM1, and GD3 for HS:19(GM1$^+$ GT1a$^+$) LPS, could be seen, although this did not achieve statistical significance compared with the control MAb, GL117 (Fig. 7A). However, in the IgG class on day 28 (Fig. 7B), a significant increase in GQ1b and GD3 titers was seen in the anti-CD40-treated mice compared with the control antibody ($P < 0.005$ and $P < 0.05$, respectively), indicating that anti-CD40 antibody had a modest effect on expanding the IgG anti-ganglioside B-cell pool and thus could partially overcome tolerance to self gangliosides.

DISCUSSION

Gangliosides are self glycolipid structures widely distributed on extracellular surfaces throughout the body and thus subject

to normal mechanisms regulating B-cell tolerance to TI antigens, as also seen, for example, in the ABO blood group system (61). In attempts to enhance their immunogenicity in mice, many studies have converted gangliosides to TD antigens by conjugation to proteins or incorporation into protein-enriched liposomes (1, 26, 31, 38). Indeed, we show here that BALB/c mice immunized with GQ1b-ova liposomes do generate low-level anti-GQ1b responses that show characteristics of a memory response. Priming with ova is a necessary step and likely acts through the generation of an anti-ova-specific TH cell pool that then helps the B-cell pool recognizing the ganglioside to switch class and affinity mature. This model relies on uptake of liposome by B cells and subsequent presentation of ova peptides in association with major histocompatibility complex class II to the primed ova-specific TH cells. Only mice immunized i.p. with ganglioside-ova liposomes responded in this manner, whereas immunization via the FP or s.c. route, although generating strong anti-ova responses, failed to generate anti-ganglioside antibodies. These data strongly suggest that the i.p. B1-cell pool can be more readily stimulated to secrete anti-ganglioside antibodies but that the conventional B2-cell pool is highly tolerant to self gangliosides.

I.p. immunization of normal mice with *C. jejuni* LPS containing ganglioside-like epitopes typically results in transient IgM anti-ganglioside responses that lack a highly developed secondary immune response. Since the gut is the principal site of infection with LPS-bearing enteric bacteria, the production of low-affinity IgM anti-ganglioside antibodies upon exposure to *C. jejuni* LPS is consistent with models of a natural protective repertoire in early host defense (15, 53). Provided the maturation of this response is regulated, the rapid production of low-affinity antibody to host-mimicking carbohydrate structures on LPS-bearing bacteria outweighs the danger of developing autoimmune disease mediated through such antibodies.

GalNAcT$^{+/+}$ mice, which bear a normal complement of gangliosides, developed similar responses to BALB/c mice when immunized with GQ1b liposomes. In contrast, GalNAcT$^{-/-}$ mice, which express only GM3 and GD3, developed highly elevated anti-ganglioside-specific secondary responses when immunized with liposomes containing non-self GD1a or GQ1b but no response to self GD3, a quantitatively dominant tissue ganglioside in the GalNAcT$^{-/-}$ mouse. Thus, tolerance to self gangliosides is clearly the major factor that prevents the maturation of antibody responses, as previously observed in studies of GD1a ganglioside (38).

This study also clearly shows that tolerance to self gangliosides is the major factor restricting the antibody response to ganglioside-mimicking LPS core OSs. Thus, GalNAcT$^{-/-}$ mice are an important tool for studying antibody responses to *C. jejuni* LPSs that bear ganglioside-like structures. These responses in the GalNAcT$^{-/-}$ mouse also switch class to IgG and exhibit memory. It is also evident that the antibody response to ganglioside-like structures on LPS is dependent on both the ganglioside mimicked and its level of expression. For example, the GM1/GD1a ratio of 1:9 on HS:4 LPS favors the production of anti-GD1a antibodies, whereas immunization with HS:19(GM1$^+$ GD1a$^+$), with a GM1/GD1a ratio of 1:1, produces both anti-GM1 and anti-GD1a antibodies. This differential effect between HS:4 and HS:19(GM1$^+$ GD1a$^+$) LPSs may be related to the differences in efficiency of density-dependent

cross-linking of the BCR specific for GM1 and GD1a; thus, the environment created by a 9:1 ratio of GD1a over GM1 favors activation of GD1a-specific B cells.

In mice immunized with ganglioside liposomes containing ova, or with ganglioside-protein conjugates, the signals necessary for generating class-switching and memory responses are dependent upon the presence of protein. BCR clustering mediated by repeating carbohydrate epitopes, as found in TI-2 antigens, can often lead to B-cell proliferation with antibody production in the absence of additional stimuli. However, our ganglioside liposomes, designed to mimic TI-2 antigens, clearly required protein (in the form of ova) to be effective immunogens.

It is unclear from our experiments how class switching and memory responses were generated in response to the ganglioside-mimicking core OS structures in ganglioside-deficient mice. The LPS was delivered in CFA at the first immunization but subsequently in protein-free IFA. One possibility is that the lipid associated with bacterial polysaccharide antigens could be presented via CD1d to generate ganglioside-specific T cells; however, there is no previously defined example by which such T cells could provide cognate help to polysaccharide-specific B cells (20, 58). LPS is a TI-1 antigen that acts as a polyclonal B-cell activator; such responses are principally IgM and do not exhibit memory. We saw some evidence that such polyclonal activation occurred and that this was in part directed against GD3 (see below). Other than GD3 responses, the anti-ganglioside antibody response to LPS was critically dependent upon the core OS structure, exhibiting clear evidence of mimicry.

As an alternative mechanism, the lipid A moiety of LPS might be providing a secondary signal to drive the maturation of anti-core OS responses. We found the responses of C3H/HeJ mice, hyposensitive to lipid A due to a mutation in Tlr4 (3, 13, 33, 52, 53), were diminished in comparison to those of normally responding C3H/HeN mice, bearing in mind that the responses to core OS structures in ganglioside-tolerant C3H/HeJ and C3H/HeN mice would not be expected to be as high as in GalNAcT$^{-/-}$ mice. This provides in vivo evidence that lipid A signaling via Tlr4 is an important secondary signaling pathway contributing to the B-cell response to TI epitopes within LPS core OS structures.

The terminal disialosyl structure of ganglioside GD3, also present on HS:10 LPS, appears to be a dominant antigen in the mouse. Even GalNAcT$^{-/-}$ mice, which contain large amounts of GD3, generated low but significant anti-GD3 responses when immunized with HS:10, although they did not respond to GD3 liposomes. This further emphasizes the potent stimulatory properties of LPS in comparison to liposomes. GQ1b liposomes that also contain this terminal disialosyl epitope generated anti-GQ1b responses in BALB/c and GalNAcT$^{+/+}$ mice, whereas in contrast, GD1a-immunized GalNAcT$^{+/+}$ mice did not develop anti-GD1a responses. In addition to anti-GD3 responses generated through GD3-specific BCR on B cells, it is also evident that anti-GD3 antibodies can arise through polyclonal B-cell activation, mediated by lipid A. Thus, C3H/HeN mice immunized with HS:4 LPS frequently developed anti-GD3 antibody responses, although no GD3-mimicking structures are present on this LPS. The predominance of anti-GD3 antibodies arising from both antigen-spe-

cific and nonspecific B-cell activation indicate that this specificity forms an important part of the natural antibody repertoire in mice, most likely produced by peritoneal B1 cells, involved in early host defense against enteric bacteria.

The role of CD40 ligation, using stimulating antibodies, in substituting for cognate T-cell help has been previously considered and tested with respect to polysaccharide antigens (12, 16). We thus considered this a possible mechanism for driving anti-ganglioside antibody responses following immunization with LPS in the absence of any protein adjuvant. We observed a very modest increment in ganglioside responses to LPS, but this was not observed in parallel experiments with ganglioside liposomes (data not shown). Thus, although CD40 is clearly critical to accessory signaling in cognate T-cell help, we were unable to reproduce the effect to any great extent using this experimental paradigm.

In human subjects with uncomplicated enteritis caused by *C. jejuni* strains containing self-ganglioside mimics in the core OS structures, one would predict that antibody responses to the self carbohydrate structures should be suppressed. Indeed, acute-phase anti-ganglioside antibodies do not arise in this clinical group (6, 47). However, in the small proportion of subjects with *Campylobacter* enteritis who develop GBS, tolerance is clearly broken in that high-titer class-switched anti-ganglioside antibodies arise in response to ganglioside mimics in the LPS. Why such individuals are unable to maintain tolerance in the setting of this infection is unknown. There is no evidence that such individuals express smaller amounts of tissue gangliosides than normal, as is the case with GalNAcT$^{-/-}$ mice. It seems more likely that any negative selection is overcome by powerful TD help provided by elements of the infection. The class switching to the TD IgG1 and IgG3 subclasses that occurs in GBS supports this view and also suggests that such B cells originate in the B2 compartment. A T helper repertoire could arise de novo as part of the infectious episode triggering GBS or could be stimulated from the memory compartment, the latter possibly providing a more potent TD environment. In either of these situations, the time course of B-cell antibody production would be that of a primary response, as is the pattern seen in GBS. Positive selection by self antigen, LPS, or other microbial components of B cells in the B1 compartment that accounts for low-affinity predominantly IgM anti-carbohydrate antibodies would be unlikely to result in the high-titer, class-switched anti-ganglioside antibodies seen in GBS (24). Irrespective of the mechanisms by which anti-ganglioside antibodies arise in GBS, these experiments show that ganglioside-mimicking *C. jejuni* LPS, when combined with appropriate TD help, provided here by protein adjuvants, can induce a high-titer class-switched antibody response exhibiting memory and that the major negative regulator of this response is tolerance to self gangliosides.

ACKNOWLEDGMENTS

REFERENCES

1. **Alfonso, M., and J. Zeuthen.** 1996. Generation of human monoclonal antibodies against ganglioside antigens and their applications in the diagnosis and therapy of cancer. Acta Oncol. **35:**287–295.

2. **Allos, B. M.** 1997. Association between *Campylobacter* infection and Guillain-Barre syndrome. J. Infect. Dis. 176(Suppl. 2):S125–S128.

3. **Anderson, K. V.** 2000. Toll signaling pathways in the innate immune response. Curr. Opin. Immunol. **12:**13–19.

4. **Ang, C. W., M. A. De Klerk, H. P. Endtz, B. C. Jacobs, J. D. Laman, F. G. van der Meche, and P. A. van Doorn.** 2001. Guillain-Barre syndrome- and Miller Fisher syndrome-associated *Campylobacter jejuni* lipopolysaccharides induce anti-GM1 and anti-GQ1b antibodies in rabbits. Infect. Immun. **69:**2462–2469.

5. **Ang, C. W., M. Koga, B. C. Jacobs, N. Yuki, F. G. van der Meche, and P. A. van Doorn.** 2001. Differential immune response to gangliosides in Guillain-Barre syndrome patients from Japan and The Netherlands. J. Neuroimmunol. **121:**83–87.

6. **Ang, C. W., J. D. Laman, H. J. Willison, E. R. Wagner, H. P. Endtz, M. A. De Klerk, A. P. Tio-Gillen, N. Van den Braak, B. C. Jacobs, and P. A. Van Doorn.** 2002. Structure of *Campylobacter jejuni* lipopolysaccharides determines antiganglioside specificity and clinical features of Guillain-Barre and Miller Fisher patients. Infect. Immun. **70:**1202–1208.

7. **Ang, C. W., N. Yuki, B. C. Jacobs, M. Koga, P. A. Van Doorn, P. I. Schmitz, and F. G. Van Der Meche.** 1999. Rapidly progressive, predominantly motor Guillain-Barre syndrome with anti-GalNAc-GD1a antibodies. Neurology **53:**2122–2127.

8. **Archelos, J. J., and H. P. Hartung.** 2000. Pathogenetic role of autoantibodies in neurological diseases. Trends Neurosci. **23:**317–327.

9. **Aspinall, G. O., S. Fujimoto, A. G. McDonald, H. Pang, L. A. Kurjanczyk, and J. L. Penner.** 1994. Lipopolysaccharides from *Campylobacter jejuni* associated with Guillain-Barre syndrome patients mimic human gangliosides in structure. Infect. Immun. **62:**2122–2125.

10. **Aspinall, G. O., C. M. Lynch, H. Pang, R. T. Shaver, and A. P. Moran.** 1995. Chemical structures of the core region of *Campylobacter jejuni* O:3 lipopolysaccharide and an associated polysaccharide. Eur. J. Biochem. **231:**570–578.

11. **Aspinall, G. O., A. G. McDonald, H. Pang, L. A. Kurjanczyk, and J. L. Penner.** 1994. Lipopolysaccharides of *Campylobacter jejuni* serotype O:19: structures of core oligosaccharide regions from the serostrain and two bacterial isolates from patients with the Guillain-Barre syndrome. Biochemistry **33:**241–249.

12. **Barr, T. A., and A. W. Heath.** 1999. Enhanced in vivo immune responses to bacterial lipopolysaccharide by exogenous CD40 stimulation. Infect. Immun. **67:**3637–3640.

13. **Beutler, B.** 2000. Tlr4: central component of the sole mammalian LPS sensor. Curr. Opin. Immunol. **12:**20–26.

14. **Chen, Z. C., M. Z. Radic, and U. Galili.** 2000. Genes coding evolutionary novel anti-carbohydrate antibodies: studies on anti-Gal production in alpha 1,3 galactosyltransferase knock out mice. Mol. Immunol. **37:**455–466.

15. **Dighiero, G., and N. R. Rose.** 1999. Critical self-epitopes are key to the understanding of self-tolerance and autoimmunity. Immunol. Today. **20:**423–428.

16. **Dullforce, P., D. C. Sutton, and A. W. Heath.** 1998. Enhancement of T cell-independent immune responses in vivo by CD40 antibodies. Nat. Med. **4:**88–91.

17. **Fagarasan, S., and T. Honjo.** 2000. T-independent immune response: new aspects of B cell biology. Science **290:**89–92.

18. **Goodyear, C. S., G. M. O'Hanlon, J. J. Plomp, E. R. Wagner, I. Morrison, J. Veitch, L. Cochrane, R. W. Bullens, P. C. Molenaar, J. Conner, and H. J. Willison.** 1999. Monoclonal antibodies raised against Guillain-Barre syndrome-associated *Campylobacter jejuni* lipopolysaccharides react with neuronal gangliosides and paralyze muscle-nerve preparations. J. Clin. Investig. **104:**697–708.

19. **Guerry, P., C. M. Szymanski, M. M. Prendergast, T. E. Hickey, C. P. Ewing, D. L. Pattarini, and A. P. Moran.** 2002. Phase variation of *Campylobacter jejuni* 81–176 lipooligosaccharide affects ganglioside mimicry and invasiveness in vitro. Infect. Immun. **70:**787–793.

20. **Gumperz, J. E., and M. B. Brenner.** 2001. CD1-specific T cells in microbial immunity. Curr. Opin. Immunol. **13:**471–478.

21. **Hahn, A. F.** 1998. Guillain-Barre syndrome. Lancet **352:**635–641.

22. **Hartung, H. P., R. Kiefer, R. Gold, and K. V. Toyka.** 1996. Autoimmunity in the peripheral nervous system. Baillieres Clin. Neurol. **5:**1–45.

23. **Hartung, H. P., J. D. Pollard, G. K. Harvey, and K. V. Toyka.** 1995. Immunopathogenesis and treatment of the Guillain-Barre syndrome—part II. Muscle Nerve **18:**154–164.

24. **Havouis, S., G. Dumas, I. Chambaud, P. Ave, M. Huerre, A. Blanchard, G. Dighiero, and C. Pourcel.** 2002. Transgenic B lymphocytes expressing a human cold agglutinin escape tolerance following experimental infection of mice by *Mycoplasma pulmonis*. Eur. J. Immunol. **32:**1147–1156.

25. **Heath, A. W., W. W. Wu, and M. C. Howard.** 1994. Monoclonal antibodies to murine CD40 define two distinct functional epitopes. Eur. J. Immunol. **24:**1828–1834.

26. **Helling, F., A. Shang, M. Calves, S. Zhang, S. Ren, R. K. Yu, H. F. Oettgen, and P. O. Livingston.** 1994. GD3 vaccines for melanoma: superior immunogenicity of keyhole limpet hemocyanin conjugate vaccines. Cancer Res. **54:**197–203.

27. Ho, T. W., G. M. McKhann, and J. W. Griffin. 1998. Human autoimmune neuropathies. Annu. Rev. Neurosci. 21:187–226.
28. Ho, T. W., H. J. Willison, I. Nachamkin, C. Y. Li, J. Veitch, H. Ung, G. R. Wang, R. C. Liu, D. R. Cornblath, A. K. Asbury, J. W. Griffin, and G. M. McKhann. 1999. Anti-GD1a antibody is associated with axonal but not demyelinating forms of Guillain-Barre syndrome. Ann. Neurol. 45:168–173.
29. Hughes, R. A., R. D. Hadden, N. A. Gregson, and K. J. Smith. 1999. Pathogenesis of Guillain-Barre syndrome. J. Neuroimmunol. 100:74–97.
30. Hughes, R. A., and J. H. Rees. 1997. Clinical and epidemiologic features of Guillain-Barre syndrome. J. Infect. Dis. 176(Suppl. 2):S92-S98.
31. Jennemann, R., C. Gnewuch, S. Bosslet, B. L. Bauer, and H. Wiegandt. 1994. Specific immunization using keyhole limpet hemocyanin-ganglioside conjugates. J. Biochem. (Tokyo) 115:1047–1052.
32. Kawashima, I., O. Nakamura, and T. Tai. 1992. Antibody responses to ganglio-series gangliosides in different strains of inbred mice. Mol. Immunol. 29:625–632.
33. Krutzik, S. R., P. A. Sieling, and R. L. Modlin. 2001. The role of Toll-like receptors in host defense against microbial infection. Curr. Opin. Immunol. 13:104–108.
34. Ledeen, R. W. 1985. Gangliosides of the neuron. Trends Neurosci. 10:169–174.
35. Ledeen, R. W., and R. K. Yu. 1982. Gangliosides: structure, isolation, and analysis. Methods Enzymol. 83:139–191.
36. Linton, D., M. Gilbert, P. G. Hitchen, A. Dell, H. R. Morris, W. W. Wakarchuk, N. A. Gregson, and B. W. Wren. 2000. Phase variation of a beta-1,3 galactosyltransferase involved in generation of the ganglioside GM1-like lipo-oligosaccharide of Campylobacter jejuni. Mol. Microbiol. 37:501–514.
37. Lugaresi, A., M. Ragno, F. Torrieri, G. Di Guglielmo, P. Fermani, and A. Uncini. 1997. Acute motor axonal neuropathy with high titer IgG and IgA anti-GD1a antibodies following Campylobacter enteritis. J. Neurol. Sci. 147: 193–200.
38. Lunn, M. P., L. A. Johnson, S. E. Fromholt, S. Itonori, J. Huang, A. A. Vyas, J. E. Hildreth, J. W. Griffin, R. L. Schnaar, and K. A. Sheikh. 2000. High-affinity anti-ganglioside IgG antibodies raised in complex ganglioside knock-out mice: reexamination of GD1a immunolocalization. J. Neurochem. 75: 404–412.
39. Martin, F., and J. F. Kearney. 2001. B1 cells: similarities and differences with other B cell subsets. Curr. Opin. Immunol. 13:195–201.
40. Mayer, L. D., M. B. Bally, M. J. Hope, and P. R. Cullis. 1986. Techniques for encapsulating bioactive agents into liposomes. Chem. Phys. Lipids 40:333–345.
41. Mond, J. J., A. Lees, and C. M. Snapper. 1995. T cell-independent antigens type 2. Annu. Rev. Immunol. 13:655–692.
42. Moran, A. P. 1997. Structure and conserved characteristics of Campylobacter jejuni lipopolysaccharides. J. Infect. Dis. 176(Suppl. 2):S115–S121.
43. Moran, A. P., B. J. Appelmelk, and G. O. Aspinall. 1996. Molecular mimicry of host structures by lipopolysaccharides of Campylobacter and Helicobacter spp.: implications in pathogenesis. J. Endotox. Res. 3:521–531.
44. Moran, A. P., and J. L. Penner. 1999. Serotyping of Campylobacter jejuni based on heat-stable antigens: relevance, molecular basis and implications in pathogenesis. J. Appl. Microbiol. 86:361–377.
45. Moran, P., and D. T. O'Malley. 1995. Potential role of lipopolysaccharide of Campylobacter jejuni in the development of Guillain-Barre syndrome. J. Endotox. Res. 2:233–235.
46. Nachamkin, I., B. M. Allos, and T. Ho. 1998. Campylobacter species and Guillain-Barre syndrome. Clin. Microbiol. Rev. 11:555–567.
47. Nachamkin, I., B. M. Allos, and T. W. Ho. 2000. Campylobacter. ASM Press, Washington, D.C.
48. Nam Shin, J. E., S. Ackloo, A. S. Mainkar, M. A. Monteiro, H. Pang, J. L.

49. Penner, and G. O. Aspinall. 1998. Lipo-oligosaccharides of Campylobacter jejuni serotype O:10. Structures of core oligosaccharide regions from a bacterial isolate from a patient with the Miller-Fisher syndrome and from the serotype reference strain. Carbohydr. Res. 305:223–232.
49. Ozawa, H., M. Kotani, I. Kawashima, and T. Tai. 1992. Generation of one set of monoclonal antibodies specific for b-pathway ganglio-series ganglio-sides. Biochim. Biophys. Acta 1123:184–190.
50. Penner, J. L., and G. O. Aspinall. 1997. Diversity of lipopolysaccharide structures in Campylobacter jejuni. J. Infect. Dis. 176(Suppl. 2):S135–S138.
51. Prenderghast, M. M., and A. P. Moran. 2000. Lipopolysaccharides in the development of Guillain-Barre syndrome and Miller Fisher forms of acute inflammatory peripheral neuropathies. J. Endotox. Res. 6:341–359.
52. Qureshi, S. T., P. Gros, and D. Malo. 1999. Host resistance to infection: genetic control of lipopolysaccharide responsiveness by TOLL-like receptor genes. Trends Genet. 15:291–294.
53. Qureshi, S. T., P. Gros, and D. Malo. 1999. The Lps locus: genetic regulation of host responses to bacterial lipopolysaccharide. Inflamm. Res. 48:613–620.
54. Salloway, S., L. A. Mermel, M. Seamans, G. O. Aspinall, J. E. Nam Shin, L. A. Kurjanczyk, and J. L. Penner. 1996. Miller-Fisher syndrome associated with Campylobacter jejuni bearing lipopolysaccharide molecules that mimic human ganglioside GD3. Infect. Immun. 64:2945–2949.
55. Schwerer, B., A. Neisser, and H. Bernheimer. 1999. Distinct immunoglobulin class and immunoglobulin G subclass patterns against ganglioside GQ1b in Miller Fisher syndrome following different types of infection. Infect. Immun. 67:2414–2420.
56. Sheikh, K. A., T. W. Ho, I. Nachamkin, C. Y. Li, D. R. Cornblath, A. K. Asbury, J. W. Griffin, and G. M. Mckhann. 1998. Molecular mimicry in Guillain-Barre syndrome. Ann. N. Y. Acad. Sci. 845:307–321.
57. Snapper, C. M., H. Yamaguchi, M. A. Moorman, and J. J. Mond. 1994. An in vitro model for T cell-independent induction of humoral immunity. A requirement for NK cells. J. Immunol. 152:4884–4892.
58. Sugita, M., P. J. Peters, and M. B. Brenner. 2000. Pathways for lipid antigen presentation by CD1 molecules: nowhere for intracellular pathogens to hide. Traffic 1:295–300.
59. Takamiya, K., A. Yamamoto, K. Furukawa, S. Yamashiro, M. Shin, M. Okada, S. Fukumoto, M. Haraguchi, N. Takeda, K. Fujimura, M. Sakae, M. Kishikawa, H. Shiku, and S. Aizawa. 1996. Mice with disrupted GM2/GD2 synthase gene lack complex gangliosides but exhibit only subtle defects in their nervous system. Proc. Natl. Acad. Sci. USA 93:10662–10667.
60. Tettamanti, G., and L. Riboni. 1993. Gangliosides and modulation of the function of neural cells. Adv. Lipid Res. 25:235–267.
61. Watkins, W. M. 1980. Biochemistry and genetics of the ABO, Lewis, and P blood group systems. Adv. Hum. Genet. 10:1–136.
62. Willison, H. J., and J. Veitch. 1994. Immunoglobulin subclass distribution and binding characteristics of anti-GQ1b antibodies in Miller Fisher syndrome. J. Neuroimmunol. 50:159–165.
63. Willison, H. J., J. Veitch, A. V. Swan, N. Baumann, G. Comi, N. A. Gregson, I. Illa, J. Zielasek, and R. A. Hughes. 1999. Inter-laboratory validation of an ELISA for the determination of serum anti-ganglioside antibodies. Eur. J. Neurol. 6:71–77.
64. Winer, J. B. 2001. Guillain Barre syndrome. Mol. Pathol. 54:381–385.
65. Yuki, N., M. Takahashi, Y. Tagawa, K. Kashiwase, K. Tadokoro, and K. Saito. 1997. Association of Campylobacter jejuni serotype with antigangli-side antibody in Guillain-Barre syndrome and Fisher's syndrome. Ann. Neurol. 42:28–33.
66. Yuki, N., M. Yamada, M. Koga, M. Odaka, K. Susuki, Y. Tagawa, S. Ueda, T. Kasama, A. Ohnishi, S. Hayashi, H. Takahashi, M. Kamijo, and K. Hirata. 2001. Animal model of axonal Guillain-Barre syndrome induced by sensitization with GM1 ganglioside. Ann. Neurol. 49:712–720.

A New Substrate Specificity for Acyl Transferase Domains of the Ascomycin Polyketide Synthase in *Streptomyces hygroscopicus**

Christopher D. Reeves‡, Loleta M. Chung, Yaoquan Liu, Qun Xue§, John R. Carney, W. Peter Revill, and Leonard Katz

From Kosan Biosciences, Inc., Hayward, California 94545

Ascomycin (FK520) is a structurally complex macrolide with immunosuppressant activity produced by *Streptomyces hygroscopicus*. The biosynthetic origin of C12-C15 and the two methoxy groups at C13 and C15 has been unclear. It was previously shown that acetate is not incorporated into C12-C15 of the macrolactone ring. Here, the acyl transferase (AT) of domain 8 in the ascomycin polyketide synthase was replaced with heterologous ATs by double homologous recombination. When AT8 was replaced with methylmalonyl-CoA-specific AT domains, the strains produced 13-methyl-13-desmethoxyascomycin, whereas when AT8 was replaced with a malonyl-specific domain, the strains produced 13-desmethoxyascomycin. These data show that ascomycin AT8 does not use malonyl- or methylmalonyl-CoA as a substrate in its native context. Therefore, AT8 must be specific for a substrate bearing oxygen on the α carbon. Feeding experiments showed that [¹³C]glycerol is incorporated into C12-C15 of ascomycin, indicating that both modules 7 and 8 of the polyketide synthase use an extender unit that can be derived from glycerol. When AT6 of the 6-deoxyerythronolide B synthase gene was replaced with ascomycin AT8 and the engineered gene was expressed in *Streptomyces lividans*, the strain produced 6-deoxyerythronolide B and 2-demethyl-6-deoxyerythronolide B. Therefore, although neither malonyl-CoA nor methylmalonyl-CoA is a substrate for ascomycin AT8 in its native context, both are substrates in the foreign context of the 6-deoxyerythronolide B synthase. Thus, we have demonstrated a new specificity for an AT domain in the ascomycin polyketide synthase and present evidence that specificity can be affected by context.

Ascomycin (FK520) is closely related to tacrolimus (FK506), which is used to prevent xenograft rejection in human patients. Dosing of tacrolimus is difficult because metabolism varies between patients and different co-administered drugs (1–3). Because initial metabolism is due to cytochrome P450-mediated demethylation of the 13-methoxy group (4, 5), we wished to replace the 13-methoxy group with a hydrogen or methyl group and determine whether this increased metabolic stability. Because these analogues could not be obtained by current

chemical methods, we sought the desired analogues of ascomycin modified at C13 (Fig. 1) using PKS¹ engineering (6, 7).

The macrolactone precursor of ascomycin is biosynthesized by a large PKS complex consisting of a loading module for a shikimate-derived starter unit; 10 modules for malonyl, methylmalonyl, or other PKS extender units; and a peptide synthetase module for addition of pipecolate (8–13). FK520 and FK506 have methoxy groups at C13 and C15, which could be derived by post-PKS hydroxylation followed by O-methylation or by direct incorporation of an extender unit with an oxygen at the α carbon. Feeding of [¹³C₂]acetate was reported to label C8-C9 and C20-C23 of the macrolactone ring, as expected, but not C12-C15 in either FK520 or FK506 (8). A [1-¹³C]erythrose feed, used to establish that the dihydroxycyclohexane starter unit is derived from shikimate, unexpectedly labeled C12 and C14, implying that the extender unit is more readily derived from erythrose than from acetate.

Sequence analysis of the ascomycin gene cluster from *Streptomyces hygroscopicus* (14) showed that it contains close homologues of the genes in the FK506 cluster (9–11) that encode the three PKS subunits, the peptide synthetase, the lysine cyclodeaminase, the C9 hydroxylase, the 31-O-methyltransferase, and the putative 9-hydroxyl oxidase. In the flanking regions of the FK520 cluster, additional genes were found with proposed roles in synthesis of precursors, including a putative methoxymalonyl-ACP precursor for the 13- and 15-methoxy groups of FK520 (14).

The choice of extender unit by a modular PKS system is determined by the acyl transferase (AT) domain of each module (6, 15–17). Comparison of methylmalonyl-CoA- and malonyl-CoA-specific AT domain sequences shows that they cluster into two groups with sequence motifs that diverge according to the specificity of the domain (15). More recently, AT domains specific for ethylmalonyl units have been identified, and they are most closely related to the methylmalonyl-specific domains (18). In addition, there is circumstantial evidence that some domains are specific for an extender unit with oxygen on the α carbon (19–21). Despite the availability of the *Escherichia coli* malonyl-CoA:ACP transacylase crystal structure (22) and extensive biochemical experiments with both the rat fatty acid synthase and several bacterial PKSs (23–27), the structural basis for AT domain substrate specificity has not been established.

Here we describe replacement of the ascomycin AT8 domain with AT domains specific for malonyl or methylmalonyl ex-

---

---

¹ The abbreviations used are: PKS, polyketide synthase; ACP, acyl carrier protein; AT, acyl transferase (appended number designates the module where the domain is from); LC-MS, liquid chromatography-mass spectrometry; 13-DMA, 13-desmethoxyascomycin; 13-MDMA, 13-methyl-13-desmethoxyascomycin; 6-DEB, 6-deoxyerythronolide B; DEBS, deoxyerythronolide B synthase; thio^S, thiostrepton-sensitive.

FIG. 1. **Structures of ascomycin and engineered analogues.** The extender unit incorporated by module 8 of the ascomycin PKS and the engineered versions thereof are highlighted with *gray* in each structure.
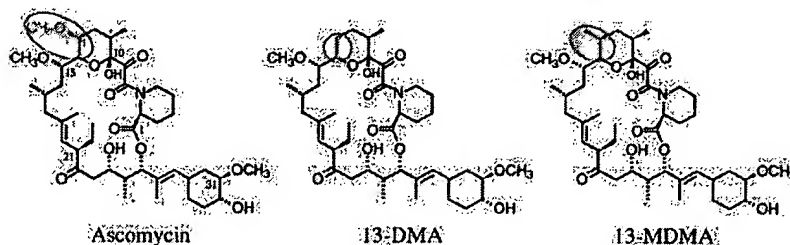
tender units, resulting in the production of analogues modified at C13 and showing that ascomycin AT8 is specific for an extender unit bearing oxygen on the α carbon. Precursor labeling experiments showed that ascomycin PKS modules 7 and 8 use an extender unit that can be derived from glycerol. In addition, we show that the specificity of this AT domain can be altered by placing it into a foreign PKS context.

EXPERIMENTAL PROCEDURES

Strains and Media—The ascomycin-producing strain, *S. hygroscopicus* ATCC 14891, was plated on SY medium (10 g of soluble starch, 2 g of yeast extract, and 20 g of agar per liter) to prepare spore stocks and grown in TSBGM (tryptic soy broth supplemented with 50 mM TES buffer, pH 7, and 1% glucose) for production of ascomycin or its analogues. Growth and transformation of *Streptomyces lividans* K4-114 has been described previously (28). Use of the phage vector KC515 followed established procedures (28).

Preparation of Phage Carrying AT Replacement Cassettes—PKS module 8 was isolated as a 4.6-kb *SphI* fragment from cosmid pKOS65-C31 (14) and cloned into Litmus28 (New England Biolabs), and the orientation with a unique *SacI* site proximal to the *SpeI* site of the polylinker was used (pKOS60-21). A synthetic linker was ligated between the *SpeI* and *SacI* sites and then subsequently ligated between the *SphI* and *AflII* sites to give pKOS60-29, which was used as a template to isolate regions flanking AT8 by PCR. The PCR mixtures for all reactions described herein contained (50 μl, total volume) 1 μl of template (either diluted plasmid DNA, undiluted genomic DNA, or high-titer phage stock), 10× Pfu buffer, 10× z-deoxynucleotide triphosphate mix (200 μM each deoxynucleotide triphosphate except 100 μM dGTP and 100 μM 7-deaza-dGTP; Roche Molecular Biochemicals), 10% Me₂SO, 400 nM of each primer, and 1 μl of cloned *Pfu* polymerase (Stratagene). Reactions were cycled 25–30 times at 95 °C for 30 s, 60 °C for 30 s, and 72 °C for 2 min. To amplify the 5′-flanking region, the forward primer was 5′-CGACTCACTAGTGGGCAGATCTGGC-3′, and one of two reverse primers was used: 1) 5′-CACGCCTAGGCCGGTCG-GTCTCGGGCCAC-3′, which introduced an *AvrII* site near the 3′ end of the ketoacyl synthase domain, or 2) 5′-GCGGCTAGCTGCTCGC-CCATCGCGGGATGC-3′, which introduced an *NheI* site near the 5′ end of the AT boundary. These PCR products were cloned as *SpeI* to *AvrII* and *SpeI* to *NheI* fragments into Litmus28 and Litmus38, respectively, to give pKOS60-37-4 and pKOS60-37-2. The 3′-flanking region was isolated using a forward primer (5′-GATGTACAGCTCGAGTCG-GCACGCCCGGCCGCATC-3′) that introduced an *XhoI* site at the AT/dehydratase boundary plus a *BsrGI* site to facilitate the construction; the reverse primer was 5′-CGACTCACTTAAGCCATGCATCC-3′. This PCR product was isolated as a *BsrGI* to *AflII* fragment and ligated into pKOS60-37-4 cut with *Acc65I* and *AflII* or pKOS60-37-2 cut with *BsrGI* and *AflII*, giving pKOS60-39-13 and pKOS60-39-1, respectively.

Heterologous AT domains were obtained by PCR using primers that introduced *AvrII* and *XhoI* or *NheI* and *XhoI* sites at the 5′ and 3′ ends, respectively. Each heterologous AT was cloned into pKOS60-39-13 (*AvrII-XhoI*) or pKOS60-39-1 (*NheI-XhoI*) to create a series of AT replacement cassettes. Each replacement cassette was isolated as a *BglII* to *NsiI* fragment and ligated to KC515 DNA cut with *BamHI* and *PstI*, and the ligation mixture was introduced into *S. lividans* TK24 by transfection. The resulting plaques were purified, and high-titer phage stocks were prepared as described previously (28). Recombinant phage preparations were checked by PCR using a pair of primers annealing within the dehydratase/keto reductase-flanking sequence.

Construction of Strains with AT8 Replaced by Heterologous ATs—Spores of *S. hygroscopicus* (10⁷) were suspended in Difco nutrient broth, heat-shocked at 50 °C for 10 min, and mixed with an equal number of plaque-forming units of recombinant phage in Difco nutrient broth. The mixture was spread on R2YE plates (28), and after an overnight incubation at 30 °C, plates were overlaid with 1.25 mg of thiostrepton

suspended in 1 ml of H₂O. After 7–10 days, sporulating colonies were streaked on SY agar containing 50 μg/ml thiostrepton. Colonies were picked from these plates after about 5 days and macerated in 200 μl of H₂O using a microfuge pestle. Half the suspension was inoculated into a 25 × 150-mm tube with two 4-mm glass beads and 5 ml of TSBGM; the other half was inoculated into the same medium with 50 μg/ml thiostrepton. After 2–3 days, a 1.5-ml sample of each thiostrepton-containing culture was harvested for total DNA isolation, and a 0.75-ml sample was prepared for LC-MS analysis by adding an equal volume of MeCN and clarifying by centrifugation. DNA was isolated by the SDS, proteinase K, phenol method (28) and analyzed by Southern blot hybridization using the digoxigenin labeling and detection kits supplied by Roche Molecular Biochemicals. Each culture grown without thiostrepton was spread on an SY agar plate to obtain spores to screen for the second recombination event.

Selected spore preparations from the nonselective propagation plates above were titered and spread on several plates at about 100–200 colonies/plate. When colonies were sufficiently sporulated, they were replica-plated onto SY agar plates containing 50 μg/ml thiostrepton. After 4–5 days, putative thio^S recombinants were identified and clonally isolated. These were grown in 5-ml TSBGM tube cultures for 3 days, and the broth was extracted as described above for LC-MS analysis (see below). Strains producing 13-DMA or 13-MDMA were designated KOS45-170 and KOS60-135, respectively.

Precursor Labeling Studies—[¹³C₂]Glycine and [¹³C₃]glycerol were obtained from Cambridge Isotope Laboratories. [¹³C₂]Glycolate, a mixture of ethyl [¹³C₂]bromoacetate (Aldrich; 98% ¹³C; 1.0 g), sodium acetate (1.0 g), and anhydrous *N,N*-dimethylformamide (15 ml), was stirred at 80 °C for 3 h. Water was added, and the mixture was extracted three times with Et₂O. The combined organic layers were washed twice with H₂O, washed once with brine, and dried over Na₂SO₄. After removal of solvent, a clear oil (0.45 g) was obtained. ¹H NMR (CDCl₃): δ 4.59 (2H, dd, *J* = 149, 4.8 Hz), 4.23 (2H, qd, *J* = 7.2, 3.2 Hz), 2.16 (3H, s), 1.29 (3H, t, *J* = 7.2 Hz). The acetate was dissolved in MeOH (15 ml), 0.5 M LiOH (15 ml) was added, and the mixture was stirred overnight at room temperature. After neutralization with 2 N HCl, the mixture was extracted twice with ether. The aqueous layer was dried under high vacuum to give [¹³C₂]lithium glycolate (508 mg; containing some sodium acetate and NaCl). ¹H NMR (D₂O): δ 3.88 (2H, dd, *J* = 143.6, 4.4 Hz). ¹³C NMR (D₂O): δ 179.1 (d, *J* = 55 Hz), 60.3 (d, *J* = 55 Hz).

[*methyl*-¹³C]Methoxyacetic acid:ethyl diazoacetate (1.8 ml) was added dropwise to a stirred solution of Rh₂(OAc)₄ (10 mg) in [¹³C]methanol (Isotec; 99 atom% ¹³C; 1.0 g). After 4 h, the mixture was diluted with 10 ml of hexanes and filtered through a 1 cm plug of silica gel. The silica was washed with 3:1 hexanes/ether, and the eluates were combined and concentrated to give 1.35 g of ethyl [*methyl*-¹³C]methoxyacetate as a colorless liquid. ¹H NMR (CDCl₃): δ 4.24 (2H, q, *J* = 7.2 Hz), 4.03 (2H, d, *J*$_{CH}$ = 4.8 Hz), 3.45 (3H, d, *J*$_{CH}$ = 142 Hz), 1.31 (3H, t, *J* = 7.2 Hz). The ester was dissolved in 2 ml of MeOH and treated with 10 ml of 6 N NaOH for 12 h. The mixture was extracted three times with CH₂Cl₂, and then the aqueous phase was acidified to below pH 2 using concentrated HCl and diluted with 100 ml of saturated aqueous NaCl before continuous extraction with ether for 24 h. The ether extract was dried over MgSO₄, filtered, and evaporated to yield 1.5 g of an oil. Bulb-to-bulb distillation under reduced pressure yielded clean [*methyl*-¹³C]methoxyacetic acid (0.70 g). ¹H NMR (CDCl₃): δ 4.09 (2H, d, *J*$_{CH}$ = 4.8 Hz), 3.48 (3H, d, *J*$_{CH}$ = 142 Hz).

[*methyl*-¹³C]Methoxymalonic acid:5-diazo-Meldrum's acid (2 g), [¹³C]methanol (2 g), Rh₂(OAc)₄ (250 mg), and toluene (25 ml) were mixed in an Ace pressure tube. The capped tube was heated at 140 °C for 2 h, the reaction was filtered, and the filtrate was evaporated. The residue was dissolved in H₂O and extracted three times with EtOAc. The combined organic layers were dried over MgSO₄, filtered, and evaporated to yield an oil (1.3 g), which was identified as a mixture of dimethyl methoxymalonate and monomethyl methoxymalonate. The oil

was dissolved in MeOH (5 ml), 6 N NaOH (10 ml) was added, and the mixture was left overnight at room temperature. After cooling on ice, the mixture was acidified to pH < 1 with HCl and filtered. The filtrate was dried under high vacuum to yield a yellow solid (1 g). To remove the inorganic salt, the solid was extracted three times with acetone; the acetone extracts were evaporated to give methoxymalonic acid as a solid (0.65 g). ^{1}H NMR (acetone-d$_6$): δ 4.47 (1H, d, J = 4 Hz), 3.46 (3H, d, J = 143 Hz). ^{13}C NMR (acetone-d$_6$): δ 167.0, 79.9, 57.5 (enriched).

Cultures grown in TSBGM were harvested at 24 h, washed twice, and resuspended in 100 mM MES, pH 6.0, 1% glucose to the original culture volume. The resting cell suspension was shaken in baffled flasks at 30 °C and 175 rpm. The ^{13}C-labeled precursors were added in three equal portions at 24, 36, and 48 h to obtain 0.5 g/liter final concentration. Resting cell cultures were harvested at 56 h by adding half the volume of the culture of MeOH. The resulting broth/extract was clarified by centrifugation and loaded at 25 ml/min onto a column of Diaion HP-20ss pre-equilibrated in MeOH-H$_2$O (2:1). The column volume was ⅟₂₀ the volume of the broth/extract. The column was eluted at 8 ml/min with MeOH-H$_2$O at ratios of 1:2 (2 column volumes), 1:1 (4 column volumes), 7:3 (4 column volumes), and 9:1 (4 column volumes). The 9:1 eluent was concentrated to give crude ascomycin, which was chromatographed over Bond-Elut ODS solid phase extraction cartridges by eluting with MeOH-H$_2$O (9:1). This material was suitable for NMR analysis.

Expression of DEBS with AT6 Replaced by Ascomycin AT8—The *Streptomyces* expression vector pKAO127 containing the SCP2* replicon and the DEBS genes expressed via the *actI* promoter and *actII*-ORF4 transcription activator were described previously (29). Constructs with *Spe*I and *Pst*I sites engineered at the eryAT6 boundaries have also been described previously (6). The ascomycin AT8 was isolated by PCR with primers that introduced a *Spe*I site at the 5′ boundary and an *Nsi*I site at the 3′ boundary. The PCR product was cloned into Litmus28 to give pKOS38-178, which was checked by sequencing, and subsequently inserted between the engineered *Spe*I and *Pst*I sites flanking DEBS AT6. This was assembled into the DEBS expression construct pKOS38-187. The construct was introduced into *S. lividans* K4-114 by standard protoplast transformation (28), and the transformants were cultured in R5 medium for production of the 6-DEB analogue.

LC-MS Analysis—Samples were analyzed by on-line extraction by LC-MS using a system comprised of a 10 port, 2 position switching valve/injector, Beckman System Gold HPLC, an Alltech evaporative light scattering detector, and a PE SCIEX API100 LC-mass spectrometer equipped with an atmospheric pressure chemical ionization source. For ascomycin analogue analyses, whole cultures were extracted by adding 1 volume of MeCN and clarified by centrifugation. Sample (250 μl) was loaded onto an Upchurch 4.3 × 10 mm ODS guard column that had been pre-equilibrated for 1 min with 0.1% acetic acid at 1 ml/min, with the eluate being diverted to waste. At 30 s postinjection a linear gradient to 1:1 MeCN-H$_2$O (0.1% acetic acid) over 1 min was started, with the eluate still diverted to waste. At 2 min, the direction of flow through the guard column was reversed, and the eluent was diverted onto a Metachem Inertsil ODS-3 column (5 μm; 4.6 × 150 mm) at 50 °C pre-equilibrated with 1:1 MeCN-H$_2$O (0.1% acetic acid). A linear gradient from 50% to 100% MeCN (0.1% acetic acid) at 1 ml/min over 5 min and then 100% MeCN (0.1% acetic acid) for 4 min was monitored by evaporative light scattering and mass spectrometry. For 6-DEB and 2-demethyl-6-DEB, 100 μl of clarified whole broth was loaded onto the guard column after a 1 min pre-equilibration with H$_2$O at 1 ml/min. At 30 s postinjection, a linear gradient to 15% MeCN over 1 min was initiated. At 2 min, the direction of flow through the guard column was reversed, and the eluent was diverted onto a Metachem Inertsil ODS-3 column (5 μm; 4.6 × 150 mm) pre-equilibrated with 15% MeCN. A linear gradient from 15% to 100% MeCN at 1 ml/min over 6 min and then 100% MeCN for 3 min was monitored by evaporative light scattering and mass spectrometry.

RESULTS

Replacement of AT8 in the Ascomycin PKS—We previously hypothesized that AT8 of the ascomycin PKS selects the unusual precursor methoxymalonyl-ACP leading to direct incorporation of the methoxy group at C13 (14). To explore this, ascomycin AT8 was replaced with heterologous ATs of known specificity by double homologous recombination using the phage vector KC515 as shown in Fig. 2. Between 10 and 100 thiostrepton-resistant colonies were obtained after infection

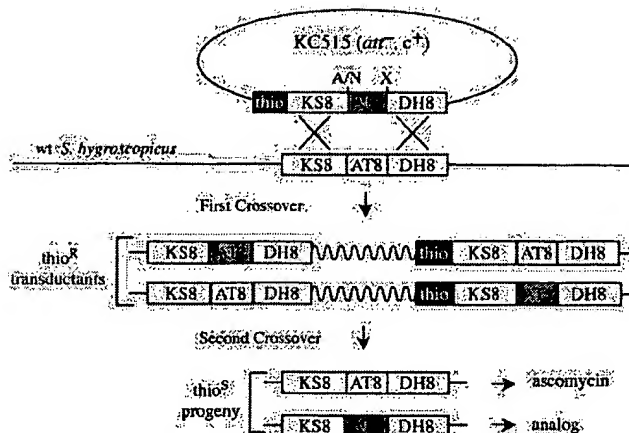Fig. 2. **Diagram showing how *S. hygroscopicus* strains were engineered to replace AT8 in the ascomycin PKS with AT domains of other specificity.** Each AT replacement cassette was delivered on the KC515 phage vector, and thiostrepton-resistant recombinants were selected. Isolates that had crossed over at either the ketoacyl synthase 8 or dehydratase 8 sequence were observed by Southern blot analyses. Analysis of the thio^S isolates indicated that both types of second crossover events occurred, giving wild-type revertants or strains containing the heterologous AT replacement, which produced the predicted ascomycin analogue. See "Experimental Procedures" for details.

with recombinant phages, whereas KC515 alone gave no thiostrepton-resistant colonies. Ten isolates each of lysogens from the rapamycin AT3 or erythromycin AT2 construct were analyzed in detail. None produced detectable ascomycin or related products, consistent with insertion of the phage into a gene essential for ascomycin production. Southern blot hybridization experiments (using *Xho*I or *Acc*65I digestion of genomic DNA) showed that of the erythromycin AT2 lysogens, seven arose by recombination at the ketoacyl synthase 8 sequence, and three arose by recombination at the dehydratase 8/keto reductase 8 sequence, whereas of the rapamycin AT3 lysogens, eight recombined at the dehydratase 8/keto reductase 8 sequence, one recombined at the ketoacyl synthase 8, and one apparently recombined at the dehydratase 1/keto reductase 1 sequence, which is 98% identical over 1 kb with keto reductase 8/dehydratase 8. Three lysogens from the malonyl-specific rapamycin AT12 construct also did not produce FK520, and the expected first crossover event was verified using PCR.

After growth in the absence of selection, thio^S colonies appeared at a frequency of about 0.3%, half of which produced ascomycin and had therefore reverted to wild-type. With the exception of one thio^S recombinant that produced no ascomycin-related compound, the remaining thio^S recombinants produced a compound with an LC retention time and atomic mass consistent with either 13-DMA (for the rapamycin AT12 replacement) or 13-MDMA (for the rapamycin AT3 and erythromycin AT2 replacements). The overall statistics indicated little bias for recombination via one flanking sequence over the other. After growing selected strains in laboratory-scale stirred-tank fermenters and purifying the ascomycin analogues, structures were verified by mass spectrometry and NMR analyses.[2] For the rapamycin AT3 replacement strain, only 13-MDMA was produced, and the relative stereochemistry of the 13-methyl group was the same as that of the 13-methoxy group of ascomycin. Thus, the α-methyl epimerization activity that occurs in rapamycin module 3 does not appear to reside on the AT domain, consistent with previous work (23). The 13-

---

TABLE I

Summary of results from replacement of AT8 in the ascomycin PKS

Strain	Replacement	Ascomycin-related products detected (approximate titer)
ATCC14891	Wild-type	Ascomycin (50 mg/liter), 21-methyl congener (trace)
KOS60-135	Rapamycin AT3	13-MDMA (2 mg/liter)
KOS45-170	Rapamycin AT12	13-DMA (2 mg/liter), ascomycin (0.1 mg/liter)

TABLE II

^{13}C *enrichment of* C_{12}-C_{15} *fragment in ascomycin after the feeding of various precursors*

Carbon	δ_C	$^1J(^{13}C, {}^{13}C)$	[$^{13}C_2$]Glycolate	[^{13}C]-MeO-acetate	[^{13}C]-MeO-malonate	[$^{13}C_2$]Glycine	[$^{13}C_3$]Glycerol
	ppm	*Hz*					
12	32.6	36	n.d.^{a}	n.d.^{b}	n.d.^{b}	d^c	2^d
13	73.6	36	n.d.^{a}	n.d.^{b}	n.d.^{b}	d^c	1.5^d
14	72.8	44	n.d.^{a}	n.d.^{b}	n.d.^{b}	d^c	2^d
15	75.2	44	n.d.^{a}	n.d.^{b}	n.d.^{b}	d^c	2^d

^{a} No detectable coupled signals. n.d., not detected; d, detected.

^{b} No detectable enrichment at 13- or 15-OMe signals.

^{c} Weak coupled signals, but detectable.

^{d} Intensity of ^{13}C satellites in relation to the intensity of the central peak in the ^{13}C NMR spectrum.

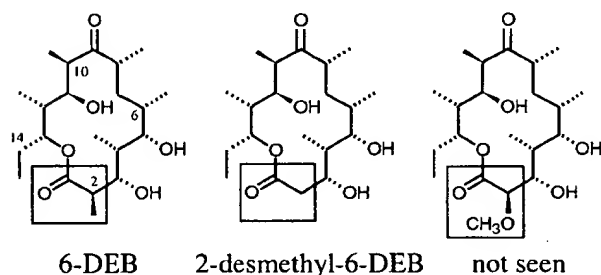6-DEB   2-desmethyl-6-DEB   not seen

FIG. 3. **Structure of 6-DEB and potential analogues.** *S. lividans* expressing DEBS produces predominantly 6-DEB. *S. lividans* expressing DEBS with AT6 replaced by ascomycin AT8 produces 6-DEB and 2-demethyl-6-DEB. No 2-methoxy-2-demethyl-6-DEB was detected. The portion of the molecules arising from incorporation by DEBS module 6 is boxed.

DMA and 13-MDMA analogues were produced at levels about 5% of parental ascomycin titers (50 mg/liter), which is better than most PKS engineering results (6). For the rapamycin AT12 replacement strain, 13-DMA was the predominant product, but a small amount (~5% of the total) of ascomycin was also observed, even after two rounds of clonal isolation. A summary of the products identified in cultures of the engineered strains is presented in Table I.

Incorporation of ^{13}C-*labeled Precursors into Ascomycin*—It was reported previously that [1,2-^{13}C]acetate can be incorporated into the macrolactone ring carbons C8, C9, and C20-C23 but not C12-C15 in either ascomycin or FK506 (8). To explore the origin of C12-C15 further, the incorporation of potential ^{13}C-labeled precursors ([$^{13}C_2$]glycolate, [*methyl*-^{13}C]methoxyacetate, [*methyl*-^{13}C]methoxymalonate, [$^{13}C_2$]glycine, and [$^{13}C_3$]glycerol) was evaluated by ^{13}C NMR experiments (Table II). No significant enrichment of the O-methyl carbon atoms was seen if either [*methyl*-^{13}C]methoxyacetate or [*methyl*-^{13}C]methoxymalonate was fed. In addition, no detectable coupled signals at C12-C15 were seen after feeding glycolate. Glycine gave weak coupled signals at C12-C15 and additional weak signals for the O-methyl carbons (at C13, C15, and C31), presumably because of metabolism via the one-carbon pool. On the other hand, glycerol feeding gave unequivocal signals resulting from $^1J_{C-C}$ for C12-C13 and C14-C15, indicating intact incorporation of two-carbon units at these positions (Table II).

Expression of DEBS with AT6 Replaced by Ascomycin AT8—Replacement of DEBS AT6 by the malonyl-specific rapamycin AT2 and expression in *S. lividans* was previously shown to give production of 2-demethyl-6-DEB instead of 6-DEB (6). To fur-

ther study the ascomycin AT8 domain, the same fusion junctions engineered in this previous construct were used to replace DEBS AT6 with ascomycin AT8. LC-MS analysis of *S. lividans* cultures expressing this construct revealed that 6-DEB and 2-demethyl-6-DEB (Fig. 3) were produced at ~7 and 3 mg/liter, respectively, or 10–20% the level of 6-DEB produced by *S. lividans* cultures expressing the wild-type DEBS genes. No 2-methoxy-2-demethyl-6-DEB was observed. Thus, ascomycin AT8 in this foreign PKS context, expressed in a strain that does not contain the methoxymalonyl precursor, selects either malonyl-CoA or methylmalonyl-CoA as alternative substrate relatively efficiently.

DISCUSSION

The results of AT8 replacement in the ascomycin PKS have proven that module 8 uses a precursor other than malonyl-CoA or methylmalonyl-CoA. Moreover, we have shown that C12-C15 arise by sequential incorporation of an extender unit that can be derived from glycerol, consistent with our previous proposal, based on gene homologies, that the direct precursor comes from the glycolytic pathway (14). Recent results have confirmed that replacement of AT7 with ATs specific for malonyl, methylmalonyl, or ethylmalonyl extenders gave the predicted 15-desmethoxy analogue.[3] Two possible reasons glycolate was not incorporated are that it was not taken up by the cells or that one of the activities needed to convert it to glycerate (*e.g.* tartronate semialdehyde synthase) was absent from *S. hygroscopicus* under the growth conditions used.

Our results are consistent with the proposal that methoxymalonyl-ACP is the substrate used by modules 7 and 8 (14). The substrate is more likely to be a methoxymalonyl thioester rather than a hydroxymalonyl thioester for the following reasons. First, aside from *fkbM*, the assigned 31-O-methyltransferase gene, *fkbG* is the only other methyltransferase gene found in the cluster (14). It is unlikely that FkbG methylates both the 13- and 15- hydroxyl groups of a post-PKS intermediate because methyltransferases are known to have very tight substrate specificity. Second, the sequence of FkbG is most similar to two methyltransferases encoded in clusters for macrolides with a methoxy group at an α carbon and is more similar to plant caffeoyl-CoA methyltransferases than to any of the enzymes known to methylate a post-PKS macrolide intermediate (14). This is consistent with FkbG methylating a precursor to the extender unit before its incorporation into the

---

polyketide chain. Finally, if hydroxymalonyl units were incorporated at these positions, the polyketide would rearrange to form the hemiketal isomers known to be favored following demethylation of these methoxy groups by mammalian liver CYP3A (4, 5), and this could interfere with subsequent biosynthetic steps. Our previous proposal that the substrate is methoxymalonyl-ACP instead of methoxymalonyl-CoA was based on the presence of an unusual ACP gene *(fkbJ)* in the set of five genes believed to encode the synthesis of this extender unit (14). If this hypothesis is correct, methoxymalonyl-specific AT domains may recognize features of the unusual ACP as an additional way to maintain tight substrate specificity.

The choice of precursor by a given AT domain is governed by its relative selectivity for the available substrates and the effective concentrations of those substrates. Clearly, there is an adequate supply of both malonyl-CoA and methylmalonyl-CoA in *S. hygroscopicus* during ascomycin production because these precursors are incorporated by other modules of the ascomycin PKS. Despite this, AT8 in its native ascomycin PKS context discriminates against these substrates because the corresponding analogues have never been observed from the wild-type strain. In addition, when the *fkbG* gene was disrupted, no ascomycin-related structures were detected,[4] showing that AT8 (and AT7) discriminates against malonyl-CoA or methylmalonyl-CoA in its native context.

Extender unit specificity is usually tight, although there are examples of relaxed specificity, such as module 4 of the epothilone PKS, which incorporates either malonyl or methylmalonyl units (30, 31), and modules in the ascomycin and monensin PKSs, which can incorporate ethylmalonyl or methylmalonyl units (8, 32). Rapamycin AT12, which is specific for malonyl-CoA in its native context, accepted the methoxymalonyl substrate to some extent, *i.e.* about 5% of the product from the engineered strain was ascomycin in the ascomycin PKS context. When ascomycin AT8 was placed into the context of DEBS module 6, both methylmalonyl-CoA and malonyl-CoA were used efficiently as substrates, even though the domain rejects these substrates in the native context, as discussed above. Recently, genes encoding methoxymalonyl-ACP biosynthesis from the ansamitocin gene cluster of *Actinosynnema pretiosum* were co-expressed along with the engineered DEBS genes in *S. lividans*, and the resulting strain produced 2-methoxy-2-demethyl-6-DEB.[5] This shows that ascomycin AT8 maintains its original substrate preference in this foreign context. On the other hand, our results also suggest that changing the context of an AT domain can affect substrate selectivity. We hypothesize that external steric forces on a domain after folding and assembly of the PKS complex can change the conformation of a domain sufficiently to affect its specificity. Replacement of a short segment of amino acids toward the C terminus of AT domains, which lies outside the homology with *E. coli* transacylase and is probably on the exterior of the domain, also has been shown to alter specificity (24). Perhaps this region is important for the interaction of the AT domain with the rest of

the PKS complex and thus can affect specificity by the mechanism hypothesized here.

Although primary sequence motifs have been identified that play a role in substrate specificity (15, 33), it has not yet been possible to identify sequence motifs correlated with specificity for the methoxymalonyl substrate. Indeed, AT domains specific for methoxymalonyl substrates appear to have evolved from either malonyl-specific domains, as in the case of the ascomycin PKS, or from methylmalonyl-specific domains, as in the case of the niddamycin and soraphen PKSs (18, 34).

---

⁴ M. Trujillo, W. P. Revill, and L. Katz, unpublished data.

⁵ Y. Kato, L. Bai, Q. Xue, W. P. Revill, T.-W. Yu, and H. G. Floss, submitted for publication.

REFERENCES

1. Sewing, K. F. (1994) *Transplant. Proc.* **26,** 3267–3269
2. Iwasaki, K., Matsuda, H., Nagase, K., Shiraga, T., Tokuma, Y., and Uchida, K. (1993) *Res. Commun. Chem. Pathol. Pharmacol.* **82,** 209–216
3. Lampen, A., Christians, U., Guengerich, F. P., Watkins, P. B., Kolars, J. C., Bader, A., Gonschior, A. K., Dralle, H., Hackbarth, I., and Sewing, K. F. (1995) *Drug Metab. Dispos.* **23,** 1315–1324
4. Iwasaki, K., Shiraga, T., Matsuda, H., Nagase, K., Tokuma, Y., Hata, T., Fujii, Y., Sakuma, S., Fujitsu, T., and Fujikawa, A. (1995) *Drug Metab. Dispos.* **23,** 28–34
5. Shiraga, T., Matsuda, H., Nagase, K., Iwasaki, K., Noda, K., Yamazaki, H., Shimada, T., and Funae, Y. (1994) *Biochem. Pharmacol.* **47,** 727–735
6. McDaniel, R., Thamchaipenet, A., Gustafsson, C., Fu, H., Betlach, M., and Ashley, G. (1999) *Proc. Natl. Acad. Sci. U. S. A.* **96,** 1846–1851
7. Katz, L. (1997) *Chem. Rev.* **97,** 2557–2576
8. Byrne, K. M., Shafiee, A., Nielson, J., Arison, B., Monaghan, R. L., and Kaplan, L. (1993) *Dev. Ind. Microbiol.* **32,** 29–45
9. Motamedi, H., Shafiee, A., Cai, S. J., Streicher, S. L., Arison, B. H., and Miller, R. R. (1996) *J. Bacteriol.* **178,** 5243–5248
10. Motamedi, H., Cai, S. J., Shafiee, A., and Elliston, K. O. (1997) *Eur. J. Biochem.* **244,** 74–80
11. Motamedi, H., and Shafiee, A. (1998) *Eur. J. Biochem.* **256,** 528–534
12. Nielsen, J. B., Hsu, M. J., Byrne, K. M., and Kaplan, L. (1991) *Biochemistry* **30,** 5789–5796
13. Shafiee, A., Motamedi, H., Dumont, F. J., Arison, B. H., and Miller, R. R. (1997) *J. Antibiot. (Tokyo)* **50,** 418–423
14. Wu, K., Chung, L., Revill, W. P., Katz, L., and Reeves, C. D. (2000) *Gene (Amst.)* **251,** 81–90
15. Haydock, S. F., Aparicio, J. F., Molnar, I., Schwecke, T., Khaw, L. E., Konig, A., Marsden, A. F., Galloway, I. S., Staunton, J., and Leadlay, P. F. (1995) *FEBS Lett.* **374,** 246–248
16. Kuhstoss, S., Huber, M., Turner, J. R., Paschal, J. W., and Rao, R. N. (1996) *Gene (Amst.)* **183,** 231–236
17. Oliynyk, M., Brown, M. J., Cortes, J., Staunton, J., and Leadlay, P. F. (1996) *Chem. Biol.* **3,** 833–839
18. Kakavas, S. J., Katz, L., and Stassi, D. (1997) *J. Bacteriol.* **179,** 7515–7522
19. Haber, A., Johnson, R. D., and Rinehart, K. L. J. (1977) *J. Am. Chem. Soc.* **99,** 3541–3544
20. Hill, A. M., Harris, J. P., and Siskos, A. P. (1998) *Chem. Commun.* **1998,** 2361–2362
21. Ono, M., Sakuda, S., Ikeda, H., Furihata, K., Nakayama, J., Suzuki, A., and Isogai, A. (1998) *J. Antibiot. (Tokyo)* **51,** 1019–1028
22. Serre, L., Verbree, E. C., Dauter, Z., Stuitje, A. R., and Derewenda, Z. S. (1995) *J. Biol. Chem.* **270,** 12961–12964
23. Khosla, C., Gokhale, R. S., Jacobsen, J. R., and Cane, D. E. (1999) *Annu. Rev. Biochem.* **68,** 219–253
24. Lau, J., Fu, H., Cane, D. E., and Khosla, C. (1999) *Biochemistry* **38,** 1643–1651
25. Marsden, A. F., Caffrey, P., Aparicio, J. F., Loughran, M. S., Staunton, J., and Leadlay, P. F. (1994) *Science* **263,** 378–380
26. Rangan, V. S., and Smith, S. (1997) *J. Biol. Chem.* **272,** 11975–11978
27. Rangan, V. S., Serre, L., Witkowska, H. E., Bari, A., and Smith, S. (1997) *Protein Eng.* **10,** 561–566
28. Kieser, T., Bibb, M. J., Buttner, M. J., Chater, K. F., and Hopwood, D. A. (2000) *Practical Streptomyces Genetics*, The John Innes Foundation, Norwich, United Kingdom
29. Kao, C. M., Katz, L., and Khosla, C. (1994) *Science* **265,** 509–512
30. Julien, B., Shah, S., Ziermann, R., Goldman, R., Katz, L., and Khosla, C. (2000) *Gene (Amst.)* **249,** 153–160
31. Tang, L., Shah, S., Chung, L., Carney, J., Katz, L., Khosla, C., and Julien, B. (2000) *Science* **287,** 640–642
32. Liu, H., and Reynolds, K. A. (1999) *J. Bacteriol.* **181,** 6806–6813
33. Reeves, C. D., Murli, S., Ashley, G. W., Piagentini, M., Hutchinson, C. R., and McDaniel, R. (2001) *Biochemistry* **40,** 15464–15470
34. Schupp, T., Toupet, C., Cluzel, B., Neff, S., Hill, S., Beck, J. J., and Ligon, J. M. (1995) *J. Bacteriol.* **177,** 3673–3679

Presentation of a T Cell Receptor Antagonist Peptide by Immunoglobulins Ablates Activation of T Cells by a Synthetic Peptide or Proteins Requiring Endocytic Processing

By Kevin L. Legge,* Booki Min,* Nicholas T. Potter,‡ and Habib Zaghouani*

From the *Department of Microbiology, University of Tennessee, Knoxville, Tennessee 37996; and ‡The Developmental and Genetic Center, University of Tennessee Medical Center, Knoxville, Tennessee 37920

Summary

T cell receptor (TCR) antagonism is being considered for inactivation of aggressive T cells and reversal of T cell–mediated autoimmune diseases. TCR antagonist peptides silence aggressive T cells and reverse experimental allergic encephalomyelitis induced with free peptides. However, it is not clear whether free antagonist peptides could reverse natural disease where the antigen is presumably available for endocytic processing and peptides gain access to newly synthesized class II MHC molecules. Using an efficient endocytic presentation system, we demonstrate that a proteolipid protein (PLP) TCR antagonist peptide (PLP-LR) presented on an Ig molecule (Ig-PLP-LR) abrogates the activation of T cells stimulated with free encephalitogenic PLP peptide (PLP1), native PLP, or an Ig containing PLP1 peptide (Ig-PLP1). Free PLP-LR abolishes T cell activation when the stimulator is free PLP1 peptide, but has no measurable effect when the stimulator is the native PLP or Ig-PLP1. In vivo, Ig-PLP1 induces a T cell response to PLP1 peptide. However, when coadministered with Ig-PLP-LR, the response to PLP1 peptide is markedly reduced whereas the response to PLP-LR is normal. Free PLP-LR coadministered with Ig-PLP1 has no effect on the T cell response to PLP1. These findings indicate that endocytic presentation of an antagonist peptide by Ig outcompete both external and endocytic agonist peptides whereas free antagonist hinders external but not endocytic agonist peptide. Direct contact with antagonist ligand and/or *trans*-regulation by PLP-LR–specific T cells may be the operative mechanism for Ig-PLP-LR–mediated downregulation of PLP1-specific T cells in vivo. Efficient endocytic presentation of antagonist peptides, which is the fundamental event for either mechanism, may be critical for reversal of spontaneous T cell–mediated autoimmune diseases where incessant endocytic antigen processing could be responsible for T cell aggressivity.

Over the last few years it has become clear that the avidity of T cell–APC interactions dictates thymic learning and tolerance to self antigens (1). Accordingly, high avidity interactions lead to elimination of the T cell, whereas low avidity interactions allow for maturation and exit from the thymus (2–4). Although this mechanism is effective in purging the immune system of autoreactivity, T cell precursors endowed with self reactivity could still be generated if the autoantigen is sequestered and does not reach for thymic presentation, is subjected to thymic crypticity, or is poorly presented (5–7). Superantigens capable of reacting with particular Vβ-TCR (8) and events that could set to motion antigen mimicry (9), epitope spreading (10), or peripheral loosening in peptide crypticity (11), may trigger activation of those self-reactive T cells and cause antigen exposure. Continuous supply of autoantigen and abundant generation of TCR ligands may be the mechanism of T cell

aggressivity. Multiple sclerosis (MS)[1], type I diabetes, and rheumatoid arthritis, all of which are thought to be T cell–mediated autoimmune diseases qualify as examples of a spontaneous break of self tolerance (12–14).

Experimental allergic encephalomyelitis (EAE) that is used as an animal model for MS can be induced in susceptible strains of mice with myelin autoantigens such as proteolipid protein (PLP) and myelin basic protein (MBP; for review see reference 15). The encephalitogenic activity of these proteins correlates with the presence of peptides that induce in vivo class II–restricted encephalitogenic T cells and

---

[1]*Abbreviations used in this paper:* aa, amino acid; EAE, experimental allergic encephalomyelitis; HA, hemagglutinin; MBP, myelin basic protein; MS, multiple sclerosis; PLP, proteolipid protein; PLP1, the peptide corresponding to aa residues 139–155 of PLP; PPD, purified protein derivative.

consequently EAE (15). The peptide corresponding to amino acid (aa) residues 139–151 of PLP (hereafter is referred to PLP1) is encephalitogenic in H-2^s SJL mice (16), and T cell lines specific for PLP1 transfer EAE into naive animals (17). Although the target antigen(s) in human MS is still debatable, the frequency of T cells specific for myelin proteins are higher in MS patients than in normal subjects (18–19). Therefore, silencing those myelin-reactive T cells may be a logical approach to reverse MS.

Interaction of T cells with altered peptide ligands could have various effects on TCR-mediated effector functions (20). These include induction of cytokine production without proliferation (21), changes in the profile of cytokines produced (22), TCR antagonism that is a state of cytokine and proliferative unresponsiveness (23–25), and anergy that is a state of cytokine and proliferative unresponsiveness to a subsequent stimulation with the agonist peptide (26). Peptide analogues represent an attractive approach to modulating the effector functions of aggressive T cells and ameliorating autoimmune diseases. A promising success was achieved in the EAE system in which mice induced for EAE with a free MBP encephalitogenic peptide or by transfer of an MBP-specific T cell clone recovered from the disease when they were treated with a peptide analogue (27, 28). Similarly, treatment of human T cells specific for MBP with a TCR antagonist peptide modulated their cytokine production profile and increased secretion of TGF-β (22). Reversal of EAE was also achieved with a TCR antagonist peptide derived from PLP1 peptide (29). Indeed, when the major TCR contacting residues within PLP1 were mutated, the resulting peptide analogue (hereafter referred to as PLP-LR), although binding to I-A^s equally as well as PLP1, does not activate PLP1-specific T cells. Instead, PLP-LR inhibits in vitro activation of the T cells by PLP1. In addition, EAE induced in mice with free PLP1 peptide resolved after treatment with free PLP-LR (29). Since only a few MHC-peptide complexes are available on the surface of APCs, and a single complex may be required to serially trigger ~200 TCRs to activate the T cells (30, 31), the ratio of antagonist versus agonist ligands on the surface of a given APC becomes a major factor as to whether injection of free peptide analogues could reverse spontaneous autoimmune disease where the autoantigen could be continuously available. Furthermore, the presentation of autoantigens may operate through an endocytic pathway loading peptides onto newly synthesized MHC molecules and generating an unsurmountable agonist–MHC target to overcome. Overcoming such obstacles may demand highly effective antagonist systems. One such approach might well be peptide presentation on autologous Ig. Ig can function as a delivery system for T cell peptides (32, 33). A 100–1,000-fold increase in T cell activation was observed when a class II–restricted peptide from the hemagglutinin (HA) of influenza virus was presented on an Ig chimera, Ig-HA (34). Similar results were obtained when a class II peptide from λ_2 phage repressor protein was expressed on an IgG1 molecule (35). The increase in T cell activation appears to result from efficient peptide loading onto MHC molecules (36).

In the present report, we asked whether Ig-mediated endocytic presentation of an antagonist peptide could out compete high endosomal antigen load and downregulate autoreactive T cells. To this end, PLP-LR antagonist peptide was expressed on an Ig molecule and the resulting Ig-PLP-LR chimera was compared with free PLP-LR for antagonism of PLP-specific T cells. The results indicate that Ig-PLP-LR inactivates PLP1-specific T cells whether the stimulator is PLP1 peptide, native PLP, or even an Ig expressing PLP1 (Ig-PLP1). However, a free PLP-LR peptide could not inhibit IL-2 production when the T cells were stimulated with APCs pulsed with Ig-PLP1 or native PLP. In vivo, when Ig-PLP1 was administered to SJL/J mice it induced a strong PLP1-specific T cell response, but when coadministered with Ig-PLP-LR, the response to PLP1 fell to almost background levels. Efficient endocytic presentation of antagonist peptides may therefore oppose the unlimited and persistent generation of endogenous self peptides that might occur in T cell–mediated autoimmune diseases such as MS.

Materials and Methods

Animals

6–8-wk-old SJL/J mice (H-2^s) were purchased from Harlan Sprague Dawley (Frederick, MD) and maintained in our animal facility for the duration of experiments. New Zealand white rabbits were purchased from Myrtle's Rabbitry (Thompson Station, TN).

Antigens

Peptides. All peptides used in these studies were purchased from Res. Genetics (Huntsville, Alabama) and purified by HPLC to >90% purity. PLP1 peptide (HSLGKWLGHPDKF) encompasses an encephalitogenic sequence corresponding to aa residues 139–151 of PLP (16). PLP-LR (HSLGKLLGRPDKF) is a mutant form of PLP1 in which Trp144 and His147 were replaced with Leu and Arg, respectively (29). PLP1 and PLP-LR bind equally well to I-A^s class II molecules (29). However, stimulation of T cell hybridomas with PLP1 in the presence of PLP-LR leads to blockade of IL-2 production by these T cells (29). PLP2 peptide (NTWTTCQSIAFPSK) encompasses an encephalitogenic sequence corresponding to aa residues 178–191 of PLP (37). This peptide binds to I-A^s class II molecules and induces EAE in SJL/J mice (37). HA110-120 peptide corresponds to aa residues 110–120 of the HA of influenza virus. HA110-120 binds to I-E^d class II molecules and is used here as control peptide (34).

Ig-PLP Chimeras. PLP1 and PLP-LR peptides were expressed on Ig chimeras that were designated Ig-PLP1 and Ig-PLP-LR, respectively. The genes used to construct these chimeras are those coding for the light (38) and heavy (39) chains of the anti-arsonate antibody, 91A3. The procedures for deletion of the heavy chain CDR3 region and replacement with nucleotide sequences coding for PLP1 and PLP-LR are similar to those described for the generation of Ig-NP (40), a chimera carrying a CTL epitope corresponding to aa residues 147–161 of the nucleoprotein of PR8 influenza A virus. In brief, the 91A3V$_H$ gene was subcloned into the EcoRI site of pUC19 plasmid and used as template DNA in PCR mutagenesis reactions (40) to generate 91A3V$_H$ fragments carrying PLP1 (91A3V$_H$-PLP1) and PLP-LR (91A3V$_H$-PLP-LR) sequences in place of CDR3. Nucleotide sequencing analysis indicated that full PLP1 and PLP-LR sequences were inserted in

the correct reading frame (not shown). The 91A3V$_H$-PLP1 and 91A3V$_H$-PLP-LR fragments were then subcloned into the EcoRI site of pSV2-gpt-Cγ2b in front of the exons coding for the constant region of a BALB/c γ2b that generated pSV2-gpt-91A3V$_H$-PLP1-Cγ2b and pSV2-gpt-91A3V$_H$-PLP1-LR-Cγ2b plasmids, respectively. These plasmids were then separately co-transfected into the non-Ig–producing SP2/0 B myeloma cells with an expression vector carrying the parental 91A3 light chain, pSV2-neo-91A3L (38, 40). Transfectants producing Ig chimeras were selected in the presence of geneticin and mycophenolic acid. Transfectants were cloned by limiting dilution, and final clones secreted 1–4 μg/ml of Ig-PLP chimeras. All the cloning, sequencing, and purification procedures are similar to those used to generate Ig-NP (40) and Ig-HA (34). Nucleotide sequences and detailed mutagenesis procedures for Ig-PLP1 and Ig-PLP-LR will be published elsewhere. Also used in these studies was Ig-W (40), a chimera encoded by wild-type genes that does not carry any PLP peptide.

Large scale cultures of transfectants were carried out in DMEM containing 10% iron enriched calf serum (Intergen Corp., Purchase, New York). Ig-PLP chimeras were purified from culture supernatant on columns made of rat anti–mouse κ chain coupled to CNBr activated Sepharose 4B (Pharmacia). To avoid cross-contamination, separate columns were used to purify the chimeras.

PLP. PLP was purified from rat brain according to a previously described procedure (41). In brief, the brain was homogenized in 2:1 vol/vol chloroform/methanol, and the soluble crude lipid extract was separated by filtration through a scintered glass funnel. PLP was then precipitated with acetone and the pellet was redissolved in a mixture of chloroform, methanol, and acetic acid and passed through a sephadex column (LH-20-100; Sigma Chemical Co., St. Louis, MO) to remove residual lipids. Removal of chloroform from the eluates and conversion of PLP into its apoprotein form were carried out simultaneously through gradual addition of water under a gentle stream of nitrogen. Subsequently, extensive dialysis against water was performed to remove residual acetic acid and methanol.

Production of Rabbit Anti–peptide Antibodies

PLP1 and PLP-LR peptides were coupled to KLH and BSA as described (42). Rabbits were immunized with 1 mg peptide–KLH conjugates in CFA and challenged monthly with 1 mg conjugate in IFA until a high antibody titer was reached as described (43). The peptide–BSA conjugates were coupled to Sepharose and used to purify anti–peptide antibodies from the rabbit antiserum.

Radioimmunoassay

Capture radioimmunoassay was used to assess expression of PLP peptides on Ig. Microtiter 96-well plates were coated with rabbit anti–peptide antibodies (5 μg/ml) overnight at 4°C and blocked with 2% BSA in PBS for 1 h at room temperature. The plates were then washed three times with PBS, and graded amounts of Ig-PLP chimeras were added and incubated for 2 h at room temperature. After three washes with PBS, captured Ig-PLP chimeras were revealed by incubating the plates with 10^5 cpm/well ^{125}I-labeled rat anti–mouse κ mAb for 2 h at 37°C. The plates were then washed five times with PBS and counted using an LKB gamma counter.

Cells

PLP1-specific T cell hybridomas 5B6 and 4E3 (29) and the IL-2–dependent HT-2 T helper were obtained from Drs. M.B. Lees and V. Kuchroo (The Eunice Kennedy Shriver Center, Wal-

tham, MA). The 5B6 and 4E3 T cells recognize PLP1 in association with I-A^s and produce IL-2 in response to it (29). However, when stimulated with PLP1 and then with PLP-LR, they become unable to produce IL-2 (29). The rat anti–mouse κ chain mAb (187.1 or American Type Culture Collection denotation, HB-58) and the mouse anti–rat κ light chain mAb (MAR 18.5 or American Type Culture Collection denotation TIB 216) were obtained from American Type Culture Collection (Rockville, MD). These hybridomas were grown to large scale and purified from culture supernatant on each other. The rat anti–mouse κ mAb was used to prepare columns on which Ig-PLP chimeras were purified from culture supernatant.

T Cell Activation Assay

Irradiated (3,000 rads) SJL splenocytes (used as APCs) were incubated in 96-well round-bottom plates (5 × 10^5 cells/well/50 μl) with graded concentration of antigens (100 μl/well). After 1 h, T cell hybridomas (5 × 10^4 cells/well/50 μl) were added and the culture was continued overnight. Activation of the T cells was assessed by measuring production of IL-2 in the culture supernatant. This was done by [^{3}H]thymidine incorporation using the IL-2–dependent HT-2 cells. In brief, culture supernatants (100 μl/well) were incubated with HT-2 cells (10^4/100 μl/well) in 96-well flat-bottom plates for 24 h. Subsequently, 1 μCi [^{3}H]thymidine was added per well and the culture was continued for an additional 12–14 h. The cells were then harvested on glass fiber filters, and incorporated [^{3}H]thymidine was counted using the trace 96 program and an Inotech β counter. The culture media used to carry out these assays were DMEM supplemented with 10% FBS, 0.05 mM 2-mercaptoethanol, 2 mM glutamine, 1 mM sodium pyruvate, and 50 μg/ml gentamycin sulfate.

Assay for Inhibition of T Cell Activation

Irradiated (3,000 rads) SJL/J splenocytes (used as APCs) were incubated in 96-well round-bottom plates (5 × 10^5 cells/well/50 μl) with the stimulator antigen (optimal dose in 50 μl/well) and graded concentration of inhibitor (100 μl/well) for 1 h. Subsequently, T cell hybridomas (5 × 10^4 cells/well/50 μl) were added and the culture was continued overnight. IL-2 production in the supernatant, which was used as measure of T cell activation, was determined using HT-2 cells, as above.

Immunization of Mice with Ig Chimeras and Peptides

Immunization with Ig-PLP1. Mice were immunized subcutaneously in the foot pads and at the base of the limbs and tail with 50 μg of Ig-PLP1 emulsified in a 200 μl mixture 1:1 vol/vol PBS/CFA. 10 d later the mice were killed by cervical dislocation, the spleens and lymph nodes (axillary, inguinal, popliteal, and sacral) were removed, single cell suspensions were prepared, and the T cell responses were analyzed as described below.

Co-immunization of Mice with Ig-PLP1 and Ig-PLP-LR, Ig-W, or PLP-LR peptide. Individual mice from three groups (four mice per group) were injected subcutaneously as above with a 200 μl mixture (PBS/CFA, 1:1 vol/vol) containing 50 μg Ig-PLP1 and 150 μg Ig-PLP-LR; 50 μg Ig-PLP1 and 150 μg Ig-W; or 50 μg Ig-PLP1 and 100 μg PLP-LR peptide. Splenic and lymph node T cell responses were analyzed at day 10 after immunization.

Assays for Spleen and Lymph Node Proliferative Responses

Lymph node and spleen cells were incubated in 96-well round-bottom plates at 4 and 10 × 10^5 cells/100 μl/well, respectively, with 100 μl of stimulator for 3 d. Subsequently, 1 μCi [^{3}H]thy-
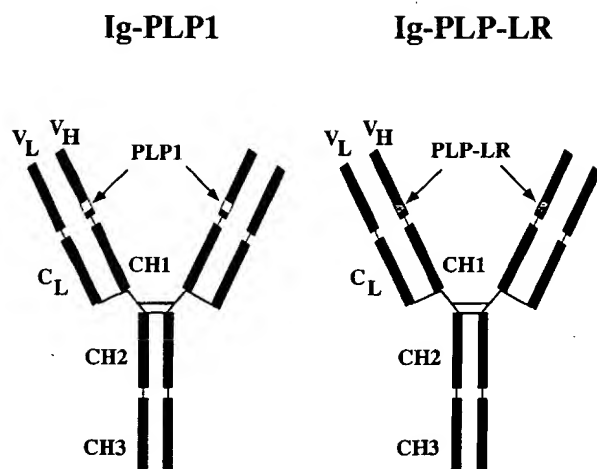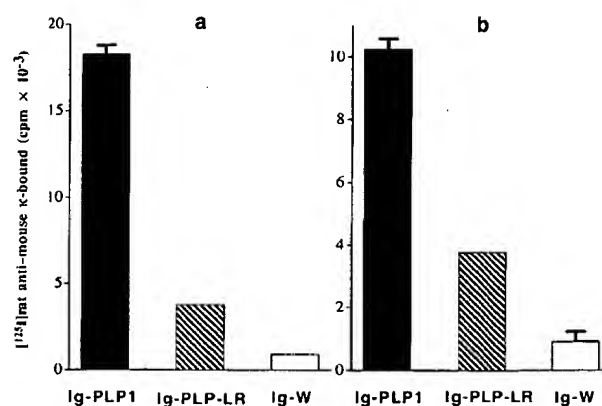
Ig-PLP1 Ig-PLP-LR

Figure 1. Schematic representation of Ig-PLP1 and Ig-PLP-LR. The CDR3 loop (D segment) of the heavy chain variable region of the antiarsonate antibody 91A3, was deleted and replaced with nucleotide sequences that encode PLP1 and PLP-LR peptides. These chimeric V_H genes were then ligated to a gene encoding a BALB/c γ2b constant region to generate complete chimeric heavy chain. These heavy chains were then co-transfected with parental 91A3 κ light chain into the non-Ig-secreting myeloma cell SP2/0 to generate a complete IgG2b,K chimera carrying PLP1 (Ig-PLP1) and PLP-LR (Ig-PLP-LR) peptide. Other chimeras were also used as controls: Ig-HA, an Ig molecule carrying in place of the D segment the HA110-120 T helper epitope from the HA and differ from Ig-PLP1 and Ig-PLP-LR only by the peptide inserted within CDR3. Ig-W is the product of unmodified (wild-type) 91A3V_H gene, BALB/c γ2b constant region, and 91A3 κ light chain. Therefore, it differs from Ig-PLP1 and Ig-PLP-LR in the CDR3 region which is the parental D segment. Ig-PLP2 is a chimera that carries aa residues 178–191 of PLP (this chimera will be described elsewhere) within the heavy chain CDR3 loop.


Figure 2. PLP peptide expression on Ig-PLP1 and Ig-PLP-LR. Rabbit antibodies to PLP1 and PLP-LR were used in a capture radioimmunoassay to demonstrate peptide expression on the chimeras. Microtiter plates were coated with affinity-purified rabbit antibodies to PLP1 (a) or to PLP-LR (b), blocked with BSA, and incubated with graded amounts (27, 9, 3, and 1 μg/ml) of Ig-PLP1, Ig-PLP-LR, or negative control Ig-W. Captured Ig were revealed with ^{125}I-labeled rat anti–mouse κ light chain mAb. Shown are the mean ± SD of triplicates obtained with 27 μg/ml of chimeras.

midine was added per well, and the culture was continued for an additional 12–14 h. The cells were then harvested on glass fiber filters, and incorporated [³H]thymidine was counted using the trace 96 program and an Inotech β counter. The stimulators were used at the following concentrations: PLP1, PLP2, and PLP-LR peptides at 15 μg/ml, and proteolipid protein (PPD) at 5 μg/ml. A control media with no stimulator was included for each mouse and used as background.

Results

Expression of PLP Peptides on Ig Molecules.   Two Ig-PLP chimeras designated Ig-PLP1 and Ig-PLP-LR were constructed to include PLP1 and PLP-LR peptides, respectively (Fig. 1). In both cases, the heavy chain CDR3 loop was deleted and replaced with nucleotide sequences coding for the selected peptide. DNA sequencing analysis indicated insertion of peptide nucleotide sequences in the correct reading frame (not shown). In addition, rabbit antibodies to synthetic PLP1 and PLP-LR peptides recognized the chimeras (Fig. 2). Indeed, when Ig-PLP1 and Ig-PLP-LR were incubated on plates coated with rabbit anti-PLP1 antibodies they were captured by these rabbit antibodies and bound ^{125}I-labeled rat anti–mouse κ chain mAb (Fig. 2 a). Similarly, both Ig-PLP1 and Ig-PLP-LR were captured by

rabbit anti–PLP-LR (Fig. 2 b). Ig-W, the wild-type 91A3 antibody without peptide and an IgM control antibody, did not show significant binding to the rabbit antibodies. Ig-PLP1 bound to both anti-PLP1 and anti-PLP-LR antibodies better than did Ig-PLP-LR, indicating that structural differences affected accessibility of the peptides to the rabbit antibodies. The above experiments also indicated that peptide expression on the chimeras did not alter heavy and light chain pairing because the rabbit antibodies bind to the PLP peptide on the heavy chain and the rat anti-κ binds on the light chain.

Presentation of Ig-PLP Chimeras to T Cells.   The CDR3 of the 91A3 Ig is permissive for peptide expression, and both class I– and class II–restricted epitopes have been efficiently processed and presented to T cells when grafted in place of the D segment (34, 40). Ig-PLP1 that includes the PLP1 peptide within CDR3 is also presented to specific T cells (Fig. 3). T cell hybridomas 5B6 and 4E3 specific for PLP1 produced IL-2 subsequent to stimulation with APCs pulsed with Ig-PLP1 as they have done when pulsed with PLP1 and native PLP. The negative controls Ig-W, Ig-HA, and PLP2 peptide did not induce the production of IL-2 by the T cells. Both Ig-PLP-LR and PLP-LR peptide do not stimulate 5B6 and 4E3 for production of IL-2 (Fig. 3). These results are expected because PLP-LR peptide is known to negate rather than stimulate IL-2 production. However, whereas these experiments could not show the processing and presentation of Ig-PLP-LR, we have evidence that PLP-LR peptide is released from the chimeras and presented to the T cells (see below).

Efficient Presentation of Ig-PLP1 to T Cells.   In spontaneous disease, exposure and continuous endocytic presentation of autoantigen may generate significant levels of MHC–agonist complexes. Ig-PLP1 was constructed for the purpose of
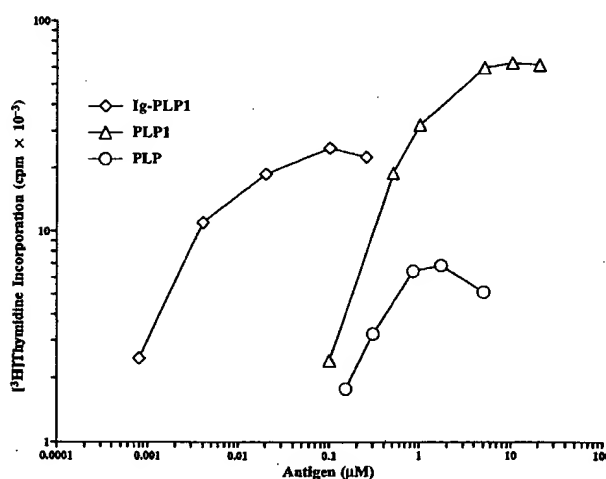
[³H]Thymidine incorporation (cpm × 10⁻³)
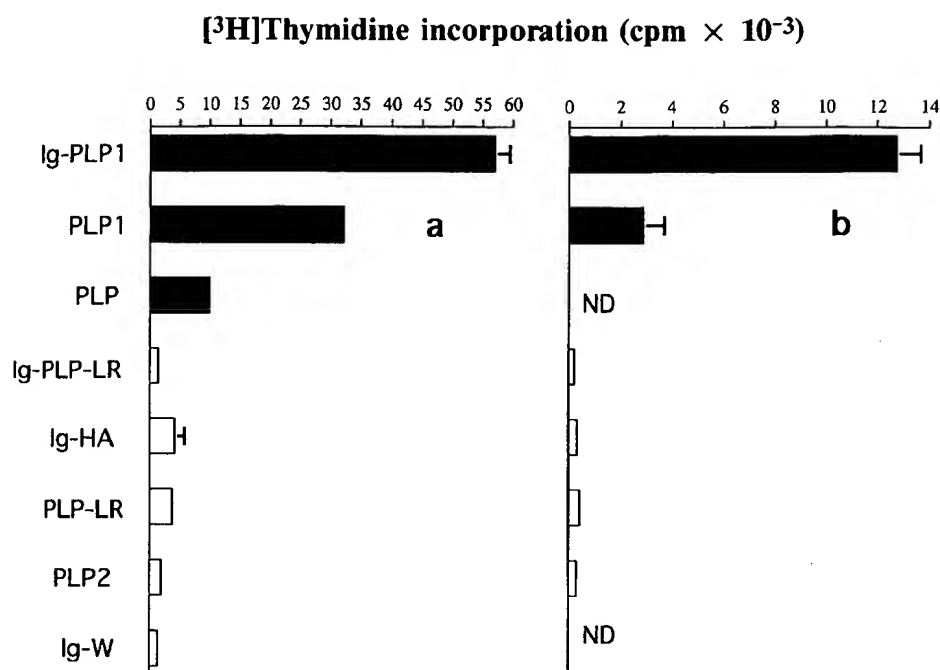
Figure 3. Presentation of Ig-PLP chimeras to PLP1-specific T cell hybridomas. Ig-PLP1 and Ig-PLP-LR were assayed for presentation to the PLP1-specific T cell hybridomas 4E3 (a) and 5B6 (b) by measurement of IL-2 production as indicated in the Materials and Methods section. Irradiated SJL/J splenocytes (as APCs) were incubated with the indicated antigens and T cells overnight, and IL-2 content of the supernatant was measured by [³H]thymidine incorporation using the IL-2-dependent HT-2 cells. The concentration of antigen was 0.1 μM for Ig-PLP1, Ig-PLP-LR, Ig-HA, and Ig-W; 1 μM for PLP1 and PLP2 peptides; and 1.7 μM for PLP. Each value represents the mean ± SD of triplicate wells.

establishing a peptide delivery system that could efficiently operate through the endocytic pathway and generate high levels of agonist ligands such that it provides a relevant system to investigate T cell antagonism in a situation similar to presentation of autoantigens. It is therefore important to determine the efficacy of Ig-PLP1 in peptide delivery and presentation to specific T cells. To this aim, dose response T cell activation assays were performed with free PLP1 peptide, native PLP, and Ig-PLP1. The results shown in Fig. 4 indicate that the PLP1 T cell epitope was better presented by Ig-PLP1 than by native PLP or by free PLP1 peptide. Although the plateau of IL-2 production was higher when the T cell stimulator is PLP1 synthetic peptide, the individual half maximal IL-2 production by the T cells required about 100-fold higher of PLP or PLP1 peptide than Ig-PLP1 (Fig. 4). The efficacy of Ig-PLP1 in peptide delivery may be related to FcR-mediated internalization and access to newly synthesized MHC molecules, as we have previously shown for Ig-HA (34, 36), whereas PLP may internalize by simple fluid phase pinocytosis, and PLP1 peptide may bind to empty MHC class II molecules at the cell surface. Overall, Ig-PLP1 is efficient in loading PLP1 peptide onto class II molecules within the endosomal compartment.

Inhibition of T Cell Activation by Ig-PLP-LR. The potency of Ig-PLP1 chimeras in peptide loading onto class II molecules provides a situation that probably resembles in vivo autoimmune circumstances, where a continuous supply of antigen may allow for abundant generation of self peptides, which could trigger T cells aggressively. The Ig-PLP1 endocytic presentation system was then used to investigate Ig-PLP-LR for inactivation of PLP1-specific T cells. As shown in Fig. 5 a, when T cells were incubated with APCs in the

presence of both PLP1 and Ig-PLP-LR, a specific decrease in IL-2 production occurred as the concentration of Ig-PLP-LR increased. These results are in agreement with a previous report that showed that efficient endocytic presentation of an antagonist form of hemoglobin outcompeted an external agonist peptide (44). A similar decline in IL-2 production was evident when the synthetic PLP-LR

Figure 4. Efficient presentation of Ig-PLP1 to 4E3 T cell hybridoma. Graded amounts of each antigen were incubated with splenic SJL/J APCs and the PLP1-specific 4E3 T cell hybridoma, and IL-2 production was measured by [³H]thymidine incorporation using the IL-2-dependent HT-2 cells as described in the legend to Fig. 3. Each point represents the mean of triplicates. The SD did not exceed 10% of the mean value. Although the maximal activation varied among the three different stimulators, the individual half maximal activation required less Ig-PLP1 (0.005 μM) than PLP (0.5 μM) or PLP1 peptide (0.6 μM).
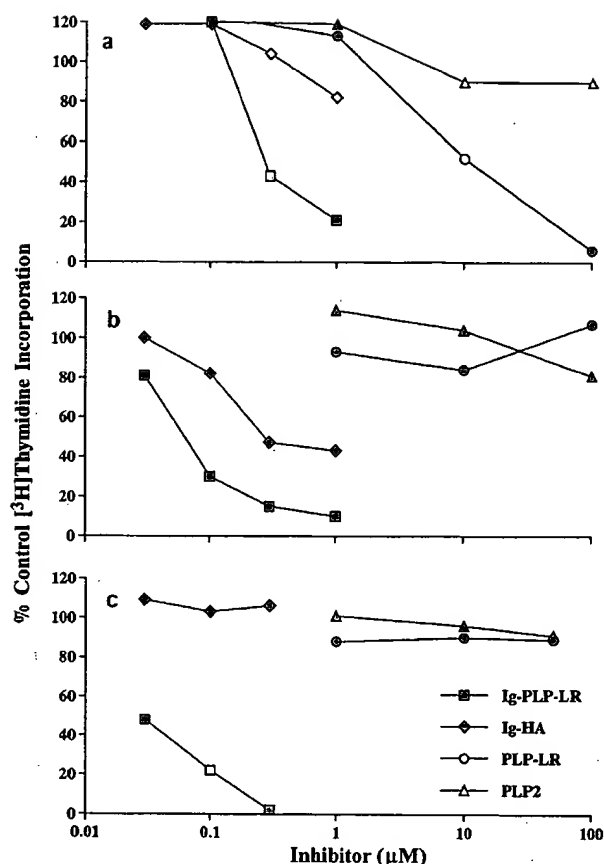
Figure 5. Antagonism of PLP1-, PLP-, and Ig-PLP1-mediated T cell activation by Ig-PLP-LR. SJL/J splenic APCs were incubated with (a) 1 μM PLP1 peptide, (b) 0.05 μM Ig-PLP1, or (c) 6.8 μM PLP in the presence of graded amounts of antagonists or controls antigens, and then assayed for activation of the PLP1-specific T cell hybridoma 4E3, by measuring IL-2 production as described in the Materials and Methods section. The antagonists were Ig-PLP-LR (squares), PLP-LR (circles), and the controls were Ig-HA (diamonds) and PLP2 (triangles). The cpm value obtained when the APCs were incubated with the stimulator but no antagonist was used as maximum [3H]thymidine incorporation. This value was 7,503 ± 1,302 for Ig-PLP1; 31,089 ± 3,860 for PLP1; and 8,268 ± 915 for PLP. The cpm value obtained when the APCs were incubated with no stimulator and no antagonist was used as background (BG). This value was 1,560 ± 323 for Ig-PLP1; 2,574 ± 290 for PLP1; and 2,127 ± 177 for PLP. The percent control thymidine incorporation was calculated as follows: (cpm obtained in the presence of test antagonist − BG)/(cpm control thymidine incorporation value − BG). Each point represents the mean of triplicates.

Figure 6. Competition for binding to class II at the endocytic level is not the mechanism for Ig-PLP-LR-mediated antagonism. SJL/J splenic APCs were incubated with native PLP (6.8 μM) in the presence of 50 μg/ml (0.3 μM) Ig-PLP2, Ig-PLP-LR, or Ig-W and 5 × 10⁴ PLP1-specific 4E3 T cells. IL-2 production was assessed by [3H]thymidine incorporation using HT-2 cells as described in the legend to Fig. 5. The percent control [3H]thymidine incorporation was calculated as in Fig. 5. Each column represents the mean ± SD of triplicates.

peptide was used during T cell activation with PLP1 peptide. Antagonistic effects were not observed with Ig-W chimera and PLP2 peptide used as negative controls (Fig. 5 a). The half maximal inhibition of IL-2 production (60% control thymidine incorporation) required 0.4 μM Ig-PLP-LR versus 9 μM PLP-LR peptide indicating a much more efficient presentation of and consequently T cell antagonism by Ig-PLP-LR (Fig. 5 a).

Further evidence that the chimera is more efficient than the free peptide in T cell antagonism is shown in Fig. 5, b and c. Ig-PLP-LR inhibited T cell activation mediated by Ig-PLP1 (Fig. 5 b) whereas free PLP-LR did not show any significant antagonism like the negative control PLP2 peptide (Fig. 5 b). Ig-W, the wild-type 91A3 Ig without peptide, showed partial inhibitory activity in Ig-PLP1-mediated T cell activation (Fig. 5 b). This is likely the result of competition for binding to the FcR on APCs because both Ig-PLP1 and Ig-W share identical IgG2b constant regions. As the concentration of Ig-W increases, less Ig-PLP1 will bind to FcR and internalize into the APCs, resulting in a diminished presentation and IL-2 production. Ig-W had similar inhibitory effects on the presentation of Ig-HA, as did the anti-FcR mAb 2.4G2 (34). Finally, Ig-PLP-LR, but not Ig-W, abolished the activation of T cells by native PLP (Fig. 5 c). However, PLP-LR and the negative control PLP2 peptide did not inhibit PLP-mediated T cell activation.

Competition for binding to class II molecules seems not to be the operative mechanism of antagonism at the endocytic level. This conclusion is drawn from the observation that Ig-PLP2, a chimera carrying PLP2 peptide (Min, B., K.L. Legge, and H. Zaghouani, manuscript in preparation), did not inhibit PLP-mediated T cell activation (Fig. 6) even though Ig-PLP2 is presented by I-Aˢ like PLP1.

In Vivo Antagonism of PLP1-specific T Cells by Ig-PLP-LR. As demonstrated in Fig. 7, when individual mice were immunized with Ig-PLP1, they developed strong PLP1-specific T cell responses in the lymph nodes (Fig. 7 a) and even significant proliferation in the spleen (Fig. 7 b). Consequently, Ig-PLP1, which is presumably processed in endocytic vacuoles like autoantigens, provides a relevant system to assay the antagonists Ig-PLP-LR and PLP-LR peptide for in vivo T cell antagonism.

The results in Fig. 8 indicate that co-immunization of mice with Ig-PLP1 and Ig-PLP-LR led to a reduced T cell
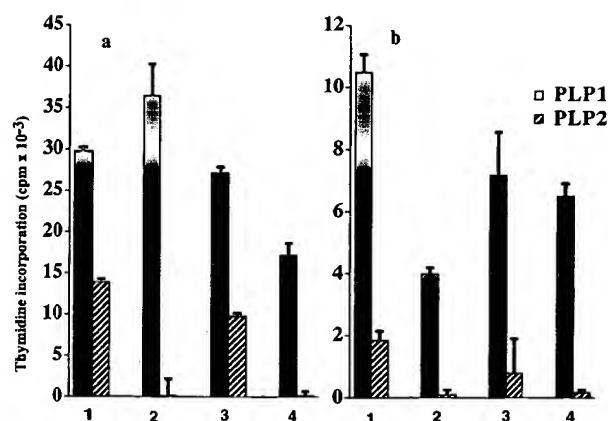
Figure 7. In vivo priming of PLP1-specific T cells by Ig-PLP1. Mice were immunized subcutaneously with 50 μg of Ig-PLP1 in CFA as described in Materials and Methods, and after 10 d, cells from the lymph nodes (a) and spleen (b) were tested for specific proliferation to PLP1. The indicated results are those obtained with 4×10^5 lymph node cells/well and 10×10^5 spleen cells/well. The stimulators PLP1 and PLP2 were used at 15 μg/ml and PPD was used at 5 μg/ml. Each value represents the mean ± SD of triplicates after deduction of BG cpms obtained with no stimulator in the media. The cpm values obtained with PPD for each mouse exceeded the cpm values obtained with PLP1 by 20–60% dependent upon each mouse. Similar results were obtained when mice were immunized with 150 μg of Ig-PLP1 per mouse (not shown). Note that some mice show proliferation with PLP2. This may be because this peptide is presented by I-A^s, like PLP1, and low affinity cells could bind to it.

Figure 8. Coadministration of Ig-PLP-LR with Ig-PLP1 reduces the response to PLP1 peptide. Mice were co-immunized with 50 μg Ig-PLP1 and 150 μg Ig-PLP-LR or 50 μg Ig-PLP1 and 150 μg Ig-W as indicated in Materials and Methods. The lymph node (a) and splenic (b) proliferative responses to PLP1 peptide were analyzed 10 d later. The lymph node cells were used at 4×10^5 cells/well and the spleen cells at 10^6 cells per well. The stimulators were PLP1 (15 μg/ml), and PPD (5 μg/ml). The indicated results are those obtained with PLP1 peptide and represent the mean ± SD of triplicates after deduction of BG cpm obtained with no stimulator in the media. The cpm values obtained with PPD were similar in both groups of mice and were 5–30% higher than the cpm values obtained with PLP1 in the mice immunized with Ig-PLP1 and Ig-W.
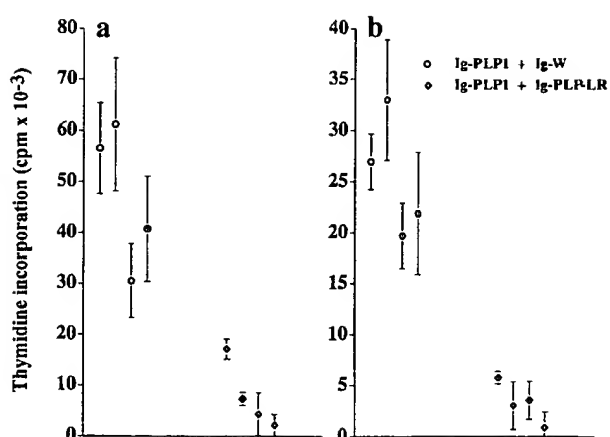
response to PLP1 when compared to responses obtained in mice injected with Ig-PLP1/Ig-W mixture. Both lymph node (Fig. 8 a) and splenic (Fig. 8 b) T cell responses were markedly reduced as a consequence of coadministration of Ig-PLP-LR with Ig-PLP1.

Because Ig-PLP-LR could induce a T cell response to PLP-LR, lymph node and spleen cells from mice immunized with Ig-PLP1/Ig-PLP-LR mixture were stimulated in vitro with PLP-LR peptide, and the specific [^{3}H]thymidine incorporation was measured and compared with PLP1 specific proliferation. The results depicted in Fig. 9 indicate that PLP-LR–specific T cells were present in both the lymph nodes (Fig. 9 a) and spleen (Fig. 9 b), and the specific proliferation to PLP-LR was two- to nine-fold higher than the proliferation to PLP1.

Mice co-immunized with Ig-PLP1 and free PLP-LR peptide showed no evidence for reduction of PLP1-specific responses (Table 1). To minimize the role of individual and experimental intrinsic variability on the overall outcome of the in vivo experiments, the PLP1-specific proliferations were expressed as percent of the individual response to PPD (Table 1). The standardized results clearly indicated a fall in the PLP1-specific response in the mice injected with Ig-PLP1 and Ig-PLP-LR relative to those injected with Ig-PLP1/Ig-W or Ig-PLP1/ PLP-LR peptide mixtures.

Discussion

Herein, we designed an endocytic antigen presentation system and evaluated fundamental mechanisms as to whether

TCR antagonist peptides could overcome antigens that because of efficient supply and access to endocytic processing could generate high levels of encephalitogenic peptides and therefore MHC–agonist complexes. In this system, PLP1 peptide and a TCR antagonist form of it, PLP-LR, were expressed on the anti-arsonate antibody 91A3, and the resulting Ig-PLP1 and Ig-PLP-LR chimeras were used to evaluate T cell antagonism in an antigen system requiring endocytic processing as it might occur in natural autoim-
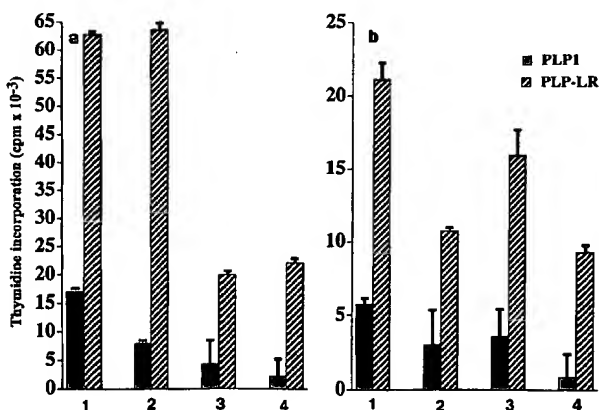
Figure 9. Mice co-injected with Ig-PLP1 and Ig-PLP-LR develop higher proliferative response to PLP-LR than PLP1 peptide. Day 10 after immunization, lymph node (a) and splenic (b) proliferative responses to PLP-LR peptide, in mice that were co-injected with Ig-PLP1 and Ig-PLP-LR and described in Fig. 8, were measured and shown here along with the responses to PLP1 peptide.

Table 1. *Ig-PLP-LR but Not Free PLP-LR Peptide Mediates T Cell Antagonism In Vivo*

| Mouse | Ig-PLP1 coadministered with | | |
	Ig-W	Ig-PLP-LR	PLP-LR peptide
		PLP1/PPD*	
		%	
1	100	28	81
2	95	40	91
3	78	37	93
4	79	25	100

Three groups of mice (four per group) were immunized with 50 μg Ig-PLP1 mixed with 150 μg Ig-W; 50 μg Ig-PLP1 mixed with 150 μg Ig-PLP-LR; and 50 μg Ig-PLP1 mixed with 100 μg PLP-LR peptide, respectively. After 10 d, the lymph nodes were removed and 4×10^5 cells were stimulated in vitro with 15 μg/ml PLP1 peptide, 15 μg PLP2 peptide, 5 μg/ml PPD, or media without stimulator and assayed for [³H]thymidine incorporation as described in Materials and Methods. The mean cpm obtained for media without stimulator was used as background (BG).
*The indicated numbers represent percentage values of PLP1-specific proliferation relative to PPD-specific proliferation and were estimated as follows: (mean cpm of triplicates obtained with PLP1 stimulation − mean cpm triplicate BG) / (mean cpm of triplicates obtained with PPD − mean cpm triplicate BG) × 100. The percentage values of PLP2-specific proliferation relative to PPD ranged between 0 and 15% indicating the absence of significant proliferation to PLP2 peptide (used as negative control).

Table 2. *Ig-PLP-LR– and PLP-LR–mediated T Cell Antagonism In Vitro*

| Antagonist | Stimulator | | |
	PLP1	PLP	Ig-PLP1
PLP-LR	+	−	−
Ig-PLP-LR	+	+	+

This summarizes the effect of PLP-LR and Ig-PLP-LR on IL-2 production by PLP1-specific T cell hybridomas when they are stimulated with APCs pulsed with Ig-PLP1, PLP1, or native PLP in the presence of PLP-LR or Ig-PLP-LR.
+, inhibition of IL-2 production and therefore antagonism; −, absence of inhibition of IL-2 production and therefore no antagonism.

mune disease. Both Ig-PLP1 and Ig-PLP-LR could be captured by rabbit antibodies to the synthetic peptides and bind rat anti–mouse κ mAb indicating peptide expression and proper pairing of the heavy and light chains (Fig. 2). Ig-PLP1 was presented to T cells in a specific manner indicating that the PLP1 peptide was released from the Ig and bound class II I-As molecules (Fig. 3). In this case, the flanking regions seem to have no interfering effect on the presentation of Ig-PLP1, as has been observed for other T cell peptides expressed on proteins unrelated to their own environment (32–35, 45, 46). The presentation of Ig-PLP1 was 100-fold better than free PLP1 peptide (Fig. 4). This observation parallels with results obtained with an IgG1 chimera expressing a T cell peptide from λ_2 phage repressor protein (35) and with Ig-HA (34). The efficacy of Ig-PLP1 in activating specific T cells is probably partly due to efficient internalization via FcR as we have previously seen for Ig-HA (34). Moreover, since Ig-PLP1 is presumably, like Ig-HA, processed in endocytic vacuoles, the released PLP1 peptides access newly synthesized class II molecules and allow for the formation of significant amounts of peptide–class II complexes (36). Ig-PLP-LR is also taken up by APCs, processed, and presented to T cells; otherwise it would not have inhibited PLP1-mediated T cell stimulation. Indeed, when APCs were incubated with PLP1 peptide in the presence of Ig-PLP-LR, there was no activation of the PLP1-specific T cell hybridomas (Fig. 5 a). Ig-PLP-LR was much more potent than free PLP-LR peptide in inhibiting PLP1-

mediated T cell activation indicating a better presentation of the peptide when delivered on the Ig chimera as was the case for PLP1. These results confirm the observation by Vidal et al. (44) showing that efficient endocytic presentation of an antagonist peptide could outcompete an external agonist and inhibit IL-2 production by specific T cells.

Furthermore, when the activation of T cells by native PLP and Ig-PLP1 was carried out in the presence of graded concentrations of Ig-PLP-LR, IL-2 production declined as Ig-PLP-LR increased. However, free PLP-LR peptide failed to inhibit T cell activation mediated by native PLP or Ig-PLP1 (Fig. 5). A maximum of 50% inhibition in IL-2 production was seen when the activation of T cells by Ig-PLP1 was carried out in the presence of Ig-W (Fig. 5 b). Ig-PLP1 and Ig-W have an identical heavy chain constant region and use the same FcR to internalize into APCs. Therefore, Ig-W could outcompete Ig-PLP1 for internalization and diminish the activation of T cells. Ig-W, had a similar effect on the presentation of Ig-HA (34), but had no effect on the activation of T cells by native PLP (Fig. 5 c).

Whereas free PLP-LR antagonized only activation mediated by free PLP1 peptide, the spectrum of antagonism by Ig-PLP-LR broadens to include antigen requiring endocytic processing such as native PLP and Ig-PLP1 (Table 2). Two lines of evidence indicated that the mechanism responsible for PLP-LR and Ig-PLP-LR–mediated inactivation of T cells was likely to be TCR antagonism rather than blockage of class II molecules. At the extracellular level, PLP2 peptide, which uses I-As class II molecules for presentation (37), did not inhibit the activation of T cells by free PLP1 peptide. At the endocytic level, Ig-PLP2, which is presented by I-As, did not antagonize native PLP for the activation of T cells. Competition for binding to class II may take place. However, a living antigen presenting system, such as the one we used, and the design of our experimental system are not suitable for optimal blockade as demonstrated by the control experiments using PLP2 peptide and Ig-PLP2 chimera. Therefore, one can speculate that TCR engagement with PLP-LR-I-As complexes on the surface of APCs antagonizes the cells rather than stimulates them. If we retain this possibility, one may ex-

plain the antagonism by Ig-PLP-LR as follows; because of efficient presentation of Ig-PLP-LR in endocytic vaccuoles, significant levels of PLP-LR–I-A^s complexes are generated. The amount of complexes on the cell surface is proportional to the amount of Ig-PLP-LR offered to the APCs. When PLP1 stimulation is carried out in the presence of Ig-PLP-LR, both PLP-LR–I-A^s and PLP1-I-A^s are present on the surface of a given APC and increase in the concentration of Ig-PLP-LR leads to higher number of PLP-LR–I-A^s complexes. Considering that ~3,500 TCRs have to be engaged for a T cell to be activated (47), and that a given complex of peptide–class II serially engages ~200 TCRs (31), a T cell is antagonized when TCR engagement with PLP-LR–I-A^s complexes override engagement with PLP1-I-A^s. Overall, because of efficient loading of PLP-LR by Ig-PLP-LR, T cell antagonism is achieved by a higher frequency of serial triggering of TCR by PLP-LR–I-A^s complexes. This is probably more conceivable when Ig-PLP-LR is engaged in antagonizing native PLP or Ig-PLP1, which are processed in endocytic vacuoles. How could Ig-PLP-LR antagonize PLP1 peptide, a stimulator that may not require processing but rather bind directly to cell surface class II molecules? One possibility is that only a limited number of PLP1–class II complexes could be generated because external PLP1 binds empty class II and/or displaces other peptides from I-A molecules. These conditions may limit the number of complexes that could be available for stimulation. Another possibility is that the turnover of cell surface MHC molecules contribute to a short stay of complexes formed at the extracellular milieu (class II molecules have been in the cell surface for some time before binding the extracellular peptide), whereas complexes formed in the endocytic compartment will reside for a normal period of time because they have just been translocated to the cell surface. This may also be the reason why PLP-LR could not antagonize Ig-PLP1 or PLP but did antagonize PLP1 peptide. Considering recent findings that complexes made of MHC–antagonist peptide engage the TCR for a shorter period of time than those made of MHC–agonist peptide (48), we lean to the possibility that external peptide forms very few complexes with a short stay at the cell surface, and endocytic processing is more effective for the generation of MHC–peptide complexes that could trigger more TCR because of longer residency at the cell surface. Overall, internalization via FcR of Ig chimeras and efficient endocytic presentation may be responsible for the broad antagonism by Ig-PLP-LR, and the formation of fewer short-lived complexes, when the peptide is externally added to the APCs, may be responsible for the inability of PLP-LR to antagonize the endocytic presentation of PLP and Ig-PLP1. Overall, this demonstrates for the first time that competition between agonist and antagonist at the endocytic level is achievable, but this only occurs when the antagonist peptide is efficiently presented within the endocytic compartment.

In vivo, when Ig-PLP1 was injected subcutaneously in the foot pads and at the base of the limbs and tail, routes that mostly target the response to the lymph nodes, a strong specific T cell response to PLP1 peptide was induced (Fig. 7). These results are expected considering that Ig-PLP1 was efficient in presenting the peptide to T cells in vitro (Fig. 4) and that Ig-HA has been shown to prime a strong HA-specific T cell response (34). However, interestingly there is a significant PLP1-specific response detected in the spleen, an organ that mostly filters and responds to systemic Ags (Fig. 7 b). One possibility we can put forth to explain these results is that Ig-PLP1, because of its long half life, was able to circulate and reach both the lymphatic and blood circulation and consequently be presented at both systemic and lymphatic sites.

Although Ig-PLP1 was efficiently presented and induced a strong in vivo T cell response, it was possible to antagonize such a response by Ig-PLP-LR (Fig. 8). Indeed, when Ig-PLP1 was coadministered to mice with Ig-PLP-LR, the response to PLP1 peptide was markedly reduced. This decline in PLP1 response was specifically induced by Ig-PLP-LR because when Ig-PLP1 was coadministered with Ig-W instead of Ig-PLP-LR, the response to PLP1 was not affected. Efficient in vivo endocytic presentation of Ig-PLP-LR may be the fundamental basis for the decline in PLP1-specific response. The failure of PLP-LR peptide to inhibit Ig-PLP1–mediated T cell activation in vitro coupled with the potency of Ig-PLP-LR in antagonizing Ig-PLP1 T cell stimulation supports the belief that Ig-PLP-LR–mediated in vivo antagonism may be related to efficient presentation. Moreover, when free PLP-LR peptide was coadministered with Ig-PLP1, there was no evidence for a decline of the PLP1 response (Table 1). The lack of antagonist effect by free PLP-LR peptide was not due to a net lower amount of injected peptide because the mice were given ~34-fold more PLP-LR in the free peptide form than Ig-PLP-LR form (on the basis of a molecular weight of 150,000 daltons, the 150 μg Ig-PLP-LR given to the mice correspond to 1 nmol of Ig that contains 2 nmol of PLP-LR peptide, whereas with a molecular weight of 1,468 daltons, the 100 μg of free PLP-LR peptide correspond to 68 nmol of peptide). The mechanism by which Ig-PLP-LR reduced the response to PLP1 is not clear. However, knowing that Ig-PLP-LR induced PLP-LR–specific T cells (Fig. 9) when it was coadministered with Ig-PLP1, it can be speculated that these PLP-LR–specific T cells downregulate PLP1-specific T cells (49). Although there was induction of PLP-LR–specific response when free PLP-LR peptide was administered with Ig-PLP1 (not shown), there was no evident reduction in the proliferative response to PLP1. Further studies are required to identify any qualitative differences among T cells induced by Ig-PLP-LR and those induced by PLP-LR peptide. Another possibility that could explain the reduction in T cell response to PLP1 is in vivo antagonism by PLP-LR–MHC complexes. Ig-PLP1 and Ig-PLP-LR have identical isotypes and could bind the same FcR and internalize into the same APCs. Simultaneous presentation of PLP-LR and PLP1 by the same APCs could, as is seen in the in vitro assays, be responsible for the antagonism of PLP1-specific T cells by Ig-PLP-LR. The striking features associated with this endocytic antagonist system are

1051   Legge et al.

its high efficacy and its broad spectrum of activity against free peptides and most importantly autoantigens which require endocytic processing. Indeed, our data demonstrate for the first time that competition between agonist and antagonist is achievable at the endocytic level and ensures downregulation of autoreactive T cells, in vivo. Efficient endocytic presentation of peptide analogues may operate through mechanisms that could overcome the abundant MHC–agonist complexes generated in spontaneous disease subsequent to the eruption and continuous endocytic presentation of autoantigens.

References

1. Jameson, S.C., K.A. Hogquist, and M.J. Bevan. 1995. Positive selection of thymocytes. *Annu. Rev. Immunol.* 13:93–126.
2. Sebzda, E., V.A. Wallace, J. Mayer, R.S.M. Yeung, T.W. Mak, and P.S. Ohashi. 1994. Positive and negative thymocyte selection induced by different concentrations of a single peptide. *Science (Wash. DC).* 263:1615–1618.
3. Ashton-Rickardt, P.G., A. Bandeira, J.R. Delaney, L. Van Kaer, H.-P. Pircher, R.M. Zinkernagel, and S. Tonegawa. 1994. Evidence for a differential avidity model of T cell selection in the thymus. *Cell.* 76:651–663.
4. Hsu, B.L., B.D. Evavold, and P.M. Allen. 1995. Modulation of T cell development by an endogenous altered peptide ligand. *J. Exp. Med.* 181:805–810.
5. Cibotti, R., J.M. Kanellopoulos, J.-P. Cabaniols, O. Halle-Panenko, K. Kosmatopoulos, E. Sercarz, and P. Kourilsky. 1992. Tolerance to a self-protein involves its immunodominant but does not involve its subdominant determinants. *Proc. Natl. Acad. Sci. USA.* 89:416–420.
6. Mamula, M.J. 1993. The inability to process a self-peptide allows autoreactive T cells to escape self-tolerance. *J. Exp. Med.* 177:567–571.
7. Liu, G.Y., P.J. Fairchild, R.M. Smith, J.R. Prowle, D. Kioussis, and D.C. Wraith. 1995. Low avidity recognition of self-antigen by T cells permits escape from central tolerance. *Immunity.* 3:407–415.
8. Brocke, S., A. Gaur, C. Piercy, A. Gautam, K. Gijbels, C.G. Fathman, and L. Steinman. 1993. Induction of relapsing paralysis in experimental autoimmune encephalomyelitis by bacterial superantigen. *Nature (Lond.).* 365:642–644.
9. Wucherpfennig, K.W., and J.L. Strominger. 1995. Molecular mimicry in T cell–mediated autoimmunity: viral peptides activate human T cell clones specific for myelin basic protein. *Cell.* 80:695–705.
10. McRae, B.L., C.L. Vanderlugt, M.C. Dal Canto, and S.D. Miller. 1995. Functional evidence for epitope speading in the relapsing pathology of experimental autoimmune encephalomyelitis. *J. Exp. Med.* 182:75–85.
11. Sercarz, E.E., P.V. Lehmann, A. Ametani, G. Benichou, A. Miller, and K. Moudgil. 1993. Dominance and crypticity of T cell antigenic determinants. *Annu. Rev. Immunol.* 11:729–766.
12. Steinman, L. 1996. Multiple sclerosis: a coordinated immunological attack against myelin in the central nervous system. *Cell.* 85:299–302.
13. Tisch, R., and H. McDevitt. 1996. Insulin-dependent diabetes mellitus. *Cell.* 85:291–297.
14. Feldmann, M., F.M. Brennan, and R.N. Maini. 1996. Rheumatoid arthritis. *Cell.* 85:307–310.
15. Martin, R., H.F. McFarland, and D.E. McFarlin. 1992. Immunological aspects of demyelinating disease. *Annu. Rev. Immunol.* 10:153–187.
16. Tuohy, V.K., Z. Lu, R.A. Sobel, R.A. Laursen, and M.B. Lees. 1989. Identification of an encephalitogenic determinant of myelin proteolipid protein for SJL mice. *J. Immunol.* 142:1523–1527.
17. Kuchroo, V.K., R.A. Sobel, J.C. Laning, C.A. Martin, E. Greenfield, M.E. Dorf, and M.B. Lees. 1992. Experimental allergic encephalomyelitis mediated by cloned T cells specific for a synthetic peptide of myelin proteolopid protein: fine specificity and T cell receptor V_β usage. *J. Immunol.* 148:3776–3782.
18. Zhang, J., S. Markovic-Plese, B. Lacet, J. Raus, H.L. Weiner, and D.A. Hafler. 1994. Increased frequency of interleukin 2–responsive T cells specific for myelin basic protein and proteolipid protein in peripheral blood and cerebrospinal fluid of patients with multiple sclerosis. *J. Exp. Med.* 179:973–984.
19. Chou, Y.K., D.N. Bourdette, H. Offner, R. Whithan, R.Y. Wang, G.A. Hashim, and A.A. Vandenbark. 1992. Frequency of T cells specific for myelin basic protein and myelin proteolipid protein in blood and cerebrospinal fluid in multiple sclerosis. *J. Neuroimmunol.* 38:105–113.
20. Evavold, B.D., J. Sloan-Lancaster, and P.M. Allen. 1993. Tickling the TCR: selective T cell functions stimulated by altered peptide ligands. *Immunol. Today.* 14:602–609.
21. Evavold, B.D., and P.M. Allen. 1991. Separation of IL-4 production from Th cell proliferation by an altered T cell receptor ligand. *Science (Wash. DC).* 252:1308–1310.
22. Windhagen, A., C. Scholz, P. Höllsberg, H. Fukaura, A. Sette, and D.A. Hafler. 1995. Modulation of cytokine pat-

terns of human autoreactive T cell clones by a single amino acid substitution of their peptide ligand. *Immunity*. 2:373–380.

23. De Magistris, M.T., J. Alexander, M. Coggeshall, A. Altman, F.C.A. Gaeta, H.M. Grey, and A. Sette. 1992. Antigen analog–major histocompatibility complexes act as antagonist of the T cell receptor. *Cell*. 68:625–634.

24. Jameson, S.C., F.R. Carbone, and M.J. Bevan. 1993. Clone-specific T cell receptor antagonist of major histocompatibility complex class I–restricted cytotoxic T cells. *J. Exp. Med.* 177:1541–1550.

25. Racioppi, L., F. Ronchese, L.A. Matis, and R.N. Germain. 1993. Peptide–major histocompatibility complex class II complexes with mixed agonist/antagonist properties provide evidence for ligand-related differences in T cell receptor–dependent intracellular signaling. *J. Exp. Med.* 177:1047–1060.

26. Sloan-Lancaster, J., B.D. Evavold, and P.M. Allen. 1993. Induction of T-cell anergy by altered T-cell–receptor ligand on live antigen-presenting cells. *Nature (Lond.).* 363:156–159.

27. Brocke, S., K. Gijbels, M. Allegretta, I. Ferber, C. Peircy, T. Blankenstein, R. Martin, U. Utz, N. Karin, D. Mitchell et al. 1996. Treatment of experimental encephalomyelitis with a peptide analogue of myelin basic protein. *Nature (Lond.).* 379:343–346.

28. Karin, N., D.J. Mitchell, S. Brocke, N. Ling, and L. Steinman. 1994. Reversal of experimental autoimmune encephalomyelitis by a soluble peptide variant of a myelin basic protein epitope: T cell receptor antagonism and reduction of interferon γ and tumor necrosis factor α production. *J. Exp. Med.* 180:2227–2237.

29. Kuchroo, V.K., J.M. Greer, D. Kaul, G. Ishioka, A. Franco, A. Sette, R.A. Sobel, and M.B. Lees. 1994. A single TCR antagonist peptide inhibits experimental allergic encephalomyelitis mediated by a diverse T cell repertoire. *J. Immunol.* 153:3326–3336.

30. Pinet, V., M. Vergelli, R. Martin, O. Bakke, and E.O. Long. 1995. Antigen presentation mediated by recycling of surface HLA-DR molecules. *Nature (Lond.).* 375:603–606.

31. Valitutti, S., S. Müller, M. Cella, E. Padovan, and A. Lanzavecchia. 1995. Serial triggering of many T-cell receptors by a few peptide–MHC complexes. *Nature (Lond.).* 375:148–151.

32. Zanetti, M., F. Rossi, P. Lanza, G. Filaci, R.H. Lee, and R. Billetta. 1992. Theoretical and practical aspects of antigenized antibodies. *Immunol. Rev.* 130:125–150.

33. Zaghouani, H., Y. Kuzo, H. Kuzo, N. Mann, C. Daian, and C. Bona. 1993. Engineered immunoglobulin molecules as vehicles for T cell epitopes. *Int. Rev. Immunol.* 10:265–278.

34. Zaghouani, H., R. Steinman, R. Nonacs, H. Shah, W. Gerhard, and C. Bona. 1993. Presentation of a viral T cell epitope expressed in the CDR3 region of a self immunoglobulin molecule. *Science (Wash. DC).* 259:224–227.

35. Zambidis, E.T., and D.W. Scott. 1996. Epitope-specific tolerance induction with an engineered immunoglobulin. *Proc. Natl. Acad. Sci. USA.* 93:5019–5024.

36. Brumeanu, T.D, W.J. Swiggard, R.M. Steinman, C. Bona, and H. Zaghouani. 1993. Efficient loading of identical viral peptide onto class II molecules by antigenized immunoglob-

ulin and influenza virus. *J. Exp. Med.* 178:1795–1799.

37. Greer, J.M., V.K. Kuchroo, R.A. Sobel, and M.B. Lees. 1992. Identification and characterization of a second encephalitogenic determinant of myelin proteolipid protein (residues 178–191) for SJL mice. *J. Immunol.* 149:783–788.

38. Sanz, I., and D.J. Capra. 1987. V_k and J_k gene segments of A/J Ars-A antibodies: somatic recombination generates the essential arginine at the junction of the variable and joining regions. *Proc. Natl. Acad. Sci. USA.* 84:1085–1089.

39. Ruthban, G.A., F. Otani, E.C.B. Milner, D.J. Capra, and P.H.W. Tucker. 1988. Molecuar characterization of the A/J J558 family of heavy chain variable region segments. *J. Mol. Biol.* 202:383–395.

40. Zaghouani, H., M. Krystal, H. Kuzu, T. Moran, H. Shah, Y. Kuzu, J. Schulman, and C. Bona. 1992. Cells expressing an H chain Ig gene carrying a viral T cell epitope are lysed by specific cytolytic T cells. *J. Immunol.* 148:3604–3609.

41. Lees, M., and J.D. Sakura. 1978. Preparation of proteolipids. *In* Research Methods in Neurochemistry. N. Marks and R. Rodnight, editors. Plenum Press, New York. 345–370.

42. Zaghouani, H., D. Goldstein, H. Shah, S. Anderson, M. Lacroix, G. Dionne, R.C. Kennedy, and C. Bona. 1991. Induction of antibodies to the envelope protein of the human immunodeficiency virus by immunization with monoclonal anti-idiotypes. *Proc. Natl. Acad. Sci. USA.* 88:5645–5649.

43. Zaghouani, H., S.A. Anderson, K.E. Sperber, C. Daian, R.C. Kennedy, L. Mayer, and C. Bona. 1995. Induction of antibodies to the human immunodeficiency virus type 1 by immunization of baboons with immunoglobulin molecules carrying the principal neutralizing determinant of the envelope protein. *Proc. Natl. Acad. Sci. USA.* 92:631–635.

44. Vidal, K., B.L. Hsu, C.B. Williams, and P.M. Allen. 1996. Endogenous altered peptide ligands can affect peripheral T cell responses. *J. Exp. Med.* 183:1311–1321.

45. Hahn, Y.S., V.L. Braciale, and T.J. Braciale. 1991. Presentation of viral antigen to class I major histocompatibility complex–restricted cytotoxic T lymphocyte. Recognition of an immunodominant influenza hemagglutinin site by cytotoxic T lymphocyte is independent of the position of the site in the hemagglutinin translation product. *J. Exp. Med.* 174:733–736.

46. Chimini, G., P. Pala, J. Sire, B.R. Jordan, and J.L. Maryanski. 1989. Recognition of oligonucleotide-encoded T cell epitopes introduced into a gene unrelated to the original antigen. *J. Exp. Med.* 169:297–303.

47. Viola, A., and A. Lanzavecchia. 1996. T cell activation determined by the T cell receptor number and tunable thresholds. *Science (Wash. DC).* 273:104–106.

48. Lyons, D.S., S.A. Leiberman, J. Hampi, J.J. Boniface, Y. Chien, L.J. Berg, and M.M. Davis. 1996. A TCR binds to antagonist ligands with lower affinities and faster dissociation rates than do agonist. *Immunity.* 5:53–61.

49. Nicholson, L.B., J.M. Greer, R.A. Sobel, M.B. Lees, and V.K. Kuchroo. 1996. An altered peptide ligand mediates immune deviation and prevents autoimmune encephalomyelitis. *Immunity.* 3:397–405.

Adjuvant internal radiation therapy in a model of colorectal cancer-derived hepatic metastases

MA Burton[1] and BN Gray[2]

[1]Rural Biomedical Research Group, School of Science and Technology, Charles Sturt University, Wagga Wagga 2650, Australia; [2]University Department of Surgery, Lions Cancer Institute, Royal Perth Hospital, Perth 6001, Australia.

Summary Selective internal radiation therapy (SIR therapy) is a technique whereby metastatic liver cancer is irradiated by embolising microspheres containing the radionuclide yttrium-90 into the hepatic arterial circulation. To date this technique has not been used as an adjuvant therapy, but rather to treat established metastases in the liver. This study evaluated the use of two intrahepatic radiation doses delivered on radioactive microspheres for the treatment of small, growing micrometastases. Three groups of five rats were each inoculated with tumour spheroids into the portal vein. The resultant liver micrometastases were treated with either 10 or 20 MBq of yttrium-90 microspheres or a sham dose of non-radioactive microspheres injected into the portal vein 2 days following tumour inoculation. The livers of each animal were examined for the presence of metastases after a further 21 days and liver function tests were performed. At the time of sacrifice there was no obvious normal liver damage in any of the rats treated with microspheres. The livers of the sham-treated animals contained extensive signs of tumour deposition. A mean of 34 tumours were taken from the livers of each of the sham-treated animals, whereas only a single tumour was found in one animal treated with 10 MBq of yttrium and eight small tumours from two animals treated with 20 MBq. Liver function tests demonstrated a significant short-term increase in alkaline phosphatase levels in the radiation-treated animals compared with shams, but there were no other indications of any effects on liver function. These results indicate a potential role for SIR therapy in an adjuvant setting with colorectal cancer.

Keywords: adjuvant; liver; metastases; yttrium; internal radiotherapy

The occurrence of liver metastases is a common development from a number of different forms of malignancy but is especially prevalent in patients first diagnosed with primary colorectal cancer. Hepatic metastases are evident in approximately a quarter of patients at initial diagnosis, but this is more than doubled at the time of death (Bengmark and Hafstrom, 1969). Approximately 70% of the metastases attributed to tumours of the large bowel are found in the liver, and half the deaths from bowel cancer result from disease in the liver (Gray, 1980).

Over the past two decades there have been many randomised clinical trials that have assessed the potential of adjuvant chemotherapy and radiotherapy to improve survival in patients undergoing resection for primary tumours of the large bowel. The past 3 years has seen a resurgence of interest in this area as several of these trials have now demonstrated positive results (Gray et al., 1987; Laurie et al., 1989; Moertel et al., 1990).

Of particular interest is the fact that three of the prospectively randomised trials have demonstrated an improvement in survival with the use of regional perfusion chemotherapy of the liver as an adjuvant treatment (Taylor et al., 1985; Gray et al., 1987; Wolmark et al., 1990). In all three of these clinical trials a relatively small dose of chemotherapy was delivered directly into the portal venous circulation following removal of the primary tumour in patients who had either stage B or C large bowel cancer. These data indicate that elimination or suppression of micrometastases within the liver in patients at high risk of developing clinically obvious recurrent cancer can translate into a survival improvement when the chemotherapy is given directly into the portal venous circulation.

In earlier studies we have shown that even very small subclinical metastases derive their blood supply almost entirely from the hepatic artery and that metastases as small as 1 mm in diameter have a well-defined arterial blood supply and that this arterial supply will occur in a short period of time (Archer and Gray, 1989). Microscopic deposits smaller than this are nourished by diffusion of nutrients from the portal vein before they have developed their own arterial blood supply. Therefore, it might be expected that cytotoxic drugs delivered into the portal vein would only be effective against micrometastases of much less than 1 mm in diameter and that they would have little effect on larger 'micrometastases'.

We have shown that this is exactly what does happen in an animal model of liver metastases. In these studies it was shown that portal venous chemotherapy is only effective against metastatic tumour deposits that have not had time to develop their own arterial blood supply. Portal venous chemotherapy had little effect on metastases as small as 1 mm in diameter, whereas the same chemotherapy delivered via the hepatic artery was highly effective in eliminating these tumour deposits (Archer and Gray, 1990). This effect may be associated with the low tissue penetration of the chemotherapy drugs, which are unable to diffuse from the portal veins to the arterial feeding vessels of the larger deposits.

As would be expected, many studies have established that the objective response rate for treatment of liver metastases is considerably higher when the chemotherapy is delivered directly into the hepatic arterial circulation, as opposed to systemic therapy (Daly et al., 1987; Archer and Gray, 1990). SIR therapy is a technique developed by our group for selectively concentrating radioactive microspheres containing yttrium-90 into the vascular compartment of malignant tumours within the liver (Burton and Gray, 1989; Gray et al., 1989, 1992). In patients with liver metastases derived from the large bowel, the objective response rate of established metastases to treatment by SIR therapy exceeds that of other treatment techniques, including hepatic perfusion chemotherapy (Gray et al., 1992). The yttrium-90 used in SIR therapy has a relatively long penetration distance relative to chemotherapeutic drugs and may provide therapeutic levels of radiation from portal veins to hepatic arteries. Therefore, there is obvious potential to use SIR therapy as an adjuvant treatment for patients undergoing resection of primary tumours of the large bowel but who are at high risk of developing liver metastases.

Correspondence: MA Burton

The current study was designed to evaluate the potential of using a relatively small and a high intrahepatic radiation dose delivered on radioactive microspheres via the portal vein to retard the growth of micrometastases in an animal model of liver metastasis.

Materials and methods

Tumour model

A total of 15 mixed sex Wistar rats with mean body weight of 290.0 g (45.9 g s.d.) were randomly assigned to three equal groups for the purposes of the study. The tumour cell line used was derived from DMH-induced colonic carcinomas and was delivered on tumour spheroids using the method of Archer and Gray (1988). Briefly, the model entails harvesting tumour cells which adhere in a monolayer to ion exchange spheroids of 32–45 μm diameter. The spheroids with their load of tumour cells can then be injected into the portal vein, where they travel into the liver and embolise portal vessels. Tumour deposits will then grow at the site of embolisation and do not move into the venous system, thus confining the seeded tumour to the liver. Growth rates and a detailed methodology have been described previously (Archer and Gray, 1988).

Radioactive microspheres

The radioactive microspheres used in the study were closely sized resin-based particles of 32.5 ± 2.5 μm diameter containing the highly energetic isotope yttrium-90. The isotope is a pure beta emitter with a half life of 64 h, a maximum range in tissue of 11 mm and a mean range of 4.5 mm (Klemp et al., 1989). The microspheres have a specific gravity of <2.0 and have been shown not to leach activity in vivo, and the particles distribute evenly throughout the liver when delivered intravascularly. The microspheres are stable and cause minimal tissue reaction even after being in the liver for extensive periods (Gray et al., 1990). The activity of the microspheres was approximately 65 Bq per sphere and a stock suspension was dispensed at a concentration of 50 MBq per ml of distilled water.

The radiation dose to liver tissue was based initially on an estimated average liver weight of 15 g for each animal treated. Absorbed dose for tissue was calculated as 1.82 Gy for every 37 MBq per kg of liver (Mantravadi et al., 1982). The calculation was thus derived from the following equation:

$$\text{Activity (MBq)} = [\text{dose (Gy)} \times \text{weight (g)} \times 0.037]/1.82$$

The calculation however, is based on homogeneous distribution of dose throughout the tissue substance. This is not the case with point sourced radiation as provided on microspheres distributed primarily in the tumour and liver vasculature. There will be areas of extremely high dose near the microspheres and of low dose away from them. The mean doses described in the calculation are thus overstated by a constant fraction related to the tissue volume not receiving the maximum doses and doses are therefore designated as 'inferred' doses. This concept has been described in detail previously (Fox et al., 1991), but basically means that approximately 86% of the normal tissue receives less than the dose that would be expected with perfectly uniform distribution, and 34% of the tissue receives less than one-third of that dose.

Protocol

A laparotomy was performed under general anaesthetic (Pentabarbital, 60 mg kg^{-1}) on each animal and the portal vein cleared distally to the liver. A total of 4×10^5 tumour spheroids were then injected directly into the portal vein in a volume of 0.5 ml of saline carrier. The animals were recovered and resultant tumours allowed to grow in the liver at the sites of random spheroid embolisation. After a further

2 days when the tumours were still less than 1 mm in diameter, the animals were again injected intraportally with one of the following three treatments, assigned at random:

1. Approximately 3.0×10^5 radioactive microspheres carrying a total activity of 20 MBq of ^{90}Y. In a 15 g liver this will equate to an inferred tissue dose of approximately 66 Gy.
2. Approximately 1.5×10^5 radioactive microspheres carrying a total activity of 10 MBq of ^{90}Y. In a 15 g liver this will equate to an inferred tissue dose of approximately 33 Gy.
3. Approximately 3.0×10^5 non-radioactive microspheres, equivalent to the number of microspheres in the high-dose group.

Animal body weights were measured periodically throughout the period from treatment to eventual sacrifice. On day 21 post tumour deposition each animal received a barbiturate overdose and the liver was removed and fixed in 10% phosphate-buffered formalin. At that time a 1.0 ml blood sample was also taken for examination of standard liver function tests. Venous blood samples were also taken from an extra group of five rats without tumour seeded to the liver as a control for the liver function tests in the animals from the treatment groups. Following liver fixation the lobes were separated and sectioned into thin slices (approximately 3 mm) for examination of the presence of tumour deposits. Tumours were numbered individually and those associated with each lobe combined and weighed.

Results

All animals tolerated the microsphere treatments without difficulty and post-operative recovery, including activity patterns and general condition, did not vary significantly between the groups. There was, however, a small drop (less than 5%) in body weight in the group receiving 20 MBq of ^{90}Y microspheres immediately following treatment which was resolved within 12 days. This may have been related to the larger radiation dose since neither the sham-treated animals nor those treated with 10 MBq exhibited this response. The latter animals all increased and maintained mean body weight following the operation (Figure 1).

At the time of sacrifice there was no obvious damage to the liver of treated animals that could be associated with the radioactive microspheres. The livers of the animals treated with the non-radioactive microspheres demonstrated extensive signs of tumour deposition but otherwise there was no damage to the normal liver parenchyma. One animal in the 10 MBq group had a small number of tumour deposits sit-

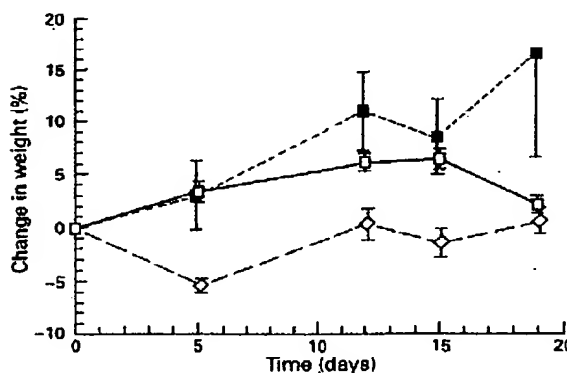Figure 1 Changes in body weight of rats treated with a high ($\diamond$) and a low ($\blacksquare$) dose of ^{90}Y microspheres and a sham-treated group ($\square$) receiving non-radioactive microspheres injected into the portal vein. Means are presented with standard error bars.

Although portal venous chemotherapy is only effective in treating very small micrometastases, radiation treatment using the SIR therapy technique but also delivered via the portal vein, as opposed to the hepatic artery, should theoretically have much greater potential to destroy small metastatic deposits by virtue of the fact that the effective penetration distance of yttrium-90 beta-radiation is of the order of 3 mm (Klemp et al., 1989). Adjuvant SIR therapy should be able to destroy micrometastases up to several millimetres in diameter as it does not rely on diffusion of drug from a nearby portal venous radicle.

The results of these animal experiments clearly show that the administration of a single dose of yttrium-90 can greatly inhibit the clinical development of liver metastases in animals that are harbouring large numbers of microscopic metastases. This has major potential implications for the treatment of patients who are known at the time of treatment of the primary tumour to have a high probability of having microscopic tumour deposits within their liver.

The small deposits of tumour that did grow in three of the ten animals treated with radiation probably resulted from slight inhomogeneity of distribution of the microspheres from lobe to lobe. This may lead to areas of liver that are insufficiently irradiated to suppress the metastases and is a common occurrence in the multilobulate liver of the rat. Studies from this laboratory using sheep liver as an organ model (Burton et al., 1988) have shown that this does not occur to the same extent where the liver is bilobular as in the human and distribution is relatively homogeneous. We have also experienced severe inhomogeneity when ceramic microspheres are used rather than the SIR spheres. This is attributed to the high specific density of ceramic microspheres, causing sedimentation in the vasculature, and thus making them unsuitable for clinical use.

The post-treatment liver function tests demonstrate abnormalities of liver enzyme function that are consistent with some damage to the normal liver parenchyma. However, these tests were performed on the 19th day following treatment and do not reflect alterations to long-term function of the liver that has been subjected to irradiation by yttrium-90. In patients with established liver metastases we have shown that it is possible to deliver inferred liver radiation doses of the order of 74 Gy without any obvious long-term sequelae (Gray et al., 1990), and more recently patients are routinely receiving inferred doses of up to 92 Gy again without measureable toxicity. Furthermore, as both the low (42 Gy) and high (76 Gy) radiation doses used in these animal experiments gave similar results, it may be possible to use even lower doses to produce this same result.

On theoretical grounds, it would seem more appropriate to use adjuvant SIR therapy via the hepatic arterial supply, rather than via the portal vein. While this is true, the realities of surgical practice are that it is technically much easier to cannulate a vein in the portal circulation than the hepatic artery. If adjuvant SIR therapy is to be accepted as a clinical modality, the ease of use by the general surgical community is a major factor to be considered. In addition, it must be ensured that radioactive microspheres do not pass through the liver and enter the pulmonary circulation. Where radioactive microspheres are currently used clinically, a pretreatment procedure involves assessment of lung uptake of activity by analysis of distribution of injected ^{99}Tc-labelled macroaggregated albumin particles of similar size to microspheres. If excessive activity is breaking through the liver to the lung then the treatment is not continued. A similar procedure would need to be employed in the adjuvant setting.

The use of SIR therapy should now be evaluated as an adjuvant treatment for patients at high risk of developing liver metastases.

References

ARCHER S AND GRAY BN (1988). A new reproducible model of hepatic and peritoneal metastases from colonic carcinoma. *Eur. J. Cancer Clin. Oncol.*, 24, 1623–1632.

ARCHER S AND GRAY BN. (1989). Vascularisation of small liver metastases. *Br. J. Surg.*, 76, 545–548.

ARCHER S AND GRAY BN. (1990). Comparison of portal vein chemotherapy with hepatic artery chemotherapy in the treatment of liver metastases. *Am. J. Surg.*, 159, 325–329.

BENGMARK S AND HAFSTROM L. (1969). The natural history of primary and secondary malignant tumours of the liver. I. The prognosis for patients with hepatic metastases from colonic and rectal carcinoma by laparotomy. *Cancer*, 23, 198–204.

BURTON MA AND GRAY BN. (1989). Intraoperative dosimetry of yttrium-90 in liver tissue. *Nucl. Med. Biol.*, 16, 495–498.

BURTON MA. GRAY BN AND COLETTI A. (1988). Effect of angiotensin II on blood flow in the transplanted sheep squamous cell carcinoma. *Eur. J. Cancer. Clin. Oncol.*, 24, 1373–1376.

DALY J, KEMENY N, SIGMUNDSON E, ODENMAN P AND THOM A. (1987). Regional infusion for colorectal hepatic metastases. *Arch. Surg.*, 122, 1273–1277.

FOX R, KLEMP P, EGAN G, BURTON MA AND GRAY BN. (1991). Dose distribution following selective internal radiation therapy. *Int. J. Radiat. Oncol. Biol. Phys.*, 21, 463–467.

GRAY BN. (1980). Colorectal cancer, natural history of disseminated disease. *Aust. NZ J. Surg.*, 50, 643–648.

GRAY B, DEZWART J AND FISHER R. (1987). The Australia and New Zealand trial of adjuvant chemotherapy in colon cancer. In *Adjuvant Therapy of Cancer*, Vol. V. Jones S and Salmon S (eds) pp. 537–546. Grune & Stratton: New York.

GRAY BN, BURTON MA, KELLEHER DL AND ANDERSON J. (1989). Selective internal radiation therapy (SIR) therapy for treatment of liver metastases: measurement of response rate. *J. Surg. Oncol.*, 42, 192–196.

GRAY BN, BURTON MA, KELLEHER DK, KLEMP PF AND MATZ L. (1990). Tolerance of the liver to the effects of yttrium-90 radiation. *Int. J. Radiat. Oncol. Biol. Phys.*, 18, 619–623.

GRAY BN, ANDERSON J, BURTON MA AND KLEMP P. (1992). Regression of liver metastases following treatment with yttrium-90 microspheres. *Aust. NZ J. Sur.*, 62, 105–110.

KLEMP P, PERRY A, FOX R, BURTON MA AND GRAY BN. (1989). Aspects of radiation protection during the treatment of liver cancer using yttrium-90 labelled microspheres. *Radiat. Protect. Aust.*, 7, 70–73.

LAURUE J, MOERTEL C AND FLEMMING T. (1989). Surgical adjuvant therapy for large bowel carcinoma; an evaluation of levamisole and the combination of levamisole and 5FU. *J. Clin. Oncol.*, 7, 1447–1456.

MANTRAVADI R, SPIGOS D, TAN W AND FELIX FL. (1982). Intra-arterial yttrium-90 in the treatment of hepatic malignancy. *Radiology*, 142, 783–786.

MOERTEL C, FLEMING T AND McDONALD J. (1990). Levamisole and fluorouracil for adjuvant therapy of resected colon cancer. *N Engl. J. Med.*, 322, 352–358.

TAYLOR I, MACHIN D AND MULLER M. (1985). A randomised controlled trial of adjuvant portal vein cytotoxic perfusion in colorectal cancer. *Br. J. Surg.*, 72, 359–363.

WOLMARK N, FISHER B AND WICHERMAN D. (1990). Portal vein 5-FU adjuvant therapy of carcinoma of the colon: a brief report of NSABP protocol C-02. In *Adjuvant Therapy of Cancer*, Vol. VI, Salmon S (ed.) pp. 435–438. WB Saunders: London.

324

uated at the site of tumour spheroid injection in the region of the portal vein, indicating spillage of tumour at the time of tumour implantation.

The mean weight of residual normal liver tissue at sacrifice for the sham-treated group and groups treated with 10 MBq and 20 MBq was 10.38 g (2.07 g s.d.), 11.52 g (1.72 g s.d.) and 12.87 g (1.78 g s.d.) respectively. Using the measured weights of the treated livers with the tumour weights subtracted, this calculates to an inferred liver dose delivered to the animals of approximately 42.3 Gy and 76.4 Gy for the low and high radiation doses.

Table I describes the extent of tumour deposition resulting from portal venous seeding of the tumour spheroids in the different treatment groups. The sham-treated animals grew large numbers of tumours in each liver lobe. A mean of 34 (11 s.d.) tumours were taken from each animal with a total mass of 29.2 g for the group. A single animal with a single tumour was recorded in the 10 MBq group, while two animals with a total of eight tumours were found in the group treated with 20 MBq. No clear pattern of distribution was determined for the deposition of tumours in any of the groups.

The mean tumour weight in the sham-treated animals was 0.16 g (0.08 g s.d.), while the mean tumour weight in the radioactive microsphere-treated animals was 0.01 g and 0.05 g respectively for the 10 MBq and 20 MBq groups.

Liver function tests were carried out on all animals and the means and standard deviations of each test are described in Table II. There were no significant differences between any of the groups in relation to either bilirubin, albumin or protein levels in the serum. Statistical significance was tested by one-way ANOVA followed by Bonferroni correction. Aspar-

tate aminotransferase levels did not show any significant difference in any group compared with control animals, but the sham group demonstrated significantly higher levels ($P < 0.05$) than the group treated with 20 MBq. Serum alkaline phosphatase levels were significantly increased ($P < 0.05$) in both radiation-treated groups compared with controls but not in the sham group compared with controls. This was reflected in the significant increases in these levels for the radiation-treated groups compared with sham-treated controls.

Discussion

These experiments were designed to simulate in an animal model the clinical scenario of patients with microscopic liver metastases. This is a common event in clinical practice when patients undergo surgical removal of a primary tumour of the gastrointestinal tract but do not apparently have any clinically detectable metastatic disease in their liver. However, the fact that many of these patients do subsequently develop overt liver metastases indicates that microscopic liver metastases were present at the time of the initial surgery. This phenomenon has underscored the rationale for using portal venous chemotherapy as an adjuvant therapy for patients with stage B and C large bowel cancer undergoing resection of the primary tumour. The results of clinical trials in this patient group have now shown that the use of adjuvant chemotherapy given via the portal vein can result in a significant survival advantage for the patients having this additional form of treatment (Taylor et al., 1985; Gray et al., 1987; Wolmark et al., 1990).

Table I Number and weight of seeded tumour deposits forming in different lobes of the rats' liver after treatment with two doses of ^{90}Y microspheres and sham-treated animals with non-radioactive microspheres

Treatment	Left medial No.	Left medial Wt	Right medial No.	Right medial Wt	Left lateral No.	Left lateral Wt	Other lobes No.	Other lobes Wt
Sham	*(total of 172 tumours weighting 29.2 g)*							
1	--	--	5	1.01	4	1.75	20	4.15
2	1	0.03	3	0.59	1	0.03	10	0.66
3	11	2.47	14	4.01	15	4.72	4	0.65
4	--	--	1	0.16	17	1.55	24	1.85
5	8	0.79	7	1.00	10	1.68	17	2.14
10 MBq	*(total of one tumour weighing 0.01 g)*							
1	--	--	--	--	--	--	--	--
2	--	--	--	--	--	--	--	--
3	--	--	--	--	--	--	--	--
4	1	0.01	--	--	--	--	--	--
5	--	--	--	--	--	--	--	--
20 Mbq	*(total of eight tumours weighing 0.57 g)*							
1	--	--	--	--	--	--	6	0.56
2	--	--	--	--	--	--	--	--
3	--	--	--	--	--	--	2	0.01
4	--	--	--	--	--	--	--	--
5	--	--	--	--	--	--	--	--

Table II Changes in standard liver function tests of untreated rats compared with animals treated with non-radioactive and radioactive microspheres

	Bilirubin ($\mu mol\ ml^{-1}$)		Albumin ($g\ l^{-1}$)		Protein ($g\ l^{-1}$)		AST ($U\ l^{-1}$)		Alkaline phosphates ($U\ l^{-1}$)	
Control	1	--	32.3	3.5	53.7	4.9	125.0	99.9	207.0	50.1
Sham	1	--	33.6	1.7	56.4	3.3	203.2	34.8	258.2	18.9
	NS		NS		NS		NS		NS	
10 MBq	1	--	35.3	0.5	58.8	1.7	154.3	33.9	341.3	31.5
	NS		NS, NS		NS, NS		NS, NS		*, †	
20 MBq	1	--	35.0	1.3	58.2	1.1	140.0	43.3	327.6	37.0
	NS		NS, NS		NS, NS		NS, †		*, †	

Data are expressed as means followed by standard deviations. Significance is given below the means for comparison of controls with the treated groups shown first ($*P < 0.05$) and shams compared with radiation treatments second ($†P < 0.05$). In no case was a significant difference measured between the high and low radiation treatments (NS = $P > 0.05$).

Immunoassays with rolling circle DNA amplification: A versatile platform for ultrasensitive antigen detection

Barry Schweitzer*, Steven Wiltshire*, Jeremy Lambert*, Shawn O'Malley*, Kari Kukanskis*, Zhengrong Zhu[†], Stephen F. Kingsmore*, Paul M. Lizardi[‡], and David C. Ward[†§]

*Molecular Staging Incorporated, 66 High Street, Guilford, CT 06437; [†]Department of Genetics, Yale University School of Medicine, 333 Cedar Street, New Haven, CT 06510; and [‡]Department of Pathology, Yale University School of Medicine, 333 Cedar Street, New Haven, CT 06510

This contribution is part of the special series of Inaugural Articles by members of the National Academy of Sciences elected on May 2, 2000.

Contributed by David C. Ward, May 22, 2000

We describe an adaptation of the rolling circle amplification (RCA) reporter system for the detection of protein Ags, termed "immunoRCA." In immunoRCA, an oligonucleotide primer is covalently attached to an Ab; thus, in the presence of circular DNA, DNA polymerase, and nucleotides, amplification results in a long DNA molecule containing hundreds of copies of the circular DNA sequence that remain attached to the Ab and that can be detected in a variety of ways. Using immunoRCA, analytes were detected at sensitivities exceeding those of conventional enzyme immunoassays in ELISA and microparticle formats. The signal amplification afforded by immunoRCA also enabled immunoassays to be carried out in microspot and microarray formats with exquisite sensitivity. When Ags are present at concentrations down to fM levels, specifically bound Abs can be scored by counting discrete fluorescent signals arising from individual Ag–Ab complexes. Multiplex immunoRCA also was demonstrated by accurately quantifying Ags mixed in different ratios in a two-color, single-molecule-counting assay on a glass slide. ImmunoRCA thus combines high sensitivity and a very wide dynamic range with an unprecedented capability for single molecule detection. This Ag-detection method is of general applicability and is extendable to multiplexed immunoassays that employ a battery of different Abs, each labeled with a unique oligonucleotide primer, that can be discriminated by a color-coded visualization system. ImmunoRCA-profiling based on the simultaneous quantitation of multiple Ags should expand the power of immunoassays by exploiting the increased information content of ratio-based expression analysis.

prostate-specific antigen | human IgE | IgG | ELISA | immuno-microarrays

A ntibody-based detection systems for specific Ags are versatile and powerful tools for various molecular and cellular analyses, as well as clinical diagnostics (1). The power of such systems originates from the considerable specificity of Abs for particular antigenic epitopes. There are, however, numerous examples where important biological markers for cancer, infectious disease, or biochemical processes are present at too low a concentration in body fluids or tissues to be detected by using conventional immunoassays. Recent advances in the field of low-level Ag detection include the development of stronger fluorochromes and chemiluminescent substrates for use in ELISAs, immunofluorescence-based staining and immunoblotting (2), and the application of signal amplification methods such as tyramide deposition (3). Although these techniques can be quite powerful, greater sensitivity and specificity are often required, particularly when working with limited amounts of sample material or when Ag density is extremely low. With these needs in mind, we have adapted the recently described rolling circle amplification (RCA) reporter system (4) for the detection of protein Ags.

The use of DNA amplification for the detection of Abs bound to Ag has been documented previously (5–10). In immuno-PCR, a unique DNA sequence tag is associated with a specific Ab using streptavidin-biotin interactions, alternative bridging moieties, or covalent linkage. Abs bound to Ag are then detected by PCR amplification of the associated DNA tag. Multiple Abs and multiple DNA tags have been used (10) to analyze several Ags simultaneously. Although immuno-PCR was shown to be significantly more sensitive than ELISA, gel electrophoresis was required after DNA amplification in solution to separate and/or quantitate the different amplified DNA tags. The requirements for thermal cycling and product separation by gel electrophoresis have restricted the widespread adoption of immuno-PCR as an alternative to ELISA and have precluded its utility in immunohistochemical or array formats.

RCA driven by DNA polymerase can replicate circularized oligonucleotide probes with either linear or geometric kinetics under isothermal conditions (4). Using a single primer, RCA generates hundreds of tandemly linked copies of the circular template within a few minutes. In ImmunoRCA, the 5' end of this primer is attached to an Ab. In the presence of circular DNA, DNA polymerase, and nucleotides, the rolling circle reaction results in a DNA molecule consisting of multiple copies of the circle DNA sequence that remains attached to the Ab (Fig. 1). The amplified DNA can be detected in a variety of ways, including direct incorporation of hapten-labeled or fluorescently labeled nucleotides, or by hybridization of fluor-labeled or enzymatically labeled complementary oligonucleotide probes. ImmunoRCA, therefore, represents a novel approach for signal amplification of Ab–Ag recognition events. Although RCA reactions can be carried out with either linear or geometric kinetics (4), the signal-generation paradigm we have used in this study is based exclusively on the linear RCA model. Here, we describe the construction of Ab–DNA conjugates and demonstrate the utility of using these conjugates to detect Ags in several different immunoRCA formats.
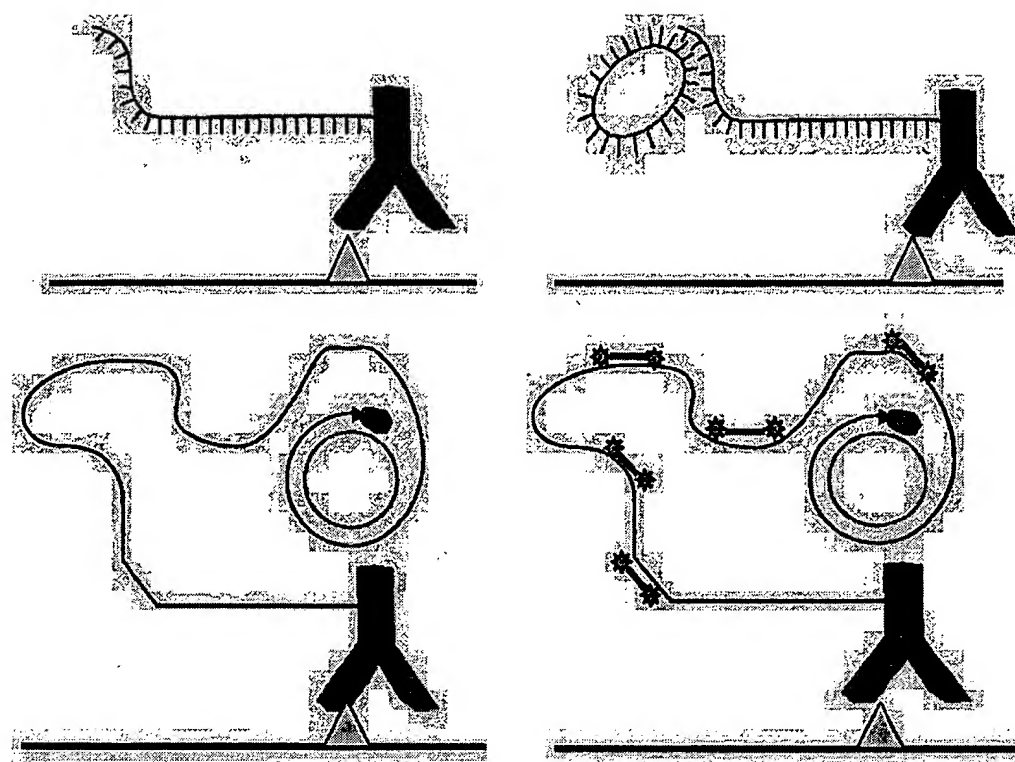
Methods

Oligonucleotide Synthesis. All oligonucleotides used in this study were synthesized on a PerSeptive Biosystems (Framingham, MA) Expedite DNA Synthesizer and purified by reverse-phase HPLC. Thiol- and fluor-modified phosphoramidites were purchased from Glen Research (Sterling, VA) and Amersham Pharmacia, respectively. Circle DNAs were constructed as previously described (4). The sequences used for immunoRCA detection of (i) prostate-specific Ag (PSA) and avidin were as follows: conjugate primer 1, 5'-thiol-AAA AAA AAA AAA AAA CAC AGC TGA GGA TAG GAC AT-3'; circle 1,

Fig. 1. Schematic of immunoRCA assay. (*Top Left*) A reporter Ab conjugated to an oligonucleotide binds to a test analyte that is captured on a solid surface by covalent attachment or by a capture Ab. (*Top Right*) A DNA circle hybridizes to a complementary sequence in the oligonucleotide. (*Bottom Left*) The resulting complex is washed to remove excess reagents, and the DNA tag is amplified by RCA. (*Bottom Right*) The amplified product is labeled *in situ* by hybridization with fluor-labeled oligonucleotides.

5'-CTC AGC TGT GTA ACA ACA TGA AGA TTG TAG GTC AGA ACT CAC CTG TTA GAA ACT GTG AAG ATC GCT TAT TAT GTC CTA TC-3'; detectors, 5'-FITC-AAC AAC ATG AAG ATT GTA-DNP-3', 5'-FITC-TCA GAA CTC ACC TGT TAG-DNP-3', 5'-FITC-ACT GTG AAG ATC GCT TAT-DNP-3'; (*ii*) for IgE and sheep IgG: conjugate primer 2, 5'-thiol-GTA CCA TCA TAT ATG TCC GTG CTA GAA GGA AAC AGT TAC A-3'; circle 2, 5'-TAG CAC GGA CAT ATA TGA TGG TAC CGC AGT ATG AGT ATC TCC TAT CAC TAC TAA GTG GAA GAA ATG TAA CTG TTT CCT TC-3'; detectors, 5'-Cy3-TAT ATG ATG GTA CCG CAG-Cy3-3', 5'-Cy3-TGA GTA TCT CCT ATG ACT-Cy3-3', 5'-Cy3-TAA GTG GAA GAA ATG TAA-Cy3-3' [for CACHET (condensation of amplified circles after hybridization of encoding tags) experiments, detectors for circle 2 had DNP instead of Cy3 on the 3' ends].

Ab–DNA Conjugates. The following Abs were used to construct DNA conjugates in the course of this study: rabbit anti-mouse IgG (generously provided by DAKO), mouse monoclonal anti-human IgE, mouse monoclonal anti-biotin, rabbit anti-sheep IgG, and rabbit anti-avidin. The conjugation of one of the Abs, the mouse mAb against human IgE, is described in the supplemental data on the PNAS web site (www.pnas.org) as an example for the other conjugations.

ELISA. Ninety-six-well plates (Nunc Maxisorb) were incubated with 100 μl of 2 μg/ml goat polyclonal anti-human IgE per well for 2 h at 37°C and then overnight at 4°C. Plates were washed three times with 100 μl of Tris-buffered saline (TBS)/0.05% Tween 20, and then blocked with 5% nonfat dry milk for 2 h at 37°C. Plates were washed again, followed by addition of the IgE analyte at variable concentrations in a 100-μl volume. After a 37°C incubation for 30 min, plates were washed three times. In the conventional ELISA experiments, anti-human IgE–alkaline phosphatase conjugate was added to each well and incubated at 37°C for 30 min. After plates

were washed, the alkaline phosphatase substrate 4-methylumbelliferyl phosphate (MUP) was added, and fluorescence levels were read after 20 min on a BioTek (Winooski, VT) FL600 plate reader at an excitation wavelength of 360 nm and an emission wavelength of 460 nm. In the immunoRCA experiments, anti-human IgE–DNA conjugate (5 ng/μl) was added to each well in a 60-μl volume and incubated at 37°C for 30 min. After plates were washed three times, circle 1 DNA (170 nM) in 60 μl of φ29 buffer (250 mM Tris·HCl (pH 7.5)/50 mM MgCl2/1 mg/ml BSA/1 mM dATP/1 mM dCTP/1 mM dGTP/0.75 mM dTTP/0.25 mM FITC-12-dUTP) was added to each well, and incubated at 37°C for 30 min. RCA reactions were initiated by addition of 1.5 μl of φ29 DNA polymerase (0.4 units/μl, generously provided by Amersham Pharmacia) and continued for 30 min at 37°C. RCA products were detected by addition of an anti-FITC–alkaline phosphatase conjugate. After a 37°C incubation for 30 min, plates were washed three times, 4-methylumbelliferyl phosphate (MUP) substrate was added, and fluorescence levels were read after 20 min.

Magnetic Bead Immunoassay. Streptavidin-coated magnetic beads (Bangs Laboratories, Carmel, IN) were coated with a solution of 16 μg/ml biotinylated polyclonal anti-human IgE (PharMingen) in TBS, washed three times in TBS/0.05% Tween 20, and blocked overnight with 2 mg/ml BSA. Beads were incubated with human IgE (25 ng/ml) in TBS for 20 min at room temperature and washed three times. Detection of IgE by using a conventional anti-IgE-alkaline phosphatase conjugate or an immunoRCA conjugate was carried out as described above for the ELISA.

Detection of PSA on Microspots. *Preparation of microspots.* Clean glass slides were chemically functionalized by immersing in a solution of mercaptopropyltrimethoxysilane [1% vol/vol in 95% ethanol (pH 5.5)] for 1 h. Slides were rinsed in 95% ethanol for 2 min, dried under nitrogen, and heated at 120°C for 4 h. Thiol-derivatized slides were activated by immersing in a 0.5 mg/ml solution of the heterobifunctional crosslinker *N*-[γ-

maleimidobutyryloxy]succinimide ester (GMBS; Pierce) in 1% dimethylformamide, 99% ethanol for 1 h at room temperature. Slides were rinsed with ethanol, dried under nitrogen, and stored in a vacuum dessicator until use. Spotting of goat anti-PSA polyclonal Ab (BioSpecifics, Lynbrook, NY) onto the slides was accomplished by pipetting 0.2 μl of 0.5 mg/ml solution in a grid pattern. Hand-spotted arrays were blocked with 2% BSA (protease free), air-dried, and stored under nitrogen at 4°C until use.

Ag capture. Purified human PSA (BiosPacifics, Emeryville, CA) was diluted in PBS to the desired concentration. Ten μl of the PSA dilution was spotted onto a coverslip (Hybrislip, Grace Biolabs Inc., Bend, OR) that was then inverted onto the slide over the area of the array. The slide was incubated at 37°C for 30 min in a humidified chamber, washed twice for 2 min in PBS/0.05% Tween 20, and tapped dry. Ten microliters of a 1:5,000 dilution in PBS of monoclonal anti-PSA Ab was added to the array. The slide was incubated at 37°C for 30 min in a humidified chamber, washed twice, and tapped dry. Finally, rabbit anti-mouse IgG-DNA conjugate (10 ng/μl in PBS) was added to the array and incubated at 37°C for 30 min in a humidified chamber. Slides were washed twice and tapped dry.

RCA reaction. Circle 1 DNA (200 nM) in 10 μl φ29 buffer [250 mM Tris·HCl (pH 7.5)/50 mM MgCl$_2$/1 mg/ml BSA] was added to the array and incubated at 45°C for 30 min. Ten microliters of RCA reaction mixture (2 mM dATP/2 mM dCTP/2 mM dGTP/1.5 mM dTTP/0.5 mM FITC-dUTP/φ29 buffer/0.4 units/μl φ29 polymerase) was added to the array and incubated at 37°C for 30 min. The slide was washed in 2× SSC/0.05% Tween 20 for 5 min with agitation at room temperature, followed by a wash in 2× SSC. Slides were dried under nitrogen, and the array portion of the slide was covered with Prolong Antifade (Molecular Probes). Fluorescent imaging was done on a Zeiss epifluorescence microscope equipped with a charge-coupled device (CCD) imaging system and a ×100 objective. Fluorescence quantitation was performed by using IPLAB software (Scanalytics, Inc., Fairfax, VA).

Detection of IgE on Microarrays. *Preparation of microarrays.* Glass slides were functionalized with thiol-silane and activated with GMBS as described above. A solution of polyclonal goat anti-human IgE (BiosPacifics; 0.5 mg/ml) was spotted onto the slides by using a pin-tool type microarrayer (GeneMachines, San Carlos, CA).

Antigen capture. Each microarray was blocked by adding a 50-μl volume of a 2 mg/ml BSA solution in 50 mM glycine (pH 9.0) and incubating for 1 h at 37°C in a humidity chamber. After blocking, slides were twice washed by immersion of the slides into a coplin jar containing 1× PBS/0.05% Tween 20 and allowing the slides to stand in wash for 2 min followed by a 1-min 1× PBS wash. A 10-μl volume of human IgE at various concentrations was immediately added to each microarray and incubated for 30 min at 37°C in a humidity chamber, and then washed as described above.

ImmunoRCA. Goat anti-human IgE (BioSpecifics) was labeled with biotin using the BiotinTag Micro Biotinylation Kit (Sigma). Ten microliters of the Ab at 2.5 ng/μl in PBS/0.05% Tween 20/1 mM EDTA was applied to each array and incubated at 37°C for 30 min in a humid chamber. Slides were washed twice for two minutes in PBS/0.05% Tween 20. A mouse monoclonal anti-biotin Ab conjugated to primer 1 was annealed with 50 nM circle 1 in PBS/0.05% Tween 20/1 mM EDTA at 37°C for 30 min. Ten microliters was applied to each array and incubated at 37°C for 30 min in a humid chamber, and then slides were washed twice. A 20-μl volume of reaction solution containing T7 native DNA polymerase (0.01 units/μl)/1 mM dNTPs/0.04 mg/ml ssDNA-binding protein/20 mM Tris·HCl (pH 7.4)/10 mM MgCl$_2$/25 mM NaCl was then added to each microarray. The slides were incubated at 37°C for 45 min, and the reaction was stopped by washing the

slides in a 2× SSC/0.05% Tween 20 solution at room temperature. A 20-μl solution of 0.5 μM DNA decorators was added to each array and allowed to hybridize to the RCA product for 30 min at 37°C. Slides were washed in 2× SSC at room temperature and spin-dried. Slides were scanned in a General Scanning (Watertown, MA) Luminomics 5000 microarray scanner, and fluorescence was quantitated by using QUANTARRAY software.

Detection of Single Ab-Ag Complexes. *Preparation of capture slides.* Slides were coated with 4-aminobutyl-dimethylmethoxysilane and derivatized with 1,4-phenylene-diisothiocyanate as previously described (11). A mixture of an avidin capture reagent, the oligonucleotide 5'-NH$_2$-GG$_{18}$G-biotin-3', and an anti-digoxigenin IgG capture reagent, digoxigenin-succinyl-ε-aminocaproic acid hydride, each at a concentration of 5 μM, were spotted onto the activated slide surface in an array format (8–10 spots/array). Chemical coupling was allowed to proceed for 2 h before blocking unreacted functional groups as previously described (11).

Binding of Ags to capture slides. Various concentrations of avidin and sheep antidigoxigenin IgG, either singly or in defined molar ratios, were spiked into normal human serum. The spiked serum (1.0 μl) was applied to the capture arrays, and the slides were incubated in a moist chamber at 37°C for 30 min. The slides then were washed twice in PBS/Tween 20 and air-dried. Five microliters of a mixture of 7.5 nM rabbit anti-avidin-primer-1 conjugate and 7.5 nM rabbit anti-sheep IgG Ab-primer-2 conjugate was applied to each array spot and incubated at 37°C for up to 2.5 h. The slides were washed eight times (1 min each) and air-dried. Five microliters of 0.2 μM solution of the two circular probes (circle 1 and circle 2) in 2× SSC/0.1% Tween 20/3% BSA/0.1% sonicated herring sperm DNA was applied to each spot. After hybridization at 37°C for 20 min, the slides were washed with 2× SSC/0.1% Tween 20 at 37°C for 5 min and air-dried.

RCA-CACHET Reactions. Five microliters of RCA reaction mixture (50 mM NaCl/50 mM Tris·HCl (pH 7.2)/5 mM MgCl$_2$/0.5 mM each dNTP/1 mM DTT/0.04 mg/ml ssDNA-binding protein/0.5 units/μl Sequenase) was applied to each spot, and the slides were incubated at 37°C for 15 min. After the slides were washed, they were air-dried, and 5 μl of a solution containing 0.2 μM double labeled (fluor + 2,4-DNP) detector probes were applied to each array. Slides were incubated in the moist chamber for 30 min at 37°C, then washed five times and air-dried. To collapse the RCA products into point sources of fluorescence so that single Ag-Ab complexes could be enumerated, 5 μl of 33 nM sheep anti-DNP IgM in PBS was added to each array spot, and slides were incubated at 37 °C for 45 min, washed for 3 min in 2× SSC at room temperature, and then air-dried. Prolong Antifade solution (Molecular Probes) was applied to the slide, and the slide was covered with a 20× 20-mm coverslip. Separate FITC and Cy3 fluorophore microscope images were captured by using a ×63 objective lens, and individual RCA products in each field were counted manually. The FITC and Cy3 image were merged electronically, and RCA signals were pseudocolored green and red.

Results

Preparation and Characterization of Ab-DNA Conjugates. The covalent coupling strategy described by Hendrickson *et al.* (10) was used with several modifications to construct Ab-DNA conjugates for immunoRCA applications. Each batch of conjugate synthesized was subjected to several quality control checks, including agarose gel (Fig. 6, see the supplemental data) and SDS/PAGE gel analyses (not shown). In addition, competitive ELISA experiments were carried out to assess the ability of the conjugate to bind cognate Ag. In these assays, the matching unconjugated and DNA-conjugated Abs were assessed in parallel for their ability to compete with a reporter Ab for binding to Ag. The conjugated Abs, each coupled to ≈3 oligonucleotides
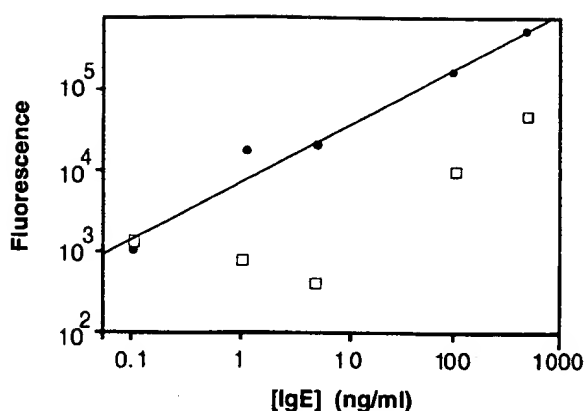
Fig. 2. Comparison of immunoRCA and conventional immunoassay in an ELISA format. Filled circles, ELISA of human IgE with immunoRCA, using an anti-human IgE-DNA conjugate; open squares, ELISA of human IgE with an anti-human IgE-alkaline phosphatase conjugate.

a 40-mer oligonucleotide (primer-2) consisting of a primer sequence that is complementary to a portion of a DNA circle designated circle 2; this conjugate was used in an immunoRCA reaction as described in *Methods*. The lowest level of IgE that could be detected over background (no IgE) was 0.1 ng/ml (Fig. 2). This result indicated that the Ab–DNA conjugate formed an effective sandwich complex in response to IgE; furthermore, it established that a covalently coupled oligonucleotide can function effectively as an RCA primer both in solution (see above) and as a surface-immobilized protein adduct. In the conventional ELISA, the reporter Ab was the monoclonal anti-human IgE Ab conjugated to alkaline phosphatase. As shown in Fig. 2, the immunoRCA assay gave a dose-response over a greater range of IgE concentration than the conventional assay. In addition, the immunoRCA assay, even in its less amplified linear mode, could detect IgE levels approximately two orders of magnitude lower than those detected by the conventional ELISA assay.

Comparison of Conventional and RCA-Based Microparticle Immunoassays. The utility of immunoRCA in a microparticle format was also investigated to examine the flexibility of the method. Microparticle assays are often the format of choice for clinical immunoanalyzers because of favorable performance characteristics for high-throughput automated platforms (13). Human IgE was again selected as the test analyte, but this sandwich assay was performed by using avidin-coated magnetic microparticles and biotinylated polyclonal anti-human IgE capture Abs. ImmunoRCA with the anti-IgE-DNA conjugate gave approximately 75-fold more signal than detection with an anti-IgE-alkaline phosphatase conjugate with the same amount of input IgE (25 ng IgE/ml).

Ultrasensitive Detection of PSA on Microspots. Several features of immunoRCA that make it suitable for solid-phase detection were demonstrable by using detection of PSA as a model system. For this application, immunoRCA was configured in an indirect sandwich assay format. Briefly, goat anti-PSA polyclonal Ab was immobilized on thiol-silane-coated microscope slides that had been activated with the heterobifunctional crosslinker GMBS. Purified human PSA in various concentrations was added, and the slide was incubated at 37°C and then washed to remove unbound protein. A mouse monoclonal anti-PSA Ab was used to form the second part of the immuno-sandwich complex. This complex was detected with a polyclonal rabbit anti-mouse IgG Ab that had been conjugated to an oligonucleotide containing a sequence for priming an RCA

per mole of protein, exhibited nearly equivalent avidity for Ag as the unconjugated forms (Fig. 7, see the supplemental data). Finally, the ability of the Ab–DNA conjugates to serve as primers for RCA reactions was examined. Ab–primer conjugate gave more RCA reaction product than an equimolar amount of unconjugated primer in the presence of a complementary circle DNA (Fig. 8, see the supplemental data), consistent with the observation that each Ab is conjugated to more than one primer. Neither form of primer gave an appreciable product in the absence of complementary circle or in the presence of a non-complementary circle (data not shown).

Comparison of Conventional and RCA-Based ELISAs. ImmunoRCA assays were first investigated in a single analyte ELISA format to demonstrate the feasibility of the sandwich configuration and to confirm the utility of the Ab–DNA conjugates. Human IgE was selected as the first test analyte because of its clinical importance in the assessment of allergic disorders (12). The immunoRCA sandwich assay for human IgE was performed by using microtiter plates coated with a polyclonal anti-human IgE capture Ab. Two ELISAs were carried out. In one assay, the reporter Ab was a monoclonal anti-human IgE Ab conjugated to
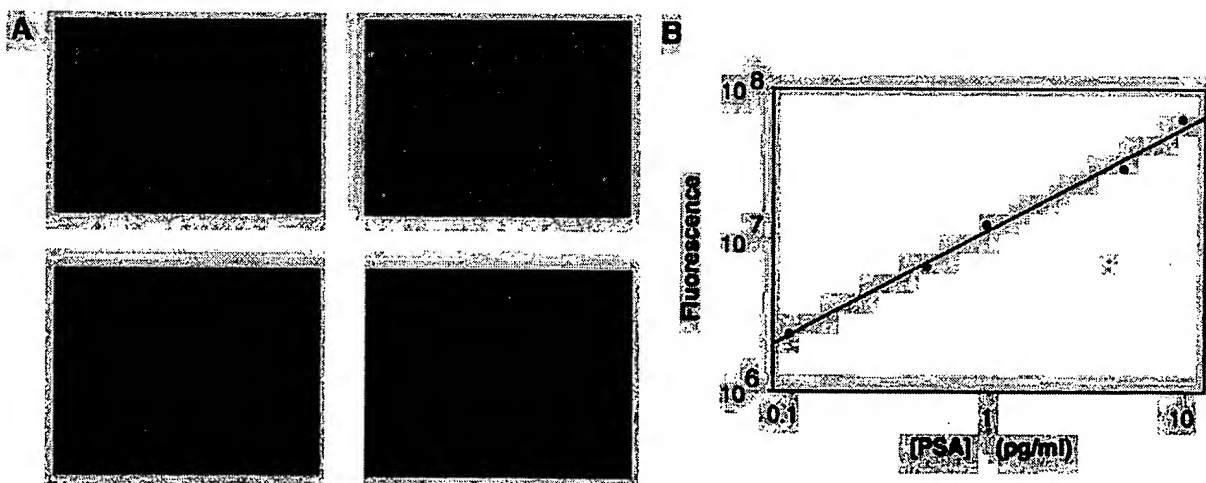

Fig. 3. Detection of PSA by immunoRCA in a microspot assay. (A) Fluorescent microscope images of immunoRCA signals obtained with different concentrations of human PSA captured on microspots of anti-human PSA Ab. Concentrations: (*Upper Left*) 5 pg/ml PSA; (*Lower Left*) 0.5 pg/ml PSA; (*Upper Right*) 0.1 pg/ml PSA; (*Lower Right*) 0 pg/ml PSA. (B) Fluorescence in microscope images was quantitated as described in *Methods* and plotted versus PSA concentrations incubated on microspots.
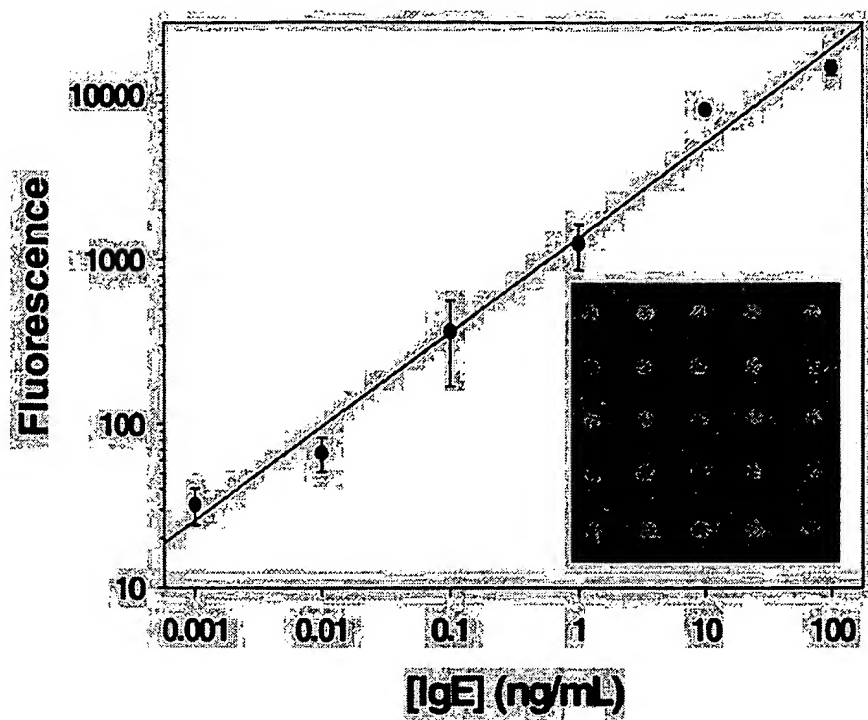
Fig. 4.   ImmunoRCA anti-human IgE microarray dose-response for purified IgE. Signals from six microarray spots were averaged for each point, and the background (no IgE) signal was subtracted. (*Inset*) Microarray scanner image of anti-human IgE array incubated with 1 ng/ml IgE.

reaction. RCA was carried out by the addition of reaction mixture containing circle DNA, DNA polymerase, and dNTPs including FITC-dUTP. As shown in Fig. 3*A*, in this direct labeling protocol, fluorescence was clearly detectable over background (no PSA) at 0.1 pg/ml PSA. Quantitation of the fluorescence with a CCD-camera-equipped microscope indicated that the signal was linear over at least 2 logs of PSA concentration (Fig. 3*B*).

Detection of IgE on Glass Microarrays. The results with PSA demonstrated that immunoRCA could be used for ultrasensitive Ag

detection on a glass surface. These experiments, however, were carried out by using hand-spotted arrays and a CCD-camera for detection, limiting the density of the arrays and the dynamic range of the detection, respectively. Therefore, similar immunoRCA experiments were performed in a sandwich format on microarrays of polyclonal goat anti-human IgE Ab spotted onto glass slides by using a pin-tool type microarraying robot. In these microarrays, approximately 0.5 nl of Ab solution was deposited in each spot, spots had a diameter of approximately 200 μm, and the spot-to-spot spacing was 250 μm. The anti-IgE microarrays were incubated with
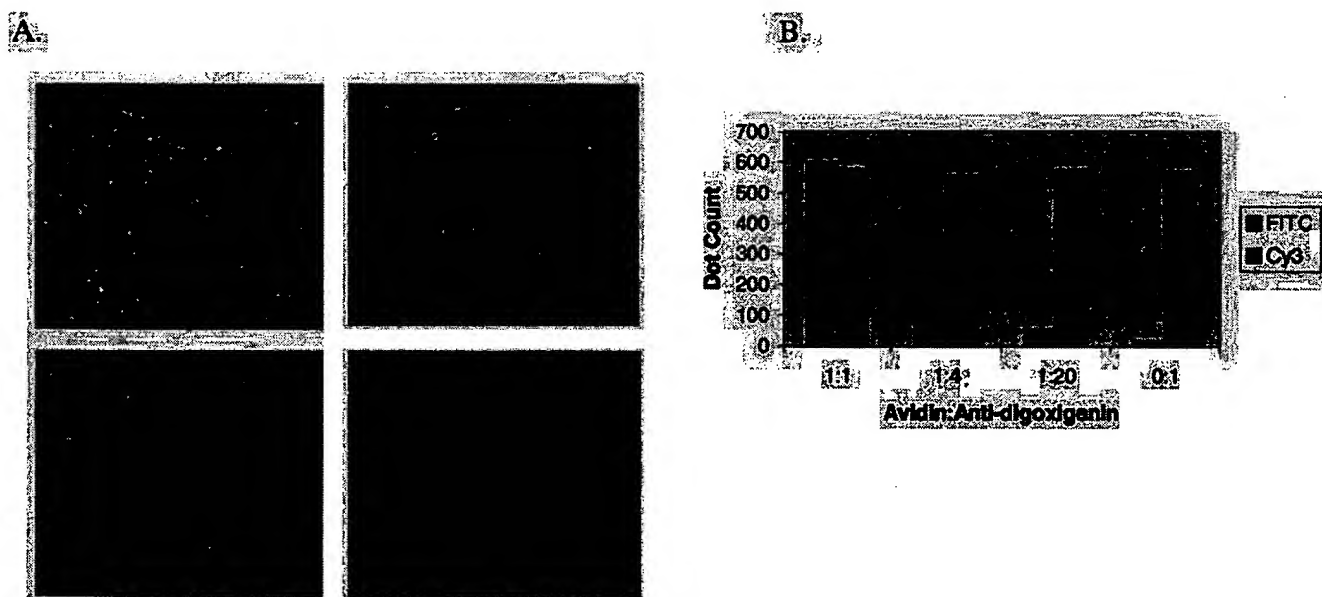

Fig. 5.   Dual Ag detection using immunoRCA-CACHET. (*A*) The RCA products from the anti-avidin and the anti-sheep Ab conjugates were decorated with fluorescein- and Cy3-labeled detector oligonucleotides, respectively. Each image shown is the superimposition of two separate images, with fluorescein and Cy3 signals pseudocolored in green and red, respectively. (*Upper Left*) Avidin:anti-digoxigenin (anti-dig) = 1:1; (*Upper Right*) avidin:anti-dig = 1:4; (*Lower Left*) avidin:anti-dig = 1:20; (*Lower Right*) avidin:anti-dig = 0:1. (B) Quantitation of avidin (FITC) and anti-digoxigenin (Cy3) signals.

human IgE, and bound Ag was detected with a biotinylated anti-human IgE Ab and an anti-biotin mAb that had been conjugated to an oligonucleotide containing an RCA-priming sequence. RCA was carried out as described in *Methods*, and the RCA product was detected by hybridization with a complementary oligonucleotide labeled with the fluorophore Cy3. Fluorescence was measured with a microarray scanner, with a dynamic range of approximately 5 logs. As shown in Fig. 4 *Inset*, microarray spots were clearly seen at low (1 ng/ml) levels of IgE. In other experiments, as little as 1 pg/ml IgE was detected by immunoRCA, and with a dynamic range of approximately 5 logs (Fig. 4).

Direct Quantitation of Individual Ag–Ab Complexes. RCA is a generic reporter system for the detection of immobilized nucleic acid analytes and has already been shown to permit the visualization and quantitation of individual nucleic acid hybridization events, including discrimination of point mutations by imaging of fluorescent dots by using a two-color labeling system (4). To test the feasibility of detecting two (or more) proteins simultaneously in a single-molecule-counting mode, avidin and sheep anti-digoxigenin IgG were chosen as test analytes because of their wide-spread use as detector reagents in molecular studies. Biotin and digoxigenin, in a 1:1 ratio, were covalently coupled to glass slides to act as analyte capture reagents and were spotted in an array format. Avidin and anti-digoxigenin IgG were mixed in different ratios, diluted in serum to simulate complex biological samples, and then spotted onto the array. The two Ags then were detected with anti-avidin-primer-1 and anti-sheep IgG-primer-2 conjugates. The immunoRCA products were condensed to 0.3- to 0.7-μm spots by crosslinking with an anti-DNP IgM (the CACHET reaction), and single fluorescence spots were counted during microscopic examination. The discrete fluorescence signals had either a pure fluorescein or pure Cy3 spectra (Fig. 5A). Whereas the possibility exists that some of these signals arose from aggregates of analyte molecules, the absence of signals with mixed spectra (yellow) indicated that each dot was generated by a single Ab–Ag complex. Quantitation of the avidin (green) and sheep anti-digoxigenin IgG (red) signals demonstrated that the ratio of green/red signals closely corresponded to the known input ratios of the two protein Ags (Fig. 5B), further suggesting a 1-to-1 correspondence between Ab–Ag complexes and signals.

We have examined the efficiency of the single molecule detection process as illustrated in the two-color experiment described above by titrating a known amount of a single Ag (avidin) and counting the number of RCA signals. A comparison of the number of input molecules with RCA signals produced indicated that the overall efficiency of molecular detection ranged from 0.5% to 5% in different experiments. These studies provided further confirmation that the sensitivity of immunoRCA was in the subattomole range (data not shown). It remains to be seen whether implementation of the geometric mode of RCA will provide further improvements in sensitivity.

Discussion

DNA tags are ideal molecular labels for multiple analyte detection because different specific sequences can be arbitrarily associated with each individual analyte. In most published examples of immunoPCR, a specific DNA tag is associated with an Ab by means of biotin–streptavidin bridges. Direct covalent coupling of DNA to Ab, as described by Hendrickson *et al.* (10), has advantages for the implementation of simple assay formats, because fewer reagent mixing and washing steps are required; furthermore, variability in the stoichiometry of the assembled components can be avoided. We have adopted the covalent coupling strategy used by Hendrickson *et al.*, for use in a signal amplification strategy termed ImmunoRCA. By employing several modifications and improvements in the synthetic and puri-

fication strategies, these conjugates can be produced in high yields with a high degree of purity (supplemental Fig. 6). Characterization of these conjugates indicated that the Abs had not lost avidity for Ags (supplemental Fig. 7); in addition, the oligonucleotides retained efficiency for priming an RCA reaction (supplemental Fig. 8).

The detection of IgE by using an anti-IgE Ab-DNA conjugate in an ELISA format was used to establish the feasibility of immunoRCA-based assays (Fig. 2). Covalent linkage of the RCA primer to the reporter Ab guaranteed that the surrogate relationship between the analyte and the amplified RCA product was maintained throughout the assay. One tangible benefit of immunoRCA over conventional methods of signal amplification was a significantly enhanced immunoassay sensitivity (Fig. 2): the immunoRCA IgE sandwich assay exhibited a two to three order of magnitude increase in sensitivity over the conventional ELISA. This level of increased sensitivity was similar to that observed for immunoPCR in an ELISA format (10). In the immunoPCR assay, however, the amplified DNA products were first generated by thermocycling and then quantified separately by gel electrophoresis. Because the amplification products of the RCA reaction remain associated with the Ab in the immunoRCA assay, the signal amplification and read-out can be carried out in the same multiwell plate. Finally, immunoRCA is compatible with a number of DNA polymerases; three different polymerases (φ29, T7 native, and T7 Sequenase) were used in various experiments reported in the current study.

The features that make immunoRCA a powerful technology for signal amplification in ELISAs also give it an advantage for other immunoassay formats. ImmunoRCA was compatible with a microparticle-based immunoassay format; in fact, the signal observed in the immunoRCA experiment was significantly greater than that obtained with conventional signal amplification for the same amount of analyte. This result suggests that immunoRCA may be adaptable for use in automated clinical immunoanalyzers, which often use microparticles as their assay format (13). It should also be noted that no effort was made in this assay (or in any other assay described in this study) to optimize Ab choice, Ab matching, etc. for the immunoRCA process. Such optimization measures are anticipated to improve sensitivity of immunoRCA reactions further.

ImmunoRCA is ideally suited for microarray applications. During the entire isothermal RCA reaction, the resulting amplified DNA molecule remains covalently attached to the Ab–Ag complex. On microarrays, this process results in an approximately 3 log increase in detectable fluorescent signal over nonamplified signal detection approaches (data not shown). A distinctive feature of RCA is the ability to precisely localize signals arising from a single DNA reporter molecule, thus enabling the visualization of individual recognition events on a solid surface. When the long ssDNA product of RCA is decorated by hybridization to many complementary oligonucleotides labeled with both a reporter fluorophore and a hapten, such as 2,4-dinitrophenol, all of the fluorophores can be collapsed into a point source of light. When the number of molecular signals is extremely high, the signal from a spot on a microarray can be read by using aggregate fluorescence. When the number of surface-bound Ags is smaller, however, the signals can be scored as discrete single molecule counts (Figs. 4 and 5), and subattomoles of analyte can be visualized. ImmunoRCA carried out on microarrays thus provides assays with an extremely wide dynamic range; combining single molecule counting and total fluorescence output indicates a dynamic range between 6 and 7 logs. Incorporation of molecular beacon type detector probes (14) into the immunoRCA assay could also eliminate post hybridization washing steps because unhybridized beacons are nonfluorescent.

Proof-of-principle for the use of immunoRCA in a microspot or microarray format was obtained by using PSA, IgE, avidin, and anti-digoxigenin IgG as the test analytes. PSA is the current

"gold-standard" serum tumor marker for the screening of men for prostate cancer and for persistence or recurrence of disease after therapy (15). Although elevation of PSA levels in peripheral blood in advanced disease can usually be monitored by standard immunodiagnostic procedures such as ELISAs, which have a sensitivity limit of approximately 100 pg/ml, this level of sensitivity may be insufficient for detecting residual disease after radical prostatectomy (16). As shown in Fig. 3, immunoRCA can detect as little as 0.1 pg/ml PSA (300 zeptomoles) in a microspot assay, which is three orders of magnitude more sensitive than standard immunoassays for PSA. The Ab used as the conjugate in this experiment was a rabbit anti-mouse IgG polyclonal Ab; this reagent can serve as a "universal" conjugate to detect any mouse mAb with high sensitivity. The ultimate sensitivity of any immuno-RCA assay will undoubtedly be limited by the specificity and avidity of the Ab–Ag binding recognition and the impact of large RCA products bound to the Ab on these parameters. Additional studies will be required to more precisely define these issues.

The utility of immunoRCA in microarray-based immunoassays was examined further by using high-density arrays of anti-IgE on a glass slide. The results from these experiments (Fig. 4) indicate that immunoRCA has high sensitivity, a wide dynamic range, and excellent spot-to-spot reproducibility. Recently, a microarray-based immunoassay was reported that used alkaline phosphatase conjugates and the fluorescent substrate ELF for detection (17). The ELF-based assay required a specially constructed CCD-based camera to read the signal, and a sensitivity of approximately 10 ng/ml was achieved. In another report, Abs labeled with a near-infrared dye were used to detect IgG subclasses on a microarray (18); this system also required a specially designed imaging system and achieved a detection limit of approximately 15 ng/ml. In contrast, signal amplification by immunoRCA gives sensitivity in the pg/ml range and allows the assay results to be read with commonly available microarray scanners. In other work not presented here, we have demonstrated that immunoRCA can be used to detect allergen-specific IgEs on microarrays with excellent clinical sensitivity and specificity (S.W., S.O., J.L., K.K., S.F.K., and B.S., unpublished data). The Ab used as the conjugate in this experiment was a monoclonal anti-biotin Ab; this reagent can be used to detect any biotinylated polyclonal or monoclonal Ab, as well as any other protein, nucleic acid, or small molecule that can be biotinylated.

A logical extension of immunoRCA is the detection of Ags in tissues and cytological specimens. Indeed, initial experiments indicate that immunoRCA can readily detect low abundance membrane receptor molecules and intranuclear Ags that are very difficult to visualize by using conventional immunohistochemical techniques (Maltzman, W., Visconti, R., Wheeler, V., and Kingsmore, S., unpublished data). Future applications of immunoRCA include array-based protein-expression-profiling (where multiple Ags can be detected and quantitated simultaneously, yielding precise information on their relative abundance), the measurement of protein–protein interactions, and drug discovery or toxicology. Finally, it is conceivable that DNA or RNA aptamers may be substituted for Abs as the recognition moieties in immunoRCA. For example, combinatorial selection has permitted the generation of DNA aptamers of relatively high affinity that bind the anion-binding exosite of thrombin (19), or the prion protein (20). If aptamer affinities could be improved to the point that they approached the binding constants typical of Ag-Ab interactions, then it may become possible to implement the use of aptamer-RCA reporter systems of considerable simplicity and power. The detection reagent in such an assay would be a synthetic oligonucleotide, combining in a single DNA molecule the dual functions of molecular recognition and RCA priming.

1. Gosling, J. P. (1990) Clin. Chem. 36, 1408–1427.
2. Diamandis, E. P. & Christopoulos, T. K., eds. (1996) Immunoassay (Academic, San Diego).
3. van Gijlswijk, R. P., Zijlmans, H. J., Wiegant, J., Bobrow, M. N., Erickson, T. J., Adler, K. E., Tanke, H. J. & Raap, A. K. (1997) J. Histochem. Cytochem. 45, 375–382.
4. Lizardi, P. M., Huang, X., Zhu, Z., Bray-Ward, P., Thomas, D. C. & Ward, D. C. (1998) Nat. Genet. 19, 225–232.
5. Sano, T., Smith, C. L. & Cantor, C. R. (1992) Science 258, 120–122.
6. Ruzicka, V., Marz, W., Russ, A. & Gross, W. (1993) Science 260, 698–699.
7. Zhou, H. R., Fisher, J. & Papas, T. S. (1993) Nucleic Acids Res. 21, 6038–6039.
8. Sano, T., Smith, C. & Cantor, C. R. (1993) Science 260, 699.
9. Sano, T. & Cantor, C. R. (1991) BioTechnology 9, 1378.
10. Hendrickson, E. R., Hatfield, T. M., Joerger, R. D., Majarian, W. R. & Ebersole, R. C. (1995) Nucleic Acids Res. 23, 522–529.
11. Guo, Z., Guifoyle, R. A., Thiel, A. J., Wang, R. & Smith, L. M. (1994) Nucleic Acids Res. 22, 5456–5465.
12. Knauer, K. A. & Adkinson, N. F. (1983) in Allergy: Principles and Practice, eds. Middleton, P., Reed, D. & Ellis, M. (Mosby, St. Louis), pp. 673–688.
13. Chan, D. W., ed. (1996) Immunoassay Automation: An Updated Guide to Systems (Academic, San Diego).
14. Tyagi, S. & Kramer, F. R. (1996) Nat. Biotech. 14, 303–308.
15. Catalona, W. J., Smith, D. S., Wolfert, R. L., Wang, T. J., Rittenhouse, H. G., Ratliff, T. L. & Nadler, R. B. (1995) J. Am. Med. Assoc. 274, 1214–1220.
16. Lu-Yao, G. L., Mclerran, D., Wasson, J. & Wennberg, J. E. (1993) J. Am. Med. Assoc. 269, 2633–2655.
17. Mendoza, L. G., McQuary, P., Mongan, A., R. Gangadharan, R., Brignac, S. & Eggers, M. (1999) Biotechniques 27, 778–788.
18. Silzel, J. W., Cercek, B., Dodson, C., Tsay, T. & Obremski, R. J. (1998) Clin. Chem. 44, 2036–2043.
19. Bock, L. C., Griffin, L. C., Latham, J. A., Vermaas, E. H. & Toole, J. J. (1992) Nature (London) 355, 564–566.
20. Weiss, S., Proske, D., Neumann, M., Groschup, M. H., Kretzschmar, H. A., Famulok, M., Winnacker, E. L. (1997) J. Virol. 71, 8790–8797.

Quantitation of DNA Sequences in Environmental PCR Products by a Multiplexed, Bead-Based Method

Alexander Spiro and Mary Lowe*

Physics Department, Loyola College in Maryland, Baltimore, Maryland 21210

A first application of a multiplexed, bead-based method is described for determining the abundances of target sequences in an environmental PCR product. Target sequences as little as 0.3% of the total amount of DNA can be quantified. Tests were conducted on 16S ribosomal DNA sequences from microorganisms collected from contaminated groundwater.

We are developing a multiplexed, bead-based method involving polystyrene microspheres, nucleic acid hybridizations, and flow cytometry instrumentation with an aim towards environmental field testing. High-throughput, quantitative methods which can simultaneously measure the abundances of many microorganisms would help us gain a broader view of microbial activity involved with degrading, eliminating, or immobilizing contaminants in the environment (4, 9). When PCR is used, a critical step is the accurate measurement of the amount of individual sequences in the PCR product derived from community DNA. In this paper, we developed a procedure for multiplexed quantitation of PCR products using the bead method in a manner which can lead to high-throughput testing. Measurements were made on 16S ribosomal DNA sequences obtained from groundwater contaminated with TCE and TKEBS at the Lawrence Livermore National Laboratory, Well-834-D3, Site 300.

Microorganisms were collected by passing groundwater through filters. A phenol chloroform-isoamyl alcohol method, adapted from reference 1, was used to extract DNA. The 16S rRNA gene was amplified from community DNA or plasmid DNA obtained from clones using bacterial primers 338Fbs2 (5′[Biotin]*T*C*C*T*A CGG GAG GCA GC) and 907R (5′CCG TCA ATT CMT TTR AGT TT; Oligos Etc.) (3), where 338Fbs2 was synthesized with a 5′ biotin modification, 12-carbon linker, five phosphorothioate bonds (*), and reverse-phase high-performance liquid chromatography purification (Synthegen, Inc.). The terms "PCR mix," "environmental PCR product," and "pure PCR product" refer to PCR products prepared from no-template DNA, community DNA, and plasmid DNA, respectively. Typical concentrations were 50 to 60 fmol/μl for a pure PCR product and 12 or 13 fmol/μl for the environmental PCR product.

Capture probes for four target sequences labeled d006, d011, d023, and *Geothrix* (Gx) and a universal probe 533FA (3) were designed, synthesized, and attached to beads, as described in reference 7. The bead probes were designated plain/d006, 154/d023, 138/d011, 134/Gx, and 133/533FA, where 154/

d023 means that the d023 capture probe was attached to bead type 154.

A "bead mix" and single-stranded amplicons were prepared according to reference 7. In each tube, 17 μl of single-stranded amplicons was combined with 34 μl of bead mix containing five types of bead probes (10,000 beads of each type) and were hybridized at 46°C for 2 h. The beads were then washed in 46°C 1× TMAC buffer (7). Twelve microliters of a 20-μg/ml streptavidin-R-phycoerythrin (Molecular Probes) solution, prepared in 1× TMAC buffer at room temperature, was added to the hybridization mix, vortexed, and incubated at 46°C for 10 min. The beads were then washed two times in 46°C 1× TMAC buffer and resuspended in 100 μl of 1× TMAC buffer at room temperature.

The beads were detected with a Luminex 100 flow cytometer. The intensity values of the reporter signals were converted into units known as molecules of equivalent soluble fluorochrome (MESF) using Quantum 27 (R-PE) Reference Standards (Bangs Laboratories, Inc.) according to standard procedures. Cytometry data were analyzed with FCS Express version 1.065 (De Novo Software). The mean intensity (I_s) of the reporter signal and intersample standard deviation (SD) were determined by running ≤ 7 replicate tubes. A similar procedure was used for the background signal (I_b). The uncertainty in the fluorescence response $F = I_s - I_b$ was calculated using the standard error SD in the difference of means (5).

The quality of the bead probes was checked as follows. The background signal for each bead probe was determined using PCR mix as the analyte. A typical value for plain/d006 was 203 ± 25 MESF with higher values for the fluorescent beads. Sequence discrimination was evaluated by exposing bead probes to noncomplementary pure or environmental PCR products diluted with PCR mix. No cross-hybridization signal was found.

An example of the flow cytometer output is shown in Fig. 1, demonstrating the fluorescence response of the bead probes after hybridization to 115 fmol of environmental PCR product. A visual comparison between Fig. 1a and b shows that the reporter signals for 138/d011, 154/d023, and 133/533FA in the environmental sample are higher than the background, indicating the presence of d011 and d023. For a given bead population, the standard error of the mean intensity was $\leq 3\%$ of the mean intensity; however, intersample variability was larger.

* Corresponding author. Mailing address: Physics Department, Loyola College in Maryland, 4501 N. Charles St., Baltimore, MD 21210. Phone: (410) 617-2709. Fax: (410) 617-2646. E-mail: mlowe@loyola.edu.
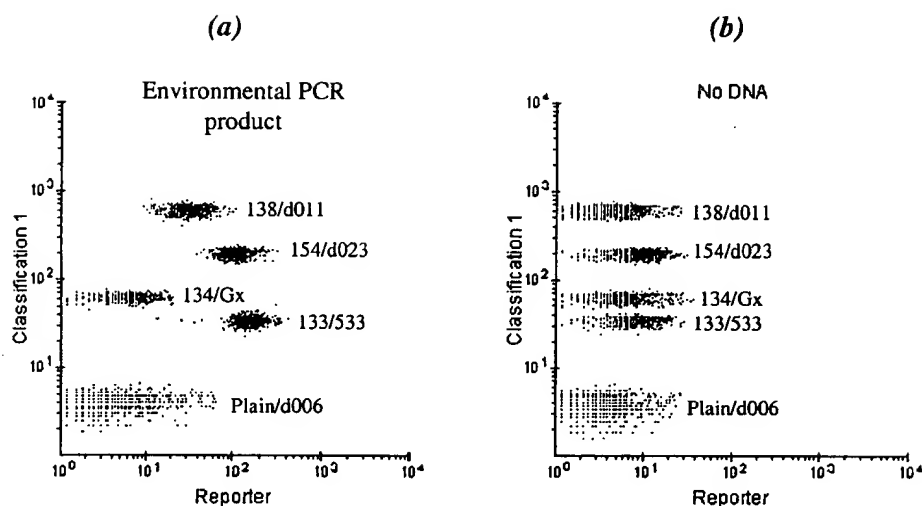
(a)   *(b)*

FIG. 1. Fluorescence detection of the bead-probes with the Luminex 100 flow cytometer. The dot plots show the orange reporter signal (abscissa) and the red bead classification color (ordinate). (a) Analyte-containing 16S ribosomal DNA from the contaminated well. (b) Negative control (PCR mix).

For a measurement of abundance, the fluorescence response must be related to the actual amount of a sequence in the PCR product.

Since the hybridization efficiency between probes and targets can vary considerably, standard concentration curves were developed for each probe. We have found that the concentration response in the environmental PCR product is different from that in the pure PCR product. Therefore, quantitation was accomplished by adding known amounts (C_i) of a target (measured in, for example, fmoles) to a fixed amount of environmental PCR product, containing an unknown amount (C_e) of that target. The total amount of target in the analyte was therefore $C = C_e + C_i$.

Model. To determine C_e, a model equation was developed. Estimates in reference 7 showed that not more than a few tenths of a percent of the total amount of target DNA in the analyte actually hybridize to capture probes on the bead surface. In this case, the fluorescence response of a specific target sequence may be described by a Scatchard-type equation for a unireactant system (probe-target) (6): $F_i = [k_a I_{max}(C_e + C_i)]/[1 + k_a(C_e + C_i)]$ (equation 1), where F_i is the fluorescence response of a particular target in the sample (with background subtracted); $k_a = K_a/V$; K_a is the association constant; V is the reaction volume, and I_{max} is the maximum response corresponding to complete saturation occurring at $k_a(C_e + C_i) \gg 1$.
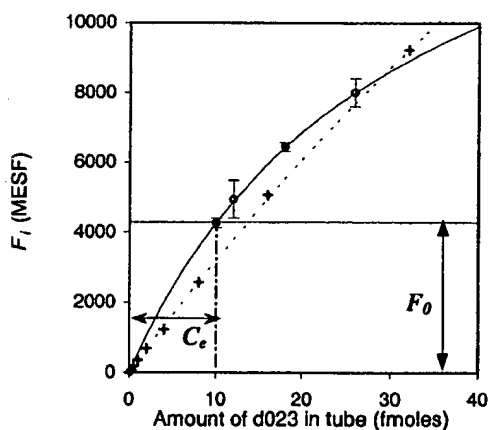
FIG. 2. Application of model to determine the amount (C_e) of d023 in the environmental PCR product (106 fmol). F_i, indicated by O, is shown for C_i at 0, 2, 8, and 16 fmol. C_e was determined from equation 2 by using errors given by S_D. The solid line is a weighted, nonlinear fit to equation 1. The "+" symbols and the dotted line are the F_i and fit for pure d023 PCR product diluted in PCR mix.
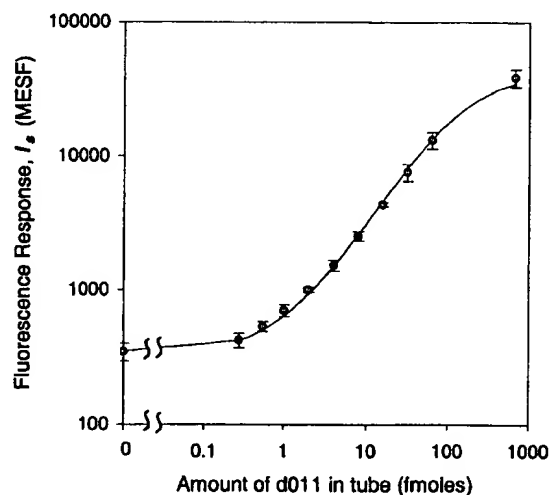
FIG. 3. Concentration curve of pure d011 PCR product diluted in PCR mix. The reporter signal I_s is displayed on the ordinate axis indicating that $I_b = 348 \pm 51$ MESF for 138/d011 beads. The solid line is a weighted, nonlinear fit to the model. The error bars represent intersample SD.

TABLE 1. Fitting parameters associated with the standard curve for each target sequence in an analyte consisting of either pure or environmental PCR product[a]

Target sequence	Pure PCR		Environmental PCR	
	k_a	I_{max}	k_a	I_{max}
d023	$(5.23 \pm 0.98) \times 10^{-3}$	$64,100 \pm 12,000$	$(31.80 \pm 0.04) \times 10^{-3}$	$17,700 \pm 200$
d011	$(7.20 \pm 1.10) \times 10^{-3}$	$41,400 \pm 6,300$	$(29.8 \pm 7.5) \times 10^{-3}$	$11,800 \pm 3,000$
d006	$(7.84 \pm 0.92) \times 10^{-3}$	$31,200 \pm 3,700$	$(8.86 \pm 0.98) \times 10^{-3}$	$20,900 \pm 2,300$
Gx	$(2.25 \pm 0.43) \times 10^{-3}$	$26,000 \pm 5,100$	$(27.1 \pm 0.2) \times 10^{-3}$	$2,200 \pm 200$

[a] Units used are fmoles^{-1} and MESF for k_a and I_{max}, respectively.

In practice, k_a, I_{max}, and C_e must be determined experimentally. Equation 1 represents a system of equations where $i = 0$, 1, 2, 3... This model assumes (i) that there is no cross-hybridization, consistent with our observations, and (ii) that parameters k_a and I_{max} are constant for all C_i.

At minimum, three spiking values are required to determine C_e, k_a, and I_{max}. When $C_o = 0$ (no spike), equation 1 yields a simple, exact solution: $C_e = [\alpha C_1 C_2]/[C_2(1 - \alpha) - C_1]$ (equation 2), where $\alpha = F_0(F_2 - F_1)/[F_1(F_2 - F_0)]$. Parameters I_{max}, k_a, and C_e can also be determined by directly fitting equation 1 to the experimental data $\{C_i, F_i\}$.

Verification of model. The model was tested by spiking equimolar mixtures of pure PCR products for d006, d011, and d023 and Gx into 106 fmol of environmental PCR product, using PCR mix as diluent. The C_e value for each sequence was calculated from equation 2 using $C_i = 0$, 8, and 16 fmol. The uncertainties in C_e were determined from S_D and conventional error propagation formulas (2). C_e was found to be 10.0 ± 4.7 fmol (9.4%) for d023, 4.3 ± 1.2 fmol (4.1%) for d011, and 0.31 ± 0.17 fmol (0.3%) for d006, where the percentage refers to the relative abundance out of 106 fmol of environmental PCR product. In the case of 138/Gx beads, F_0 was -16 ± 24 MESF, indicating that this sequence was not detected (0%) in the environmental PCR product within the error. Except for d023, the relative abundances of d011, d006, and Gx were in agreement with cloning and sequencing results based on 63 clones. The cloning results were 28.6% (17.9 to 41.4) for d023; 4.8% (0.99 to 13.3) for d011; 1.6% (0.04 to 8.53) for d006; and 0% (0.00 to 4.64), where the bracketed numbers represent the 95% confidence interval determined by using Minitab software (J. H. Klotz, L. M. Leemis, and K. S. Trivedi, Letter, Am. Statistician **50**:388–389, 1996).

Figure 2 illustrates the experimental data $\{C_i, F_i\}$ for d023 and a weighted, nonlinear fit of equation 1 using the calculated C_e to obtain k_a and I_{max} (Table 1). For this and other sequences, the fits using the model equation are excellent.

The values of k_a and I_{max} are different in the pure and environmental PCR products, indicating different hybridization conditions (see dotted and solid curves in Fig. 2). Concentration curves for pure PCR products were obtained with equimolar mixtures of d023, d011, and d006 and Gx diluted in PCR mix. Parameters k_a and I_{max} were calculated by a weighted, nonlinear fit of equation 1 with $C_e = 0$ (Table 1). In general I_{max} is greater in the pure PCR product than in the environmental PCR product. As shown in Fig. 3 for d006, the excellent fit to the experimental concentration curve spanning

3 orders of magnitude in the amount of target DNA in the tube again supports the model equation for this system.

We sought further validation of the model by comparing our values for the dissociation constant K_d ($= 1/K_a$) to those in the literature. In our experiments the K_d values for a 570-nucleotide target DNA hybridized to a 20-mer capture probe ranged from 2.5×10^{-9} M for d006 to 8.7×10^{-9} M for Gx. Detailed studies (8) of hybridizations on microparticle surfaces between a short target (22-mer) and a particle-bound 22-mer capture probe obtained K_d values of $\sim 10^{-9}$ M at 50°C. Our values are similar but somewhat higher; we speculate that this may be due to a decrease in hybridization efficiency for long-target DNA. We note, however, that the design of the capture probe can affect the hybridization response more than the target sequence length.

As expected, there is substantial variation of the coefficients k_a and I_{max} for different target sequences, most likely due to secondary structure. In practice, for assays targeting a broad array of microorganisms, it will be impossible to design probes with the desired specificity and identical coefficients. Good quantitation will therefore require separate determination of k_a and I_{max} for each control strain. Correspondingly, fine quantitation with universal probes is probably not achievable, as demonstrated by the data for 133/533FA beads in which the total amount of DNA was found to be 17.6 ± 10.5 fmol, compared to 106 fmol determined by gel-based quantitation.

The coefficients k_a and I_{max} are different between an environmental sample and a pure PCR product. Cross-hybridization is unlikely to be the cause since none was observed in our experiments. (For example, the Gx capture probe subjected to noncomplementary pure or environmental PCR products produced no signal.) At this time, we suggest two possible causes: (i) chemicals in the groundwater or extraction process which reduce the efficiency of hybridization or labeling and (ii) many similar sequences in the PCR product which interfere with each other. Tests on more types of environmental samples will be required to elucidate this point.

In summary, we have developed and verified a quantitative method for multiplexed determination of abundances in environmental PCR products.

REFERENCES

1. **Barns, S. M., R. E. Fundyga, M. W. Jeffries, and N. R. Pace.** 1994. Remarkable archaeal diversity detected in a Yellowstone National Park hot spring environment. Proc. Natl. Acad. Sci. USA **91:**1609–1613.
2. **Bevington, P. R.** 1969. Data reduction and error analysis for the physical sciences. McGraw-Hill Book Co., New York, N.Y.
3. **Dojka, M. A., P. Hugenholtz, S. K. Haack, and N. R. Pace.** 1998. Microbial diversity in a hydrocarbon- and chlorinated-solvent-contaminated aquifer undergoing intrinsic bioremediation. Appl. Environ. Microbiol. **64:**3869–3877.
4. **Pieper, D. H., and W. Reineke.** 2000. Engineering bacteria for bioremediation. Curr. Opin. Biotechnol. **11:**2626.
5. **Press, W. H., S. A. Teukolsky, W. T. Vetterling, and B. P. Flannery.** 1992. Numerical recipes in C: the art of scientific computing, 2nd ed. Cambridge University Press, Cambridge, United Kingdom.
6. **Segel, I. H.** 1976. Biochemical calculations, 2nd ed. John Wiley & Sons, New York, N.Y.
7. **Spiro, A., M. Lowe, and D. Brown.** 2000. A bead-based method for multiplexed identification and quantitation of DNA sequences using flow cytometry. Appl. Environ. Microbiol. **66:**4258–4265.
8. **Stevens, P. W., M. R. Henry, and D. M. Kelso.** 1999. DNA hybridization on microparticles: determining capture-probe density and equilibrium dissociation constants. Nucleic Acids Res. **27:**1719–1727.
9. **Wackett, L. P., and D. C. Hershberger.** 2001. Biocatalysis and biodegradation. ASM Press, Washington, D.C.

Prognostic Significance of Fluorescence Intensity of Surface Marker Expression in Childhood B-Precursor Acute Lymphoblastic Leukemia. A Pediatric Oncology Group Study

By Michael J. Borowitz, Jonathan Shuster, Andrew J. Carroll, Michael Nash, A. Thomas Look, Bruce Camitta, Donald Mahoney, Stephen J. Lauer, and D. Jeanette Pullen

This report describes the prognostic significance of the intensity of surface membrane antigen expression in a series of 1,231 children older than 1 year with newly diagnosed B-precursor acute lymphoblastic leukemia (ALL) treated on Pediatric Oncology Group (POG) treatment protocols. All patients had dual-color flow cytometric immunophenotyping performed at a central reference laboratory with a standard panel of monoclonal antibodies. The flow cytometers used in the study were calibrated with a standard fluorescence microparticle that permitted conversion of relative fluorescence channels to standard units of mean equivalents of soluble fluorochrome (MESF). In univariate analysis, fluorescence intensity of CD45 and CD20 was significantly associated with event-free survival (EFS), whereas other markers showed no significant correlation with outcome. Patients whose blasts were greater than the 75th percentile of intensity for CD45 (corresponding to 18,000 MESF units with CD45-FITC, or about 8% of the intensity of normal lymphocytes) fared significantly worse than those with lower-density CD45, and those whose blasts were greater than the 25th percentile of intensity for CD20 (corresponding to 17,900 MESF units with CD20-PE) had a poorer EFS. The intensity of both CD45 and CD20 was independently correlated with outcome. There was no significant correlation between intensity of expression of either antigen and traditional clinical risk factors, ploidy, or t(9;22) or t(1;19). All patients with t(4;11) had CD45 intensity greater than the 75th percentile, but CD45 intensity retained its prognostic significance after adjusting for t(4;11). In multivariate analysis, both CD45 intensity greater than the 75th percentile and CD20 intensity greater than the 25th percentile were significantly correlated with poor outcome independently of previously reported poor prognostic factors including National Cancer Institute (NCI) risk group, ploidy, trisomies of 4 and 10, and adverse translocations including t(1;19), t(9;22), and t(4;11). We conclude that in childhood B-precursor ALL, the intensity of expression of CD20 and CD45 provides prognostic information not available from simple consideration of antigen expression as positive or negative, and adds to that obtained from traditional clinical and biologic risk factors.
© 1997 by The American Society of Hematology.

IMMUNOPHENOTYPIC characterization of acute lymphoblastic leukemia (ALL) in childhood is important for directing therapy and predicting outcome. With the large number of monoclonal antibodies directed against hematopoietic cell surface antigens, it is now possible to demonstrate considerable phenotypic heterogeneity among cases of ALL. Although classification into major immunologic categories is well accepted,[1-5] the importance of detailed subclassification is more controversial. Markers such as CD10, CD24, or myeloid cell surface antigens have been associated with outcome, although the independent prognostic importance of these is less well established.[6-14]

Although flow cytometry is widely used for performing immunophenotyping studies in acute leukemia, little attention has been given to standardizing the criteria for concluding that antigens are present on leukemic cells. In most studies, rigid criteria based on "percent positive" cells are used, even though procedures for standardizing the denominator used to calculate these percentages are rarely specified. Moreover, antigen distributions in leukemia are often such that it is not appropriate to analyze them as percent positives;

specifically, distributions may be unimodal but of low intensity so that they overlap with control distributions. Arbitrarily enumerating events to the right of a negative control may result in the calculation of an inappropriate numeric value.

Fluorescence intensity may provide a better descriptor of antigen distribution on leukemic cells than percent positives. Unfortunately, commercial flow cytometers measure only relative fluorescence in units called channels. Changes in instrument set-up, service, or replacement, as well as changes in monoclonal antibodies, all change the relative channel value of the same fluorescent signal. This limits the ability to use relative fluorescence to compare studies performed over time.

In the past few years, methods for standardizing fluorescence using fluorescent microparticles have been developed.[15-18] These methods take advantage of the fact that measurable amounts of fluorochromes can be attached to beads and assayed in the flow cytometer. Relative channel values are generated and plotted against the known values for the fluorochrome, expressed in units known as mean equivalents of soluble fluorescein (MESF), to produce a standard curve. The fluorescent channel of an unknown sample can then be read from this standard curve. In this way, it is possible to measure fluorescence in absolute rather than relative terms.

In this study, we used a set of fluorescent microparticles to standardize fluorescence intensity measurement of monoclonal antibody–defined cell surface antigens in pediatric B-precursor ALL. The fluorescence intensity of two markers, CD45 and CD20, is highly prognostic of outcome independently of traditional clinical and other biologic risk factors.

SUBJECTS AND METHODS

Patient population. From January 1991 to January 1994, 1,314 patients aged 1.0 to 21.9 years were entered onto Pediatric Oncology

Group (POG) treatment studies for patients with newly diagnosed B-precursor ALL. Although the study did not terminate until November 1994, patients entered after January 1994 were excluded from the study after we became aware of a change in calibration procedures for the microparticles (Schwartz A., personal communication, December 1995). Specimens from all patients were sent by overnight courier to the immunophenotyping reference laboratory at Duke University (through late 1993) or Johns Hopkins University (after 1993), to the cytogenetics reference laboratory at the University of Alabama at Birmingham, and to the ploidy reference laboratory at St. Jude Children's Research Hospital. Cytogenetic and ploidy studies were performed as previously described.[19] Informed consent for reference laboratory studies and for treatment was obtained using forms approved by local institutional review boards.

Among 1,314 patients, 1,231 had sufficient material to perform a complete analysis of antigen density for all markers; 1,258 had satisfactory data for determination of antigen density of CD20 and CD45. Although the material was suitable for confirmation of B-precursor phenotype in the remaining patients, these had either excessive contamination with uninvolved peripheral blood or insufficient cells for complete phenotypic characterization and therefore were not included in this analysis. Eight hundred twenty-two of 1,231 patients had informative cytogenetic studies (ie, at least two abnormal metaphases).

Immunophenotyping. Ficoll-Hypaque–enriched blasts at a concentration of 5×10^6/mL were stained in a final volume of 100 μL by two-color immunofluorescence with a panel of monoclonal antibodies directly conjugated with fluorescein isothiocyanate (FITC) or phycoerythrin (PE). Stained cells were analyzed by flow cytometry on a FACScan flow cytometer (Becton Dickinson Immunocytometry Systems, San Jose, CA), which was calibrated daily with a set of standardized beads (Caribbean Microparticles Inc, San Juan, Puerto Rico). These consisted of a set of beads each with a different known amount of either FITC or PE expressed in units of MESF. A standard curve was constructed each day by plotting MESF values for the beads against the median channel in which the peak was displayed.[18] Fluorescence intensity data were collected using a logarithmic amplifier, but channel values were expressed on a linearized 256- or 1,024-channel scale.

Antibodies CD10, CD34, and CD45 were tested with FITC conjugates, and CD19, CD20, CD22, and HLA-DR were tested with PE conjugates. CD9 and CD24 were tested by indirect immunofluorescence using an FITC-conjugated Fab'(2) goat antimouse secondary antibody. Appropriate isotype controls were also tested. Although the duration of the study was such that it was not possible to use a single lot of antibody, the same vendor was used for the entire study and there was relatively little between-lot variability in fluorescence intensity. All antibodies were from Becton Dickinson, except for CD19-PE and CD9 (Immunotech, Westbrook, ME) and CD24 (Boehringer, Mannheim, Germany). A minimum of 5,000 events were collected for each pair of antibodies, and list mode data were analyzed using Lysys or, in later experiments, Lysys II software (Becton Dickinson). For analysis, an initial display of forward-angle light scatter versus right-angle light scatter was used to construct a mononuclear cell gate, and the reactivity of cells in the gate was determined for each marker. Antibodies were considered positive when there was a significant shift (usually about 20 channels with 256-channel full scale) in the curve of an antibody-stained sample compared with an isotype control, provided it could be determined that this shift was not due to reactivity of normal cells contaminating the gate used for analysis. This latter point was determined from inspection of all the antibody combinations run, based on knowledge of the expected position of normal cells on multiparameter displays. In addition to this method of visually comparing displays to determine positivity, the percent positive events was also recorded using

traditional methods based on setting the gate on mononuclear cells and comparing control and test histograms. With this method, analysis was made using the arbitrary value of 20% as the criterion for positivity.

In addition to recording whether each marker was positive or negative, we also recorded the intensity of antigen expression based on determining the median channel value of the positive population. Although channel values are expressed in arbitrary units, these were converted to standard MESF units by reading from the standard curve obtained by plotting the known MESF values of the standard beads against their channel values. In some experiments, MESF values for blasts were compared directly with MESF values for residual normal lymphocytes in the population. In these experiments, blast populations were distinguished from the residual lymphocytes on dual-parameter displays of CD45 versus right-angle light scatter, separate gates were established on each population, and the median channel of each gated population was used to compute the corresponding MESF value from the same curve.

Treatment. Patients were assigned to standard-risk (POG 9005) or poor-risk (POG 9006) protocols based on age, white blood cell count, and blast ploidy. Briefly, children were assigned to POG 9005 using previously published age and white blood cell count criteria or if DNA ploidy was greater than 1.16 irrespective of age and white blood cell count.[20] Other patients were considered poor risk. In addition, patients with central nervous system disease, t(9;22), or t(1;19) were considered poor risk independently of other factors. Sixty-five percent of the patients were assigned to 9005 and 35% to 9006, although the two studies had equivalent numbers of failures. Infants less than 1 year old were not included in this study.

Standard-risk patients were treated with vincristine, L-asparaginase, and prednisone for induction and randomized for intensification to either 12 courses of intravenous (IV) methotrexate (MTX) (1 g/m² over 24h/IV 6-mercaptopurine (6-MP) (1 g/m² over 6h) or 12 courses of oral MTX (30 mg/m² per dose every 6 h for six doses)/ IV 6-MP. The poor-risk protocol consisted of four-drug induction (vincristine, L-asparaginase, prednisone, and daunorubicin) followed by randomization for intensification to either 12 courses of the IV MTX/IV 6-MP regimen or an alternating drug regimen of IV MTX/ 6-MP, followed by VM-26 and cytosine arabinoside, followed by another MTX/6-MP course, and finally followed by daunorubicin, cytosine arabinoside, vincristine, prednisone, and PEG asparaginase. All patients received standard-dose MTX/6-MP as continuation therapy for 2 years and central nervous system prophylaxis with intrathecal MTX or triple intrathecal medications.

Statistical methods. Univariate analyses of prognostic markers were conducted using the log-rank test[21] stratified for study (standard-risk v high-risk) using event-free survival (EFS) as the dependent variable. EFS is defined as the time from registration to relapse, progression, death, second cancer, or last contact, whichever occurs first. EFS curves were constructed by the Kaplan-Meier method[22] with the standard errors of Peto et al.[21] The overall results should take priority over all subset results (ie, standard- v poor-risk), as subsets have much lower statistical power to observe true differences. In addition, subset results were not an a priori objective of the study. To assess cutoff points and the independent importance of the CD variables found to be significant, multivariate analysis was constructed by the forward stepwise Cox method for proportional hazards, with EFS as the dependent variable.[23] Independent variables included four binary variables (negative, and cutoffs at the first three quartiles) for each significant CD variable, along with National Cancer Institute (NCI) consensus risk group, study (standard- v poor-risk, the latter defined by age ≥ 10 years or white blood cell count >50,000[24]); trisomy of both chromosomes 4 and 10; or bad translocation [t(4;11), t(9;22), or t(1;19)]. The risk ratio is the estimated ratio of instantaneous likelihood of failure, ie, adverse to favorable

Table 1. Prognostic Significance of Antigen Expression in Childhood B-Precursor ALL by Univariate Analysis (P values)

	All Patients > 20%	Intensity		
Antigen		All Patients	Standard-Risk Patients	Poor-Risk Patients
CD10	.08	.14	.28	.28
CD19	*	.65	.11	.69
CD20	.01	.005	.34	.01
CD22	<.001	.33	.38	.54
HLA-DR	*	.63	.84	.76
CD34	.92	.60	.73	.48
CD9	.91	.18	.81	.18
CD24	.28	.68	.53	.04
CD45	.81	<.0001	.08	.0001

Analysis of failure rates of patients in different groups was conducted with the log-rank test. In the column marked "v 20%," patients were considered positive for each marker if 20% of blasts were positive; in columns marked "intensity," patient populations were determined based on intensity distributions. Standard-risk and poor-risk patients were treated on study protocols 9005 and 9006, respectively.

* Only 3 patients were CD19⁻ and 2 patients HLA-DR⁻.

value of the factor. Clinical correlations were made by the Kruskal-Wallis nonparametric test for quantitative factors and the Pearson χ^2 test for qualitative factors.

The prognostic significance of each factor was assessed using a traditional 20% positive cutoff and as five groups using intensity of expression, including negative plus each of the four quartiles for cases in which blasts were considered positive (ie, cutoff points were defined at the 25th, 50th, and 75th percentiles of the fluorescence intensity variable MESF for each marker). This division into multiple groups allowed for investigation of nonmonotonic trends (for example, a trend other than one in which the higher the value of a variable, the more favorable the outcome). The decision to use quartiles was arbitrary, but follows the common practice among clinical investigators to place patients into prognostic groups while allowing for flexible choices of cutoff points.

RESULTS

Prognostic significance of surface antigen expression. Each marker in the panel was evaluated in univariate analysis to determine its prognostic significance for EFS. Expression of CD10, CD19, HLA-DR, CD34, CD9, or CD24 was not significantly correlated with outcome whether results were expressed as positive using the arbitrary 20% positive cutoff or based on intensity (Table 1). CD22 was significant only when the percent positive cutoff was used; examination of this latter phenomenon in more detail revealed that this was due to a high failure rate (12 patients) among a small number of patients (n = 23) in whom CD22 was less than 20%. However, CD20 expression was an adverse prognostic marker using either the arbitrary percentage cutoff for positivity or based on intensity, whereas CD45 expression was only significant when intensity was considered.

Intensity distributions for CD45 and CD20 were examined in more detail. MESF values for CD45-FITC that corresponded to the 25th, 50th, and 75th percentiles were represented by 6,250, 10,900, and 18,000 MESF units, respectively; for CD20-PE, the corresponding values were 17,900,

31,900, and 62,900. To put this in perspective, 24 cases with MESF values for the blasts closest to the 75th percentile cutoff (mean MESF, 17,600 ± 800) were compared with normal lymphocytes in the same specimen; the corresponding value for CD45 on these residual normal lymphocytes was 236,000 ± 70,000. Expressed as a relative value, the average ratio of the MESF value of CD45 on the blasts to that on the lymphocytes was .081 ± .024. There were insufficient normal residual CD20⁺ B cells to calculate a similar relative value for CD20.

Results were also investigated separately for standard- and poor-risk patients treated on studies 9005 and 9006, respectively. In five-way analysis, no marker was significant among standard-risk patients, although a trend was seen with CD45 intensity (P = .08). However, among poor-risk patients, both CD45 and CD20 intensities were significantly associated with outcome. CD24 intensity was marginally significant in higher-risk patients.

Prognostic significance of CD45 and CD20 intensity. Table 2 presents treatment failure rates as a function of fluorescence intensity of CD45. Patients who are CD45⁻ or CD45⁺ up to the 75th percentile of intensity show little difference in outcome, but patients who are CD45-brightest (4th quartile) are at much higher risk of treatment failure. Kaplan-Meier plots of EFS for these patients are illustrated in Fig 1. Table 3 illustrates similar data for CD20 fluorescence intensity. The increased risk of treatment failure is seen at a lower intensity level (at the 2nd quartile and above). For both CD45 and CD20, fluorescence intensity shows a better correlation with treatment failure than does classification as positive or negative.

In multivariate analysis, CD45 and CD20 intensity are independent prognostic factors for poor outcome. In this analysis, the strongest prognostic relationship of CD20 is above and below the median rather than at the 25th percentile. Figure 2 shows a Kaplan-Meier plot of outcome of all patients using risk groups defined by the combination of CD45 and CD20 intensity. The poorest EFS was seen among patients who were both CD45-bright and CD20-bright. Such patients accounted for about 8% of total patients; these represented about 14% of patients registered to the high-risk study and 5% of patients on the standard-risk study. The 3-year EFS of this poor-risk group is 59% ± 13%, compared with 84% ± 2% among patients who are neither CD45- nor CD20-bright. Other groups (CD45-bright, CD20-less bright; or CD20-bright, CD45-less bright) show intermediate survival.

Correlation of CD45 and CD20 intensity with other prognostic parameters. Patients with bright CD20 or CD45

Table 2. Prognostic Significance of Fluorescence Intensity of CD45 Expression in Childhood B-Precursor ALL by Univariate Analysis

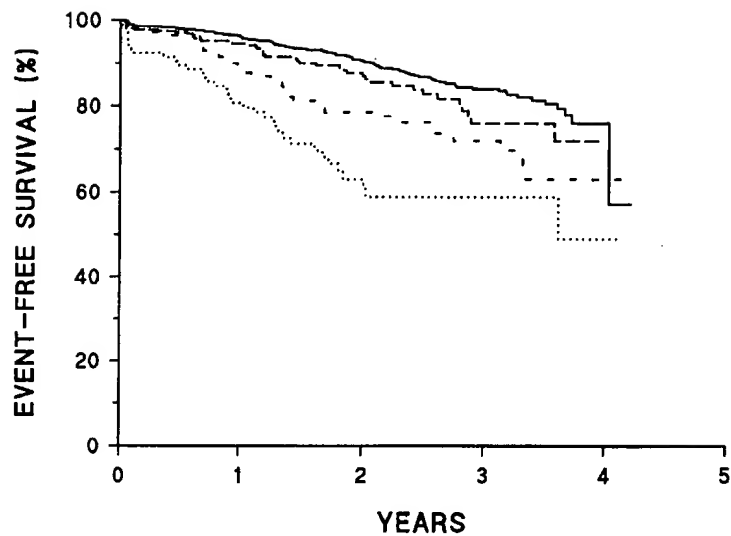| CD45 Intensity	No.	No. of Failures	Expected
Negative	195	25	28.5
1st quartile	278	35	49.9
2nd quartile	285	41	49.8
3rd quartile	288	47	49.9
4th quartile	244	72	41.9

P < .0001.

Fig 1. Prognostic significance of CD45 intensity. Kaplan-Meier survival plots of patients classified as shown in Table 2. ——, CD45⁻ or intensity in dimmest quartile; - - -, CD45 intensity in second quartile; - - -, CD45 intensity in third quartile; · · ·, CD45 intensity in brightest quartile. The curves are significantly different (*P* < .001).

were not significantly different from other patients with respect to other known important prognostic factors including age, white blood cell count, incidence of hyperdiploidy, trisomies of 4 and 10, or presence of the Philadelphia chromosome (data not shown). However, all 12 patients with t(4;11) were in the CD45-bright (>75th percentile) group; CD45 intensity remained prognostic even after adjusting for t(4;11) patients.

Multivariate analysis. Each marker shown to be of prognostic significance in univariate analysis was put into a multivariate Cox linear regression model along with other known prognostic factors including NCI risk group, ploidy involving trisomies of chromosome 4 and 10, adverse translocations [t(1;19), t(9;22), or t(4;11)], and treatment regimen. A second analysis was made substituting flow hyperdiploidy (DNA index [DI] > 1.16) for the cytogenetic analysis, because there were significantly more patients for whom there were informative data with flow ploidy compared with cytogenetics.

In these analyses, the intensity of expression of CD45 (>75th percentile) and CD20 (>25th percentile) was again independently prognostic. The cutoff point for CD45 was again at the 75th percentile and that for CD20 was at the 25th percentile, as it had been in univariate analysis. Additional variables found to be significant included NCI risk group, trisomies of 4 and 10, and adverse translocations. In patients

Table 3. Prognostic Significance of Fluorescence Intensity of CD20 Expression in Childhood B-Precursor ALL by Univariate Analysis

CD20 Intensity	No.	No. of Failures	Expected
Negative	466	65	84.5
1st quartile	204	35	41.0
2nd quartile	211	40	35.1
3rd quartile	226	39	32.8
4th quartile	189	42	27.4

P < .005.

with only satisfactory flow ploidy, NCI risk group and flow hyperdiploidy (DI > 1.16) were significant. The final models are illustrated in Tables 4 and 5.

DISCUSSION

The independent prognostic significance of expression of particular surface membrane antigens within an immunologically defined subgroup of ALL is controversial. In part, this reflects the close association between expression of particular surface markers and other biologic measurements of disease expression, particularly cytogenetics.[25-28] However, varying analytic approaches used for measuring these antigens and for defining positivity may also play a role.

In this study, we calibrated the flow cytometers with a well-characterized fluorescent microparticle to quantify the fluorescence intensity of antigen expression. We found that the description of antigen expression using intensity was more powerful than either qualitative or quantitative dichotomous discrimination of "positives" and "negatives" for predicting early EFS in pediatric B-precursor ALL. Specifically, patients with the brightest expression of CD45 (>75th percentile) or relatively bright (>25th percentile) CD20 expression had an increased risk of treatment failure independently of each other and of other traditional risk factors including age, white blood cell count, DNA ploidy, or adverse chromosomal translocations. The risk ratios of treatment failure in final multivariate models for CD45 or CD20 ranged from 1.5 to 1.9, compared with relative risks of approximately 2.0 for other traditional adverse risk factors. Although these analyses were based on the entire cohort of patients, the clinical relevance of these results appeared most pronounced in the high-risk stratum.

We found no significant association between CD20 intensity and any other clinical or laboratory features known to be associated with adverse prognosis. However, there was a strong association between bright CD45 expression and t(4;11): all patients with t(4;11) expressed CD45 at intensity
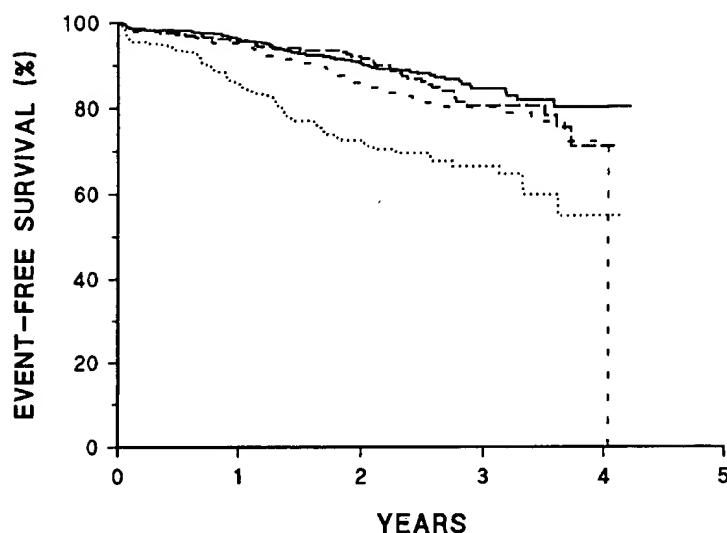
Fig 2. Prognostic significance of the combination of CD45 and CD20 intensity. Kaplan-Meier survival plots of all patients classified by risk group based on intensity of CD45 and CD20 expression. CD45 poor risk implies > 75th percentile of intensity; CD20 poor risk implies > 50th percentile of intensity. ——, CD45 and CD20 good risk (57% of patients); — — —, CD45 good risk, CD20 poor risk (24% of patients); - - -, CD45 poor risk, CD20 good risk (11% of patients); · · ·, CD45 and CD20 poor risk (8% of patients). The curves are significantly different (P < .001).

levels that put them in the upper quartile. In fact, preliminary studies suggest that bright CD45 expression is a more sensitive method for predicting t(4;11) than our previously published algorithm based on expression of CD10, CD24, and CD15.[22] Despite this strong correlation, the adverse prognostic association of bright CD45 expression was not completely explained by the poor outcome of t(4;11) patients, as only 12 patients in our series had t(4;11). It also appears unlikely that the adverse outcome of CD45-bright patients can be explained by other 11q23 translocations involving the MLL gene, as non-t(4;11) MLL translocations are relatively rare in this patient population (Behm, Carroll, and Shuster, unpublished observations, May 1996).

In normal B-cell development, CD45 is expressed more intensely as B cells mature.[29] However, we do not believe that the poor outcome of this patient population reflects the fact that their leukemic blasts represent a later stage of maturation. In the first place, as already noted, CD45 is particularly intense on the subset of "immature" leukemias associated with t(4;11). In addition, there was no correlation between intensity of CD45 expression with other differentiation-related markers such as CD34. Whether CD45 expression per se is somehow important in determining response to therapy or whether it is a surrogate for an as yet undefined biologic marker is uncertain. CD45 is a tyrosine phosphatase,

and as such may play a role in the regulation of growth via tyrosine kinase phosphorylation pathways.[30] Whether this plays any role in leukemia remains to be determined.

Although CD45 is ubiquitous on hematologic cells, about 15% to 20% of B-precursor ALL is negative for CD45,[6] although the sensitivity of the method used for detection may affect this number. Behm et al[6] showed that patients with CD45⁻ blasts fared better than CD45⁺ cases; however, this was due to the high correlation of CD45 negativity and hyperdiploidy. They did not investigate the bright CD45⁺ patients as a separate subgroup. However, Caldwell et al[7] also showed that patients with bright CD45 fared worse than those with lower-density expression. However, the series was relatively small and multivariate analysis was not performed. Moreover, the patient population was heterogeneous with respect to immunophenotype, and unlike our series, it included some patients with T-ALL. However, in light of our results, it is likely that Caldwell et al were measuring a similar correlation between outcome and CD45 intensity.

CD20 has rarely been considered an important prognostic factor in childhood B-precursor ALL.[9] Although we found a modest relationship between CD20 expression and outcome when expressed as positive or negative using an arbitrary percent positive cutoff, it was not nearly as strong as the consideration of intensity of expression; in multivariate analysis, intensity of expression was an independent significant

Table 4. Multivariate Analysis of Risk of Treatment Failure in Childhood B-Precursor ALL Patients With Informative Cytogenetic and Immunophenotyping Studies (N = 822)

Adverse Variable	P	Estimated Risk Ratio (95% confidence limits)
NCI poor-risk group	<.001	2.1 (1.5-2.9)
Not both +4 and +10	.002	2.3 (1.4-4.0)
Brighter than 1st-quartile CD20	.006	1.6 (1.1-2.2)
Brightest-quartile CD45	.008	1.6 (1.1-2.2)
t(1;19), t(4;11), or t(9;22)	.04	1.5 (1.0-2.3)

Table 5. Multivariate Analysis of Risk of Treatment Failure in Childhood B-Precursor ALL Patients With Satisfactory Ploidy and Immunophenotypic Studies (N = 1,211)

Adverse Variable	P	Estimated Risk Ratio (95% confidence limits)
NCI poor-risk group	<.001	2.1 (1.5-2.9)
DNA < 1.16	.009	1.7 (1.1-2.4)
Brightest-quartile CD45	<.001	1.9 (1.4-2.6)
Brighter than 1st-quartile CD20	.004	1.5 (1.1-1.9)

prognostic factor. Thus, the failure of other investigators to note the importance of CD20 expression may be due to analytic problems in standardizing the most important discriminating values. Differences in therapy may also contribute to variability within the literature.

Relatively few investigators have examined the intensity of expression of surface markers other than CD45 in ALL.[31-34] Look et al,[31] and more recently Lavabre-Bertrand,[33] studied the relationship of CD10 intensity to a number of patient characteristics. The latter study showed that CD10 intensity correlated with cytogenetic abnormalities, and also demonstrated that leukemic blasts often expressed levels of CD10 different from those of normal B precursors.

Ideally, for our results to be compared across studies and ultimately to be used to stratify patients, it would be useful to have an absolute reproducible value for a poor prognostic marker. The MESF value of 18,000, representing our 75th percentile value for CD45, has some limitations as such a marker. First, the change in calibration value of the bead since the inception of this study would likely slightly change the absolute value for this cutoff in subsequent studies. Second, even if this problem had not occurred, differences in antibody formulation will produce variations in this absolute value. A possible mechanism to overcome these limitations is suggested by the recent study by Bikoue et al.[35] These investigators quantified the number of antigenic sites for CD45 on normal lymphocytes, monocytes, and granulocytes and found them to be stable across individuals. This suggests that normal cells might serve as internal standards for quantitative measurement. Although we did not have sufficient granulocytes or monocytes to evaluate, most cases had residual normal lymphocytes that could be readily separated from the blast population. When we compared the blast intensity of our cases at the 75th percentile cutoff with that of residual lymphocytes, we found that their fluorescence intensity corresponded to a relative intensity value of about 8% that of normal lymphocytes. An attempt to standardize CD20 cutoff values in a similar fashion was unsuccessful; this may, in part, be due to the small number of normal B cells that were present in the specimens. It would have been more difficult to determine a target value for the CD20 cutoff in any case because, depending on the analysis, the cutoff point for CD20 intensity as a significant variable was sometimes at the 25th percentile and sometimes at the 50th percentile. In future studies, we will investigate whether the use of an internal standard can provide a more reproducible method for measuring fluorescence intensity than the set of beads used in this study. In addition, the bead-based technologies used by Bikoue et al and other groups make possible direct readings of antibody binding sites independently of instrument, antibody, and fluorochrome.[15,18,33] Such an approach to a more reproducible method of antigen density determination will also be investigated in future studies.

Although it might be tempting to conclude that patients whose blasts express CD45 at a level greater than 8% of that seen in normal lymphocytes should be treated more aggressively, we would urge caution before adopting such a strategy. In the first place, our own approach in the POG has been to confirm a new prognostic finding in a second

prospective study before adopting it in our treatment design. Second, we do not yet know the interlaboratory or even the intralaboratory reproducibility of quantitation of intensity by this method. Finally, we should emphasize that the 75th percentile value was an arbitrary cutoff based on dividing our patient population into quartiles, and there is no inherent biologic significance to these cutoffs. However, arbitrary cutoffs are commonly used for all prognostic factors that are continuous variables, including age, white blood cell count, and ploidy.

However, despite the immediate practical limitations, our investigation has shown that measurement of antigen density of CD45 and CD20 provides important prognostic information in childhood B-precursor ALL. These results could lead to investigations on possible biologic attributes of leukemic cells with these phenotypic properties. In addition, future studies directed at confirming these results and further improving interlaboratory standardization could lead to more accurate methods for selecting therapy for children with ALL.

REFERENCES

1. Crist WM, Grossi CE, Pullen DJ, Cooper MD: Immunologic markers in childhood acute lymphocytic leukemia. Semin Oncol 12:105, 1985

2. Pui C-H, Behm FG, Crist WC: Clinical and biologic relevance of immunologic marker studies in childhood acute lymphoblastic leukemia. Blood 82:343, 1993

3. Borowitz MJ: Immunologic markers in childhood acute lymphoblastic leukemia. Hematol Oncol Clin North Am 4:743, 1990

4. Bradstock KF: The diagnostic and prognostic value of immunophenotyping in acute leukemia. Pathology 25:367, 1993

5. Ludwig W-D, Raghavachar A, Thiel E: Immunophenotypic classification of acute lymphoblastic leukaemia. Baillieres Clin Haematol 7:235, 1994

6. Behm FG, Raimondi SC, Scell MJ, Look AT, Rivera GK, Pui C-H: Lack of CD45 antigen on blast cells in childhood acute lymphoblastic leukemia is associated with chromosomal hyperdiploidy and other favorable prognostic features. Blood 79:1011, 1992

7. Caldwell CW, Patterson WP, Hakami N: CD45 expression and prognosis in acute lymphoblastic leukemia. Blood 81:562, 1993

8. Borowitz MJ, Shuster JJ, Civin CI, Carroll AJ, Look AT, Behm FG, Land VJ, Pullen DJ, Crist WM: Prognostic significance of CD34 expression in childhood B-precursor acute lymphocytic leukemia. A Pediatric Oncology Group Study. J Clin Oncol 8:1389, 1990

9. De Rossi G, Grossi C, Foa R: Immunophenotype of acute lymphoblastic leukemia cells: The experience of the Italian Cooperative Group (Gimema). Leuk Lymphoma 9:221, 1993

10. Kristensen JS, Jensen AW, Jensen IM, Pedersen B, Ellegaard J, Hokland P: Hybrid acute leukemia: Therapeutic implications of immunological phenotyping. Anal Cell Pathol 4:69, 1992

11. Ludwig WD, Harbott J, Reider H, Bartram CR, Komischke B, Sperling C, Teichmann JV, Seibt-Jung H, Notter M, Odenwald E, Nehmer A, Thiel E, Riehm H: Incidence and prognostic significance of immunophenotypic subgroups in childhood acute lymphoblastic leukemia: Experience of the BFM-ALL Study 86, in Ludwig WD, Thiel E (eds): Recent Advances in Cell Biology of Acute Leukemia—Impact on Clinial Diagnosis and Therapy. Berlin, Germany, Springer, 1993, p 269

12. Wiersma SR, Ortega J, Sobol E, Weinberg KA: Clinical importance of myeloid-antigen expession in acute lymphoblastic leukemia of childhood. N Engl J Med 324:800, 1991

13. Pui CH, Behm FG, Singh B, Rivera GK, Schell MJ, Roberts

WM, Crist WM, Mirro J: Myeloid-associated antigen expression lacks prognostic value in childhood acute lymphoblastic leukemia treated with intensive multiagent chemotherapy. Blood 75:198, 1990

14. Pui CH, Hancick ML, Rivera GK, Look AT, Andlund JT, Behm F: Clinical significance of CD34 expression in childhood acute lymphoblastic leukemia. Blood 82:889, 1993

15. Poncelet P, Carayon P: Cytofluorometric quantification of cell-surface antigens by indirect immunofluorescence using monoclonal antibodies. J Immunol Methods 85:65, 1985

16. Vogt RF, Cross GD, Henderson LO, Phillips DL: Model system evaluating fluorescein-labelled microbeads as internal standards to calibrate fluorescence intensity on flow cytometers. Cytometry 10:294, 1989

17. Brando B, Sommaruga E: Nationwide quality control trial on lymphocyte immunophenotyping flow cytometer performance in Italy. Cytometry 14:294, 1995

18. Schwartz A, Repollet EF, Vogt R, Gratama JW: Standardizing flow cytometry—Construction of a standardized fluorescence calibration plot using matching spectral calibrators. Cytometry 26:22, 1996

19. Crist WM, Carroll AJ, Shuster JJ, Behm FG, Whitehead M, Vietti TJ, Look AT, Mahoney D, Ragab A, Pullen DJ, Land VJ: Poor prognosis of children with pro-B acute lymphoblastic leukemia is associated with the t(1;19)(q23;p13): A Pediatric Oncology Group Study. Blood 76:117, 1990

20. Trueworthy R, Shuster J, Look T, Crist W, Borowitz M, Carroll A, Frankel L, Harris M, Wagner H, Haggard M, Mosijczuk A, Pullen J, Steuber P, Land V: Ploidy of lymphoblasts is the strongest predictor of treatment outcome in B-progenitor cell acute lymphoblastic leukemia of childhood: A Pediatric Oncology Group Study. J Clin Oncol 10:606, 1992

21. Peto R, Pike MC, Armitage P, Brewlow NE, Cox DR, Howard SV, Mantel N, McPherson K, Peto J, Smith PG: Design and analysis of randomized clinical trials requiring prolonged observation of each patient. II. Analysis and examples. Br J Cancer 35:1, 1977

22. Kaplan EL, Meier P: Nonparametric estimation from incomplete observations. J Am Stat Assoc 53:457, 1958

23. Bartolucci AA, Fraser MD: Comparative step-up and composite tests for selecting prognostic indicators associated with survival. Biometr J 19:437, 1977

24. Smith M, Arthur D, Camitta B, Carroll AJ, Crist W, Gaynon P, Gelber R, Heerema N, Korn EL, Link M, Murphy S, Pui C-H, Pullen J, Reaman G, Sallan SE, Sather H, Shuster J, Simon R, Trigg M, Tubergen D, Uckun F, Ungerleider R: Uniform approach to risk classification and treatment assignment for children with acute lymphoblastic leukemia. J Clin Oncol 14:18, 1996

25. Pui CH, Williams DL, Roberson PK: Correlation of karyotype and immunophenotype in childhood acute lymphoblastic leukemia. J Clin Oncol 6:56, 1988

26. Uckun FM, Gajl-Peczalska KJ, Provisor AJ, Heerema NA: Immunophenotype-karyotype associations in human acute lymphoblastic leukemia. Blood 73:271, 1989

27. Pui C-H, Frankel LS, Carroll AJ, Raimondi SC, Shuster JJ, Head DR, Crist WM, Land VJ, Pullen DJ, Steuber PC, Behm FG, Borowitz MJ: Clinical characteristics and treatment outcome of childhood acute lymphoblastic leukemia with the t(4;11)(q21;q23): A collaborative study of 40 cases. Blood 77:440, 1991

28. Borowitz MJ, Hunger SP, Carroll AJ, Shuster JJ, Pullen DJ, Steuber CP, Cleary ML: Predictability of the t(1;19)(q23;p13) from surface antigen phenotype: Implications for screening cases of childhood acute lymphoblastic leukemia for molecular analysis: A Pediatric Oncology Group Study. Blood 82:1086, 1993

29. Shah VO, Civin CI, Loken MR: Flow cytometric analysis of human bone marrow. IV. Differential quantitative expression of T-200 common leukocyte antigen during normal hematopoiesis. J Immunol 140:1861, 1988

30. Mustelin T, Coggeshall KM, Altman A: Rapid activation of the T-cell tyrosine protein kinase pp56lck by the CD45 phosphotyrosine phosphatase. Proc Natl Acad Sci USA 86:6302, 1989

31. Look AT, Melvin SL, Brown LK, Dockter ME, Roberson PK, Murphy SB: Quantitative variation of the common acute lymphoblastic leukemia antigen (gp100) on leukemic marrow blasts. J Clin Invest 73:1617, 1984

32. Lavabe-Bertrand Y, George F, Brunet C, Sampol J: Quantitative immune phenotyping: A new dimension for the monitoring of haematopoietic malignancies. Nouv Rev Fr Hematol 36:373, 1994

33. Lavabre-Bertrand T, Janossy G, Ivory K, Peters R, Secker-Walker L, Porwit-MacDonald A: Leukemia associated changes identified by quantitative flow cytometry. I. CD10 expression. Cytometry 18:209, 1994

34. Lavabre-Bertrand T, Duperray C, Brunet C, Poncelet P, Exbrayat C, Bourquard P, Lavabre-Bertrand C, Brochier J, Navaro M, Janossy G: Quantification of CD24 and CD45 antigens in parallel allows a precise determination of B cell maturation stages. Relevance for the study of B cell neoplasia. Leukemia 8:402, 1994

35. Bikoue A, George F, Poncelet P, Mutin M, Janossy G, Sampol J: Quantitative analysis of leukocyte membrane antigen expression: Normal adult values. Cytometry 26:137, 1996

Technical Advance

Sensitive Immunoassay of Tissue Cell Proteins Procured by Laser Capture Microdissection

Nicole L. Simone,* Alan T. Remaley,[†]
Lu Charboneau,* Emmanuel F. Petricoin III,[‡]
Janice W. Glickman,[†] Michael R. Emmert-Buck,*
Thomas A. Fleisher,[†] and Lance A. Liotta*

From the Laboratory of Pathology, National Cancer Institute,
and the Clinical Pathology Department,[†] Clinical Center,
National Institutes of Health, Bethesda, Maryland; and the
Division of Cytokine Biology,[‡] Center for Biologics Evaluation
and Research, Food and Drug Administration, Washington, DC*

Coupling laser capture microdissection (LCM) with sensitive quantitative chemiluminescent immunoassays has broad applicability in the field of proteomics applied to normal, diseased, or genetically modified tissue. Quantitation of the number of prostate-specific antigen (PSA) molecules/cell was conducted on human prostate tissue cells procured by LCM from fixed and stained frozen sections. Under direct microscopic visualization, laser shots 30 μm in diameter captured specific cells from the heterogeneous tissue section onto a polymer transfer surface. The cellular macromolecules from the captured cells were solubilized in a microvolume of extraction buffer and directly assayed using an automated (1.5 hour) sandwich chemiluminescent immunoassay. Calibration of the chemiluminescent assay was conducted by developing a standard curve using known concentrations of PSA. After the sensitivity, precision, and linearity of the chemiluminescent assay was verified for known numbers of solubilized microdissected tissue cells, it was then possible to calculate the number of PSA molecules per microdissected tissue cell for case samples. In a study set of 20 cases, using 10 replicate samples of 100 laser shots per sample, the within-run (intraassay) SD was approximately 10% of the mean or less for all cases. In this series the number of PSA molecules per microdissected tissue cell ranged from 2 $\times$ 10^4 to 6.3 $\times$ 10^6 in normal epithelium, prostate intraepithelial neoplasia (PIN), and invasive carcinoma. Immunohistochemical staining of human prostate for PSA was compared with the results of the soluble immunoassay for the same prostate tissue section. Independent qualitative scoring of anti-PSA immuno-histochemical staining intensity paralleled the LCM quantitative immunoassay for each tissue subpopulation and verified the heterogeneity of PSA content between tissue subpopulations in the same case. Extraction buffers were successfully adapted for both secreted and membrane-bound proteins. This technology has broad applicability for the quantitation of protein molecules in pure populations of tissue cells. (Am J Pathol 2000, 156:445–452)

As the field of molecular biology moves beyond genomics to proteomics,[1] there is a growing need to monitor the levels of expressed proteins directly in developing, diseased, or genetically altered tissues. Tissues are complicated three-dimensional structures composed of multiple subpopulations of cells interacting with each other and with the extracellular matrix. The amount and type of proteins expressed by cells in their native tissue environment may be quite different from those of cultured or transplanted cells. Although immunohistochemistry provides valuable information concerning the localization of antigenic epitopes in histological sections of tissue, it does not readily permit quantitation of proteins in individual cell populations.[2] Moreover, it has not been possible to calibrate the intensity of immunohistochemical staining with the actual number of antigen molecules in the stained tissue cells. Consequently, there is a great need for technology that can directly measure the quantitative level of specific proteins in actual microscopic tissue cells. Quantitative immunoassays of molecular markers in specific subpopulations of tissue cells, as compared to current global subjective immunohistochemical assessment, can provide precise objective values that may potentially be useful in diagnostic or therapeutic decisions.

Laser capture microdissection (LCM) is a technology recently developed by our laboratory[3–5] and commercialized by Arcturus Engineering (www.arctur.com). LCM enables the user to procure pure cells from stained heterogeneous tissue under direct high-power microscopic

visualization. The cells of interest are transferred to a polymer film that is activated by laser pulses. The exact morphology of the procured cells (with intact DNA, RNA, and proteins) is retained and held on the transfer film. Direct visualization of the captured cells, with their histology intact, ensures that the correct population of cells is obtained.

In the present report we examine the sensitivity and precision of a complete procedure for conducting quantitative prostate-specific antigen (PSA) immunoassay[6] of stained human prostate tissue cells selected and procured by LCM. PSA was chosen as the analyte prototype for technology development because of its importance as a prostate marker and the known cellular heterogeneity of expression of PSA by prostate immunohistochemistry.[2] Precision analysis was conducted for different numbers of laser shots. Comparisons of the number of PSA molecules per cell were made between different stages of prostate cancer progression in the same prostate and compared with PSA immunohistochemistry scoring.

Materials and Methods

Case Materials

Tissue was obtained following an Institutional Review Board-approved protocol from both the Urologic Oncology Branch of the National Cancer Institute (Bethesda, MD) and the Mayo Clinic (Rochester, MN). After surgery, the tissue samples were immediately flash frozen in liquid nitrogen. The tissue was then embedded in O.C.T. compound and stored at −80°C. Cases were selected based on the histology present in the tissue sections so that normal glands, prostate intraepithelial neoplasia (PIN), and adjacent carcinoma could be compared within the same patient. Prostate tissue cases were selected to include ample stroma to serve as a negative control. Lung tissue was used as a second negative control.

Sectioning and Staining

The O.C.T.-embedded tissue blocks were cut with a cryostat into 8-μm sections. After cutting, the sections were immediately placed on dry ice and stored at −80°C. Only one section was thawed and dissected at a time, to minimize degradation of proteins. Frozen sections on plain untreated glass slides were fixed with 70% ethanol for 10 seconds. After fixing, the slides were washed in deionized water; stained with Mayer's hematoxylin for 30 seconds, followed by another water wash, bluing solution for 30 seconds, and a wash in 70% ethanol; and then stained with eosin for 90 seconds. The slide was then dehydrated with two 10-second washes in 95% ethanol and two 10-second washes with 100% ethanol. Finally, the slide was placed in xylene for 30 seconds.

Laser Capture Microdissection

The Arcturus PixCell II system incorporates an Olympus IX-50 microscope containing a microscope slide stage that is moved by a joystick.[4] The operator uses the joy-

stick to position the tissue under a fixed laser beam that can be focused from a 7.5-μm to a 30-μm diameter. The LCM transfer film is fixed to the undersurface of a vial cap (CapSure TM TF-100 transfer film carrier, 5-mm-diameter optical-grade transparent plastic; the matching vial is Brinkmann no. 22 36 430-8). The LCM cell procurement time was always less than 15 minutes. A 5.0–10.0-μl droplet of the extraction buffer was applied to the surface of the film containing the selected cells for 1 minute. The cap with the droplet on its undersurface was then inserted in the mouth of the matching vial containing 45 μl of the immunoassay dilution buffer. The sealed vial sample receptacle was frozen at −20°C and stored for less than 48 hours before assay. The thawed sample was held at 4°C for no longer than 2.5 hours before introduction into the immunoassay module.

Extraction Buffer

Buffer A was 1/1000 dilution of the following stock: 50 mmol/L Tris-HCl, 1% NP-40, 0.1% Na deoxycholate,150 mmol/L NaCl, 4 mmol/L EDTA, aprotinin (10 mg/ml), leupeptin (10 mg/ml), 10 mmol/L Na pyrophosphate, 2 mmol/L Na orthovanate, and 100 mmol/L phenylmethylsulfonyl fluoride. Buffer B was "T-Per" tissue protein extraction liquid reagent (obtained from Pierce; catalog no. 78510). Buffer C was 10 mmol/L Tris-HCl (pH 7.4), 0.1% Triton X-100,1.5 mmol/L EDTA, 10% glycerol.

PSA Immunoassay: Microparticle Enzyme Immunoassay

PSA was measured by an automated two-site chemiluminescent assay, using the ultrasensitive PSA reagent kit on the Immulite immunoassay analyzer called the Immulite Third Generation PSA assay[6] (Diagnostic Products Corp., Los Angeles, CA). This assay is a solid-phase two-site sequential chemiluminescent immunometric assay. The solid phase, a polystyrene bead enclosed within a test vial, is coated with an antibody specific for PSA. The sample microdissected cell proteins solubilized in a buffer are introduced into the test unit and incubated for 30 minutes at 37°C. PSA in the sample binds to the surface of the bead. Unbound proteins are removed by washing. An alkaline phosphatase-labeled polyclonal goat anti-PSA antibody is introduced, and the test unit is incubated for another 30-minute cycle. After a further wash, the chemiluminescent substrate, a phosphate ester of adamantyl dioxetane, is introduced. The substrate undergoes hydrolysis, accompanied by the emission of light. The light is measured by a luminometer. Relative light units (RLUs) reflect the photons detected by the photomultiplier tube, which is proportional to the concentration of PSA in the sample.

Immunohistochemistry

Immunohistochemistry staining for PSA was conducted using an adaptation of the method as described by Fend et al.[7] The frozen sections were desiccated and then
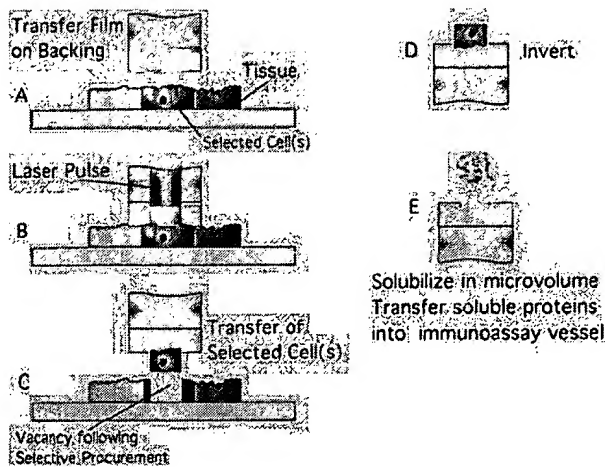
Figure 1. Extraction of proteins. Fixed, stained, microscopic tissue cells of interest are selected using LCM and transferred onto the area of the polymer surface activated by the laser beam. The captured cells are exposed to concentrated extraction buffer in a microvolume. The solubilized proteins are diluted in the immunoassay buffer and incubated with a solid-phase capture antibody specific for the analyte (Materials and Methods). Chemiluminescent detection is conducted with a labeled secondary antibody through a sandwich binding step.

fixed in acetone. After washing with 3% goat serum, the primary antibody (Dako A562) was incubated for 1 hour at room temperature. Avidin/biotin was used to label the secondary antibody, and peroxidase/diaminobenzidine was used as the substrate.

Results

Tissue Cell Procurement

Figure 1 describes the steps of LCM cell procurement and protein solubilization. Figure 2 is an example of LCM cell procurement of prostate epithelial cells. The full staining characteristics of the procured cells are retained, allowing for the precise enumeration of the number of cells transferred to the polymer cap film. The yield of procured pure epithelial or carcinoma cells encompassed within a standard 30-μm shot and the precision of cellular procurement were tested by visually counting the number of cells removed from the tissue and transferred to the film.

LCM Cell Yield Precision

Table 1 compares the number of laser shots with the average total number of microdissected cells for a series of example prostate cases. A standard laser spot diameter of 30 μm encompasses a mean number of five to seven cells. Individual tissue cells can vary in their packing density, their shape, and their volume. Consequently, the imprecision of the cell yield is greater with fewer laser shots. The SD for the number of cells procured by one shot was approximately 50% of the mean. In contrast, when 15, 25, or 100 shots were procured, the SD of cell yield was reduced progressively to less than 10% of the mean.
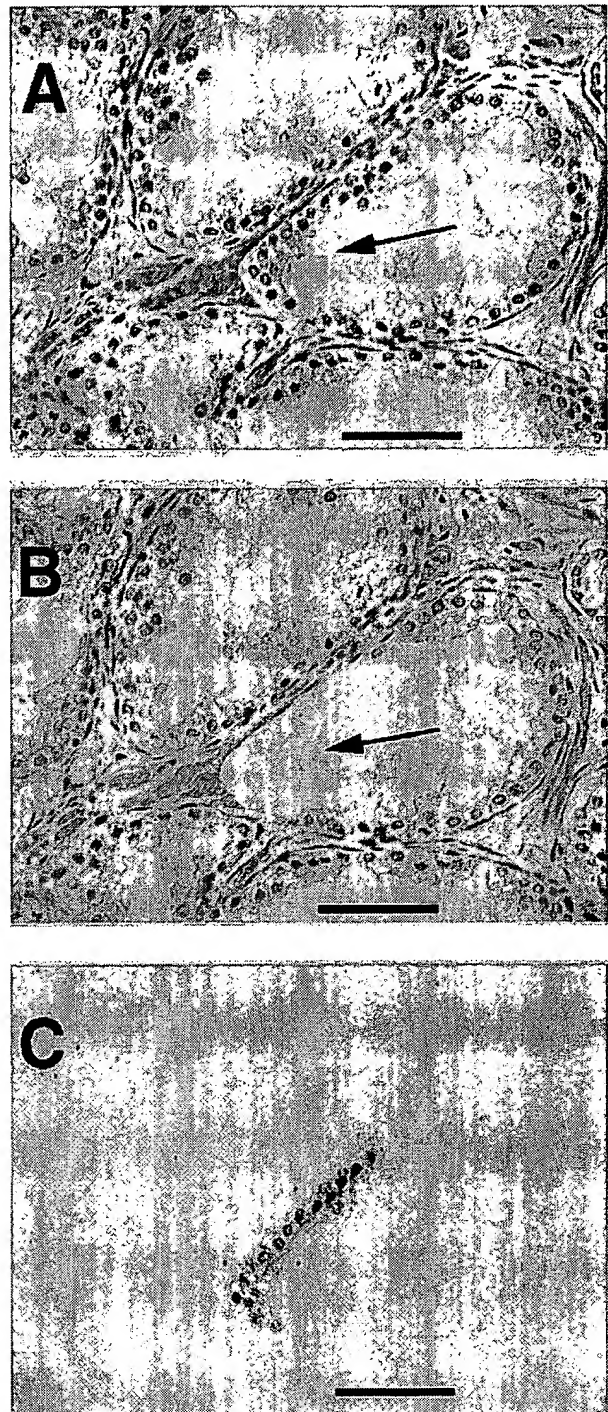
Figure 2. Visualization of LCM-procured cells. Laser capture microdissection (LCM) using the Arcturus Pixcell II was performed to selectively transfer only a portion of the epithelial lining of a prostate gland to the polymer film. H&E-stained prostate tissue: target region designated by **arrow**. **A:** Before LCM. **B:** Tissue after LCM; two shots. Note the vacancy left by the removal of selected cells. The bar represents 30 μm. **C:** Epithelial cells transferred to cap surface.

Solubilization of Proteins from LCM-Procured Cells

After placement of a 5-μl microvolume of extraction buffer on the transfer surface containing the tissue cells, visual

Table 1. Laser Capture Microdissection Tissue Cell Procurement Recovery

Prostate tissue cell type procured by LCM	No. of laser shots (30 μm diameter) procured per sample (n = no. of replicate samples per case)	Total cell no. procured per sample (mean ± SD)	Mean cell no. procured per laser shot
Case 121 carcinoma	1 shot (n = 10)	6.78 ± 3.7	6.7
Case 121 carcinoma	15 shots (n = 10)	102 ± 3.4	6.8
Case 130 epithelium	100 shots (n = 10)	506 ± 12	5.1
Case 140 epithelium	25 shots (n = 10)	128.7 ± 12.8	5.1
Case 140 epithelium	50 shots (n = 10)	284 ± 17.1	5.6
Case 140 carcinoma	50 shots (n = 10)	277 ± 17.9	5.5

Prostate tissue was stained with H&E and dehydrated in xylene. The histological diagnosis of the pure cell population microdissected is shown in the first column. The number of laser shots comprising a sample and the number of replicate samples per case are listed in the second column. Cells captured on the transfer film were visually counted under ×200 magnification (third column). The mean cell number per shot is calculated by dividing the total number of cells procured in the sample by the number of shots comprising the sample.

confirmation was obtained, establishing the complete solubilization of the stained cells. This took less than 1 minute. The transfer cap with the extracted cellular proteins was inserted into the mouth of a vial containing the immunoassay buffer. After analysis, the transfer caps were counterstained to ensure complete solubilization of the cells. The extraction buffer diluted in the assay buffer did not interfere with the immunoassay background level or linear calibration. Buffers A and B (described in Materials and Methods) were found to be highly suitable for solubilization and extraction of the PSA cytoplasmic protein from cells. Buffer C was determined to be suitable for membrane proteins. Her-2-Neu, a membrane-bound receptor, was solubilized in Buffer C from LCM-microdissected breast carcinoma cells and successfully measured using the Oncogene Science Diagnostics HER2/neu enzyme-linked immunosorbent assay (data not shown).

Calibration Curve

Negative tissues or zero controls produced a value of 80,000 to 140,000 RLUs, compared to PSA positive samples that ranged from 600,000 to 10,000,000 RLUs. The calibration curve used for measurement of PSA in serum according to the Immulite package insert was applied to the measurement of cellular tissue proteins procured by LCM. A specific calibration curve for LCM-procured samples was developed with the LCM-extracted cellular proteins in the buffer solution. As shown in Figure 3, A and B, the standard curve using spiked known concentrations of PSA showed a high degree of linearity (R^2 = 0.98) over a wide dynamic range (0.002–10 ng/ml). A strong degree of linearity was also observed between the number of laser shots independently procured in a case sample and the number of PSA molecules assayed (Figure 3C and Table 2). A parallel study was conducted on nine microdissected case samples. A representative example series is shown in Table 3. The assay was conducted in duplicate on both undiluted and diluted (10 serial) samples, and the observed and expected values were compared. For all nine case samples the linear correlation between the observed and the expected values was greater than R^2 = 0.95. Thus the LCM-Immulite PSA immunoassay maintains good linearity over the calibration range.

Sensitivity

The detection limit of the assay, defined as the concentration two standard deviations above the signal response of a tissue extraction sample free of PSA (zero dose) (Table 2), was found to be 0.002 ng/ml. The "functional sensitivity," defined as the lowest concentration measured with an interassay CV of 20%, was 0.005 ng/ml of PSA, or approximately 4.5×10^6 molecules of PSA per assay, using an extraction buffer microvolume of 5 μl. Depending on the relative concentration of PSA expressed in the tissue cells microdissected, in some cases the number of PSA molecules encompassed in an individual shot (average of five to seven cells per shot) was above the detection limit threshold.

Within-Run Precision

The LCM-Immulite assay precision is shown in Table 1 and Figure 4. In keeping with the assumed biological heterogeneity, one laser shot exhibits a PSA measurement CV of 60.2% (n = 10), even though the mean magnitude of the signal (804,416 RLUs) is substantially greater than the mean value for 100 combined shots of background tissue (132,759). Thus, capturing 15 (analytical sensitivity threshold) to 100 laser shots of a tissue sample (this takes less than 5 minutes) provides an acceptable level of precision for a routine assay. A time course study determined (in the absence of protease inhibitors) that tissue proteins retained immunoreactivity for a total microdissection time of at least 30 minutes (data not shown).
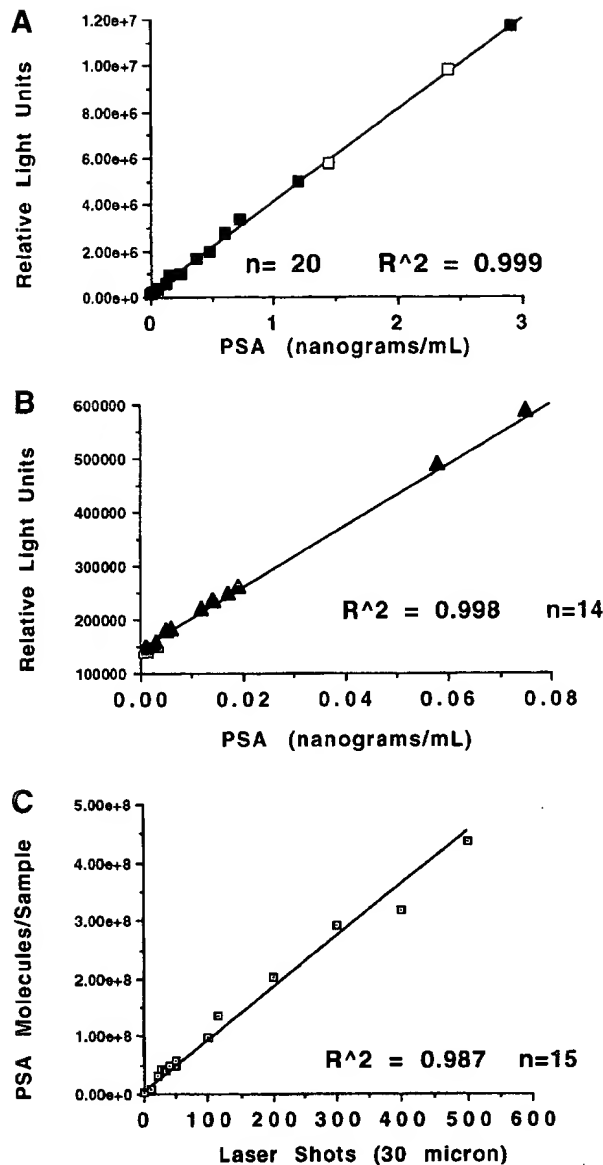
Figure 3. Standard curve and LCM shot linearity analysis. **A:** Standard curve using spiked known concentrations of PSA over the high concentration range. **B:** Standard curve using spiked known concentrations of PSA over the low concentration range. **C:** Case linearity. Individual samples of the designated number of LCM shots were independently procured from the same case. The concentration of PSA molecules assayed per sample was linearly correlated with the number of shots. n = number of individual assays.

Reproducibility

Twenty cases were randomly chosen to include 10 normal and 10 tumor cases. Based on the results of the precision studies (Tables 1 and 2), a sample of 50 shots or greater has acceptable precision but retains adequate cellular purity. Therefore, 10 replicates of 50 shots were completed for each case. The average number of PSA molecules per cell per sample and the SD of 10 within-run replicates are plotted in Figure 4. All 10 normal (epithelium) cases exhibited a PSA concentration per cell of less than 2,500,000 molecules. The SD (10 replicates of 50 shots) of every case (for both normal and cancer cases)

was approximately 10% of the mean or less. In contrast, the range of values for the cancer cases was up to sevenfold higher than the normal cases, whereas the average of all of the invasive carcinoma cases was 2,854,141 molecules. Nevertheless some tumor cases had values within or below the mean value for the normal cases. This finding validates at a molecular level, in tissue, the expected biological heterogeneity and the phenotypic instability of carcinoma cells compared to their normal counterparts.

Correlation with Tissue Immunohistochemistry

Analysis using LCM coupled with PSA immunoassays for PSA was conducted on prostate tissue sections that contained normal epithelium, carcinoma, and prostate intraepithelial neoplasia (PIN). Based on the precision analysis described above, the number of laser shots was 100. For each specimen studied, a dilution series such as that shown in Table 3, corresponding to a series of different numbers of laser shots, was prepared. This verified that conclusions based on 100 shots remained in the linear portion of the curve (Figure 3). Immunohistochemistry for PSA was conducted[6] on adjacent sections. The PSA immunoreactivity of cellular populations identical to those sampled by LCM on matched coded sections was scored independently and ranked on a scale of 0 to 3+ (Table 4). The average number of PSA molecules measured per cell ranged from 10^4 to 10^6. The immunohistochemistry scoring values paralleled the quantitation and mirrored the heterogeneity in PSA production by normal and neoplastic cell populations. Case C is an example in which the normal epithelium contained an unusually high level of PSA molecules (6.3×10^6) and was scored 3+ by immunohistochemistry. In contrast, the PIN cells contained 3.7×10^5 molecules and was scored 2+, and the tumor cells contained 1.99×10^4 and stained 1+, all in the same case (case C).

Discussion

As the field of proteomics moves from cell lines to the analysis of specific cell populations in tissue, new technology will be required to sample and measure tissue macromolecules. Modern soluble immunoassay methods employing chemiluminescence or fluorescence can achieve a level of sensitivity in the attomolar range.[8] In principle, such sensitivity is sufficient for the measurement of moderate- or even low-abundance proteins extracted from tissue cells. Nevertheless, two problems have previously hindered the application of soluble immunoassays to tissue.[9] The first is tissue microscopic cellular heterogeneity, and the second is extraction and preservation of intact proteins from stained tissue subpopulations. Simply grinding up the tissue and extracting the proteins does not produce a representative sample because the cellular population of interest may constitute a small minority of the total cells in the tissue. The tissue cells of interest are often part of complicated morphological structures that can only be correctly identified under

Table 2. Sensitivity and Within-Run Precision Study Set: Effect of Sample Size

Sample description	No. sample replicates	Mean PSA molecules per sample	CV%	Mean no. cells procured per sample (calculated mean PSA molecules/cell)
Prostate tumor 100 shots case 318	10	1.2×10^8 (7,199,673 ± 330,464)	3.9%	721 (1.7×10^5)
Prostate tumor 15 shots case 318	10	1.9×10^7 (1,178,202 ± 168,807)	15.8%	78 (2.4×10^5)
Prostate tumor single-shot case 318	10	1.2×10^7 (804,416 ± 489,353)	60.2%	5.2 (2.3×10^5)
Prostate tumor single-shot case 269	9	7.2×10^6 (602,412 ± 451,809)	74.6%	7.4 (0.97×10^5)
Buffer control	10	Negative (88,788 ± 2962)	3.5%	NA
Lung 100 shots	10	2.1×10^5 (134,413 ± 7840)	6.5%	NA
Prostate stroma 100 shots	6	2.0×10^5 (132,759 ± 7352)	5.2%	NA

The number of 30-μm laser shots comprising the sample and the histologic diagnosis are given in the first column. The number of sample replicates per case is given in the second column. The total sample of microdissected cells was dispersed in 5 μl of extraction buffer, which was then diluted in 45 μl of assay buffer. The number of molecules of PSA per sample (third column) reflects the number of PSA antigen molecules present in the original 5-μl volume. The immunoassay relative light unit (RLU) assay value, which is proportional to the concentration of PSA according to the standard curve of Figure 3, is shown in parentheses. This concentration of PSA is then converted to the number of molecules in the original sample. The number of cells microdissected, comprising the sample, is calculated by multiplying the average number of cells procured per shot (Table 1) by the number of shots. The number of molecules per cell (fourth column) is calculated by dividing the total PSA molecules in the sample by the number of cells comprising the sample.

high-power magnification. Moreover, the cells targeted for analysis can be surrounded by contaminating cells and scattered in multiple locations within a minute microscopic tissue field. Sectioning, fixing, and staining the tissue may modify the function and antigenicity of macromolecules. Finally, methods for extracting the proteins from the tissue section should maximize the yield of proteins while having no effect on the immunochemistry analysis.

Previous methods for extracting and analyzing protein macromolecules from tissue subpopulations have included UV laser ablation of unwanted tissue regions[10] and oil well isolation of tissue cells.[8] These methods were complicated and labor intensive, did not use protein stabilizers, and did not employ soluble immunoassays. The

advent of LCM now provides a means of positively selecting the desired tissue cells, even if they are scattered or in a spatially complicated distribution. Moreover, the protein macromolecules of LCM-procured cells appear to be intact and retain their functional activity.[3] An important principle of the current methodology is exposure of the microdissected cells captured on the transfer surface to a microvolume of extraction buffer. The extracted molecules are directly diluted in the immunoassay buffer. In this way the microdissected cells are exposed to adequate local concentrations of detergents and other extraction chemistries that may interfere with antibody binding reactions. After dilution in the assay buffer, the extraction chemistry has no discernible residual effect on the immunoassay performance. The procurement and

Table 3. Example Parallelism Study

Sample dilution 500 shots solubilized in 5 μl	Observed PSA (ng/ml)	Expected	Ratio: observed/ expected
1024 in 1024 case 611	1.71	—	—
512 in 1024	0.848	0.855	0.99
256 in 1024	0.429	0.427	1.004
128 in 1024	0.188	0.213	0.882
64 in 1024	0.099	0.10	0.96
32 in 1024	0.048	0.05	0.96
16 in 1024	0.023	0.025	0.92
8 in 1024	0.0096	0.012	0.80
4 in 1024	0.0056	0.006	0.93
2 in 1024	0.0023	0.003	0.76
1 in 1024	<0.002	0.001	—

One of nine cases is shown to illustrate a dilution series. Five hundred shots of LCM prostate carcinoma were solubilized in 5 μl of extraction buffer. The total volume of extraction buffer was diluted in 45 μl of assay buffer. The concentration of PSA (ng/ml) (observed mean of duplicates) in the 50 μl of assay volume was then calculated using the standard curve shown in Figure 3, A and B.
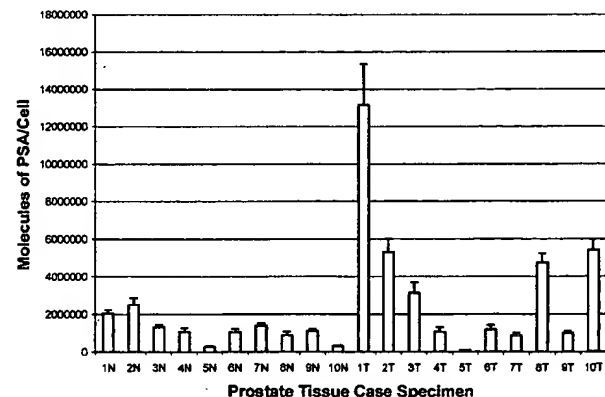
Figure 4. Case study set. N = normal prostate epithelium, T = prostate carcinoma. Ten individual within-run replicate immunoassays were performed per case for 20 separate cases. Ten replicate samples of 50 shots were individually procured from each case. The microdissected cells were solubilized in 5 μm and then diluted up to 50 μm in assay buffer. The results are expressed in mean ± SD of the number of PSA molecules per LCM microdissected cell.

Table 4. Immunohistochemistry Comparison

Case designation: prostate histological diagnosis	Molecules of PSA/cell mean per 100 shots immunoassay results	PSA immunohistochemistry pathologist's score
Case A: normal	6.66×10^4	+
Case A: tumor Gleason 4a	3.4×10^6	+ + +
Case B: normal	1.04×10^5	+ +
Case B: PIN	4.25×10^5	+ +
Case B: tumor Gleason 3a	9.52×10^4	+
Case C: normal	6.3×10^6	+ + +
Case C: PIN	3.70×10^5	+ +
Case C: tumor Gleason 2	1.99×10^4	+

Immunohistochemistry staining of human prostate tissue sections for PSA was compared with the results of the soluble immunoassay (Tables 1–3 and Figures 3 and 4) for the same prostate tissue section. Independent immunohistochemical scoring of coded specimens by the pathologist was graded as high (+ + +), medium (+ +), or low (+). PIN, Prostate intraepithelial neoplasia. Tumor, Carcinoma Gleason grade designated. Normal, Histologically normal epithelium from glands distant from the tumor in the same section. The relative concentration of measured PSA molecules per cell in a sample of 100 laser shots corresponds to the semiquantitative scoring.

extraction procedure used in the present report did not alter the tissue cellular proteins in relative abundance, molecular weight, or charge, as judged by 2-D gel electrophoresis of proteins extracted from frozen sections compared before and after LCM procurement and staining of 7500 shots (data not shown). 2-D gel analysis of microdissected prostate tissue cells revealed PSA to be of low to moderate abundance compared to other cellular proteins. The current study was performed using frozen tissue stained with H&E. Fixed tissue embedded in paraffin is superior to frozen sections at the level of microscopic histomorphological details. Formalin fixation may produce cross-links that hamper protein extraction. In contrast, we have found that ethanol-fixed,[7] paraffin-embedded tissue retains morphological details and preserves PSA immunoreactivity after microvolume extraction.

The present technology provides one of the first direct estimates of the actual number of protein molecules per tissue cell *in vivo*, for a single specific known protein of moderate to low abundance. The number of total PSA molecules in normal prostate epithelium ranged from 10^4 to 10^6 per cell. PSA is an important serum analyte used to clinically monitor prostate cancer, but it is not a specific marker of prostate cancer.[11] Previous investigators have reported great heterogeneity in the intensity of PSA immunohistochemical staining among various neoplastic and nonneoplastic populations in the prostate.[2,12–16] Populations of microdissected cells of a pure histological class (normal epithelium, PIN, or invasive cancer) would be expected to contain some level of heterogeneity in PSA expression among the population members. Sources of imprecision and assay variability should therefore include the following components: 1) precision in the number of cells captured per sample, 2) normal biological variation in the production of PSA by different cells from the same tissue and the position of the cells in the plane of the tissue section,[2,12–16] and 3) imprecision in the immunoassay itself. Comparing the precision of cell capture (Table 1) with the variability of PSA quantity measured (Table 2), the percentage coefficient of variation (CV n = 10) declines with increasing number of laser shots per sample. Acceptable precision can be obtained with a sample of 50–100 laser shots. This number of shots takes less than 5 minutes of operator time.

PSA immunolocalization in carcinoma cells is known to be increased or decreased in intensity compared with normal epithelium in the same prostate. Tissue cells positive for cytoplasmic PSA immunoreactivity contain antigen-positive material in the endoplasmic reticulum and secretory vesicles by immunoelectron microscopy and express PSA mRNA by *in situ* hybridization. Application of the new technology described in the present report (Table 4) provides quantitative confirmation of the heterogeneity in PSA expression that was previously detected only by qualitative staining. The average numbers of PSA molecules harvested per cell ranged over several logs. An immunohistochemical staining difference could be discriminated within a five- to 10-fold difference in PSA molecule number per cell. The level of variability in PSA molecules per case is further validated by the replicates of normal and invasive carcinoma cases shown in Figure 4. Here the normal cases were relatively homogeneous in the level of PSA expression, whereas the tumor cases varied considerably.

In conclusion, the combination of LCM with high sensitivity chemiluminescence immunoassay chemistry provides a protein quantitation technology that can be applied to the measurement of proteins in microscopic pure populations of stained tissue cells. The speed, sensitivity, and linearity of the assay are acceptable for routine use, even considering the expected biological heterogeneity of histologically similar cell types. LCM immunoassays can thereby supplement or complement immunohistochemistry. Several extraction buffers were found to be suitable for cytoplasmic or membrane proteins (Materials and Methods). In addition to PSA, described here, the technology has been successfully been applied to the measurement of HER-2/neu assays (data not shown). Moreover, solubilized proteins can be analyzed by nonimmunological means (eg, enzymatic activity). With the application of microfluidics, and the multiplexing of assays, it is foreseeable that entire panels of quantitative protein assays can be performed on microscopic regions of pure tissue cells. This will provide the closest possible snapshot of the *in vivo* state of the protein pathways in developing, diseased, or genetically altered tissue.

References

1. Humphrey-Smith I, Cordwell SJ, Blackstock WP: Tissue-specific variation of pea mitochondrial polypeptides detected by computerized image analysis of two-dimensional electrophoresis gels. Electrophoresis 1997, 18:1217–1242

2. Epstein JI, Eggleston JC: Immunohistochemical localization of prostate-specific acid phosphatase and prostate-specific antigen in stage A2 adenocarcinoma of the prostate: prognostic implications. Hum Pathol 1984, 15:853–859

3. Emmert-Buck MR, Bonner RF, Smith PD, Chuaqui RF, Zhuang Z, Goldstein SR, Weiss RA, Liotta LA: Laser capture microdissection. Science 1996, 274:998–1001

4. Bonner RF, Emmert-Buck, MR, Cole KA, Pohida T, Chuaqui R, Goldstein S, Liotta LA: Laser capture microdissection: molecular analysis of tissue. Science 1997, 278:1481–1483

5. Simone NL, Bonner RF, Gillespie JW, Emmert-Buck MR, Liotta LA: Laser-capture microdissection: opeing the microscopic frontier to molecular analysis. Trends Genet 1998, 14:272–276

6. Ferguson RA, Yu H., Kalyvas M., Zammit S, Diamandis EP: Ultrasensitive detection of prostate-specific antigen by a time-resolved immunofluorometric assay and the immulite immunochemiluminescent third-generation assay: potential applications in prostate and breast cancers. Clin Chem 1996, 42:675–684

7. Fend F, Emmert-Buck MR, Chuaqui R, Cole KA, Lee J, Liotta LA, Raffeld M: Immuno-LCM: laser capture microdissection of immunostained frozen sections for mRNA analysis. Am J Pathol 1999, 154: 61–66

8. Yu H, Diamandis EP: Ultrasensitive time-resolved immunofluorometric assay of prostate-specific antigen in serum and preliminary clinical studies. Clin Chem 1993, 39:2108–2114

9. Matschinsky FM, Passonneau JV, Lowry OH: Quantitative histochemical analysis of glycolytic intermediates and cofactors with an oil well technique. J Histochem Cytochem 1967, 16:29–39

10. Meier-Ruge W, Bielser W, Remy E, Hillenkamp F, Nitsche R, Unsold R: The laser in the Lowry technique for microdissection of freeze-dried tissue slices. Histochem J 1976, 8:387–401

11. Zarghami N, Levesque M., DiCosta M, Angelopoulou K, Diamandis EP: Frequency of expression of prostate-specific antigen mRNA in lung tumors. Am J Clin Pathol 1997, 108:184–190

12. Stamey TA, Graves HCB, Wehner N, Ferrari M, Freiha FS: Early detection of residual prostate cancer after radical prostatectomy by an ultrasensitive assay for prostate specific antigen. J Urol 1993, 149:787–792

13. Sinha AA, Wilson MJ, Gleason DF: Immunoelectron microscopic localization of prostatic-specific antigen in human prostate by the protein A-gold complex. Cancer 1987, 60:1288–1293

14. Qiu S, Young CYF, Bilhartz DL, Prescott JL, Farrow GM, He WW, Tindall DJ: In situ hybridization of prostate-specific antigen mRNA in human prostate. J Urol 1990, 144:1550–1555

15. Purnell DM, Heatfield BM, Trump BF: Immunocytochemical evaluation of human prostatic carcinomas for carcinoembryonic antigen, nonspecific cross-reacting antigen, β-chorionic gonadotrophin, and prostate-specific antigen. Cancer Res 1984, 44:285–292

16. Kuriyama M, Wang MC, Papsidero L, Killian CS, Shimano T, Valenzuela L, Nishiura T, Murphy GP, Chu TM: Quantitation of prostate-specific antigen in serum by a sensitive enzyme immunoassay. Cancer Res 1980, 40:4568–4662

attractive tool for clinical diagnostics, drug discovery, and treatment development and monitoring.

References

1. Wojciechowski M, Naser N, Zhang H, O'Daly JP, Henkens RW. Electroanalytical applications of disposable, colloidal gold based microarray sensors [Abstract]. 212th American Chemical Society National Meeting, August 25–29, 1996, Orlando, FL.

2. Castillo SA, Henkens RW, Kazantseva V, Naser N, O'Daly JP, Stewart TN, et al. Electrochemical assays for nucleic acid detection of disease causing agents [Abstract]. Fifth Annual Conference on Advances in Nucleic Acid Amplification and Detection, June 16–17, 1997, San Francisco, CA.

3. Zhang H, Thompson D, Sundseth R, Naser N, O'Daly JP, Wegner S, et al. Disposable sensor-based pulse amperometric detection of pathogens and DNA mutations [Abstract]. Gordon Research Conference on Electrochemistry, January 18–23, 1997, Ventura, CA.

4. Sundseth R, Thompson DM, Taylor G, Kazantseva V, Kazantsev A, Zhang H, et al. Electrochemical detection and quantitation of DNA and RNA [Abstract]. Cambridge Healthtech Institute DNA and RNA Diagnostics Meeting, May 19–21, 1998, Washington, DC.

5. Wojciechowski M, Ebeling F, Naser N, Sundseth R, Thompson DM, Henkens R. Intermittent pulse amperometry—a faster and more sensitive method for detection and quantitation of nucleic acids [Abstract]. 50th SRMACS Meeting of the American Chemical Society, November 4–7, 1998, Research Triangle Park, NC.

6. Sundseth R, Kazantseva V, Herfst C, Taylor C, Wojciechowski MA, Bonaventura C, et al. Rapid quantitation of RNA using amplified electrochemical detection [Abstract]. Cambridge Healthtech Institute's Gene Quantification Conference, February 8–10, 1999, San Diego, CA.

7. Henkens R, Bonaventura C, Kazantseva V, Moreno M, O'Daly J, Sundseth R, et al. Use of DNA technologies in diagnostics. In: Proceedings of the International Conference on Emerging Technologies. St. Paul, MN: American Phytopathological Society, 1999:in press.

8. AndCare-Electrochemical Sensing Technologies Homepage. http://www.andcare.com.

Simultaneous Quantification of Six Human Cytokines in a Single Sample Using Microparticle-based Flow Cytometric Technology

Roy Chen,[1]* Larry Lowe,[1] Jerry D. Wilson,[2] Eric Crowther, Kifle Tzeggai,[1] Jim E. Bishop,[1] and Rudi Varro[1] ([1] Becton Dickinson Immunocytometry Systems, 2350 Qume Dr., San Jose, CA 95131-1807, and [2] Pharmingen, San Diego, CA 92121; * author for correspondence: fax 408-954-2156, e-mail roy_chen@bdis.com)

The study of cytokines has been of great interest to researchers in many scientific disciplines, including cell biology and immunology. Cytokines form a sophisticated network that serves to modulate a myriad of cellular events. Within such a network, and through complex feedback mechanisms, cytokine functions are mostly interdependent. Because of the extreme complexity of the cytokine network, a simultaneous measurement of multiple cytokines in a single sample represents a desirable and effective approach.

Several methods are available to measure cytokines and their messenger RNAs. To measure cytokines secreted from cells, researchers commonly use conventional ELISA techniques. ELISA methods are generally cost-effective but restricted to measuring one cytokine at a time. Consequently, the ELISA approach requires not only multiple sample aliquots but also repetitive execution of the procedures for each cytokine of interest. The ability of flow cytometry to simultaneously acquire data for numerous particles and subsequently analyze multiple characteristics for each particle makes it a powerful technique for cell sorting and cell analyses. The application is fundamentally built on the high sensitivity of a flow cytometer to discern characteristics either within or on the surface of a cell. Several investigators have constructed microparticle-based immunoassays that use a flow cytometer to simultaneously measuring multiple analytes *(1–5)*.

This report describes the development of a uniform size microparticle-based flow cytometric method for a panel of six human cytokines—interleukin (IL)-2, IL-4, interferon-γ, tumor necrosis factor-α, IL-10, and IL-12—simultaneously measured in a single sample. The sample types included cell culture supernatant and human serum. The assays are two-site "sandwich" immunoassays configured with six pairs of antibodies, two fluorescent dyes, and particles of a uniform size. Particles (7.5 μm) are dyed to six different fluorescent intensities. The dye has an emission wavelength of ~650 nm (FL3). Each particle population of a given intensity represents a discrete population for constructing an immunoassay for a single cytokine. Each particle is covalently coupled with an antibody (Ab) against one of the six cytokines. These Ab-particles, which are unique in their FL3 intensity, serve as a capture for a given cytokine in the immunoassay panel. When these Ab-particles are used as a mixture, one can simultaneously detect six separate cytokines. We configured the assay for each cytokine in each of the two formats below.

Indirect format. The biotin-conjugated "detector" Ab is used to complete the particle-Ab-cytokine-Ab sandwich. Fluorescent dye-conjugated streptavidin is used to report the amount of bound secondary Ab. The fluorescent dye emits at ~530 nm (FL1). The fluorescence intensity measured at FL1 is proportional to the concentration of the cytokines and is quantified from a calibration curve. Direct format. The fluorescent dye is phycoerythrin (PE) which emits at ~585 nm (FL2). A PE-conjugated detector Ab is used to complete the sandwich, and the fluorescence intensity measured at FL2 is proportional to the concentration of the cytokine in the sample, which is quantified from a calibration curve. An important feature of the assay system is that the calibrators, Ab-bead reagent and the second Ab reagent are each made as mixtures for all six cytokines. Therefore, o six calibration curves can be obtained from one set of calibrators and six results can be obtained on one test sample.

We used six pairs of antibody to construct the sandwich assay for the six cytokines. The antibody used for capture and the second Ab labeled with biotin (used in the indirect

Table 1. Preliminary evaluation of the microparticle-based flow cytometric immunoassay for six human cytokines.

Analyte	Dynamic range, ng/L	Detection limit,[a] ng/L	Intraassay CV[b]% 625 ng/L	1250 ng/L	Method comparison vs ELISA[c] Correlation coefficient	n
IL-2	0–2500	2	7.7	9.1	0.92	11
IL-4	0–2500	4	6.3	6.1	0.97	11
IFN-γ[d]	0–2500	17	5.7	4.5	0.94	20
TNF-α	0–2500	10	5.5	6.7	0.97	20
IL-10	0–2500	8	6.7	6.9	1.0	20
IL-12	0–2500	14	7.8	6.4	0.98	10

[a] Detection limit is defined as a signal 2 SD above the mean of the zero calibrator.

[b] Intraassay CVs were determined by testing six samples of each of two calibrators (containing all six cytokines) at 625 and 1250 ng/L, respectively.

[c] Cell culture supernatants were used for comparison with the ELISA method as described in the text.

[d] IFN, interferon; TNF, tumor necrosis factor.

assay) or PE (used in the direct assay) are available from PharMingen in San Diego, CA. Polystyrene beads (7.5 μm) functionalized with amino groups (Bang's Laboratories) were dyed with a fluorescent dye to six discrete intensities. The maximal emission wavelength of the dye is ~650 nm (FL3). The bead population with each intensity was used to prepare a given antibody-bead for each of the six cytokines of interest. The Ab-beads were prepared via a covalent linkage based on thiol-maleimide chemistry. Covalent chemistry afforded advantages such as higher assay sensitivity and better storage stability. A FACScan flow cytometer (Becton Dickinson Immunocytometry Systems) was used to generate the data presented here. ELISA assays and reagents kits for the six cytokines of interest (PharMingen) were used as recommended for the method-comparison study.

The Indirect assay used three incubations. Ab-bead reagent (50 μL) was added to 50 μL of sample or calibrator and incubated for 30 min, followed by addition of 50 μL of Ab-biotin reagent and a further incubation for 15 min. The final incubation step involved the addition of 50 μL of streptavidin-Alexa (FL1) and a third incubation for 75 min before data acquisition was performed by a flow cytometer.

The Direct assay included one incubation. A 100-μL mixture of 50 μL each of Ab-bead reagent and Ab-PE reagent for the cytokines was added to 50 μL of sample or calibrator. The 150-μL mixture was subsequently incubated for 120 min before data acquisition with the flow cytometer.

Peripheral blood mononuclear cell samples from individual donors were cultured in RPMI 1640 either with or without lipopolysaccharide stimulation. Aliquots of the individual samples were tested with both the flow cyto-

metric and ELISA methods. In the flow cytometric method, one 50-μL sample was sufficient to provide six results vs 600 μL for ELISA. The bead reagent contained a mixture of Ab-beads for six cytokines. The Ab-PE or Ab biotin reagent contained a mixture of the second Ab components for six cytokines. Each calibrator contained a mixture of equal weights of the six recombinant cytokines; the concentrations of the cytokines in the calibrators were 0, 20, 80, 625, and 2500 ng/L, respectively.

The preliminary performance evaluation of the assays configured in the Indirect format is summarized in Table 1. Similar results were obtained from the Direct assays.

In summary, this microparticle-based flow cytometric method is an efficient method for simultaneously measuring multiple cytokines from a variety of test samples. It has comparable analytical sensitivity and a wider dynamic range than conventional ELISA.

References

1. McHugh TM. Flow microsphere immunoassays for the quantitative and simultaneous detection of multiple soluble analytes. In: Darzynkiewicz Z, Robinson JP, Crissman HA, eds. Methods cell biology, 2nd ed. Vol. 42, Part B. New York: Academic Press, 1994:575–95.

2. Fulton RJ, McDade RL, Smith PL, Kienker LJ, Kettman JR Jr. Advanced multiplexed analysis with the FlowMetrix™ system. Clin Chem 1997;43:1749–56.

3. Camilla C, Defoort JP, Delaage M, Auer R, Quintana T, Lary R, et al. A new flow cytometry based multi-assay system. 1. Application to cytokine immunoassays. Cytometry, 1998;(Suppl 9):132.

4. Collins DP. T lymphocyte functionality assay based on simultaneous femtomolar detection of GM-CSF secretion and cellular immunophenotyping by flow cytometry. Cytometry 1998;(Suppl 9):71.

5. Oliver KG, Kettman JR, Fulton RJ. Multiplexed analysis of human cytokines by use of the FlowMetrix System. Clin Chem 1998;44:2057–60.

Discrimination of different subsets of cytolytic cells in pseudorabies virus-immune and naive pigs

Tiny G. M. de Bruin, Eugene M. A. van Rooij, Yolanda E. de Visser, John J. M. Voermans, Janneke N. Samsom, Tjeerd G. Kimman and Andre T. J. Bianchi

Department of Mammalian Virology, Institute for Animal Science and Health (ID-Lelystad), Postbus 65, 8200 AB Lelystad, The Netherlands

We previously observed that pseudorabies virus (PRV)-induced, cell-mediated cytolysis in pigs includes killing by natural killer (NK) cells. We also observed that IL-2 stimulation *in vitro* of naive PBMC expands porcine NK cells. The purpose of this study was to compare the phenotypes of the cytolytic subsets stimulated *in vitro* by PRV and by IL-2. PBMC were isolated from blood of PRV-immune and naive pigs and stimulated *in vitro* with PRV or IL-2. After 6 days, the frequency of various lymphocyte subsets in these cultured PBMC was determined by flow cytometry: the cells were separated with a magnet-activated cell sorter and the cytolytic activity of the separated populations was determined. When lymphocytes were separated and analysed with FACScan, the following lymphocyte subsets were discriminated: $CD6^+$ $CD8^{bright+}$ $CD4^-$ (CTL phenotype), $CD6^+$ $CD8^{dull+}$ $CD4^+$ (the fraction containing memory T helper cells), $CD6^+$ $CD8^-$ $CD4^+$ (T helper cell phenotype), $CD6^-$ $CD8^{dull+}$ $CD4^-$ $\gamma\delta$-T^+ ($\gamma\delta$-T cell phenotype), $CD6^-$ $CD8^{dull+}$ $CD4^-$ $\gamma\delta$-T^- (NK phenotype) and $CD6^-$ $CD8^-$ $CD4^-$ $\gamma\delta$-T^- or $\gamma\delta$-T^+. Flow cytometry analysis demonstrated that PRV stimulation of immune PBMC resulted in the occurrence of more $CD6^+$ $CD8^+$ and $CD4^+$ $CD8^+$ and fewer $CD6^-$ $CD8^+$ and $\gamma\delta$-T^+ $CD8^+$ lymphocytes than IL-2 stimulation of naive PBMC ($P < 0.05$). It was demonstrated further that killing by PRV-stimulated PBMC was mediated mainly by $CD6^+$ $CD8^+$ T lymphocytes. Killing by IL-2-stimulated PBMC was mediated mainly by $CD6^-$ $CD8^+$ T lymphocytes. These results demonstrate that both natural killing and killing by classical PRV-specific CTL were detected in PRV-immune pigs, whereas IL-2 stimulation of PBMC isolated from naive pigs mainly induced natural killing.

Introduction

Pseudorabies virus (PRV) is an alphaherpesvirus that causes Aujeszky's disease in pigs. Both humoral and cellular immunity appear to be involved in the development of protective immunity to herpesviruses, which has been studied in detail for herpes simplex virus type 1 infection in humans. Previous reports have described the cellular lymphoproliferative immune response against PRV in pigs (Chinsakchai & Molitor, 1992; Kimman *et al.*, 1995*b*). Both $CD4^+$ and $CD8^+$ T lymphocytes proliferated (Kimman *et al.*, 1995*b*) after they were stimulated *in vitro* with PRV. Zuckermann & Husmann (1996) demonstrated the involvement of $CD4^+$ $CD8^+$ lymphocytes in proliferation, and this subset harbours putative memory cells. Zuckermann and co-workers also demon-

strated that $CD8^+$ T lymphocytes killed PRV-infected cells (Zuckermann *et al.*, 1990). Saalmüller *et al.* (1994*a*) demonstrated that the subset of $CD5^+$ $CD8^+$ lymphocytes might harbour classical CTL in pigs. Pauly *et al.* (1995, 1996) demonstrated in the case of classical swine fever virus infection that $CD6^+$ $CD8^+$ lymphocytes killed virus-infected target cells in an MHC-I-restricted way, whereas the natural killer (NK) cells were $CD6^-$ $CD8^+$.

Previously, we demonstrated killing of PRV-infected target cells by $CD2^+$ $CD4^-$ and $CD8^-$ or $CD8^{dull+}$ T lymphocytes (Kimman *et al.*, 1996). Their ability to kill target cells appeared to be at least partially MHC-I-unrestricted. NK cells or lymphokine-activated killer (LAK) cells therefore appeared to be involved. However, the presence of MHC-I-restricted killing was not excluded. These results could be explained by assuming that PRV-stimulated T helper lymphocytes secrete IL-2 *in vitro* that may increase natural killing. Apparently, different cytolytic subsets are involved in the killing of PRV-

Author for correspondence: Tiny de Bruin.

Fax +31 320 238668. e-mail m.g.m.debruin@jo.wag-ur.nl

infected target cells, but it is not clear which subset predominates under various circumstances.

The purpose of this study was, therefore, to investigate the significance of various cytolytic lymphocyte subsets in peripheral blood. We therefore stimulated PBMC from naive and immune pigs *in vitro* with PRV or IL-2 and separated the different subsets 6 days later by using anti- (α-)wCD6 monoclonal antibodies (MAbs). The phenotype and cytolytic function of these subsets were subsequently investigated.

Methods

■ **Virus.** Virus stocks for inoculation and challenge of pigs were prepared on SK6 cells (Kasza *et al.*, 1971) and secondary porcine kidney cells, respectively, as described by Kimman *et al.* (1995 b). Pigs were inoculated with a gE⁻ PRV strain (M141 or 783) (Gielkens *et al.*, 1989; De Wind *et al.*, 1990). The pigs were then challenged with the wild-type PRV

strain NIA-3 (McFerran & Dow, 1975). This strain was also used to infect target cells, as described by Kimman *et al.* (1995 a).

■ **Animals and experimental design.** Minnesota miniature pigs, which were inbred for swine leukocyte antigen complex (SLA) (haplotype d/d) (Sachs *et al.*, 1976), were kept under specific-pathogen-free conditions in the breeding unit of our institute. The pigs were born from unvaccinated sows and had no antibodies against PRV. Pigs were inoculated intramuscularly with 10^5 p.f.u./ml 783 or M141 at 7 months of age and were subsequently challenged three times intranasally with 10^5 p.f.u./ml NIA-3 virus, first after 3 months and then at intervals of 6 months. Flow cytometry analyses was done randomly after one (singly inoculated pigs) or several (frequently inoculated pigs) challenge inoculations. Cytolytic experiments with immune PBMC were done randomly after several challenge inoculations (frequently inoculated pigs). Uninoculated pigs, aged 7 months at the start of the experiments, were used in parallel with the immune pigs as negative controls during the experimental period. Each experiment was repeated at least five times with blood taken from two pigs per group. The different groups contained four or five pigs (Table 1). The ethics committee for animal experiments of ID-Lelystad approved the experiments.

■ **Isolation and culture of PBMC.** PBMC were obtained from PRV-inoculated and naive pigs. Blood was collected from the superior vena cava in vacuum tubes containing heparin (Venoject, Terumo Europe). Blood samples were diluted at a ratio of 1:2 in PBS, pH 7·4, layered on an equal volume (5 ml) of Lymphoprep (Nycomed Pharma) and centrifuged for 20 min at 800 g at 20 °C. PBMC at the interface were collected and washed twice in PBS. Viable cells were counted by trypan blue exclusion. These PBMC were stimulated *in vitro* with NIA-3 virus or IL-2 and used in a cytolytic assay or used for flow cytometry analysis. Note that PBMC from naive pigs were not examined with PRV

Table 1. Experimental design

The number of pigs in each group is shown. ND, Not done.

Immune status	Stimulation	
	PRV	IL-2
PRV-immune	5	4
Naive	ND	5
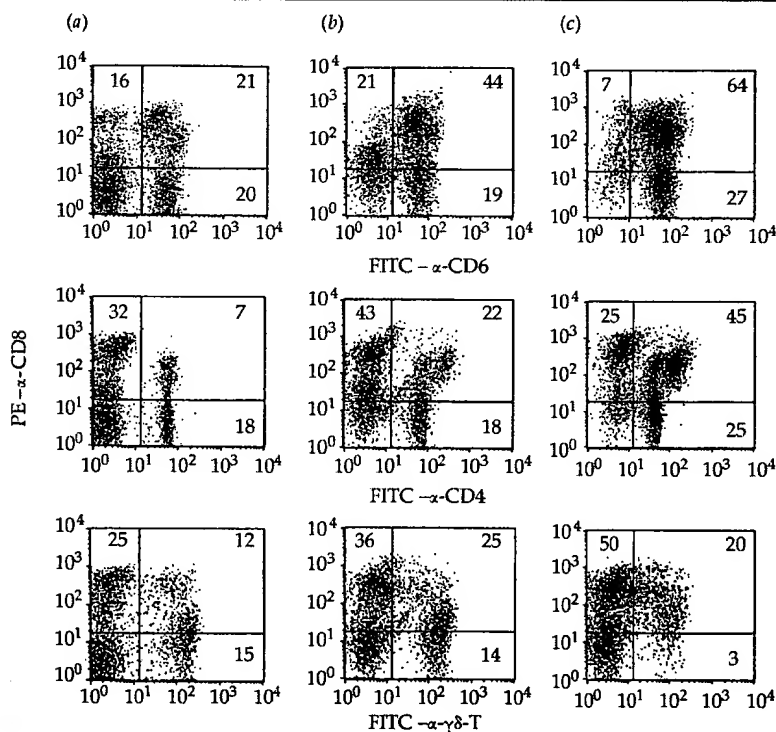
Fig. 1. Flow cytometry analysis of freshly isolated PBMC from frequently inoculated pigs (a) and PRV-stimulated PBMC isolated from singly inoculated (b) and frequently inoculated (c) pigs. Cells were double-stained with MAbs directed against porcine CD4/CD8, CD6/CD8 and γδ-T/CD8 as shown. Plots of a representative experiment are shown.
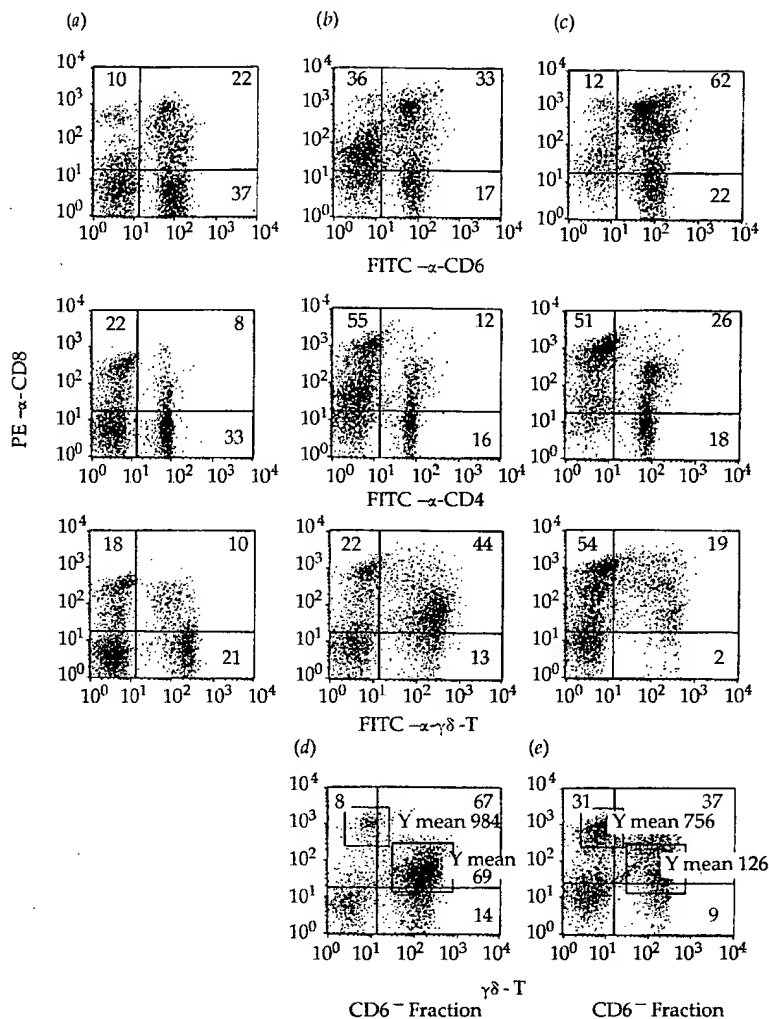
Fig. 2. (a)–(c) Flow cytometry analysis of freshly isolated PBMC from a naive pig (a) and IL-2-stimulated PBMC isolated from naive (b) and immune (frequently inoculated) (c) pigs. Cells were double-stained with MAbs directed against porcine CD4/CD8, CD6/CD8 and γδ-T/CD8. (d)–(e) Flow cytometry analysis of the CD6⁻ fraction of IL-2-stimulated PBMC isolated from naive pigs (d) and the same fraction from immune pigs (e). Cells were double-stained with MAbs directed against γδ-T/CD8. Plots of a representative experiment are shown.

stimulation because previous studies showed that PBMC of naive pigs, cultured with PRV, did not show any stimulation (Table 1).

To stimulate the cells in vitro, they were adjusted to a final concentration of 5×10^6 viable cells, with 5×10^6 p.f.u. NIA-3 virus, per ml in RPMI 1640 Dutch modification medium (ICN Biomedicals) or with 500 IU/ml recombinant human IL-2 produced in Escherichia coli (Proleukin, Eurocetus). The medium contained 10% foetal calf serum (FCS), 200 U/ml penicillin, 0·2 mg/ml streptomycin, 100 U/ml mycostatin, 0·3 mg/ml L-glutamine and 5×10^{-5} M 2-mercaptoethanol (RPMI complete medium). These cells were incubated in 6-well plates (Greiner) for 6 days and killing was determined at various intervals after inoculation.

For flow cytometry analysis, stimulated cells were adjusted to a final concentration of 1×10^6 viable cells per ml in PBS with 0·5% FCS and 0·01% NaN₃.

■ Two-colour flow cytometry analysis. PBMC were analysed on a FACScan flow cytometer (Becton Dickinson). Unfixed lymphocyte suspensions were first incubated with a mixture of two MAbs directed against the molecules of interest and then incubated with a mixture of

fluorescein isothiocyanate (FITC)-conjugated goat anti-mouse IgG2b or IgG1 (dependent on monoclonal isotype) and phycoerythrin (PE)-conjugated goat anti-mouse IgG2a (ITK Diagnostics). PBMC were incubated on ice for 30 min with saturating amounts of MAb. After each incubation, cells were washed three times in PBS containing 0·5% FCS and 0·01% NaN₃. A total of 5000 cells was examined.

PBMC were stained for the combinations γδ-T/CD8, CD4/CD8 and CD6/CD8 and the frequency of various lymphocyte subsets was determined. The following MAbs were used to characterize the lymphocytes: MAb 74.12.4, directed against porcine CD4 (IgG2b) (Pescovitz et al., 1984); MAb SL2 (11/295/33), directed against porcine CD8 (IgG2a) (Jonjic & Koszinowski, 1984); MAb a38b2, directed against porcine wCD6 (IgG1) (Saalmüller et al., 1994b); and MAb PPT16, directed against a component of the porcine γδ-T-cell receptor (TCR) (IgG2b) (Kirkham et al., 1996; Yang & Parkhouse, 1996). Cells staining positive for γδ-TCR are referred to in this article as γδ-T⁺ T lymphocytes. The separated populations were also stained with the combinations mentioned above. We could not investigate the populations after the PBMC were separated for CD8. Staining with conjugated anti-mouse

antibodies directed against IgG2a + b cross-reacted with the bead-labelled MAbs on the CD8$^+$-enriched populations. Note that the whole lymphocyte population was analysed, because after 6 days culture only a small number of lymphoblastoid cells were left (especially after IL-2 stimulation) and most lymphoblastoid cells had already matured into lymphocytes.

To illustrate how we analysed the flow cytometry results, flow cytometry plots of a representative experiment are depicted in Figs 1 and 2. We analysed the percentages of the different lymphocyte subsets by quadrant analysis (Figs 1 and 2). Student's t-test was used for statistical analysis of the results.

■ **Immunomagnetic cell sorting.** Purified CD8$^+$ and CD8$^-$ or CD6$^+$ and CD6$^-$ effector lymphocyte populations were obtained by immunomagnetic cell sorting after 6 days of *in vitro* stimulation. PBMC were labelled with MAb 11/295/33 (α-CD8, isotype IgG2a) or MAb a38b2 (α-wCD6, isotype IgG1). The PBMC were then incubated with magnetic microparticle-labelled goat anti-mouse IgG2a + b or IgG1 (dependent of the isotype of the MAb) (CLB) and subsequently incubated with FITC-conjugated F(ab')$_2$ fragment of rabbit anti-mouse immunoglobulins (Dako). PBMC were incubated on ice for 30 min with saturating amounts of antibody. After each incubation, cells were washed three times in PBS containing 0·5% BSA, 0·2 mM EDTA and 0·01% NaN$_3$. The PBMC were sorted with a magnet-activated cell sorter (MACS, Miltenyi Biotec) as recommended by the manufacturer (CLB), which resulted in the isolation of highly purified antigen-positive and antigen-negative fractions (90–98%). The purity of all sorted fractions used in the experiments was controlled by flow cytometric analyses. To ensure that the labelling procedure did not influence the reactivity of CTL, MAb-labelled unfractionated cells were also included in all cytotoxicity assays.

■ **Target cells.** The following target cells were used in the cytolytic assays: PRV-infected and uninfected L14 cells (a retrovirus-immortalized B lymphoblastoid cell line of SLA haplotype d/d) (Kaeffer *et al.*, 1990) and K562 cells (a cell line from a human erythroleukaemia) (ATCC). K562 cells were used because killing of these cells indicates that NK cells are involved (Pescovitz *et al.*, 1988). Infected L14 cells were obtained by infecting the cells 24 h before the start of the cytolytic assay with NIA-3 virus at an m.o.i. of 10. The cells were labelled by incubating various numbers of cells in a volume of 50 μl serum-free medium containing 400 μCi ^{51}Cr (Amersham, CJS4) for 2 h at 37 °C on a Rock 'n Roller (Labinco). After being labelled, the cells were washed three times in RPMI complete medium. Volumes of 50 μl medium containing 10^4 cells were added to the wells of 96-well V-bottomed microtitre plates (Nunc, Life Technologies).

■ **Cytolytic assay.** The cytolytic activity of the effector cells was measured by ^{51}Cr release. Volumes of 50 μl medium containing effector cells and 50 μl medium containing 10^4 ^{51}Cr-labelled target cells were mixed with effector:target ratios of 50:1 to 6:1. The plates were then centrifuged for 5 min at 200 g. Maximal release of ^{51}Cr was determined by adding 50 μl 20% Triton X-100. Spontaneous release was determined in wells that did not contain effector cells. Killing of the target cells was determined by measuring the release of ^{51}Cr in the supernatant after an incubation period of 5 h. Volumes of 50 μl supernatant were mixed with 100 μl Optiphase supermix liquid scintillation fluid (EG&G Instruments). Radioactivity was then measured in a Wallac Microbetaplus 1450 scintillation counter (EG&G Instruments). The percentage of specific ^{51}Cr release was calculated as 100 × (c.p.m. experimental release − c.p.m. spontaneous release)/(c.p.m. maximal release − c.p.m. spontaneous release).

Results

Comparison of phenotypes of PRV-stimulated PBMC from the singly and frequently inoculated groups

To examine the influence of subsequent PRV inoculations on the frequency of lymphocyte subsets, we compared the frequency of various lymphocyte subsets in immune PBMC from the singly inoculated group and the frequently inoculated group after stimulation *in vitro* with PRV. The percentages of CD6$^+$ CD8$^+$ (CTL phenotype, 60 ± 8%) and CD4$^+$ CD8$^+$ (fraction containing memory T helper cells, 32 ± 7%) lymphocytes were significantly higher in the frequently inoculated group than in the singly inoculated group (CTL phenotype 42 ± 7%; fraction containing memory T helper cells 22 ± 10 %). In contrast, the percentage of the $\gamma\delta$-T$^+$ CD8$^+$ lymphocyte subset (16 ± 4%) was significantly lower in the frequently inoculated group than in the singly inoculated group (25 ± 6%) (Fig. 3).

Phenotypes of PRV-stimulated and IL-2-stimulated PBMC

We subsequently examined the influence of IL-2 and PRV stimulation on the frequency of various lymphocyte subsets. When cells from immune pigs where stimulated *in vitro* with PRV, we observed the following lymphocyte subset frequencies: CD6$^+$ CD8$^+$, 49 ± 11%; CD4$^+$ CD8$^+$, 26 ± 10%; CD6$^-$ CD8$^+$, 19 ± 6%; and $\gamma\delta$-T$^+$ CD8$^+$, 21 ± 7%. When cells from immune pigs where stimulated *in vitro* with IL-2, we observed the following lymphocyte subset frequencies: CD6$^+$ CD8$^+$, 44 ± 13%; CD4$^+$ CD8$^+$, 21 ± 6%; CD6$^-$ CD8$^+$, 20 ± 10%; and $\gamma\delta$-T$^+$ CD8$^+$, 22 ± 4%. When cells from naive pigs where stimulated *in vitro* with IL-2, we observed the following lymphocyte subset frequencies: CD6$^+$ CD8$^+$, 34 ± 5%; CD4$^+$ CD8$^+$, 16 ± 5%; CD6$^-$ CD8$^+$, 29 ± 9%; and $\gamma\delta$-T$^+$ CD8$^+$, 34 ± 7%.

The frequencies of various lymphocyte subsets were compared in the IL-2-stimulated PBMC of naive pigs, the IL-2-stimulated PBMC of immune pigs and the PRV-stimulated PBMC of immune pigs. We detected significantly more CD6$^+$ CD8$^+$ (CTL phenotype) and CD4$^+$ CD8$^+$ (fraction containing memory T helper cells) and fewer CD6$^-$ CD8$^+$ (NK phenotype) and $\gamma\delta$-T$^+$ CD8$^+$ ($\gamma\delta$-T cell phenotype) lymphocytes when we compared the frequencies of various lymphocyte subsets after PRV stimulation of immune PBMC and after IL-2 stimulation of naive PBMC (Fig. 4) ($P < 0.05$).

Characterization of lymphoid subsets after cell separation with α-wCD6 MAb

CD6-negative selection. In immune and naive PBMC (after PRV or IL-2 stimulation), CD6$^-$ lymphocytes appeared to be mainly CD4$^-$ (< 8% CD4$^+$). In immune PBMC (after PRV or IL-2 stimulation), the majority of lymphocytes were $\gamma\delta$-T$^+$ CD8$^+$ ($\gamma\delta$-T cell phenotype, 25%) or $\gamma\delta$-T$^-$ CD8$^+$ (NK phenotype,
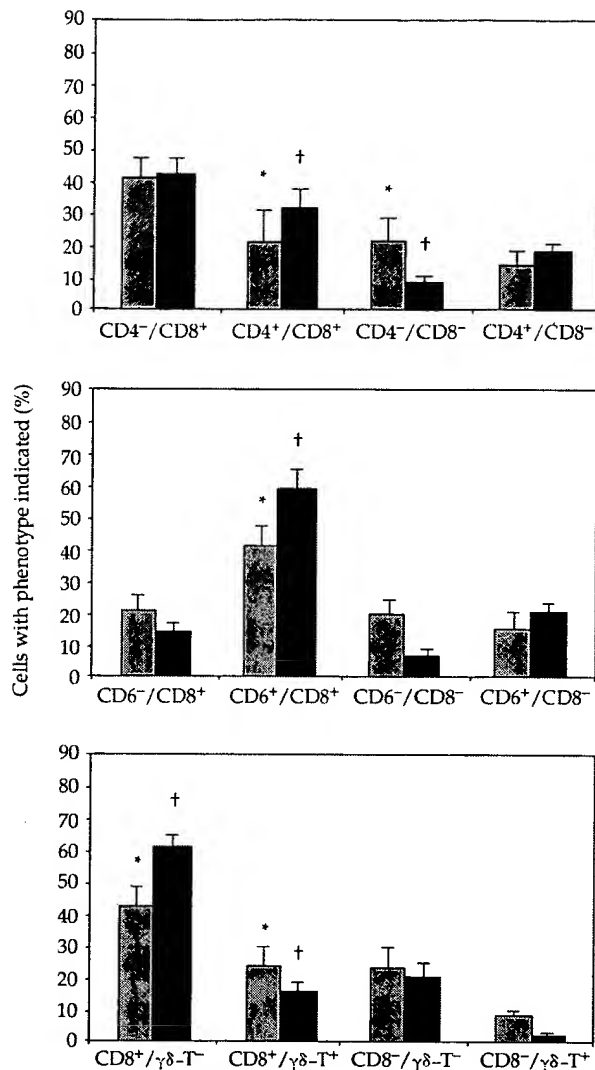
Fig. 3. Frequency of various lymphocyte subsets from singly inoculated (shaded bars) and frequently inoculated pigs (filled bars; $n = 5$) determined by flow cytometry analysis. PBMC were stimulated *in vitro* with PRV. Cells were double-stained with MAbs directed against porcine CD4/CD8, CD6/CD8 and $\gamma\delta$-T/CD8. The subset frequencies that differed significantly are indicated by * and †.
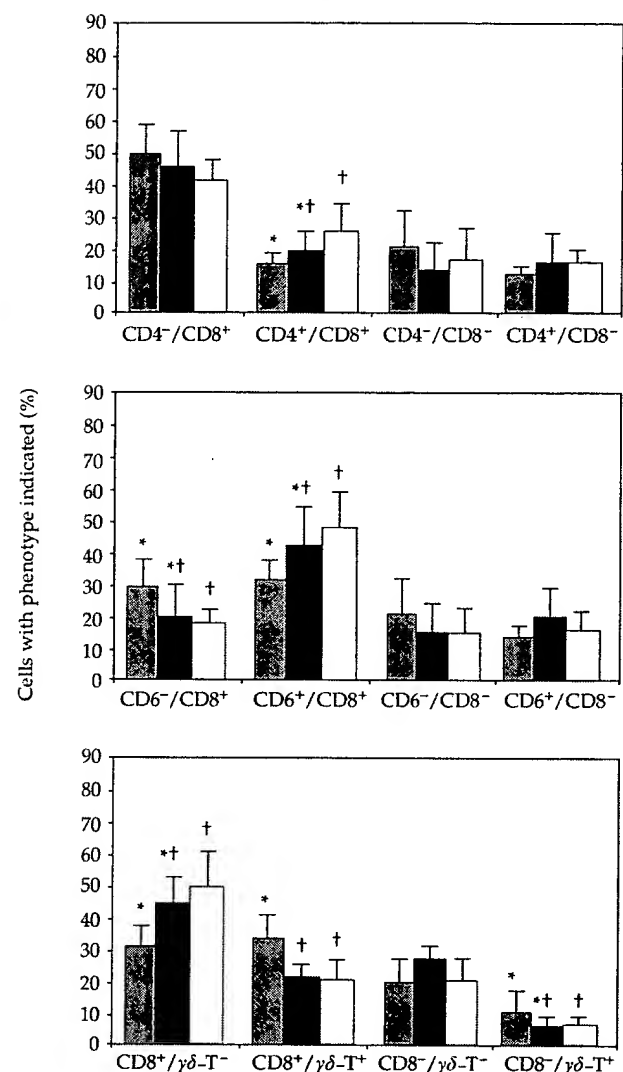

Fig. 4. Frequency of various lymphocyte subsets from IL-2-stimulated PBMC isolated from naive pigs (shaded bars; $n = 5$) and immune pigs (filled bars) and PRV-stimulated PBMC isolated from immune pigs (open bars). Cells were double-stained with MAbs directed against porcine CD4/CD8, CD6/CD8 and $\gamma\delta$-T/CD8. The subset frequencies that differed significantly are indicated by * and †.

40–41%; in bold in Table 2), whereas in naive PBMC (after IL-2 stimulation), the majority of lymphocytes were $\gamma\delta$-T$^+$ CD8$^+$ ($\gamma\delta$-T cell phenotype, 67%; in bold in Table 2). Interestingly, the expression of the CD8 antigen was higher on the $\gamma\delta$-T$^-$ CD8$^+$ (NK phenotype) lymphocytes than on the $\gamma\delta$-T$^+$ CD8$^+$ ($\gamma\delta$-T cell phenotype) lymphocytes (see the mean fluorescence values in Fig. 2d, e).

CD6-positive selection. In immune and naive PBMC (after PRV or IL-2 stimulation), the CD6$^+$ population contained CD4$^-$ $\gamma\delta$-T$^-$ CD8$^{bright+}$ (CTL phenotype), CD4$^+$ $\gamma\delta$-T$^-$ CD8$^-$ (T helper) and CD4$^+$ $\gamma\delta$-T$^-$ CD8^{dull+} (fraction containing memory T helper cells) lymphocytes (Table 2). However, in PBMC from

immune pigs after *in vitro* PRV stimulation, the percentage of CD4$^+$ $\gamma\delta$-T$^-$ CD8^{dull+} (fraction containing memory T helper cells) cells was high (68%; in bold in Table 2), whereas when PBMC isolated from immune and naive pigs were stimulated with IL-2, the percentage of CD4$^+$ $\gamma\delta$-T$^-$ CD8^{dull+} cells was low (20–30%) (Table 2).
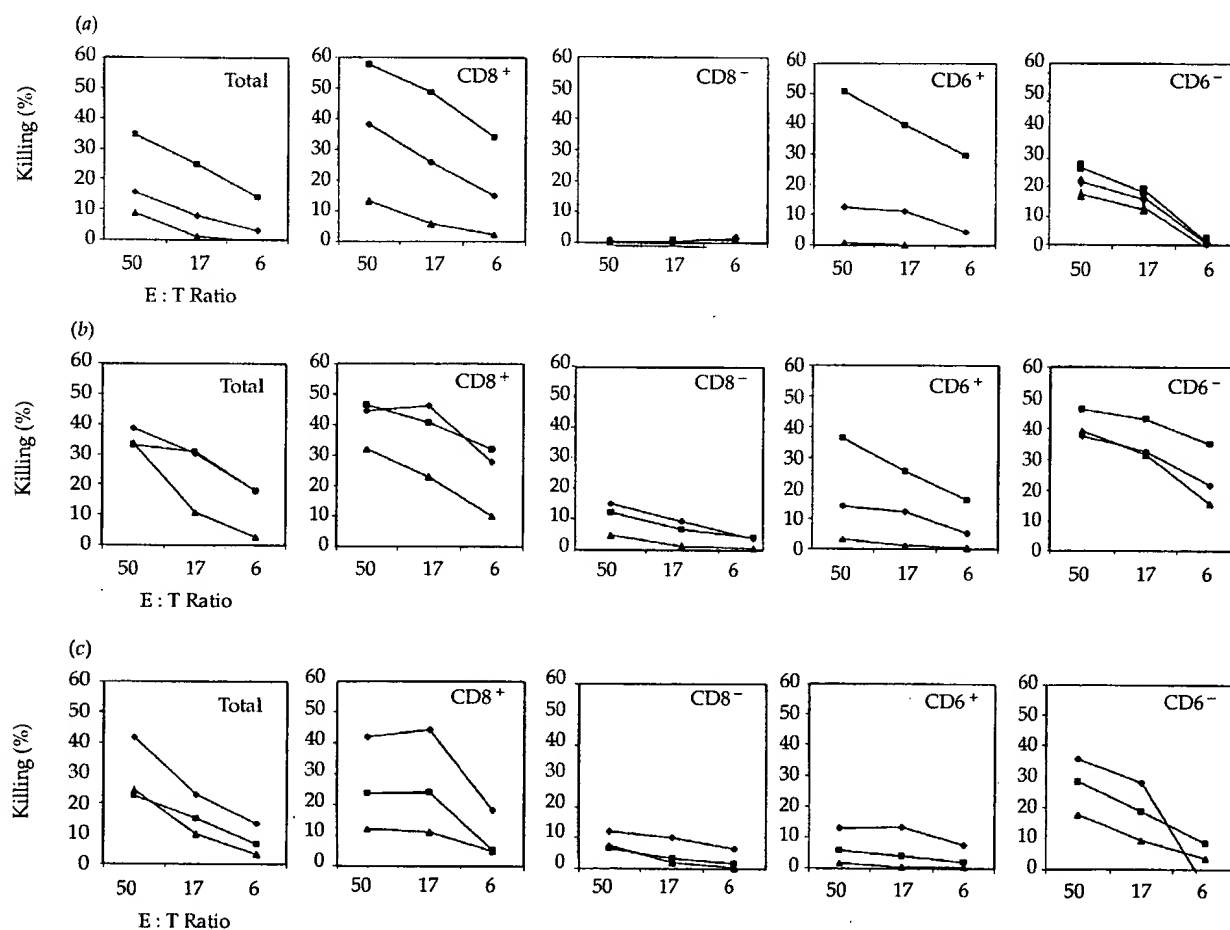
Phenotypic and functional characterization of cytolytic subsets

In none of the experiments was killing inhibited by pre-incubation with the MAbs against porcine CD8 and wCD6. PBMC from immune pigs, stimulated *in vitro* with PRV, killed

Table 2. Percentage of lymphocytes positive after separation with α-wCD6 MAb

Data are shown from a representative experiment of two in each case.

Phenotype	Immune				Naive	
	PRV stimulation		IL-2 stimulation		IL-2 stimulation	
	CD6⁻	CD6⁺	CD6⁻	CD6⁺	CD6⁻	CD6⁺
CD4⁻ CD8⁺	84	22	79	40	75	40
CD4⁺ CD8⁺	8	68	3	32	2	20
CD4⁺ CD8⁻	0	9	0	26	0	36
γδ-T⁻ CD8⁺	41	73	40	62	8	52
γδ-T⁺ CD8⁺	25	7	40	13	67	13
γδ-T⁺ CD8⁻	7	0	5	0	14	2

Fig. 5. Killing activity of CD8- and CD6-separated PBMC. PBMC that were stimulated *in vitro* with PRV or IL-2 were labelled with α-CD8 or α-wCD6 MAb and subsequently separated by MACS into CD8⁺ and CD8⁻ or CD6⁺ and CD6⁻ subpopulations, respectively. Killing of K562 cells (▲), PRV-infected L14 target cells (■) and uninfected L14 target cells (◆) is shown. PBMC isolated from immune pigs were stimulated *in vitro* with PRV (*a*) or IL-2 (*b*). PBMC isolated from naive pigs were stimulated *in vitro* with IL-2 (*c*). One representative experiment of each is shown. E : T, Effector : target.

PRV-infected L14 cells more efficiently than uninfected L14 cells (Fig. 5a). In order to dissect the activity of various subsets, these stimulated PBMC were separated for CD8 and CD6. The CD8$^+$ lymphocytes killed PRV-infected L14 cells more efficiently than uninfected L14 cells, indicating virus-specific killing (Fig. 5a). Both the total population and the enriched CD8$^+$ lymphocyte subpopulation of PRV-stimulated PBMC isolated from immune pigs killed very few K562 cells.

The CD6$^+$ lymphocytes primarily killed the PRV-infected L14 cells (Fig. 5a), indicating virus-specific killing. The CD6$^-$ lymphocytes killed the PRV-infected, uninfected L14 and K562 target cells equally well, suggesting the activity of NK cells. We could not detect more efficient killing (i.e. percentage killing of PRV-infected targets) with the enriched populations compared with the total population. However, virus-specific killing (i.e. percentage killing of PRV-infected targets minus percentage killing of uninfected targets) was more efficient with the enriched populations, indicating enrichment of virus-specific CTL after separation.

When PBMC were isolated from immune as well as naive pigs and stimulated in vitro with IL-2, these PBMC killed the PRV-infected and uninfected L14 cells equally well. In addition, these cells also killed K562 cells, suggesting the activity of NK cells (Fig. 5b, c). The IL-2-stimulated PBMC were separated for CD8 and CD6. The CD8$^+$ lymphocytes also killed PRV-infected and uninfected L14 cells and K562 cells equally well, indicating natural killing. In contrast, killing of target cells by the CD6$^+$ lymphocytes was low after IL-2 stimulation (Fig. 5c). However, in two experiments with cells from immune pigs, the PRV-infected L14 cells were killed more efficiently than the uninfected L14 cells (26 versus 7% and 36 versus 14%), indicating that virus-specific killing can be induced after IL-2 stimulation of immune PBMC. In contrast, only natural killing was found when the cells were separated by using the anti-CD8 MAb.

The K562 cells were not killed by the IL-2-stimulated CD6$^+$ lymphocytes. The CD6$^-$ lymphocytes killed PRV-infected and uninfected L14 cells equally well and K562 cells were also killed. Therefore, virus-specific killing was due to CD6$^+$ lymphocytes and natural killing was due to CD6$^-$ lymphocytes.

Discussion

We have demonstrated that we could discriminate various subsets of cytolytic cells. PRV stimulation in vitro of immune PBMC resulted mainly in CD6$^+$ CD8$^+$ lymphocytes (classical CTL phenotype and the fraction containing memory T-helper cells) and killing was mainly virus specific. In contrast, IL-2 stimulation of immune and naive PBMC resulted mainly in CD6$^-$ CD8$^+$ lymphocytes (NK and γδ-T cell phenotypes) and killing was mainly non-virus specific. In addition, flow cytometry analysis demonstrated more CD6$^+$ CD8$^+$ and CD4$^+$ CD8$^+$ and fewer CD6$^-$ CD8$^+$ and γδ-T$^+$ CD8$^+$ lymphocytes after PRV stimulation of immune PBMC compared with IL-2 stimulation of naive PBMC. Therefore, the flow cytometry data are in line with the phenotype of cytolytic cells detected after PRV (more CD6$^+$ cells) and IL-2 (more CD6$^-$ cells) stimulation.

PRV-stimulated immune PBMC killed PRV-infected target cells more efficiently than uninfected target cells and this killing was mediated by CD6$^+$ CD8$^+$ lymphocytes. These findings confirm the study of Pauly et al. (1996), who reported that CD6$^+$ CD8$^+$ lymphocytes are responsible for virus-specific MHC-restricted killing. In contrast to Pauly et al. (1996), we could not eliminate killing by the unseparated population by 'blocking' of the MHC-I molecule with a MAb (data not shown). However, both the CD6$^+$ and CD8$^+$ population showed decreased killing after 'blocking' of the MHC-I molecule, which indicated that classical CTL were present in PRV-stimulated immune PBMC. Flow cytometry analysis of the separated populations revealed that the PRV-stimulated CD6$^+$ PBMC were CD4$^-$ γδ-T$^-$ CD8$^{bright+}$ (CTL phenotype), CD4$^+$ γδ-T$^-$ CD8^{dull+} (fraction containing memory T helper

Table 3. Results summary

Frequency is scored as low ($\pm$), intermediate ($+$) or high ($+$ $+$). NT, Not tested.

| Phenotype | Immune | | | | Naive | |
| | PRV stimulation | | IL-2 stimulation | | IL-2 stimulation | |
	Frequency	Killer cell activity	Frequency	Killer cell activity	Frequency	Killer cell activity
CD4$^+$ CD8$^+$	$+$ $+$	NT	$+$	NT	$\pm$	NT
CD8$^+$ γδ-T$^+$	$+$	NT	$+$ $+$	NK-like?	$+$	NK-like?
CD8$^+$ γδ-T$^-$	$+$	NK	$+$ $+$	LAK (NK activity)	$+$	LAK (NK activity)?
CD6$^+$ CD8$^+$	$+$ $+$	CTL	$+$ $+$	NT	$+$	NT
CD6$^-$ CD8$^+$	$+$ $+$	NK	$+$	LAK (NK activity)	$+$ $+$	LAK (NK activity)

cells) or CD4$^+$ $\gamma\delta$-T$^-$ CD8$^-$ (T-helper cell phenotype). The percentage of CD4$^+$ CD8$^+$ lymphocytes was very high after PRV stimulation (68%; Table 2) compared with that of freshly isolated PBMC (Fig. 1), which indicates that these lymphocytes may contribute to killing or are themselves directly involved in killing.

In addition to the killing by CD6$^+$ lymphocytes, we also detected some killing by CD6$^-$ lymphocytes. These cells killed PRV-infected and uninfected L14 cells and K562 cells efficiently. Flow cytometry analysis of the PRV-stimulated CD6$^-$ PBMC revealed mainly $\gamma\delta$-T$^-$ CD8$^+$ (NK phenotype) and $\gamma\delta$-T$^+$ CD8$^+$ ($\gamma\delta$-T cell phenotype) lymphocytes. Therefore, these results confirm our earlier observation (Kimman *et al.*, 1996) that NK cells were induced in PRV-immune pigs.

In contrast to the predominant CD6$^+$ CD8$^+$ phenotype of cytolytic cells after PRV stimulation of immune PBMC, we demonstrated that the IL-2-stimulated cytolytic cells were mostly CD6$^-$ CD8^{dull+} lymphocytes. These CD6$^-$ CD8$^+$ lymphocytes killed all the target cells investigated, indicating MHC-unrestricted or natural killing. Flow cytometry analysis revealed that the IL-2-stimulated CD6$^-$ PBMC were mainly $\gamma\delta$-T$^-$ CD8$^+$ (NK phenotype) and $\gamma\delta$-T$^+$ CD8$^+$ ($\gamma\delta$-T cell phenotype). These findings indicate that the NK activity in the fraction containing CD6$^-$ lymphocytes is due to LAK cells or $\gamma\delta$-T lymphocytes with NK-like activity. The IL-2-stimulated PBMC isolated from naive pigs contained 67% $\gamma\delta$-T$^+$ CD8$^+$ lymphocytes. The high percentage of $\gamma\delta$-T lymphocytes, at least after IL-2 stimulation of PBMC of naive pigs, compared with the percentage in freshly isolated PBMC (Fig. 2; CD6$^-$ fraction) suggests a role in the NK activity. Killing by $\gamma\delta$-T$^+$ CD8$^+$ lymphocytes has also been reported after stimulation with an anti-CD3 MAb (Yang & Parkhouse, 1997) or with IL-2 (De Bruin *et al.*, 1997).

In addition to the killing by the CD6$^-$ lymphocytes, we also detected some killing by CD6$^+$ CD8$^+$ lymphocytes after IL-2 stimulation. These lymphocytes killed the PRV-infected and uninfected L14 target cells equally well. We demonstrated previously (De Bruin *et al.*, 1997) that IL-2-stimulated killing by CD5$^+$ CD8$^+$ lymphocytes (CTL phenotype) could be directed against infected and uninfected L14 target cells. Virus-specific killing was only detected after IL-2 stimulation of PBMC isolated from immune pigs, which indicates that PRV inoculation *in vivo* is needed to expand virus-specific CTL precursors. We did not detect killing by CD8$^-$ lymphocytes after either IL-2 or PRV stimulation, which confirms the results of Yang & Parkhouse (1997). Therefore, killing by both classical CTL and NK activity is due to CD8$^+$ lymphocytes, which confirms the results of Pescovitz *et al.* (1988). However, the α-wCD6 MAb (Pauly *et al.*, 1996) enabled us to discriminate between classical CTL and cells with NK activity (summarized in Table 3).

In PBMC from immune pigs, the percentage of PRV-induced CD6$^+$ CD8$^+$ (CTL phenotype) lymphocytes was higher in frequently inoculated pigs compared with singly inoculated pigs (Fig. 3). This result agrees with the observed increase in virus-specific killing after frequent inoculations. Similarly, the percentage of CD4$^+$ CD8$^+$ (fraction containing memory T helper cells) lymphocytes was also higher in frequently inoculated pigs than in singly inoculated pigs. These lymphocytes contribute to the PRV-specific proliferative 'helper'-like response of PBMC (Zuckermann & Husmann, 1996; Summerfield *et al.*, 1996). Direct effector functions have not yet been described for CD4$^+$ CD8$^+$ lymphocytes; therefore a cytolytic effector function can not be excluded. Besides the high percentage of CD4$^+$ CD8$^+$ lymphocytes in the CD6$^+$ population (mentioned above), the increase in CD4$^+$ CD8$^+$ lymphocytes after subsequent immunizations also indicates an important role for these lymphocytes after PRV inoculation in pigs. These findings may explain the observation that repeated immunizations with PRV vaccines are usually needed to provide a high level of protective immunity.

In conclusion, we have demonstrated that PRV stimulation induced predominantly classical CTL (CD6$^+$ CD8$^+$ lymphocytes) but also some NK cells, whereas IL-2 stimulation induced mainly LAK cells with NK activity (CD6$^-$ CD8$^+$ lymphocytes). The possible involvement of CD4$^+$ CD8$^+$ lymphocytes (the fraction containing memory T helper cells) as cytolytic effector cells against PRV-infected cells after PRV stimulation and the NK-like activity of $\gamma\delta$-T$^+$ CD8$^+$ lymphocytes after IL-2 stimulation remain to be investigated.

References

Chinsakchai, S. & Molitor, T. W. (1992). Replication and immuno-suppressive effects of pseudorabies virus on swine peripheral blood mononuclear cells. *Veterinary Immunology and Immunopathology* **30**, 247–260.

De Bruin, M. G. M., Van Rooij, E. M. A., Voermans, J. J. M., De Visser, Y. E., Bianchi, A. T. J. & Kimman, T. G. (1997). Establishment and characterization of porcine cytolytic cell lines and clones. *Veterinary Immunology and Immunopathology* **59**, 337–347.

De Wind, N., Zijderveld, A., Glazenburg, K., Gielkens, A. & Berns, A. (1990). Linker insertion mutagenesis of herpesviruses: inactivation of single genes within the Us region of pseudorabies virus. *Journal of Virology* **64**, 4691–4696.

Gielkens, A. L. J., Moormann, R. J. M., Van Oirschot, J. T. & Berns, A. J. M. (1989). Vaccine efficacy and innocuity of strain 783 of Aujeszky's disease virus. In *Vaccination and Control of Aujeszky's Disease*, pp. 27–35. Edited by J. T. Van Oirschot. Dordrecht: Kluwer Academic.

Jonjic, S. & Koszinowski, U. H. (1984). Monoclonal antibodies reactive with swine lymphocytes. I. Antibodies to membrane structures that define the cytolytic T lymphocyte subset in the swine. *Journal of Immunology* **133**, 647–652.

Kaeffer, B., Bottreau, E., Phan Thanh, L., Olivier, M. & Salmon, H. (1990). Histocompatible miniature boar model: selection of transformed cell lines of B and T lineages producing retrovirus. *International Journal of Cancer* **46**, 481–488.

Kasza, L., Shadduck, J. A. & Christofinis, G. J. (1971). Establishment, viral susceptibility, and biological characteristics of a swine kidney cell line SK-6. *Research in Veterinary Science* **13**, 46–51.

Kimman, T. G., Bianchi, A. T. J., De Bruin, T. G. M., Mulder, W. A. M., Priem, J. & Voermans, J. J. M. (1995a). Interaction of pseudorabies virus with immortalized porcine B cells: influence on surface class I and II major histocompatibility complex and immunoglobulin M expression. *Veterinary Immunology and Immunopathology* **45**, 253–263.

Kimman, T. G., De Bruin, T. G. M., Voermans, J. J. M., Peeters, B. P. H. & Bianchi, A. T. J. (1995b). Development and antigen specificity of the lymphoproliferation responses of pigs to pseudorabies virus: dichotomy between secondary B- and T-cell responses. *Immunology* **86**, 372–378.

Kimman, T. G., De Bruin, T. G. M., Voermans, J. J. M. & Bianchi, A. T. J. (1996). Cell-mediated immunity to pseudorabies virus: cytolytic effector cells with characteristics of lymphokine-activated killer cells lyse virus-infected and glycoprotein gB- and gC-transfected L14 cells. *Journal of General Virology* **77**, 987–990.

Kirkham, P. A., Takamatsu, H., Yang, H. & Parkhouse, R. M. E. (1996). Porcine CD3 epsilon: its characterization, expression and involvement in activation of porcine T lymphocytes. *Immunology* **87**, 616–623.

McFerran, J. B. & Dow, C. (1975). Studies on immunisation of pigs with the Bartha strain of Aujeszky's disease virus. *Research in Veterinary Science* **19**, 17–22.

Pauly, T., Elbers, K., König, M., Lengsfeld, T., Saalmüller, A. & Thiel, H.-J. (1995). Classical swine fever virus-specific cytotoxic T lymphocytes and identification of a T cell epitope. *Journal of General Virology* **76**, 3039–3049.

Pauly, T., Weiland, E., Hirt, W., Dreyer-Bux, C., Maurer, S., Summerfield, A. & Saalmüller, A. (1996). Differentiation between MHC-restricted and non-MHC-restricted porcine cytolytic T lymphocytes. *Immunology* **88**, 238–246.

Pescovitz, M. D., Lunney, J. K. & Sachs, D. H. (1984). Preparation and characterization of monoclonal antibodies reactive with porcine PBL. *Journal of Immunology* **133**, 368–375.

Pescovitz, M. D., Lowman, M. A. & Sachs, D. H. (1988). Expression of T-cell associated antigens by porcine natural killer cells. *Immunology* **65**, 267–271.

Saalmüller, A., Hirt, W., Maurer, S. & Weiland, E. (1994a). Discrimination between two subsets of porcine CD8$^+$ cytolytic T lymphocytes by the expression of CD5 antigen. *Immunology* **81**, 578–583.

Saalmüller, A., Aasted, B., Canals, A., Dominguez, J., Goldman, T., Lunney, J. K., Maurer, S., Pauly, T., Pescovitz, M. D., Pospisil, R., Salmon, H., Trbichavsky, I., Valpotic, I., Vizcaino, J. S., Weiland, E. & Zuckermann, F. (1994b). Analysis of monoclonal antibodies reactive with porcine CD6. *Veterinary Immunology and Immunopathology* **43**, 243–247.

Sachs, D. H., Leight, G., Cone, J., Schwarz, S., Stuart, L. & Rosenberg, S. (1976). Transplantation in miniature swine. I. Fixation of the major histocompatibility complex. *Transplantation* **22**, 559–567.

Summerfield, A., Rziha, H. J. & Saalmüller, A. (1996). Functional characterization of porcine CD4 + CD8 + extrathymic T lymphocytes. *Cellular Immunology* **168**, 291–296.

Yang, H. & Parkhouse, R. M. E. (1996). Phenotypic classification of porcine lymphocyte subpopulations in blood and lymphoid tissues. *Immunology* **89**, 76–83.

Yang, H. & Parkhouse, R. M. E. (1997). Differential expression of CD8 epitopes amongst porcine CD8-positive functional lymphocyte subsets. *Immunology* **92**, 45–52.

Zuckermann, F. A. & Husmann, R. J. (1996). Functional and phenotypic analysis of porcine peripheral blood CD4/CD8 double-positive T cells. *Immunology* **87**, 500–512.

Zuckermann, F. A., Zsak, L., Mettenleiter, T. C. & Ben-Porat, T. (1990). Pseudorabies virus glycoprotein gIII is a major target antigen for murine and swine virus-specific cytotoxic T lymphocytes. *Journal of Virology* **64**, 802–812.

OCT 0 3 2003

IN THE UNITED STATES PATENT AND TRADEMARK OFFICE

APPLICANTS : Rothberg et al.

SERIAL NUMBER : 09/814,338   EXAMINER : Young J. Kim

FILING DATE : March 21, 2001   ART UNIT : 1637

FOR : METHOD OF SEQUENCING A NUCLEIC ACID

Commissioner for Patents
P.O. Box 1450
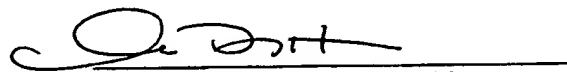Alexandria, VA 22313-1450

TRANSMITTAL LETTER

Transmitted herewith for filing in the present application are the following documents:

1. Declaration of Marcel Margulies under 37 C.F.R. § 1.132 (4 pages);
2. Exhibits 1-3 for Declaration (21 total pages);
3. Return Postcard.

If the enclosed papers are considered incomplete, the Mail Room and/or the Application Branch is respectfully requested to contact the undersigned at (212) 935-3000, New York, New York.

The Commissioner is authorized to charge any fees that may be due, or to credit any overpayment, to the undersigned's account, Deposit Account No. 50-0311 Ref. No. 21465-501 CIP 2. Please address all correspondence to customer number **35437**. A duplicate copy of this transmittal letter is enclosed herewith.

Respectfully submitted,

Ivor R. Elrifi, Reg. No. 39,529
Caryn DeHoratius, Reg. No. 45,881
Attorney/Agent for Applicants
MINTZ, LEVIN, COHN, FERRIS,
  GLOVSKY and POPEO, P.C.
The Chrysler Center
666 Third Avenue
New York, New York 10017
Tel: (212) 935-3000
Fax: (212) 983-3115

Dated: October 9, 2003

IN THE UNITED STATES PATENT AND TRADEMARK OFFICE

APPLICANTS: Jonathan M. Rothberg, et al.

ASSIGNEE: CuraGen Corporation

SERIAL NUMBER: 09/814,338   EXAMINER: Young J. Kim

FILING DATE: March 21, 2001   ART UNIT: 1637

FOR: METHOD OF SEQUENCING A NUCLEIC ACID

Commissioner for Patents
P. O. Box 1450
Alexandria, VA 22313-1450

DECLARATION OF MARCEL MARGULIES UNDER 37 C.F.R. §1.132

I, MARCEL MARGULIES, declare and state that:

1.   I am Vice President of Engineering, at 454® Life Sciences, the exclusive licensee of this application. My previous employment includes Director of New Technology Research at Perkin-Elmer's Instrument Division in Norwalk, CT, and Associate Director of the Hubble Space Telescope project.

2.   I earned my B.Sc. in Engineering from the Free University of Brussels, in Belgium, and a Ph.D. in theoretical physics from Columbia University.

3.   I have reviewed the instant application and the August 18, 2003 Office Action in this case.

4.   It is my opinion that the claimed invention represents the first massively parallel, solid-phase, whole-genome sequencing platform, which is vastly superior to previous sequencing technology for at least the reasons set out below.